LMSC-D282673
VOL I
MSC-07040, DRL-3
CR 134326

FINAL REPORT FOR

DEVELOPMENT AND DESIGN APPLICATION OF RIGIDIZED SURFACE INSULATION THERMAL PROTECTION SYSTEMS

VOLUME I

30 DEC 1972

CONTRACT NAS9-12856

PREPARED FOR NATIONAL AERONAUTICS AND SPACE ADMINISTRATION,
MANNED SPACECRAFT CENTER,
BY LOCKHEED MISSILES & SPACE COMPANY, INC.,
MANNED SPACE SUPPORT SYSTEMS, SPACE SYSTEMS DIVISION

LOCKHEED MISSILES & SPACE COMPANY, INC.
A SUBSIDIARY OF LOCKHEED AIRCRAFT CORPORATION
SPACE SYSTEMS DIVISION · SUNNYVALE, CALIFORNIA

ABSTRACT/FOREWORD

This final report presents the results of NASA Contract NAS 9-12856, "Development and Design Application of Rigidized Surface Insulation Thermal Protection Systems" performed by Lockheed Missiles and Space Company for the National Aeronautics and Space Administration, Manned Spacecraft Center, under the direction of the Thermal Technology Branch of the Structures and Mechanics Division, D. J. Tillian, COR.

The contract objective was to establish materials and design technology of the LMSC all-silica LI-900 rigid surface insulation (RSI) thermal protection system (TPS) concept for the Shuttle spacecraft. All results of contract development efforts to satisfy this objective are documented. Engineering design and analysis of RSI strain arrestor plate material selections, sizing, and weight studies are reported. A shuttle prototype test panel was designed, analyzed, fabricated, and delivered to NASA. Thermophysical and mechanical properties of LI-900 were experimentally established and reported. Environmental tests, including simulations of shuttle loads represented by thermal response, turbulent duct, convective cycling, and chemical tolerance tests are described and results reported. Descriptions of material test samples and panels fabricated for both NASA and LMSC testing are included. Descriptions of analytical sizing and design procedures are presented in a manner formulated to allow competent engineering organizations to perform rational design studies. Results of parametric studies involving material and system variables are reported. Material performance and design data are also delineated.

Areas requiring additional development effort are discussed and the conclusion drawn that no problems are foreseen that cannot be solved within the present NASA Shuttle time span. Based on the results of this contract effort, LMSC considers the LI-900 TPS to be sufficiently well developed to warrant use on the first Shuttle flight vehicle.

This report consists of two volumes. Volume I is the main body of the report and Volume II contains appendix material.

CONTENTS

SUMMARY

Of the many technological advances needed in the evolution of the Space Shuttle, the most challenging is the development of a light-weight reusable thermal protection system (TPS) capable of withstanding the extreme environments of its operational life. An all-silica rigid surface insulation (RSI) material, LMSC's LI-900, has demonstrated this capability by both analyses and test. A series of LMSC and NASA programs addressing the basic material, its coating, and its application to orbiter structure has culminated in this program, with emphasis on LI-900. The framework of the program has been structured to:

- Define material characteristics
- Develop analytical design techniques
- Display typical TPS design options
- Demonstrate life capabilities through simulated mission test exposures.

To accomplish these objectives, the program effort was categorized and defined under the following major headings:

Task A – Design and Analysis

Task B – Property Characterization

Task C – Contractor Environmental Test-Design Development

Task D – Material Production

Task E – Prototype Panel Design

A brief description of these tasks is included in the following paragraphs.

Task A – Design and Analysis. This effort evaluated the feasibility of an RSI tile attachment system that uses the strain arrestor plate concept in conjunction with a flexible strain isolator/primary structure bond. The main function of the strain arrestor plate (SAP) is to act as a strain barrier between the tile and the foam bond/primary structure, particularly at temperatures below the glassy transition range of the foam bond isolator system. With its high stiffness, high strength, and low thermal expansion characteristics, the SAP absorbs the loading transferred by the bond system from the substrate, thereby preventing high stresses in the RSI tile.

General scope of the study included:

- Selection of the optimum strain arrestor material and construction, along with compatible epoxy and strain isolator bonds. HMS X-904 graphite-epoxy was chosen on the basis of structural adequacy and low weight.

- Study of allowable tile sizes and TPS configurations for three orbiter locations (top, bottom, and sides)
- Effect of the SAP on TPS unit weight
- Design of the prototype test panel for fabrication and delivery to NASA
- Development of parametric design information that would be useful in future studies. In addition to LI-900 sizing curves, such variables as SAP in-plane stiffness, bond line thickness, tile length, bond coverage and SAP thickness and continuity were examined.

The model used for initial screening investigations considered the Area 2P skin-stringer aluminum panel delivered under the Phase II contract. As contractually specified, structural analyses were restricted to two-dimensional linearly elastic techniques.

Generally speaking, it was found that a properly designed SAP reduced tile and coating stresses under all conditions, with no weight penalty for the bottom surface TPS. Weight does increase somewhat for the side and top locations. Use of the strain arrestor plate also allows a wider range of tile sizes. It was also concluded that LI-900 RSI has the capability of withstanding the specified design conditions.

Task B – Property Characterization. This task obtained mechanical and thermophysical properties of the LI-900 material and the 0042 coating, in accordance with the Property Test Plan (LMSC-D282611) approved by NASA. Tests were conducted on material in the as-fabricated condition as well as on material subjected to 20 radiant heat cycles. The full matrix of tests, as shown in Section 3, included:

- Coating – tension and thermal expansion
- LI-900 – in-plane and transverse tension, transverse shear, thermal expansion, and thermal conductivity.

Ten data points were obtained for each mechanical test condition and three for each thermophysical condition over a range of temperature from 77°K (-320°F) to 1480°K (2200°F).

A similar matrix effort is being conducted by Battelle under NASA direction, with the exception that mechanical testing is restricted to room temperature, 700°K (800°F) and 1143°K (1600°F). A like matrix by NASA/ARC will address LI-1500 instead of LI-900.

Because of the nature of the material, special handling precautions were necessary and redesign of the mechanical test specimen and fixtures required to achieve the objectives. With the exception of the transverse shear tests it has been found that the test techniques developed are satisfactory and that the data obtained show that LI-900 is not sensitive to radiant cycling. Further development of shear test techniques is therefore required.

Experimental accuracy of the mechanical tests is discussed in Appendix B1-1, while that of the thermophysical tests is included in Section 3.2.

Task C – Contractor Environmental Test-Design Development. A test program, containing a series of four tests, was defined under this task to simulate critical environments and conditions. Because LI-900 is a relatively new variation of the all-silica RSI, a variety of performance data is needed, particularly as a result of convective testing. Tests planned were:

- Thermal Response Tests (C-1)
- Turbulent Duct Tests (C-2)
- Convective Cycling Tests (C-3)
- Chemical Tolerance Tests (C-4)

LMSC has designed and fabricated test models and submitted test plans for all four series and has conducted tests C-1 and C-4. The conduct of tests C-2 and C-3 were the responsibility of NASA/ARC and NASA/MSC respectively, although the analyses were accomplished by LMSC. All test models incorporated the SAP concept except those for C-4, the chemical tolerance tests.

The thermal response tests at LMSC evaluated the performance of LI-900 TPS under a series of radiant heat tests. Five heating tests were conducted in the LMSC HIRAD facility at one atmosphere pressure using the Area 2P temperature history of the Phase II program. This was followed by an orbit cold soak test to 117°K (-250°F) to verify the capability of the strain arrestor system. In-depth and back-face temperature predictions were correlated with the test data to verify design procedures.

Turbulent duct tests are to be conducted in the NASA/ARC 20-mw arc facility to evaluate the performance of LI-900 under turbulent heating conditions. Five cycles of heating are planned with the as-fabricated panel and temperature measurements taken through the tile and in joints parallel and perpendicular to the stream. Following these tests, successively greater amounts of artifical damage are to be induced in a tile surface by drilling and enlarging a hole in between further tests until failure appears imminent. Temperatures will be correlated with predictions and the results of the inflicted damage assessed.

A 100-cycle series of convective heating tests are planned at the NASA/MSC 10-mw arc heater facility. During the series, the model is to be removed from the holder and rotated 90 deg to obtain data with the joint parallel and perpendicular to the flow. The instrumentation array has been designed to provide surface, in-depth, joint, and arrestor plate interface temperature data. In particular, cumulative effects on the model integrity and temperature response repeatability are to be evaluated.

Chemical tolerance tests were performed to assess the contamination or degradation of LI-900 by ten different materials including dilute hydrochloric acid, dilute sodium hydroxide, acetone, methyl-ethyl-ketone, hydraulic fluid, JP-4, IRFNA, UDMH, bird excrement, and NASA/MSC NDE fluid. Exposure was by immersion or splash at one atmosphere and room temperature. The test models were weighed and measured and temperature emittance characteristics determined before and after test exposures. Following exposure and measurements, the specimens were subjected to an abbreviated Area 2P radiant lamp heating test to determine effects on the thermal characteristics.

Task D – Material Production. The LI-900 material for tasks C and E, as well as the material for MSC evaluation, was produced under this task. The LI-1500 material, specified by Supplemental Agreement 1S, was also produced under this task for MSC evaluation. Close control and material tracking were maintained throughout this task. Records of all NDE radiographs were supplied to NASA for each test specimen or model. Although the contract and supplemental agreement originally specified an aggregate of 11 cubic feet of material, a total of 19 cubic feet was actually produced and supplied.

Task E – Prctotype Panel. Design and analysis efforts on the "prototype" panel were accomplished under Task A. The panel design was reviewed with NASA/MSC for approval and authorization to proceed on 22 November. Fabrication took place in LMSC's manufacturing facilities, during which the end attachment hardware was match-drilled to NASA/MSC loading plates. The panel was instrumented with thermocouples and strain gages as specified in the Appendix E1, Environmental Test Plan For Phase III RSI Prototype Panel, developed by LMSC. The model was then transmitted to NASA/MSC for testing. Results and evaluation of these tests will be reported separately.

CONCLUSIONS

Through analysis and test, it has been demonstrated that LI-900 meets Space Shuttle mission and life requirements and is sufficiently well developed to be selected as the TPS material for the Space Shuttle orbiter.

As a result of program testing, it can be concluded that the LI-900 material/coating system has reuse capability to 1648°K (2500°F) and that its mechanical and thermal performances do not significantly degrade with use. Property data obtained were consistent within itself and with predictions. The quantity of data is sufficient for baselining preliminary design. The strength properties are not appreciably affected by high temperature reuse nor do they significantly change with temperature. Thermal conductivity was shown to be pressure-dependent and design curves for this property were validated by in-depth measurements of test temperatures. The thermal expansion characteristics of both LI-900 and its coating were shown to be compatible and, because of their low thermal expansion, the materials are thermally shock-resistant. A cold soak 116°K (-250°F) condition, followed by a reentry heat pulse, was found to have no effect on the material. It was also determined that high water content on non-waterproofed tiles can cause a slight loss of coating during the ascent/reentry thermal pressure environment, although there was no effect on heat shielding capability.

The strain arrestor plate (SAP) investigations revealed that the concept improves the mechanical performance of the combined LI-900/substrate system for all conditions. The use of the strain arrestor plate reduces tile and coating stresses under all load and temperature conditions and does not increase bottom surface TPS weight, although there is a nominal increase at side and top locations. Using a SAP permits a greater variation in tile size because of the improved mechanical performance. As a SAP matrix, Fibrite X-904 resin was found to meet requirements.

A rational design methodology was developed in the program recognizing the combined stress failure mode of RSI and utilizing the fine mesh, double-precision finite element codes (with orthotropic solid elements) found to be required for RSI stress analysis. Although the stress analyses upon which the study was based are conservative (yielding higher than actual stresses) since non-linear and creep/relaxation effects were not included, positive margins of safety were obtained or indicated at three orbiter locations (bottom, top, and side). Experimental results demonstrated the conservatism of analytical results. It is also concluded that the low LI-900 coefficient of thermal expansion reduces thermal stresses and external gap requirements.

RECOMMENDATIONS

This program has demonstrated the capability of LI-900 to satisfactorily operate within the Shuttle environment. However, questions remain to be answered prior to application to the first vehicle. LMSC recommends, therefore, that further development efforts emphasize the following subjects.

Strain Arrestor Plate. Although present linear analysis results would indicate that a strain arrestor plate (SAP) is necessary to reduce tile stresses, non-linear effects due to time (relaxation and creep) and loading in the foam bond layer should be accounted for by analysis and test before adopting this approach for final design. Concepts other than flat plates should be investigated for application to curved surfaces, odd shapes and other non-standard locations.

LI-900/Coating Properties. The need for statistical design properties will require refined mechanical test methods (particularly for shear values), including further development and verification of the failure theory through combined property testing. In addition, effort is needed to:

- By test and analysis, define RSI failure modes, damage tolerance, and accept/reject criteria for application and refurbishment.
- Investigate residual stresses in the tile and the coating (after cure/reentry)
- Evaluate more fully the mechanism involved in the occasional development of shallow cracks in the 0042 coating.
- Evaluate on-location repair of RSI tiles.
- Establish minimum LI-900 tile thickness requirements for structural integrity.

Tile Attachment. Both analysis and test are needed to develop the most efficient method. Particularly, the following are recommended:

- Test alternate attachment methods with emphasis on reliability, ease/cost of application and replacement, and ability to survive cold soak conditions (-250^{o}F).
- Investigate patterned bonds to reduce stresses and weight.
- Further investigate the effects of glass transition of bond systems.

- Perform additional tests to evaluate closed cell foams (sponge) in vacuum at various temperatures.
- Perform studies and tests to evaluate effects of protruding rivets at the primary surface.

Design Analysis. Design methods development should continue to allow the preparation of a preliminary design handbook. In addition to past results, subjects to be emphasized are:

- Improve design/analysis/techniques through non-linear 2D/3D analysis.
- Evaluate analytically, and by tests, foam/bond relaxation phenomena at all temperatures.
- By analysis and test, more completely define the interaction between the RSI and structural components.
- Evaluate buckling of skin, establish limits (buckle amplitudes, etc.).
- Develop techniques for odd-size tile and non-standard requirements such as doors, cutouts and chines.
- Perform gap studies (structural) considering NR orbiter configuration, loads, and environment.
- Evaluate dynamic effects (analytically and by tests).

Although past developments have been very encouraging, further effort is also needed to continue non-destructive evaluation (NDE) investigations with emphasis on scale-up required for Shuttle turn-around requirements.

Section 1
INTRODUCTION AND PROGRAM PLAN

1.1 INTRODUCTION

One of the most critical problems of creating a reusable Space Shuttle system is the development of a reliable reusable thermal protection system to replace previous non-reusable heat shields which are effectively consumed or degraded during recovery. Lockheed began investigating a broad range of reusable surface insulation (RSI) materials as early as 1957. In addition to an all-silica system, these included zirconium compounds, alumina, and aluminum silicates (mullites). Mullite and others were dropped as viable candidates because of their high thermal expansion, high conductivity, and poor resistance to thermal and acoustic loads. Data from this research clearly proved that an all-silica system was the best candidate for a fully reusable insulator. In 1965, Lockheed increased its activity on high lift-to-drag reentry vehicles and continued development of lightweight, all-silica thermal protection materials. This led to creation of a 240 kg/m^3 (15/ft^3) Lockheed proprietary material, called LI-1500, which achieved, in laboratory quantities, the very desirable theoretical properties of an all-silica material by strict control of material and process. In 1970, Lockheed established a pilot plant to perfect the process and provide the techniques for full production to meet Space Shuttle needs.

Lockheed's all-silica LI-1500 was tested extensively under independent development funds and under contract at Lockheed at various NASA centers and at Air Force laboratories, and was shown to meet Space Shuttle mission and life requirements.

The effort on the recent contract, NAS 9-12137 (Improvement of Reusable Surface Insulation Material), proved the feasibility of making significant improvements in reducing material density to 144 kg/cu m (9 lb/cu ft), thus creating a new lighter RSI material designated as LI-900. The present contract effort, NAS 9-12856, develops for a particular (strain arrestor plate concept) TPS design approach and material properties of LI-900 sufficiently to justify the use of LI-900 as the Space Shuttle orbiter TPS material.

The program was carried out in accordance with the contract Program Plan, LMSC-D282611, submitted to NASA-MSC on 20 July 1972 and approved by the NASA COR, Mr. D. J. Tillian. The principal tasks and associated task leaders were:

Task A – Design and Analysis	–	M. H. Kural (with co-leaders J. M. Massard and R. P. Banas)
Task B – Property Data	–	J. A. DeRuntz and A. M. C. Holmes
Task C – Environment Test	–	J. O. Doraldson

Task D – Material Production – R. M. Beasley and Y. D. Izu

Task E – Prototype Panel – B. P. Van West

Task F – Prog. Mgt. (and Reports) – R. D. Buttram/A. E. Trapp

Mr. R. D. Buttram was Project Leader for the major portion of the program until succeeded by Mr. Trapp.

This document reports the results of the successful completion of these tasks and provides technical data which show that LI-900 can be reliably produced to meet all environmental and operational needs of a rigid surface insulation material for the Space Shuttle orbiter vehicle.

1.2 PROGRAM PLAN

LMSC presented the contractually required Program Plan (LMSC-D282611) to NASA-MSC and received approval on 20 July 1972. This plan conformed with the contract Data Requirements List (DRL), set dates for program and design reviews, provided for material deliveries to meet test dates at Ames, MSC, and Battelle, and scheduled the performance of analytical, design, and test events conducted by LMSC.

Major topics presented in the Program Plan were:

- Program Description
- Management Procedures, Organization and Facilities
- Detailed Task Description and Related Manpower
- Program Phasing – Master Schedule
- Program Deliverables – Data and Materials

LMSC's master schedule (Fig. 1-1) has been updated to reflect actual and planned program milestones through 31 January 1973. Material deliveries in excess of that required under the contract and greatly accelerated delivery dates were accepted by Lockheed without cost adjustments to facilitate NASA's key requirement for evaluation of RSI materials. The project was carried cut under the technical and management direction of LMSC's Space Shuttle Support Systems TPS Program Office as a major and vital part of Shuttle program activities. Mr. Ray Buttram, the Project Leader, had full management responsibility and authority to act in all matters within the scope of this project. He was supported by staff specialists in financial management, contract management and management plans and controls. Mr. A. E. Trapp, Manager of the Space Shuttle Structures effort, succeeded Mr. Buttram as Project Leader when the latter left the company in December 1972. The project organization is shown in Fig. 1-2. This basic TPS team, under Dr. K. J. Forsberg, TPS Program Manager at LMSC, has participated in all phases of LMSC's Space Shuttle TPS efforts and its members are intimately familiar with the pioneering and current technologies developed by Lockheed under in-house independent development and past related contractual efforts.

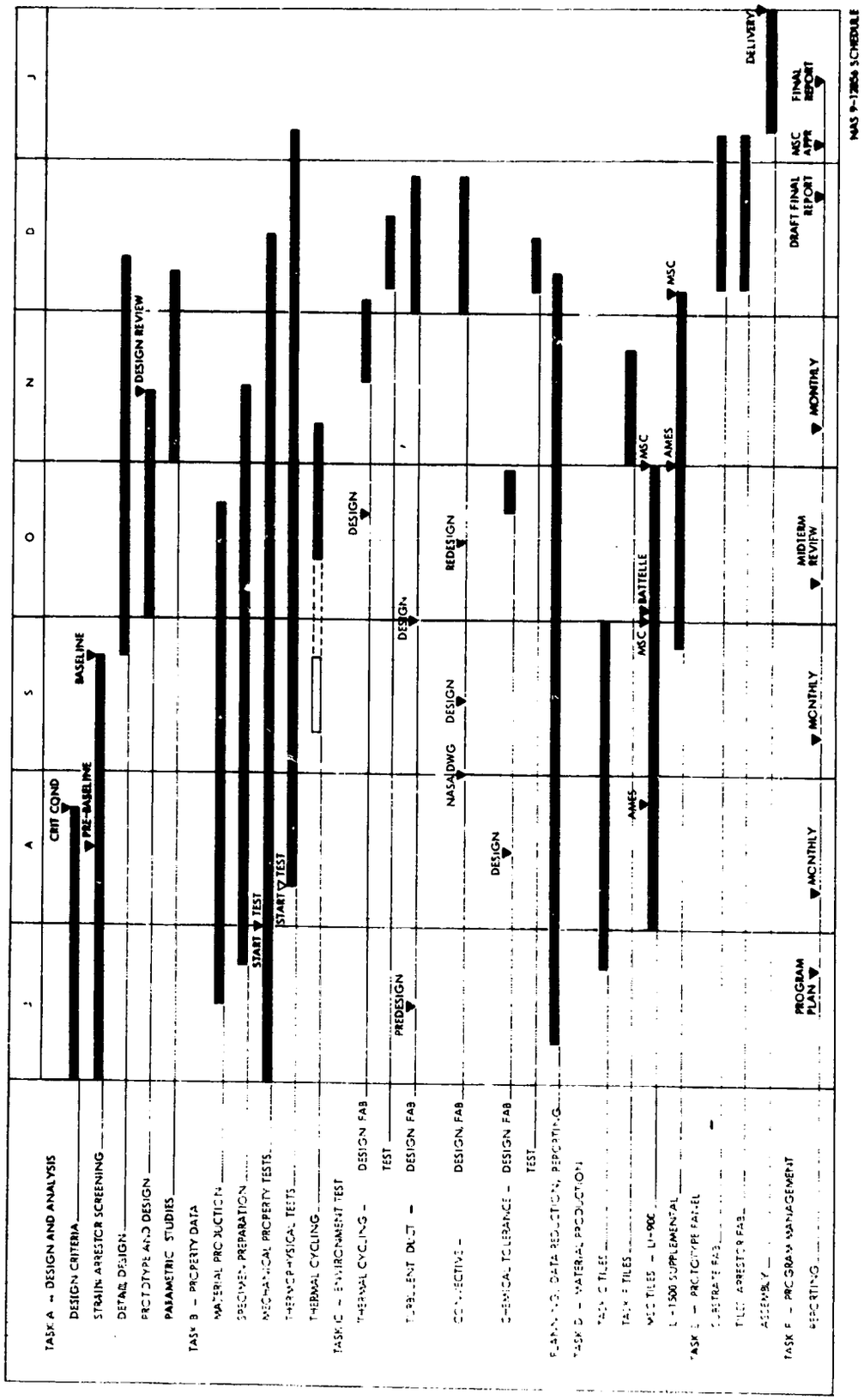

Fig. 1-1 Program Schedule

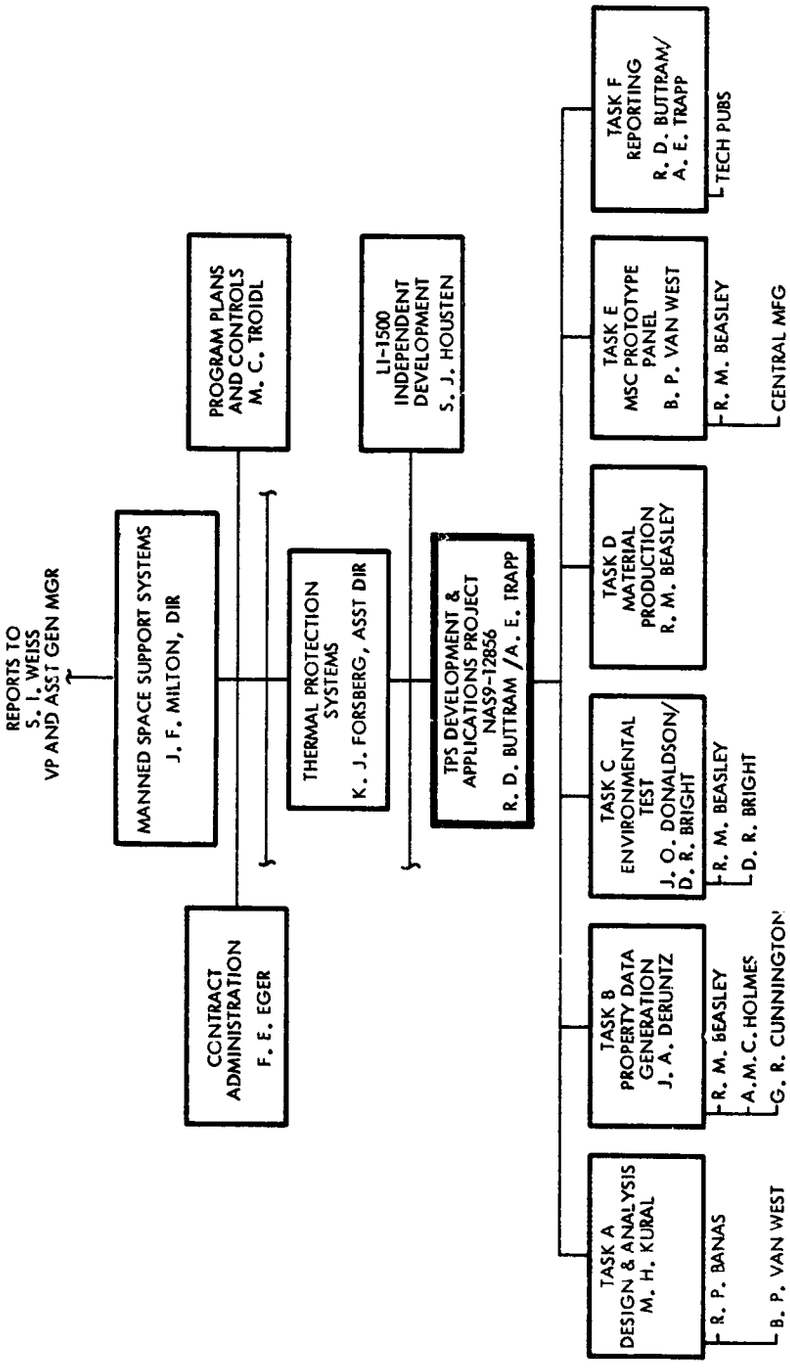

Fig. 1-2 Project Organization

Section 2

DESIGN AND ANALYSIS – TASK A

The basic objective of this task was to evaluate the feasibility of an RSI tile attachment system that uses the strain arrestor plate concept in conjunction with a flexible strain isolator/primary structure bond. The strain arrestor plate (SAP) is a high-modulus, high-strength, low thermal expansion plate placed between the RSI tile and the strain isolation bond system. Its main function is to act as a barrier between the tile and the foam bond/primary structure. In a direct bonded (non-SAP) system, primary structure strains are partially transmitted to the RSI tile through the flexible bond. At moderately low temperatures (above the glass transition range) some bond systems still work well because of their ability to maintain flexibility (strain isolation capability). However, at very low temperatures such as 116°K (-250°F), below the glass transition range, the stiffness of the available bond systems increases substantially, thereby reducing or eliminating the isolation characteristics of the attachment system. The SAP is designed to absorb the loading transferred by the bond system. Because of its high extensional stiffness, the resulting SAP strains are very low, thereby preventing high stresses in the RSI tile above. The concept is illustrated schematically for a hot primary structure/tensile load condition in Fig. 2.0-1.

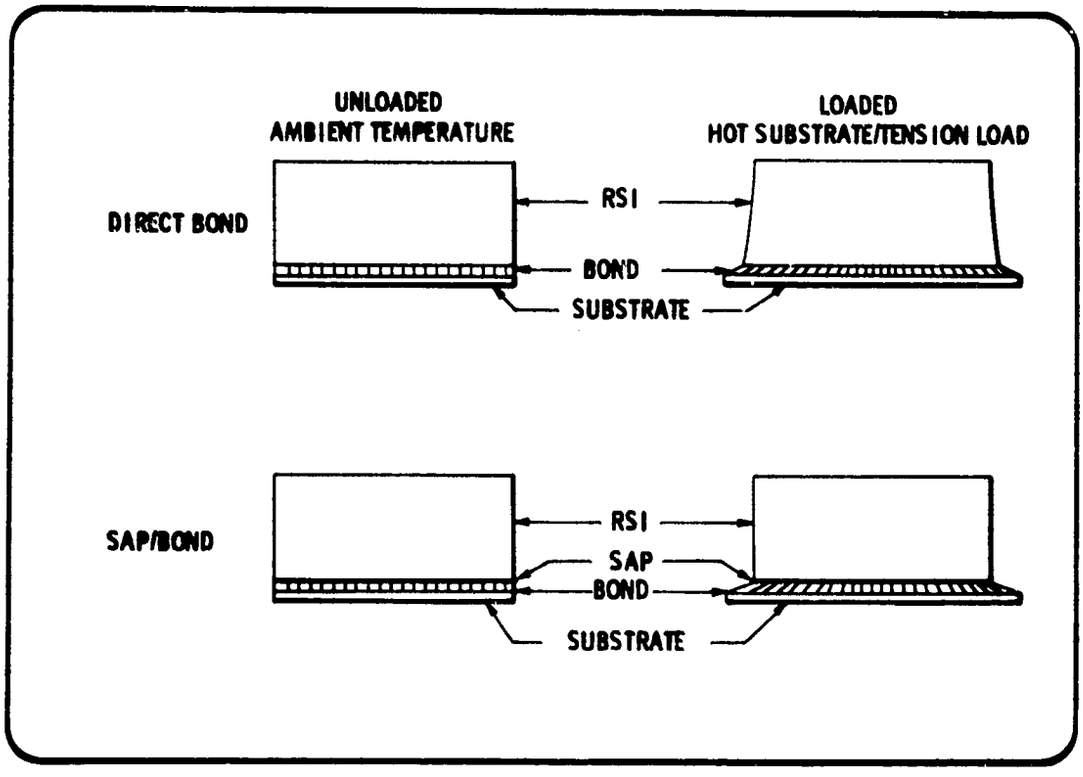

Fig. 2.0-1 Strain Arrestor Plate (SAP) Mechanics

General scope of the SAP study included:

- Selection of the optimum strain arrestor material
- Selection of compatible epoxy and strain isolator bonds
- Study of the range of allowable tile sizes for the orbiter vehicle (includes top, bottom and side locations)
- Detailed analysis of LI-900 TPS configurations at three orbiter locations (top, bottom, and sides)
- Impact of strain arrestor systems on TPS unit weight
- Design and analysis of the prototype test panel
- Design curves

Additionally, the study was limited to the following conditions:

- Use of LI-900 material
- Use of the Area 2P substrate design of Phase II for all locations
- Two-dimensional linear structural analysis and one-dimensional thermal analysis
- Consideration of only the SAP concept

The model used for initial screening investigations considered the Area 2P panel delivered under the Phase II contract. The substrate is a skin stringer aluminum panel constrained to 422°K (300°F) maximum temperature. In modeling, one-half of the panel is analyzed with an area of symmetry at the centerline.

Two models are used in the analysis – stiff direction and weak direction. The stiff direction model is pinned at the frame support end. Symmetry is simulated at the centerline by lateral and rotational restraints. The resistance of the stringers to bending results in a very stiff substrate. The weak direction model considers the stresses across the panel. In this model the stiffeners are modeled as springs. The two models are illustrated in Fig. 2.0-2.

It should be noted that under terms of Contract NAS 9-12856, structural analyses were restricted to two-dimensional linearly-elastic techniques, as embodied in the LMSC version of the Wilson finite element computer code.

The major results and conclusions from the design and analysis task are:

- Use of the strain arrestor plate (of proper design) reduces tile and coating stresses under all load and temperature conditions.
- Use of the strain arrestor plate does not increase bottom surface TPS weight. However, weight does increase at side and top surface locations.
- Use of the strain arrestor plate permits a greater variation in tile size than would otherwise be possible.

- The stress analyses upon which this study was based are conservative (higher than actual stresses), since nonlinear and creep/relaxation effects were not included.
- Adequate positive margins of safety have been attained for the prototype test panel.
- Future investigations should include nonlinear material behavior, including bond relaxation.
- RM/RL-1973 sponge, together with 0.127×10^{-3}m (0.005 in.) layers of RTV-560 constitutes a satisfactory strain isolator system at all design temperatures.
- Fibrite x-904 resin for the strain arrestor plate matrix is adequate for the SAP requirements.
- LI-900 insulation material is proven feasible for the design conditions.

Detailed discussion of the following five design and analysis subtasks are presented in this section:

- Design criteria update
- Selection of strain arrestor material
- Parametric studies
- Detail design studies
- Prototype panel design

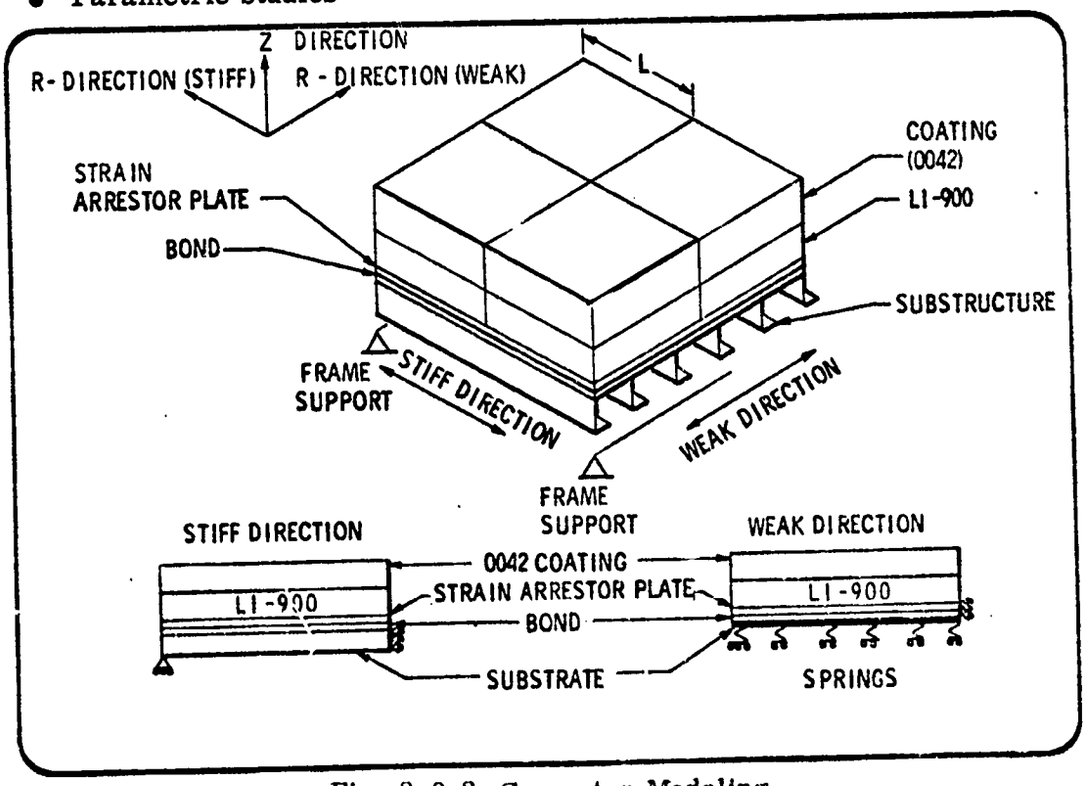

Fig. 2.0-2 Computer Modeling

2.1 DESIGN CRITERIA

The analytical work performed under the design and analysis task was based upon the design conditions and criteria specified in Phase II design activities (Ref. 2.1-1) for Area 2P. Under the current contract, the task has been expanded to assess the effects of thinner insulation with reduced surface temperatures on the orbiter side and top locations.

The insulation material used for the task was LI-900. One and two dimensional linear analyses were used for thermal and stress computations respectively. The THERM code and the LMSC version of the WILSON code were used for these analyses as described in Ref. 2.1-2. All configurations included the use of the strain arrestor plate, the concept of which was described in the introduction to this section (Section 2). The environmental conditions included entry from a 116°K (-250°F) "soak" condition in addition to Phase II design conditions as described in Ref. 2.1-1.

2.1.1 Loads and Temperatures

Three locations on the orbiter vehicle were examined – bottom, side, and top. The primary structure (substrate) for these locations was assumed to be the same, namely the substrate used for the Area 2P location on the Phase II orbiter.

Shown in Fig. 2.1-1 are the surface temperatures and the pressures for the Area 2P location representative of the bottom surface of the Shuttle orbiter. This information was supplied by NASA/MSC for both the Phase II effort (Ref. 2.1-1) and the current contract.

For the side and top, with NASA's concurrence, LMSC obtained temperature and pressure histories from the Phase C/D Shuttle proposal (Ref. 2.1-3). These are shown in Fig. 2.1-2. Because reentry for the LMSC 2020 km(1100 nm) crossrange trajectory occurs in a shorter time than for NASA's Area 2P technology contract trajectory, the touchdown time for the side and top studies was 2400 sec., rather than 3600 sec. The loading conditions for the side and top were the Area 2P conditions scaled from a 3600-sec. to a 2400-sec. touchdown time.

Substrate differential pressure applicable to all three locations is given in Fig. 2.1-3. The substrate temperature histories for all three locations are given in Figs. 2.1-4 through 2.1-6. These temperatures pertain to the substrate bond line and are given for two initial temperature conditions at the start of reentry. The substrate load histories are superimposed on each figure.

2.1.2 Material Properties – Insulation (Including Coating)

In this contract, the mechanical properties used for LI-900 in the screening studies and the parametric studies represented by the design curves presented in Subsection 2.3 were those established in the Improvement of Reusable Surface Insulation Material contract (NAS 9-12137). These values, along with coating properties, are shown in Table 2.1-1. For study purposes, average values were used.

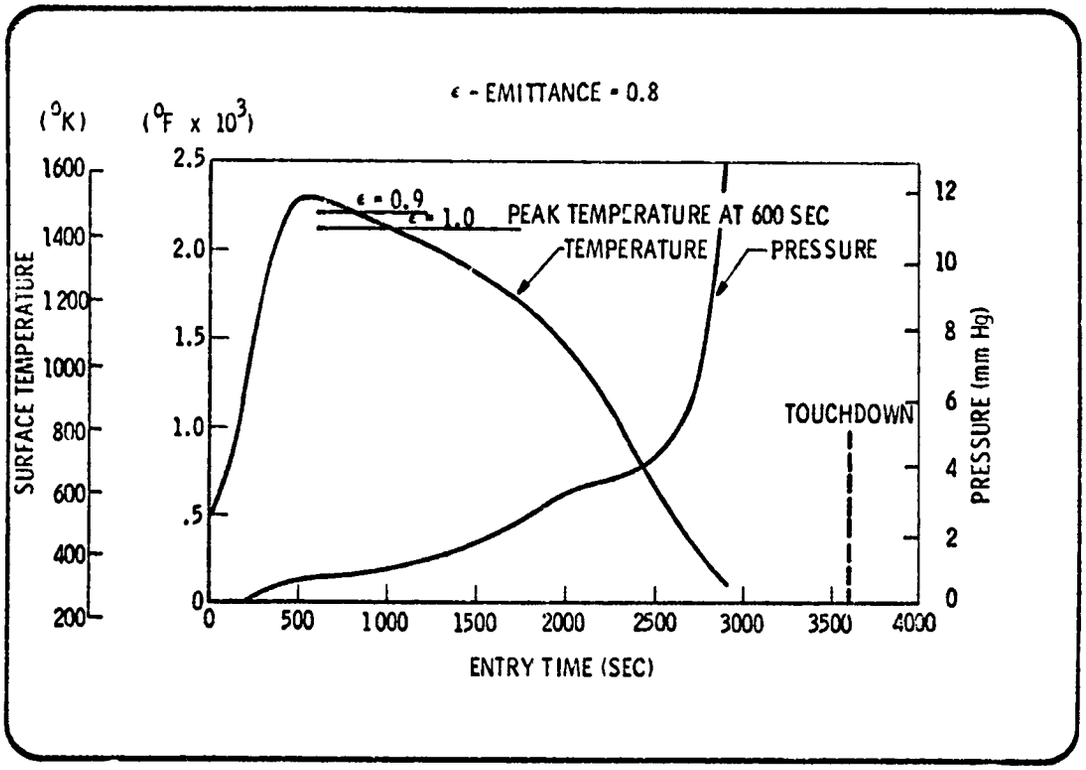

Fig. 2.1-1 Bottom Reentry Heating

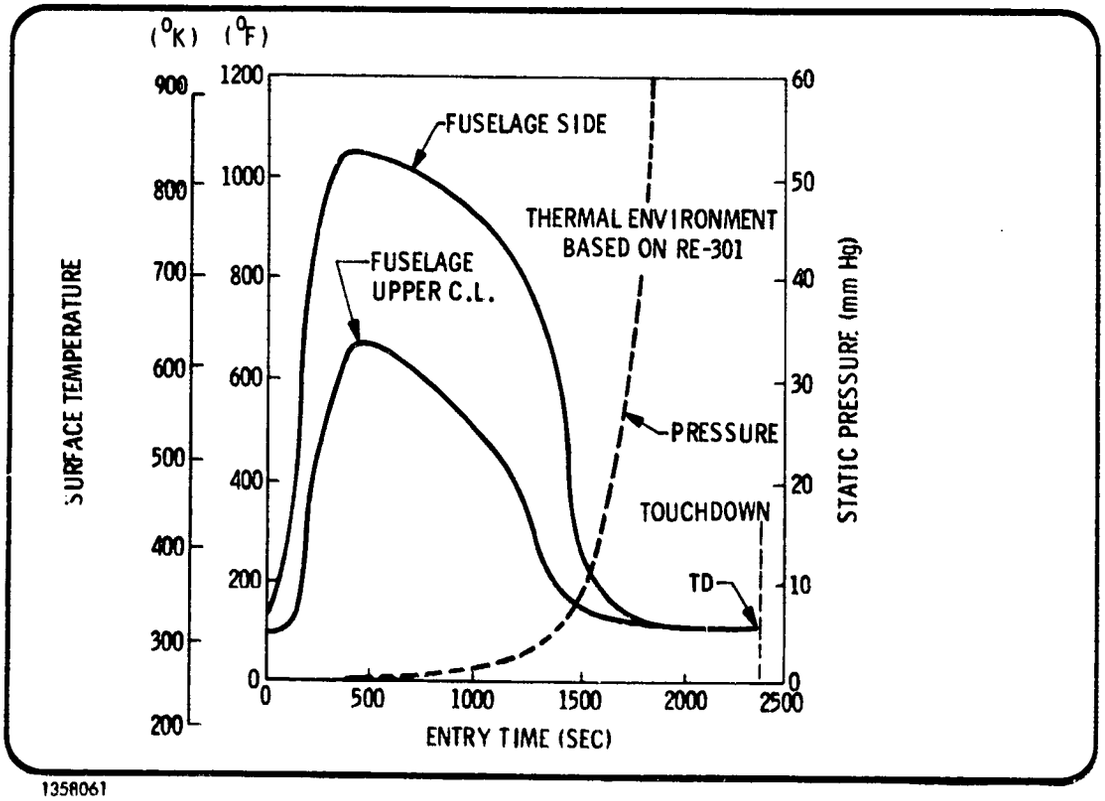

Fig. 2.1-2 Top and Side Reentry Heating

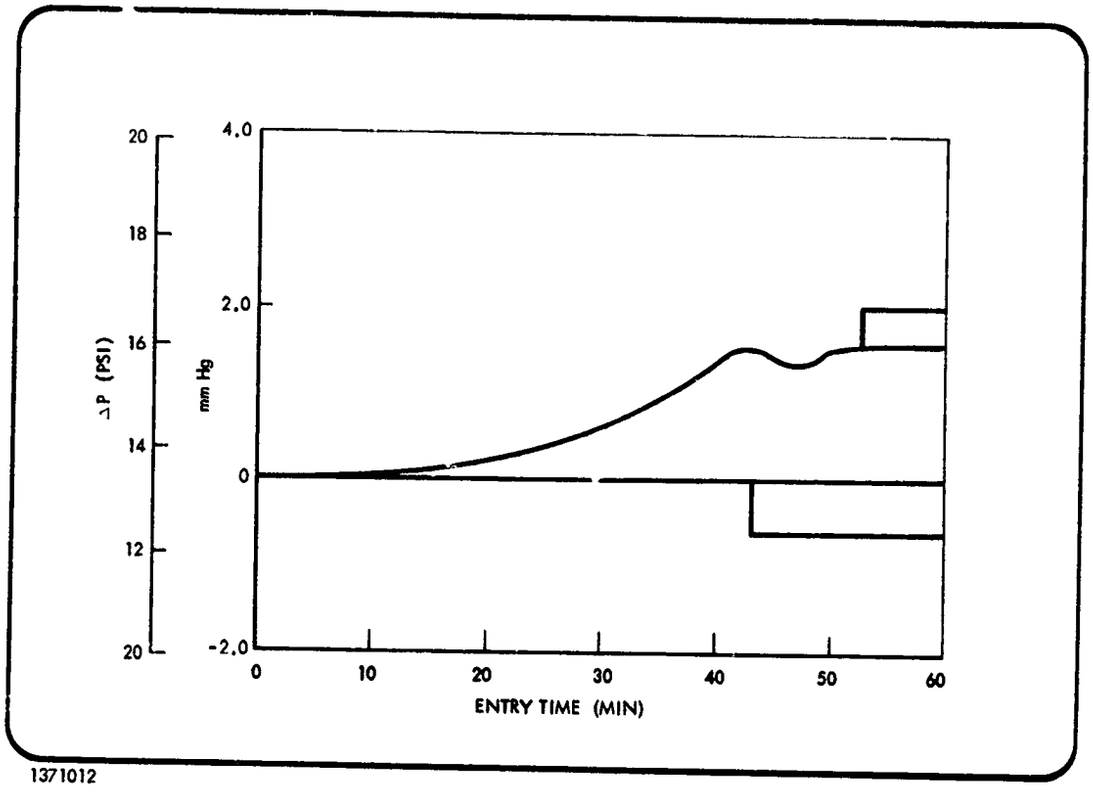

Fig. 2.1-3 Limit Differential Substrate Pressures for Entry

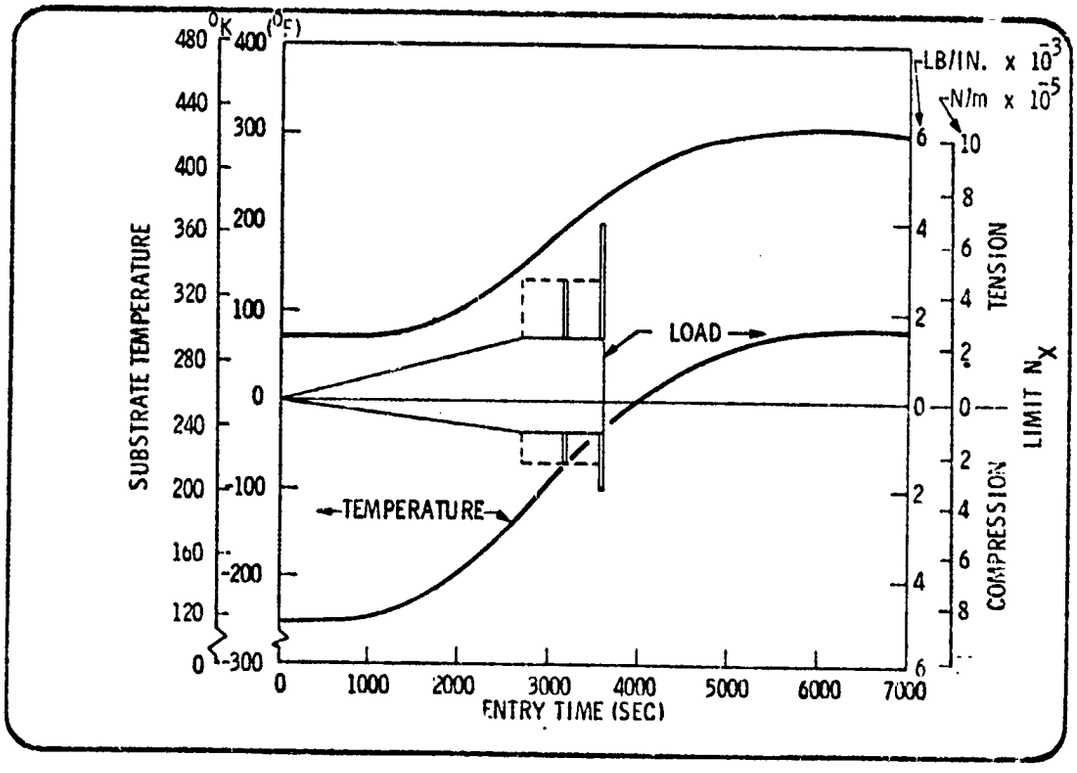

Fig. 2.1-4 Bottom Surface (Area 2P) Bond Line Temperature/Load History

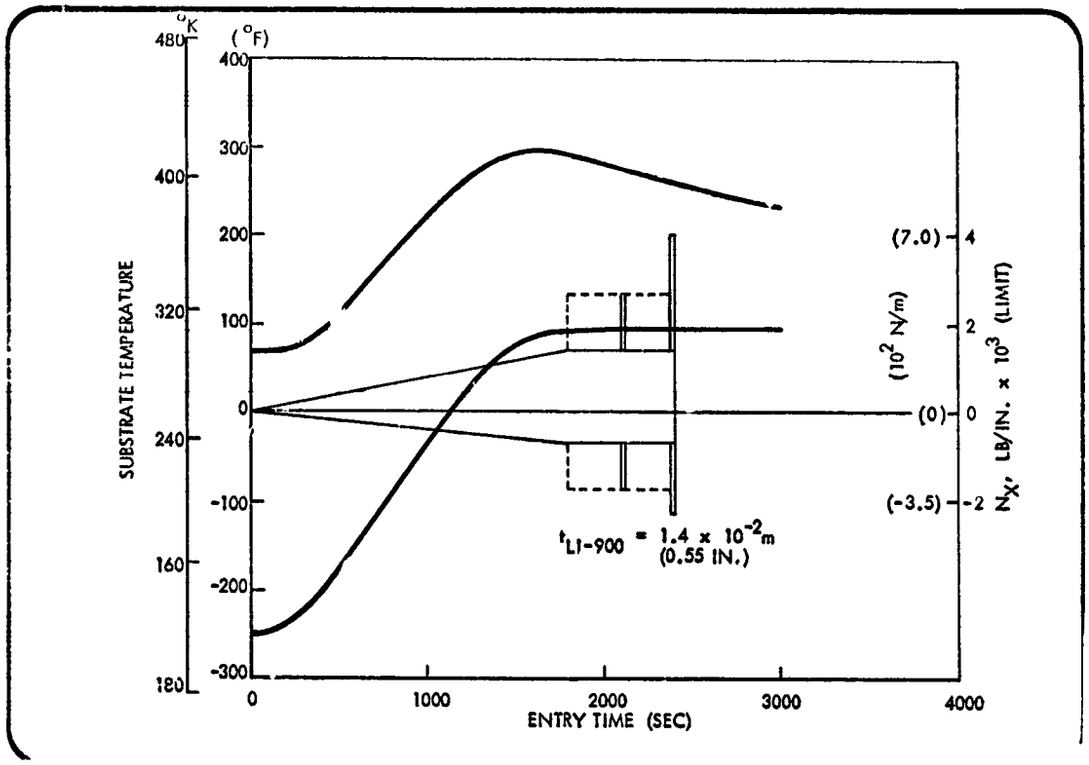

Fig. 2.1-5 Side Surface Temperature History at Bond Line

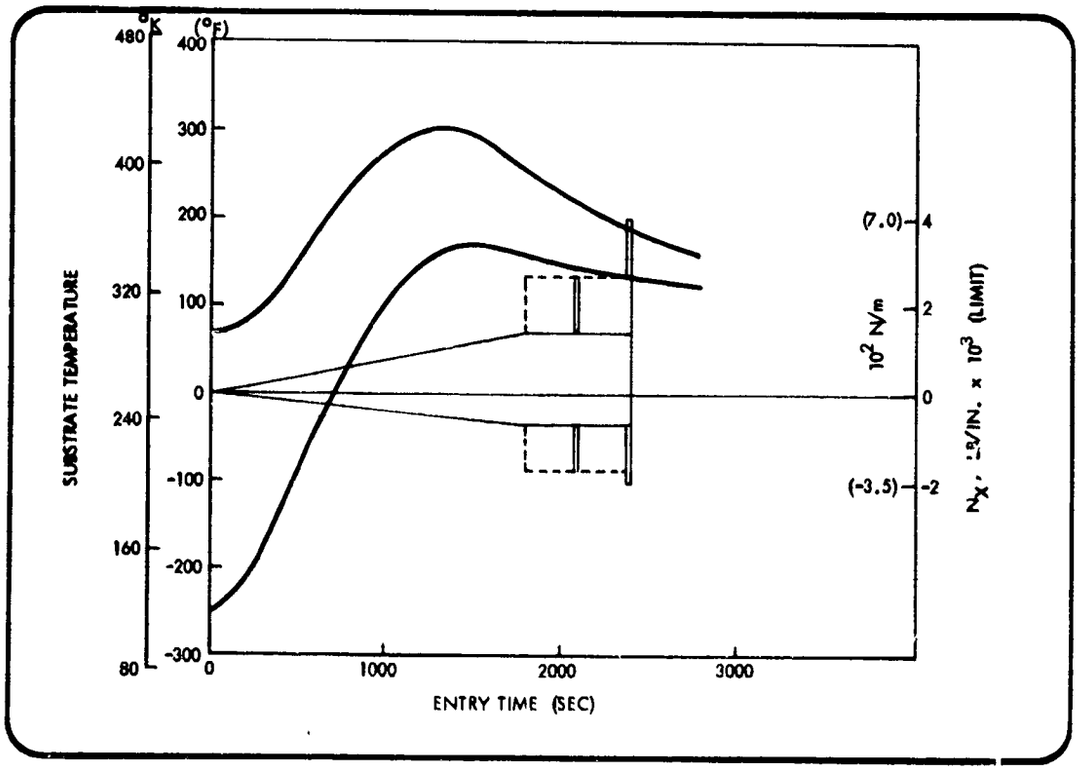

Fig. 2.1-6 Top Surface Temperature Histories at Bond Line

The detail design studies (Subsection 2.4) and the prototype test panel design (Subsection 2.5) were based on material properties for LI-900 established in Task B (Section 3) of the present contract. A summary of these properties is presented in Tables 2.1-2 and 2.1-3. The calculations were based on the average properties (elastic constants). However, the material allowables were based on combined loading and failure criteria discussed in detail in Appendix A-1.

2.1.3 Strain Arrestor Plate (SAP) Criteria

Selection of the strain arrestor plate material is based on the following criteria.

- High extensional stiffness
- High strength
- Low coefficient of thermal expansion
- Low weight
- Low cost

A detailed discussion of SAP material selection is given in Subsection 2.2.

2.1.4 Bond Criteria

Criteria for the selection of bond systems are as follows.

- Ability to function between 117°K and 450°K (-250°F and 350°F).
- Relative flexibility at the lowest design temperature, 117°K (-250°F) so that effective strain isolation will be achieved between the substrate and the SAP
- Low weight
- Low cost

2.1.5 Additional Assumptions

The calculations performed under the Design and Analysis Task were based on the load and temperature histories shown in Figs. 2.1-4 through 2.1-6. Note that the load envelopes in these figures represent limit conditions. Ultimate loads for which the structures are sized with positive margins were taken as 1.5 times the limit loads.

All screening analyses were based on butt joints and quasi-isotropic strain arrestor plates. Also the coating was considered to cover only the top surface of the tile.

Table 2.1-1

LI-900 AND 0042 COATING PROPERTIES USED FOR SCREENING STUDIES AND DESIGN CURVES

PROPERTY	LI-900 STRESS (PSI)	LI-900 MODULUS (PSI)	0042 COATING W/A = 0.12 PSF t = 0.010 IN. STRESS (PSI)	0042 COATING W/A = 0.12 PSF t = 0.010 IN. MODULUS (PSI)
TENSION (STRONG DIRECTION) (WEAK DIRECTION)	44.6 11.7	15,900 2,450	2,000	9.1×10^6
COMPRESSION (STRONG DIRECTION) (WEAK DIRECTION)	49.9	15,900	72,000	9.1×10^6
SHEAR (STRONG DIRECTION) (WEAK DIRECTION)	43.0 23.3	7,180 3,317	—	3.89×10^6
COEFFICIENT OF THERMAL EXPANSION (α)	0.3×10^{-6}		0.4×10^{-6}	
POISSON'S RATIO	0.3		0.171	

Table 2.1-2

LI-900 PROPERTIES USED FOR DETAIL DESIGN AND PROTOTYPE TEST PANEL (PSI)

MECHANICAL PROPERTY		-250°F	R.T.	400°F	800°F	1200°F	1600°F
TRANSVERSE TENSION STRESS ULTIMATE	MAX	36.0	25.0	27.3	29.4	25.6	41.5
	AVG	28.0	16.0	23.5	22.2	22.8	24.7
	MIN	19.7	9.0	19.5	17.2	16.6	19.2
TRANSVERSE TENSION MODULUS	MAX	9,575	7,925	8,380	8,900	10,500	9,560
	AVG	5,795	5,775	6,765	7,885	8,329	8,146
	MIN	2,960	3,290	4,500	7,280	7,560	7,050
IN-PLANE TENSION STRESS ULTIMATE	MAX	88.0	68.0	77.4	86.3	88.6	100.0
	AVG	66.9	50.7	69.5	74.8	58.6	66.6
	MIN	48.5	47.0	62.3	61.9	47.8	47.8
IN-PLANE TENSION MODULUS	MAX	30,300	33,600	36,450	45,900	55,500	44,000
	AVG	19,705	23,545	32,488	36,763	39,030	36,118
	MIN	13,550	19,800	29,300	26,700	32,900	24,800
TRANSVERSE SHEAR STRESS ULTIMATE	MAX	42.7	35.8	35.8	35.8	35.8	35.8
	AVG	39.4	31.5	31.5	31.5	31.5	31.5
	MIN	35.0	27.1	27.1	27.1	27.1	27.1
TRANSVERSE SHEAR MODULUS	MAX	—	—	—	—	—	—
	AVG	3,000	3,600	3,700	3,800	3,900	4,000
	MIN	—	—	—	—	—	—

POISSON'S RATIO, μ_{RZ} = 0.16 FOR ALL TEMPERATURES

THERMAL EXPANSION COEFFICIENT $\alpha = 0.40 \times 10^{-6}$ IN./IN.-°F (R.T. TO 1600°F)
$= 0.10 \times 10^{-6}$ IN./IN.-°F (-250°F TO R.T.)

Table 2.1-3

COATING (0042) PROPERTIES USED FOR DETAIL DESIGN AND PROTOTYPE TEST PANEL

MECHANICAL PROPERTY			-250°F	R.T.	400°F	800°F	1200°F	1600°F	2300°F
TENSION STRESS ULTIMATE	PSI	AVG MIN	2,000 1,180	2,100 1,140	2,079 1,187	2,054 1,245	2,029 1,302	2,000 1,360	2,000 1,360
TENSION MODULUS	PSI	AVG	10×10^6	6.0×10^6	6.2×10^6	6.5×10^6	6.7×10^6	7.0×10^6	7.0×10^6
SHEAR MODULUS	PSI		4.3×10^6	2.6×10^6	2.7×10^6	2.8×10^6	2.9×10^6	3.0×10^6	3.0×10^6

POISSON'S RATIO $\mu = 0.17$

THERMAL EXPANSION COEFFICIENT $\alpha = 0.54 \times 10^{-6}$ IN./IN.-°F (R.T. TO 1600°F)
$= 0.40 \times 10^{-6}$ IN./IN.-°F (-250°F TO R.T.)

2.1.6 REFERENCES

2.1-1 Lockheed Missiles & Space Company, "Final Report, Space Shuttle Thermal Protection System Development," Vol I, Contract NAS 9-12083, LMSC-D152738, 17 January 1972.

2.1-2 Lockheed Missiles & Space Company, "Final Report, Space Shuttle Thermal Protection System Development," Vol II – Design Methodology, Contract NAS9-12083, LMSC-D152738, 17 January 1972.

2.1-3 Lockheed Missiles & Space Company, Technical Proposal, Phase C/D Space Shuttle, Vol III, LMSC-D157364, 5 May 1972.

2.2 SELECTION OF STRAIN ARRESTOR MATERIAL

The first step in the SAP screening was the investigation of the strain arrestor material. The various steps in the screening process are illustrated in Fig. 2.2-1. As can be seen from the figure, the selection of a strain arrestor material is based on the following requirements:

- High extensional stiffness
- High strength
- Low coefficient of thermal expansion

Additional requirements include low weight and low cost.

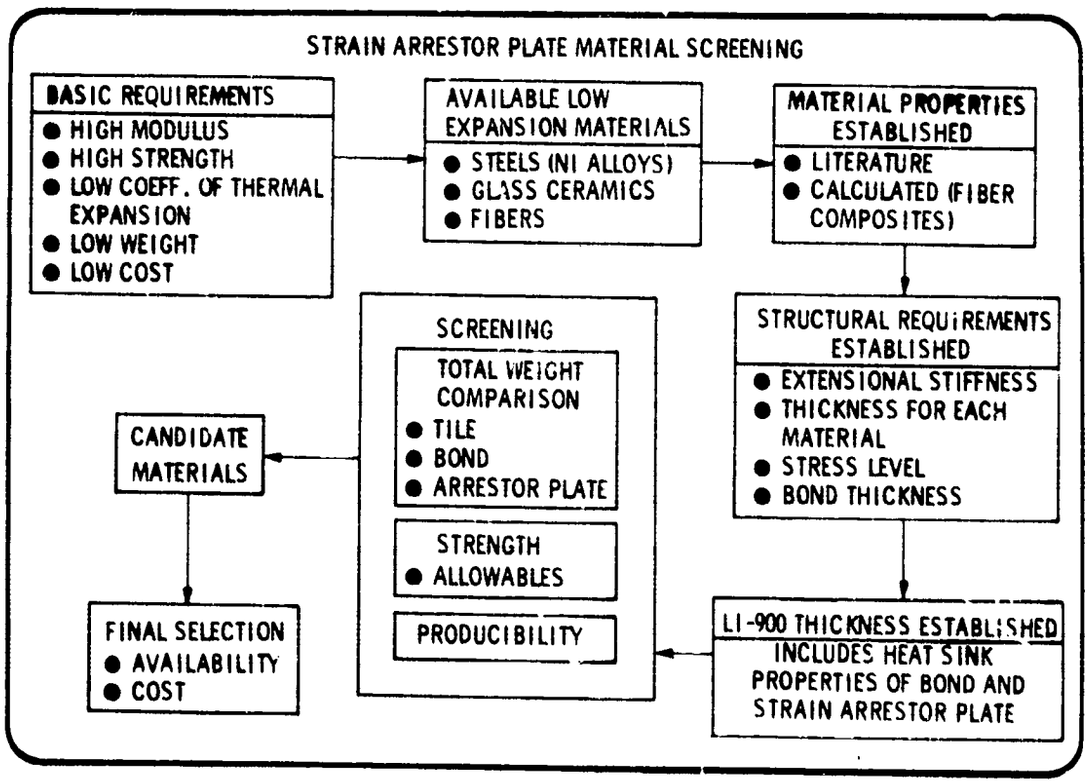

Fig. 2.2-1 Logic Sequence

Low expansion materials are relatively scarce. Among the metals, only INVAR steel seems to be a potential candidate. Glass ceramics such as CER-VIT C-101 and HERCUVIT-101 (Owens Illinois) also exhibit low thermal expansion and relatively high modulus properties. Dow Corning's fused silica ULE has similar characteristics.

The available information on fiber reinforced composite technology indicates that composite laminates can be made to meet the stringent requirements of the strain arrestor plates by using low expansion fibers. In particular, graphite fibers seem to be best suited for the present purpose. These fibers possess the following characteristics:

- High strength and stiffness
- Low density
- Negligible thermal coefficient of expansion
- Thermal and chemical stability
- Low coefficient of friction

Another fiber that has a potential use as a strain arrestor plate is the PRD-49 fiber manufactured by DuPont Co. It is relatively cheaper than graphite and exhibits excellent handling qualities. However, PRD-49 fibers have a relatively low modulus of elasticity.

In Table 2.2-1 the typical properties of various continuous fibers are shown. These fibers have been selected for the study on the basis of their high modulus and/or high strength.

The values given in Table 2.2-2 represent the unidirectional composite properties of the fibers given in Table 2.2-1. A single ply layup in the form of woven PRD-49 cloth is also included for comparison purposes. It is evident that both the Thornel 75-S and the GY-70 graphite composites seem to meet the strain arrestor plate requirements of stiffness and strength. However, these values are unidirectional and, therefore, are not necessarily representative of the final construction.

Table 2.2-3 reflects the final properties of the candidate strain arrestor plate materials. All composites are constructed to yield isotropic thermal and mechanical properties in the plane of the plate. This is accomplished by a 0 - 60 - 120 deg ply orientation of the uniaxial plies and 0 - 45 deg orientation of the PRD-49 woven cloth.

The predictions for the isotropic composites are obtained by the use of the LMSC originated "LAMINATE" compute code. The analysis techniques for the program have been reported in Ref. 2.2-7. This program is capable of predicting composite properties starting from basic fiber and matrix properties. For the present use, however, the program input has been taken from Table 2.2-2, which represents experimental results for the unidirectional composites.

Table 2.2-1

TYPICAL PROPERTIES OF LOW EXPANSION FIBERS (ROOM TEMPERATURE)

	GRAPHITE							OTHER
	THORNEL		MORGANITE		COURTAULDS		CELANESE	PRD-49
PROPERTIES	50-S	75-S	TYPE I	TYPE II	HMS	HTS	GY-70	111
YOUNG'S MODULUS $\times 10^{-6}$ (PSI)	50	75	60	40	50	32	75	19
STRENGTH $\times 10^{-3}$ (PSI)	280	320	250	350	250	300	300	270
DENSITY (LB/IN.^{3}) (LB/FT^3)	0.059 102	0.067 116	0.072 124	0.063 109	0.069 119	0.063 109	0.070 121	0.052 91
MANUFACTURER	UNION	UNION	MORGAN *	MORGAN *	COURTAULDS *	COURTAULDS *	CELANESE	E.I. DUPONT
REFERENCE	2.2-1	2.2-1	2.2-2	2.2-2	2.2-2	2.2-2	2.2-2	2.2-3

* BRITISH MADE FIBERS

Table 2.2-2

TYPICAL PROPERTIES OF UNIDIRECTIONAL COMPOSITES (ROOM TEMPERATURE)

PROPERTIES	GRAPHITE UNIDIRECTIONAL LAYERS							OTHER FIBER COMPOSITES	
	THORNEL		MORGANITE		COURTAULDS		CELANESE	DUPONT	
	50-S	75-S	TYPE I	TYPE II	HMS	HTS	GY-70	PRD-49	PRD-49 CLOTH
EPOXY RESIN	ERLB 4617		ERLA 4617	X-904	X-904	X-904	X-904	X-904	X-904
$E_{fL} \times 10^{-6}$ (PSI)	33	44	25.5	20.5	28	20	47.8	12	4.4
$E_{fL} \times 10^{-6}$ (PSI)	1.0	0.9	1.2	1.1	0.8	1.1	0.9	0.9	4.0
$E_{cL} \times 10^{-6}$ (PSI)	33	44	-	-	27	20	46.0	12	4.6
$F_{fL} \times 10^{-3}$ (PSI)	148	214	126	173	74	187	91.0	210	65
$F_{fT} \times 10^{-3}$ (PSI)	4.5	4.6	4.5	3.0	2.6	2.4	1.75	2.8	59
$F_{cL} \times 10^{-3}$ (PSI)	100	97	-	-	110	113	70.0	33.0	26
$F_{cT} \times 10^{-3}$ (PSI)	29	27	-	-	18	21	14.2	12	23
$F_{HS} \times 10^{-3}$ (PSI)	8	6.0	8.6	-	9.7	13	6.5	5	4
$G_s \times 10^{-6}$ (PSI)	-	0.64	-	-	0.6	0.75	0.6	0.6	0.4
	0.3 (t)	0.3 (t)	-	-	0.45	0.25	0.25	0.4	0.4
$\alpha_L \times 10^{-6}$ (IN./IN.-°F)	-0.35	-0.35 RT	-	-	-0.5	-0.2	-0.5	-2.8	0
$\alpha_T \times 10^{-6}$ (IN./IN.-°F)		20	-	-	20	15.5	20	25	0
s.g.		1.56	-	-	1.70	1.56	1.70	1.5	-
V/O	60%	57%	-	-	62.5%	60%	62%	60%	-
PLY THICKNESS	0.007	0.007	0.003	0.003	0.003	0.003	0.007	0.0035	0.003
REFERENCE	2.2-1	2.2-1	2.2-2	2.2-2	2.2-2	2.2-2	2.2-2	2.2-3	2.2-3

Table 2.2-3

PROPERTIES OF CANDIDATE STRAIN ARRESTOR PLATE MATERIALS

PROPERTIES	INVAR	GLASS CERAMICS		FUSED SILICA ULE	ISOTROPIC GRAPHITE COMPOSITE					PRD-49	
		CER-VIT (C-101)	HERCUVIT (101)		GY-70 X-904	HTX X-904	HMS X-904	THORNEL 50-S ERLB-4617*	THORNEL 75-S ERLB-4617	III X-904	F161 CLOTH X-904
YOUNG'S MODULUS $\times 10^{-6}$ (PSI)	21.0 19.8 (-250°F)	13.4	13.4	9.8	16.732	7.651	10.106	11.862	15.500	4.800	2.995
SHEAR MODULUS $\times 10^{-6}$ (PSI)	8.10 7.49 (-250°F)	5.3	5.3	4.2	6.388	2.953	3.830	4.506	5.872	1.841	0.960
STRENGTH $\times 10^{-3}$ (PSI)	52.5 YIELD ANNEALED	8.0	8.0	7.2	SEE FIG. 2.2-2	SEE FIG. 2.2-3	SEE FIG. 2.2-4	SEE FIG. 2.2-5	SEE FIG. 2.2-6	SEE FIG. 2.2-7	SEE FIG. 2.2-8
COEFFICIENT OF EXPANSION IN./IN.-°F $\times 10^{-7}$	1.5 (200-400°F) 0.7 (RT) 1.1 (-200°F)	1.2 @ 300°F 0 @ RT 0.4 @ -250°F	0 0 0.4 @ 238°F	0 @ 350 0 @ 75 0.4 @ 238°F	-0.308	7.971	3.056	4.146	1.816	-6.907	0
DENSITY LB/IN.^{3} LB/FT^3	0.294 508	0.090 156	0.090 156	0.079 137	0.061 106	0.056 97.3	0.061 106	0.056 97.3	0.056 97.3	0.054 93.5	0.054 93.5
SPECIFIC HEAT (BTU/LB-°F)	0.125	0.21	0.21	0.21	0.28	0.28	0.28	0.28	0.28	0.33	0.30
POISSON'S RATIO	0.29	0.25	0.25	0.17	0.320	0.296	0.319	0.316	0.320	0.304	0.559
MANUFACTURER	INTER'L NICKEL CO.	OWENS ILL	OWENS ILL	DOW CORN				UNION CARBIDE	UNION CARBIDE		
REFERENCE	2.2-4	2.2-5	2.2-5	2.2-6	COMP	COMP	COMP	COMP	COMP	COMP	COMP

*FIBRITE X-904 AND ERLB-4617 RESINS HAVE BEEN CHOSEN FOR THEIR ABILITY TO OPERATE BETWEEN -320 TO +320°F.

The estimated strength envelopes for the composite plates at room temperature are shown in Figs. 2.2-2 through 2.2-8. These predictions assume that the laminate is completely stress free, i.e., there are no self-equilibrating residual stresses in the individual layers due to the cure cycle. The two envelopes shown in the figures correspond to two different failure criteria for the individual layers, one based upon a quadratic function of the six stress components; the other, for comparative purposes only, a condition which is a generalization of the maximum strain condition first proposed by St. Venant. The former is used in the LAMINATE code and is described in Ref. 2.2-8, while the latter was incorporated in a similar code developed by H. Durlofsky of LMSC (Refs. 2.2-9, 2.2-10). The former condition is generally considered to be a better description of failure than the maximum strain condition and these are the results which will be used in the contract. The maximum strain condition has long been known to unrealistically overestimate the biaxial tensile strength because the strain in each direction is decreased by the Poisson effects due to tension in the perpendicular direction.

Strength envelopes similar to Figs. 2.2-2 through 2.2-8 are desirable for other temperatures, i.e., -250°F and 300°F; however, the present codes consider only linear elastic behavior to failure and cannot include time dependent phenomena such as creep or relaxation which are known to occur in the viscoelastic matrix materials used in fiber reinforced composites. In addition, temperature dependent properties are automatically handled by the codes.

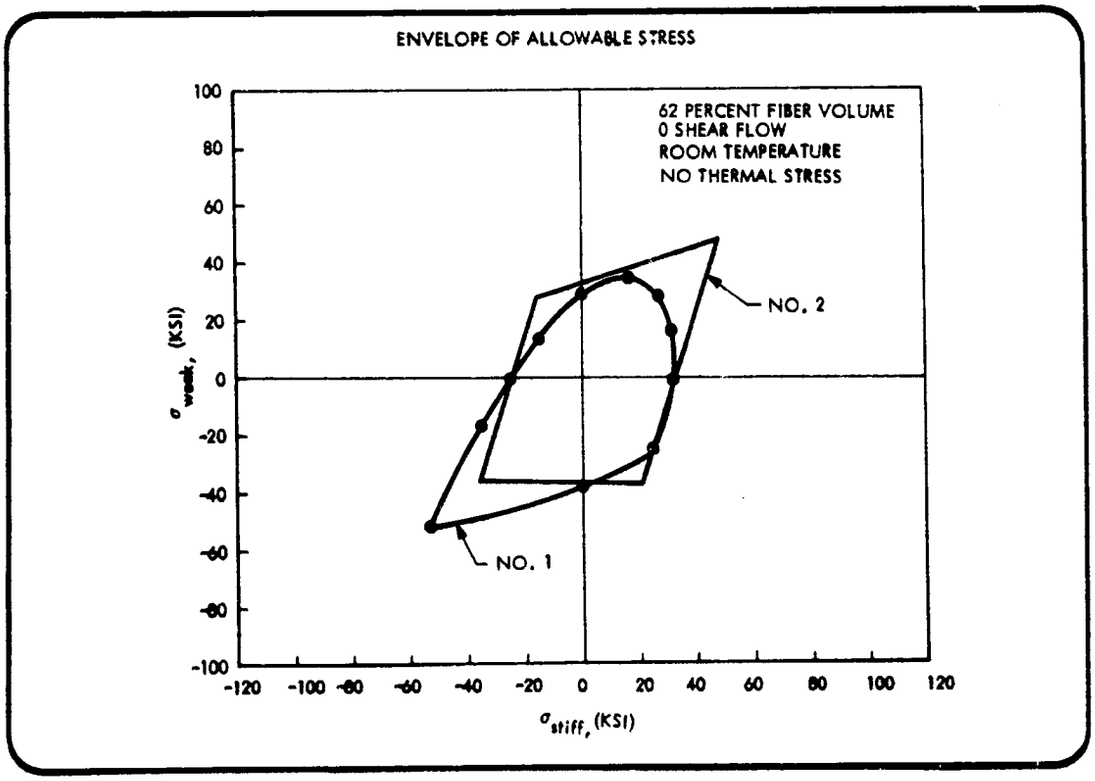

Fig. 2.2-2 GY-70/X-904 Graphite Epoxy

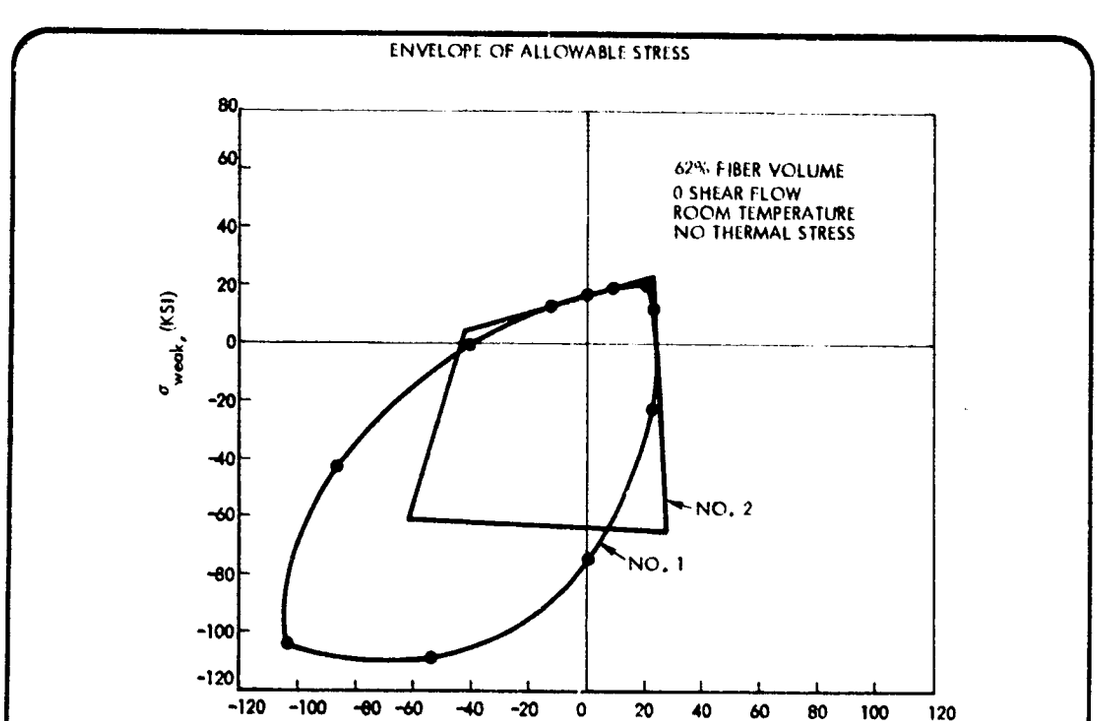

Fig. 2.2-3 HTS/X-904 Graphite Epoxy

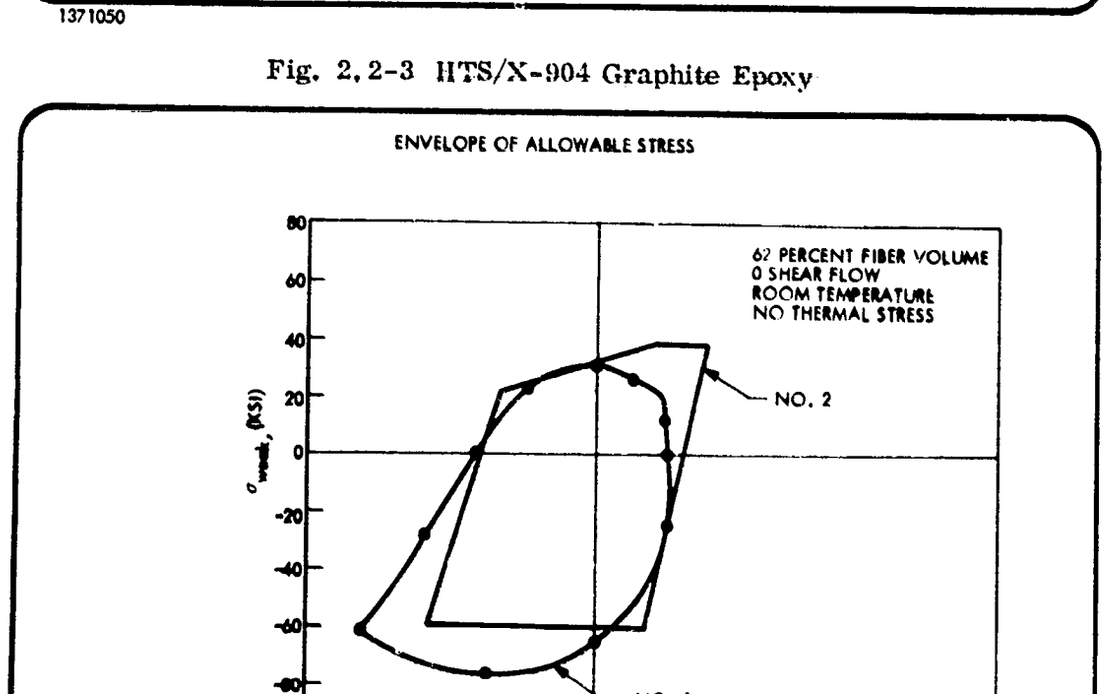

Fig. 2.2-4 HMS/X-904 Graphite Epoxy

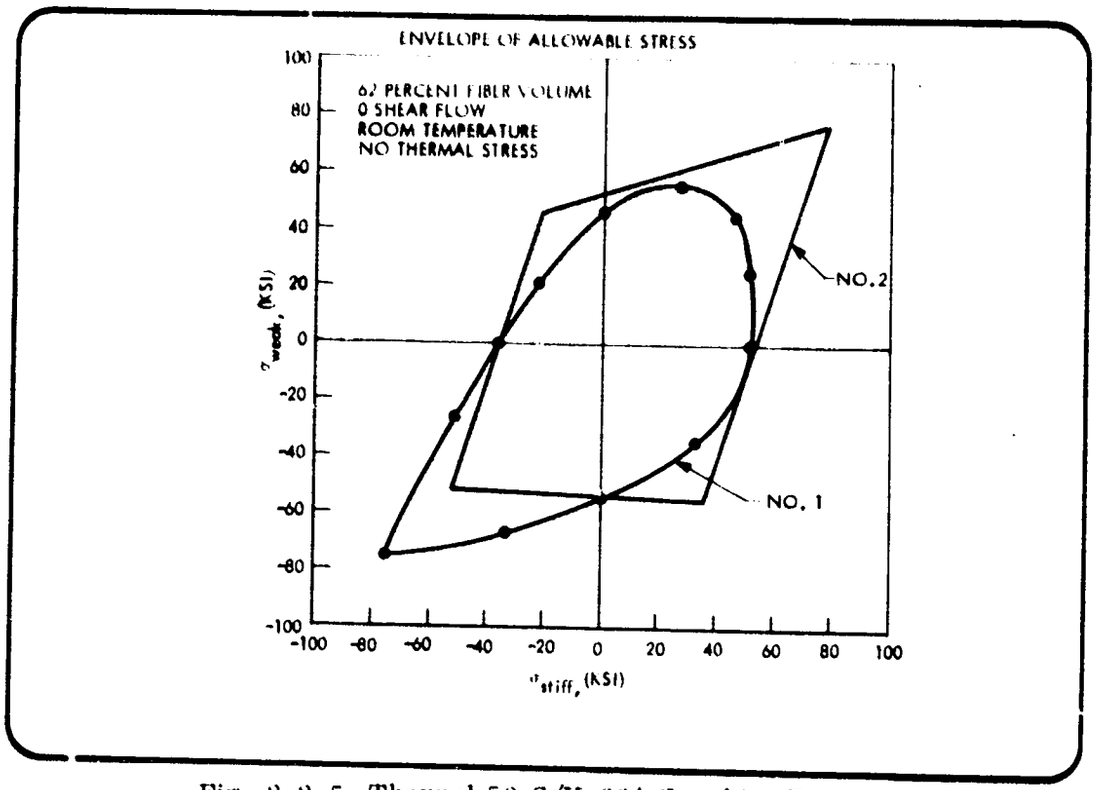

Fig. 2.2-5 Thornel 50-S/X-904 Graphite Epoxy

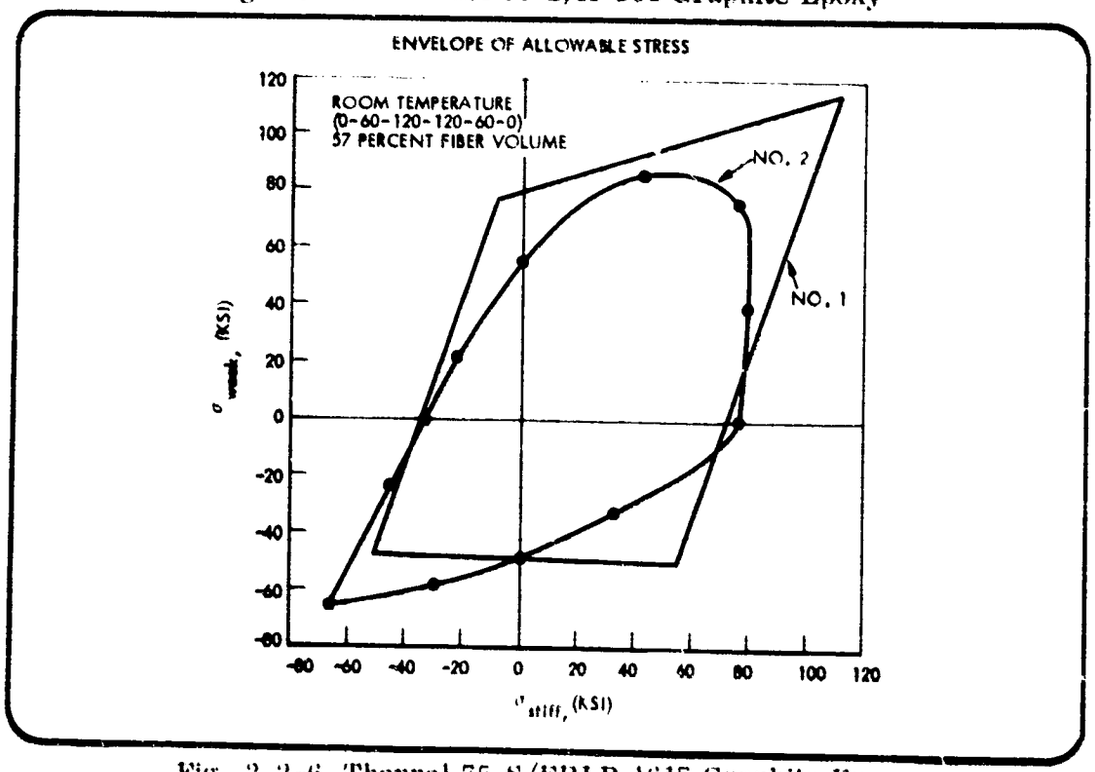

Fig. 2.2-6 Thornel 75-S/ERLB 4617 Graphite Epoxy

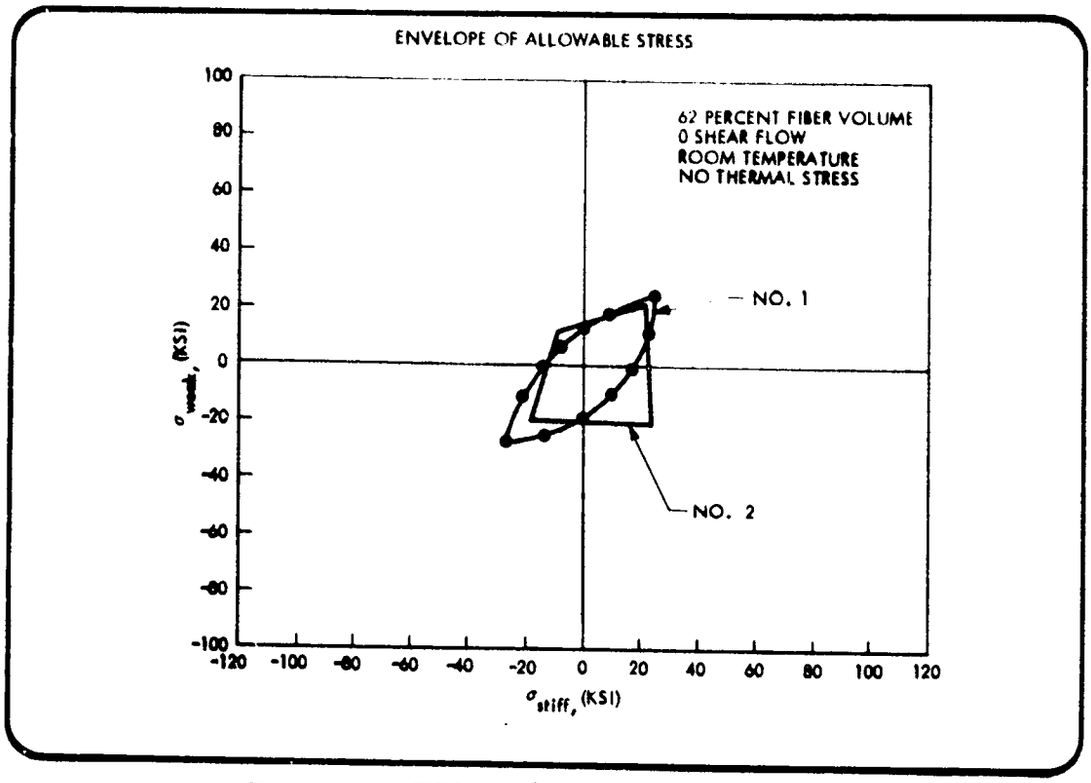

Fig. 2.2-7 PRD-49/X-904 Fiber Epoxy

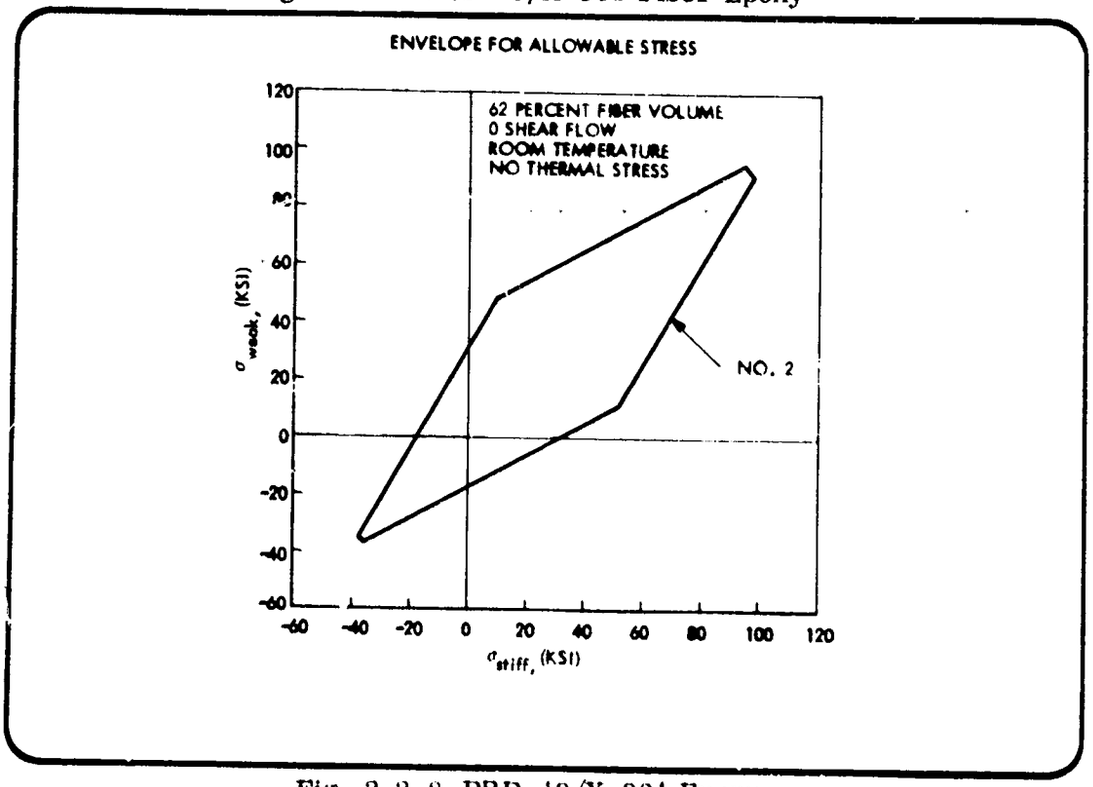

Fig. 2.2-8 PRD-49/X-904 Epoxy

The allowable strength values for materials other than composites are given in Table 2.2-3.

Weight comparisons for various strain arrestor plate materials are given in Table 2.2-4. These results have been obtained for the lower surface of the orbiter at Area 2P location for the 117°K (-250°F) critical cold soak condition.

The required strain arrestor plate thickness for each material is calculated on the basis of a general plate extensional stiffness of AE = 200,000 lb. This value has been found to be adequate for the bottom surface arrestor material screening studies.

Comparison of the strain arrestor weights (Columns 5 and 6) shows a marked advantage of the high modulus of elasticity of graphite epoxies such as GY-70/X-904 and Thornel 70-S/ERLB 4617 systems. The high stiffness of INVAR steel is offset by its high density.

The total weight of the TPS system, however, cannot be judged solely on the basis of the strain arrestor plate. Thickness of the LI-900 will vary with the heat capacity of the various arrestor plates and bond thicknesses.

In Column 8 of Table 2.2-4 these effects are included. The tile thickness calculations are based on the following heat capacity formula:

$$\text{Heat Capacity} = A_{\text{Bond}} + A_{\text{Strain Arrestor Plate}} + A_{\text{Foam}}$$

where

$A = 1/12\ \rho\, C_p\, t \quad (\text{Btu/ft}^2\text{-}^\circ\text{F})$

ρ = density (lb/ft^3)

C_p = specific heat $(\text{Btu/lb-}^\circ\text{F})$

t = thickness (in.)

$(t_{\text{RTV-Bond}})\ \text{Total} = 0.015$ in.

$t_{\text{Foam}} = 0.080$ in.

The LI-900 thicknesses are obtained from Fig. 2.2-9 using a bondline temperature of 300°F.

The total weight calculations (Columns 8 and 9) indicate that with the exception of INVAR and the PRD-49/X-904 cloth system, all candidate strain arrestor plate materials yield the same total weight.

Similar calculations using 0.020 in. foam (0.30 in. total foam bond thickness) show the same trend (see Column 12, Table 2.2-4).

Table 2.2-4

WEIGHT COMPARISON FOR STRAIN ARRESTOR PLATE MATERIALS

EXTENSIONAL STIFFNESS OF ST ARR PL AE = 200,000 LB
AREA 2P - CRITICAL CONDITION = -250°F LOWER SURFACE

AE = 200,000

(1) MATERIAL	(2) ELASTIC MODULUS (LB/IN.^{2})	(3) DENSITY (LB/IN.^{3}) (LB FT^3)	(4) REQUIRED THICKNESS (IN.)	(5) PLATE WEIGHT PER FT^2 (LB)	(6) PLATE* WEIGHT RATIO	(7) LI-900 THICKNESS 300°F BONDLINE (IN.)	(8) COMBINED LI-900, FOAM BOND AND PLATE WEIGHT/FT^2 (LB)	(9) COMBINED WEIGHT RATIO t_{BOND} = 0.09	(10) LI-900 THICKNESS FOR 0.05 FOAM-BOND (IN.)	(11) COMBINED LI-900 AND PLATE WEIGHT PER FT^2 (LB)	(12) COMBINED WEIGHT RATIO t_{BOND} = 0.05
INVAR	21 x 10^6	0.294 509	0.010	0.403	3.83	2.96	2.77	1.10	308	2.73	1.10
GLASS CERAMIC CER-VIT C-101	13.4 x 10^6	0.090 156	0.015	0.195	1.86	2.98	2.56	1.02	3.12	2.54	1.03
GLASS CERAMIC HERCUVIT 101	13.4 x 10^6	0.090 156	0.015	0.195	1.86	2.98	2.56	1.02	3.12	2.54	1.03
FUSED SILICA	9.8 x 10^6	0.079 137	0.020	0.228	2.17	2.87	2.51	1.00	3.09	2.55	1.03
GRAPHITE EPOXY GY-70 X-904	16.7 x 10^6	0.061 106	0.012	0.106	1.01	3.06	2.54	1.01	3.15	2.50	1.01
GRAPHITE EPOXY HTS X-904	7.7 x 10^6	0.036 97.3	0.026	0.211	2.01	2.92	2.53	1.01	3.06	2.51	1.02
GRAPHITE EPOXY HMS X-904	10.1 x 10^6	0.061 106	0.020	0.177	1.69	2.96	2.53	1.01	3.09	2.50	1.01
GRAPHITE EPOXY THORNEL 300 ERLB 4617	11.9 x 10^6	0.056 97.3	0.017	0.138	1.31	3.00	2.52	1.00	3.10	2.47	1.00
GRAPHITE EPOXY THORNEL 75-S ERLB 4617	15.5 x 10^6	0.056 97.3	0.013	0.105	1.00	3.02	2.50	1.00	3.14	2.47	1.00
PRD-49 III X-904	9.8 x 10^6	0.054 93.5	0.042	0.327	1.31	2.74	2.51	1.00	2.42	2.52	1.02
PRD-49 CLOTH X-904	9.8 x 10^6	0.054	0.067	0.522	4.97	2.74	2.71	1.08	2.92	2.71	1.10

* $\frac{\text{PLATE WEIGHT/FT}^2}{\text{WEIGHT OF 75-S FT}^2}$

NOTE: COMBINED WEIGHT IS BASED ON 0.080 PD FOAM + 0.015 TOTAL RTV THICKNESS — LI-900 THICKNESS FOR 300°F BONDLINE.

AE = 200,000 LB
$t_{PD\ FOAM}$ = 0.080 IN.
t_{RTV} = 0.015 IN.
$t_{FOAM\text{-}BOND}$ = 0.096 IN.

AE = 200,000 LB
$t_{PD\ FOAM}$ = 0.020 IN.
t_{RTV} = 0.015 IN.
$t_{FOAM\ BOND}$ = 0.030 IN.

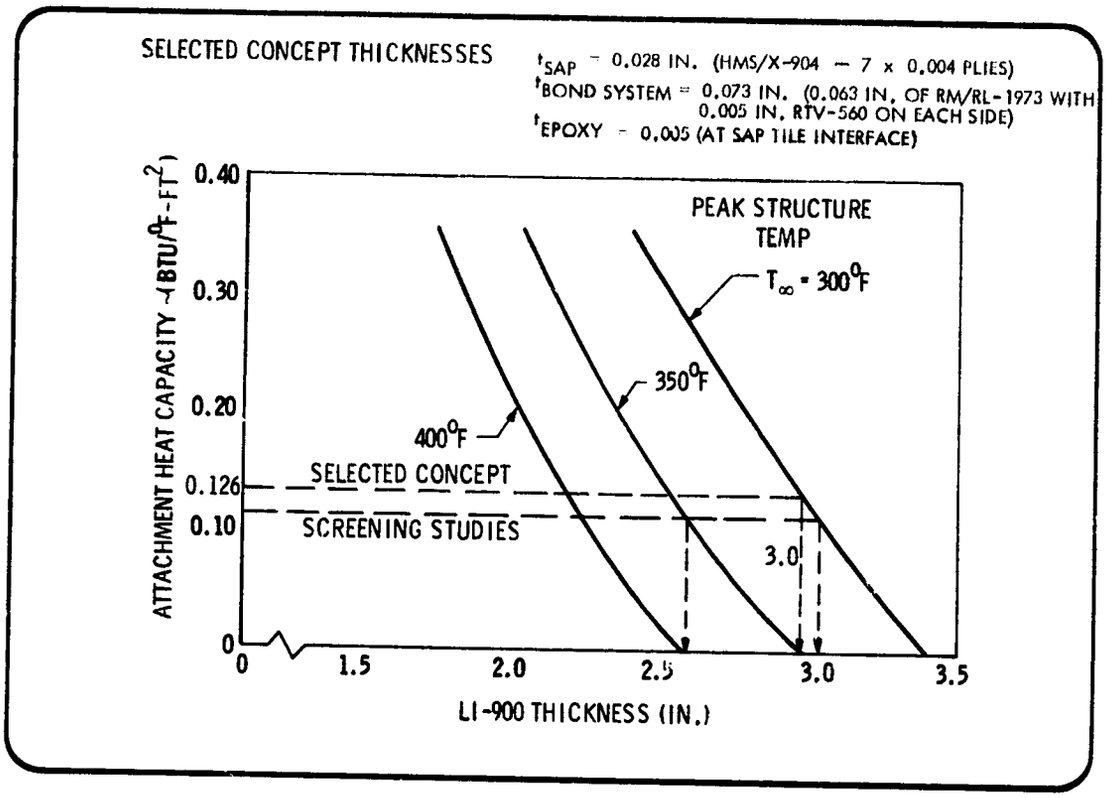

Fig. 2.2-9 Variation of LI-900 Thickness With Attachment Heat Capacity

Therefore, it is concluded that one is relatively free to choose a strain arrestor plate material from the remaining candidate materials, provided that the thickness and the strength requirements are met.

The thickness requirements eliminate the following materials:

Material	t Required	Manufacturing Limit* for At Least Three Plies
GY-70/X-904	0.012 in.	0.021 in.
Thornel 50-X/ERLB-4617	0.017 in.	0.021 in.
Thornel 70-S/ERLB-4617	0.013 in.	0.021 in.

*Minimum thickness for these plies at present is 0.007 in.

The strength requirements and the allowable strengths for the remaining candidate materials are given below:

Material	Strength Required	Allowable Strength
CERVIT C-101	34,000 psi (Comp)	8,000 psi (See Table 2.2-3)
HERCUVIT 101	34,000 psi (Comp)	8,000 psi (Sec Table 2.2-3)
Fused Silica	27,000 psi (Comp)	7,200 psi (Sec Table 2.2-3)
HTS/X-904	21,000 psi (Comp)	60,000 psi (See Fig. 2.2-2)
HMS/X-904	27,000 psi (Comp)	58,000 psi (See Fig. 2.2-3)
PRD-59-III/X-904	11,000 psi (Comp)	19,000 psi (See Fig. 2.2-6)

The stress levels (strength required) for different strain arrestor plates are obtained from Fig. 2.2-10, according to their thickness (thickness requirements are given in Table 2.2-4.

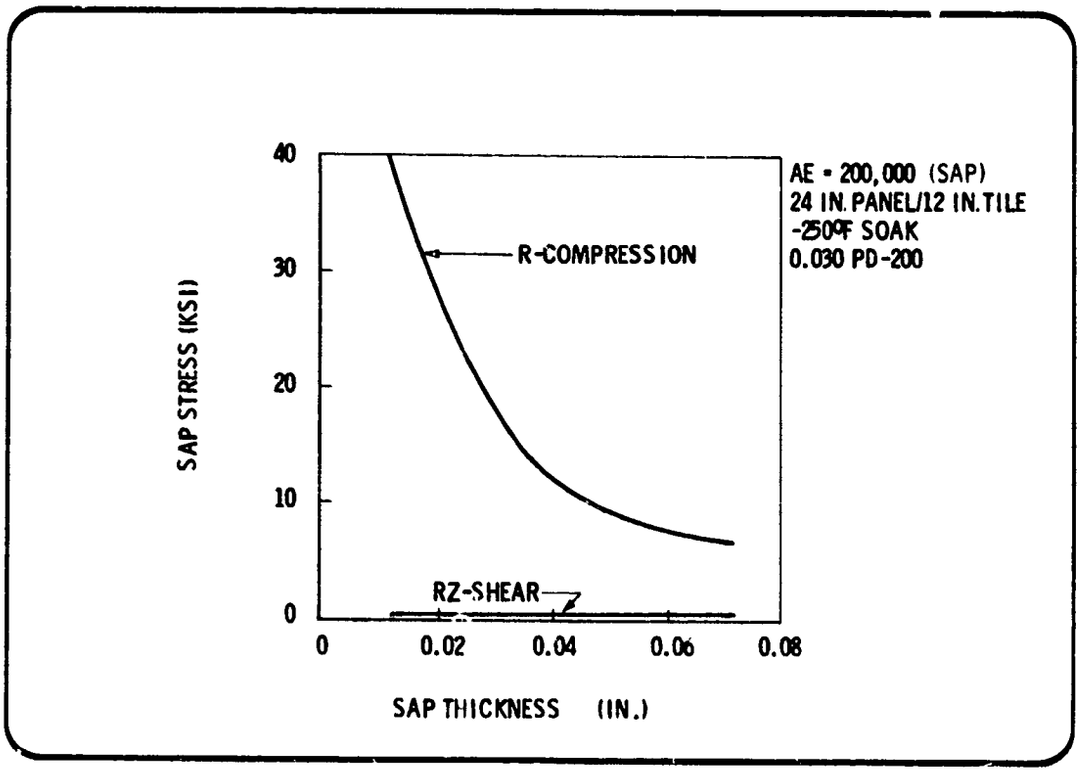

Fig. 2.2-10 Strain Arrestor Plate Stress Vs Plate Thickness

The above figures indicate that the glass ceramic materials and the fused silica do not have the required strength. The other materials meet the strength and the manufacturing requirements. This is shown in Table 2.2-5.

Table 2.2-5

SELECTED MATERIALS FOR STRAIN ARRESTOR PLATES (LOWER SURFACE)

Material	Thickness Required	Available Ply Thickness	Remarks
Graphite Epoxy HTS/X-904	0.026 in.	0.003 in.	For balanced construction six plies are required
Graphite Epoxy HMS/X-904	0.020 in.	0.003 in.	
PRD-49-III/X-904	0.042 in.	0.0035 in.	

The final selection is based on manufacturability, cost and also the bending stiffness of the strain arrestor plate. As shown in Fig. 2.2-11, excessive bending stiffness (excessive thickness) causes some tile stresses to go up. For this reason the choice has been narrowed down to HMS/X-904 graphite epoxy.

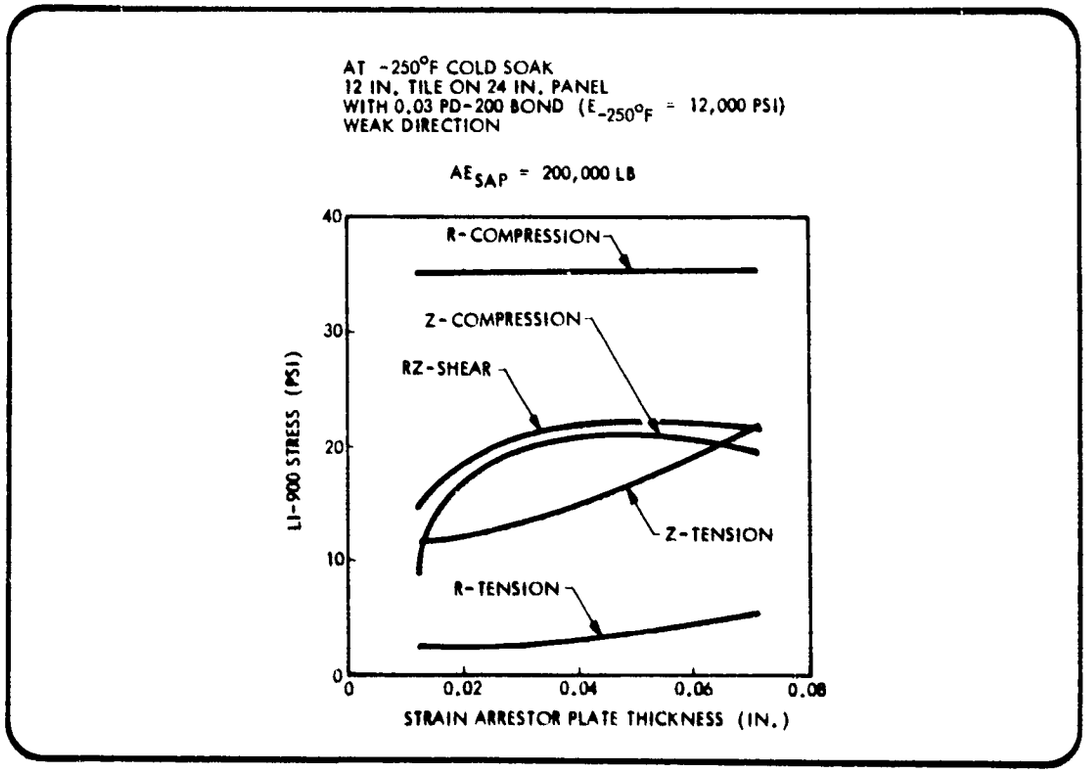

Fig. 2.2-11 LI-900 Stress Vs Plate Thickness

Results

- Weight considerations eliminated INVAR and PRD-49 cloth
- Strength requirements eliminated

  CER-VIT (8,000 psi), HERCUVIT (8,000 psi), Fused Silica (7,200 psi)
- Manufacturing requirements eliminated

	$t_{required}$
GY-70/X-904	0.012 in.
Thornel 50-X/ERLB-4617	0.017 in.
Thornel 70-X/ERLB 4617	0.013 in.

(Minimum ply thickness for these materials is 0.007 in.)

Remaining Candidate Materials

	$t_{required}$	t_{ply}
Graphite Epoxy HTS/X-904	0.026 in.	0.003 in.
Graphite Epoxy HMS/X-904	0.020 in.	0.003 in.
PRD-49-III/X-904	0.042 in.	0.0035 in.

Final Choice

HMS/X-904 Graphite Epoxy — Selected on the basis of least thickness (weight)

These results are summarized in Fig. 2.2-12.

MATERIAL	WEIGHT	STRENGTH	MANUFACTURING	PRODUCIBILITY	STRUCTURAL PREFERENCE (ALL ACCEPTABLE)
1 INVAR	NG				
2 GLASS CERAMIC CERVIT C-101		NG			
3 GLASS CERAMIC HERCUVIT 101		NG			
4 FUSED SILICA		NG			
5 GRAPHITE EPOXY GY-70/X-904			NG		
6 GRAPHITE EPOXY HTS/X-904				O.K.	2
7 GRAPHITE EPOXY HMS/X-904				O.K.	1
8 GRAPHITE EPOXY THORNEL 50-S/ERLB 4617			NG		
9 GRAPHITE EPOXY THORNEL 70-S/ERLB 4617			NG		
10 PRD-49 EPOXY 111/X-904				O.K.	3
11 PRD-49 EPOXY CLOTH/X-904	NG				

Fig. 2.2-12 Final SAP Selection

REFERENCES

2.2-1 Union Carbide Corp. Data Sheet

2.2-2 J. Hertz, J. L. Christian, M. M. Varlas, et al., "Advanced Composite Applications for Spacecraft and Missiles Phase I Final Report," Vol. II, Material Development AFML-TR-71-186, Vol. II, March 1972

2.2-3 PRD-49 Data Sheets

2.2-4 W. S. McCain and R. E. Maringer, "Mechanical and Physical Properties of INVAR and INVAR Type Alloys, DMIC Memorandum 207, August 31, 1965

2.2-5 Owens-Illinois, Inc. Data Sheet

2.2-6 Corning Glass Works Data Sheet

2.2-7 John A. DeRuntz, Jr., "Mechanical Properties of Carbon-Carbon Laminate Systems – Parameter Study, LMSC-5-B2-71-1, Jan 8, 1971

2.2-8 O. Hoffman, "The Brittle Strength of Orthotropic Materials," J. Comp. Materials, Vol. 1, No. 1, April 1967, pp. 200-206

2.2-9 H. Durlofsky, "Composite Analysis Program," Engineering Memorandum L3-1.3.1.3-M1-13, Space Shuttle Project, 24 Aug 1972

2.2-10 J. E. Ashton, et al., "Primer on Composite Materials: Analysis," Technomic Publishing Co., Stanford, Conn., 1969

2.3 PARAMETRIC STUDIES

One objective of the design and analysis task was to present the results of the parametric studies performed under this contract in a form that would be useful in future design studies of a similar nature. Such information is contained in this subsection, which presents the results of the structural screening studies. The information consists of the following:

- Sizing curves showing the required LI-900 thickness as a function of attachment heat capacity
- Temperature profiles for critical conditions
- Logic sequence for structural screening (flow charts)
- Structural screening studies for bottom location (Area 2P)
  - SAP in-plane stiffness variation
  - Bond line thickness variation
  - Tile length variation
  - Analysis model variation
  - Partial bond and bond deletion study
  - SAP thickness variation
  - Continuous SAP study
  - Results for bottom location
- Structural screening studies for side and top locations
  - LI-900 thickness variation
  - Results for side and top locations

2.3.1 Required LI-900 Thickness Versus Attachment Heat Capacity

The Phase II groundrules specified an adiabatic condition on the primary structure with the structure constrained to a maximum temperature of 300°F. In addition to the pressure effects on conductivity, the heat capacity of the attachment system and structure are also considered in sizing. The sizing curves shown in Fig. 2.3-1 for the bottom location allow a ready weight tradeoff for the various candidate SAP systems. Similar curves for the top and side locations are shown in Fig. 2.3-2.

The baseline selected for the screening studies (shown later) results in a heat capacity at the bottom location of 0.114 Btu/°F, requiring a LI-900 thickness of 3.04 inches to constrain primary structure temperature to 300°F. Relaxing this constraint to 350°F reduces the LI-900 thickness to 2.59 inches.

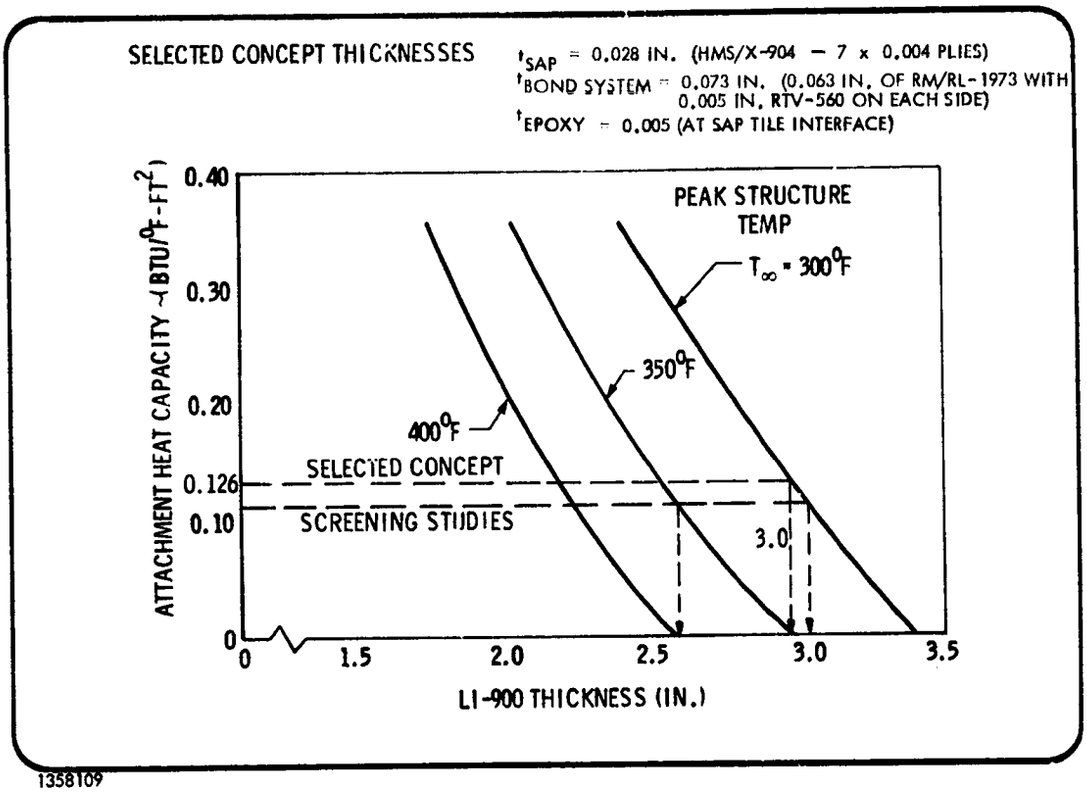

Fig. 2.3-1 Variation of LI-900 Thickness With Attachment Heat Capacity – Area 2P (Bottom)

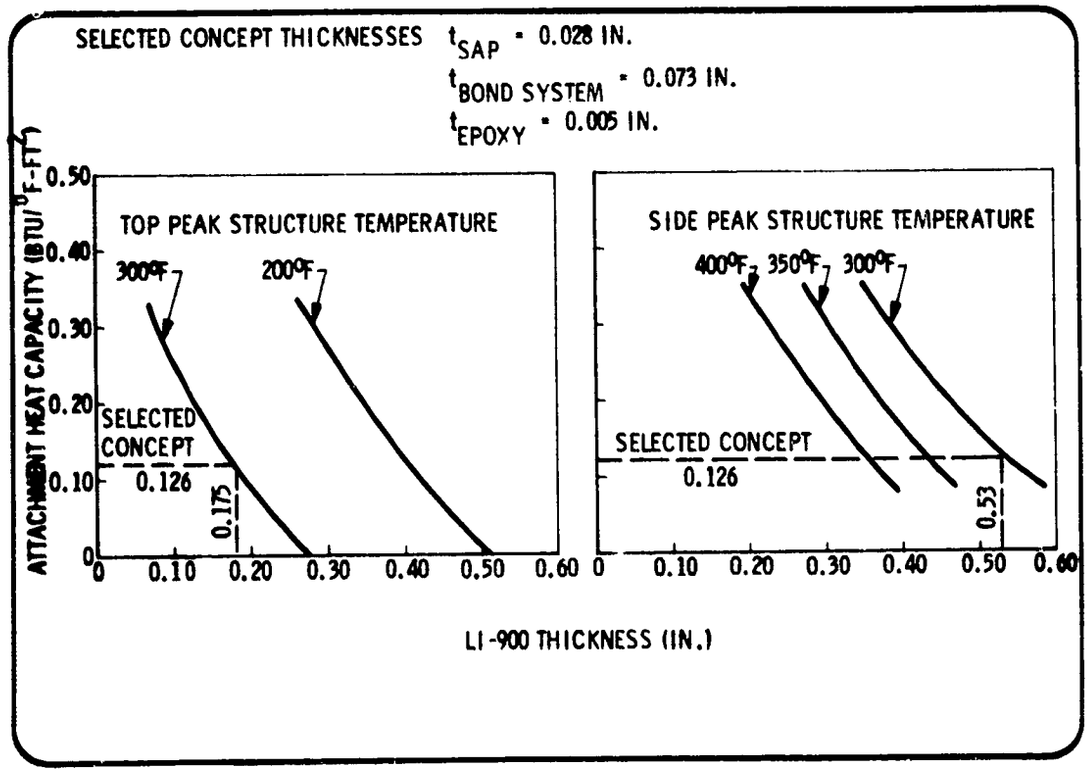

Fig. 2.3-2 Variation of LI-900 Thickness With Attachment Heat Capacity (Top and Side)

Depending on orbit conditions, the initial temperature at the start of reentry can vary from 200°F down to -250°F. The substrate (bond line) temperature history for the bottom (Area 2P) location was shown in Fig. 2.1-4 for two initial reentry temperatures, 70°F and -250°F. The 200°F initial condition is not included since it results in final substrate temperatures greater than 350°F, the nominal reuse capability of the aluminum structure. In addition to temperature, Fig. 2.1-4 shows substrate load history from the start of reentry to touchdown at 3600 seconds. The -250°F cold soak condition has been used for the majority of the screening exercises. Other critical conditions at a reentry time of 1000 seconds and at touchdown have also been considered in the design effort. For screening it has been shown that the -250°F cold soak condition results in stresses very close to the maximum values; therefore, for ease of computation, this condition has been used exclusively in the screening studies. Note from Fig. 2.1-4 that peak temperatures on the lower surface at the bond line occur after touchdown.

2.3.2 Temperature Profiles for Critical Conditions

The critical temperature profile for LI-900, GY-70, PD-200, and aluminum structure is shown in Fig. 2.3-3. The 1000-second condition results in an outer surface temperature of 2080°F and a steep gradient through the material to the -250°F backface. The screening has shown that the decrease in modulus of the bond system results in critical stresses located adjacent to the SAP. These stresses are independent of the thermal gradient through the material, which further justifies the use of the -250°F cold soak condition for screening.

At touchdown (t = 3600 seconds) the backface temperature is 250°F, assuming an initial temperature of 70°F. In addition to the high backface temperature, maximum line loads are experienced at this time. The steep thermal gradient exists through the RSI material, as shown in Fig. 2.3-4. With the SAP this condition has been shown to be less critical than the -250°F cold soak condition.

2.3.3 Logic Sequence for Structural Screening

The design effort and sizing analysis flow for the initial screening of the SAP is shown on Figs. 2.3-5 through 2.3-7. The effort shown resulted in the establishment of a preliminary baseline design for the lower surface application. However, the analysis of this design for the weak substrate plane indicated fairly high stresses for the weak direction model if a SAP AE of 200,000 lb were used.

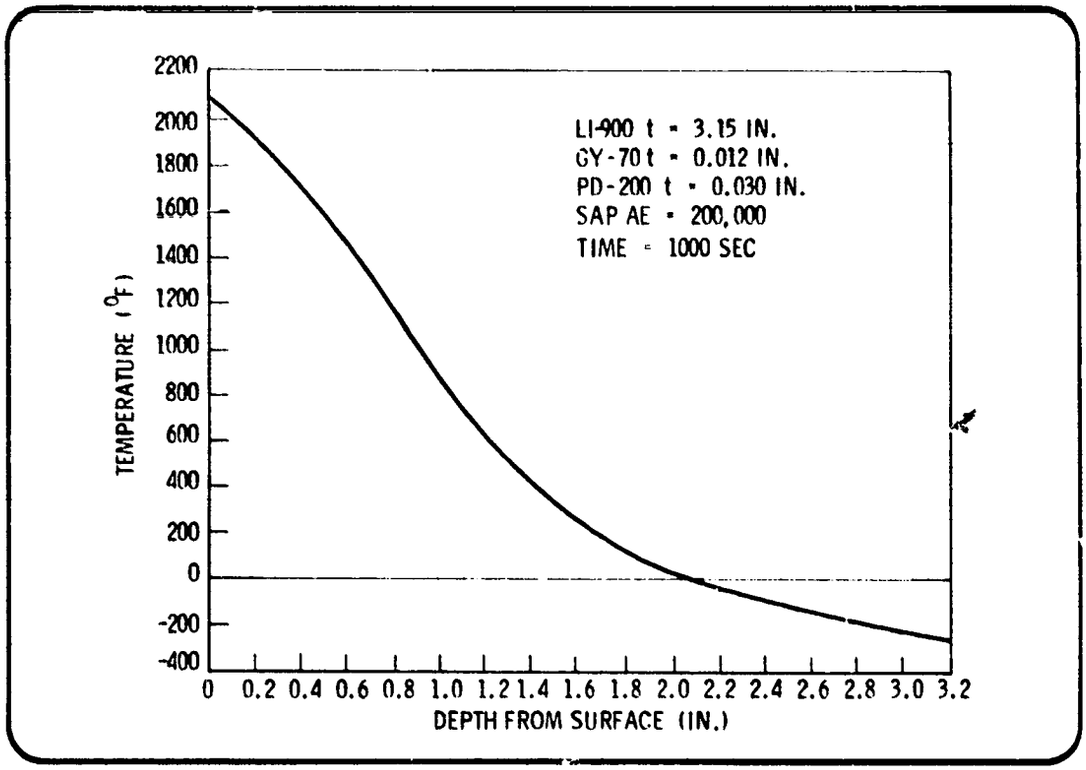

Fig. 2.3-3 Temperature Profile – LI-900, GY-70, PD-200, Aluminum

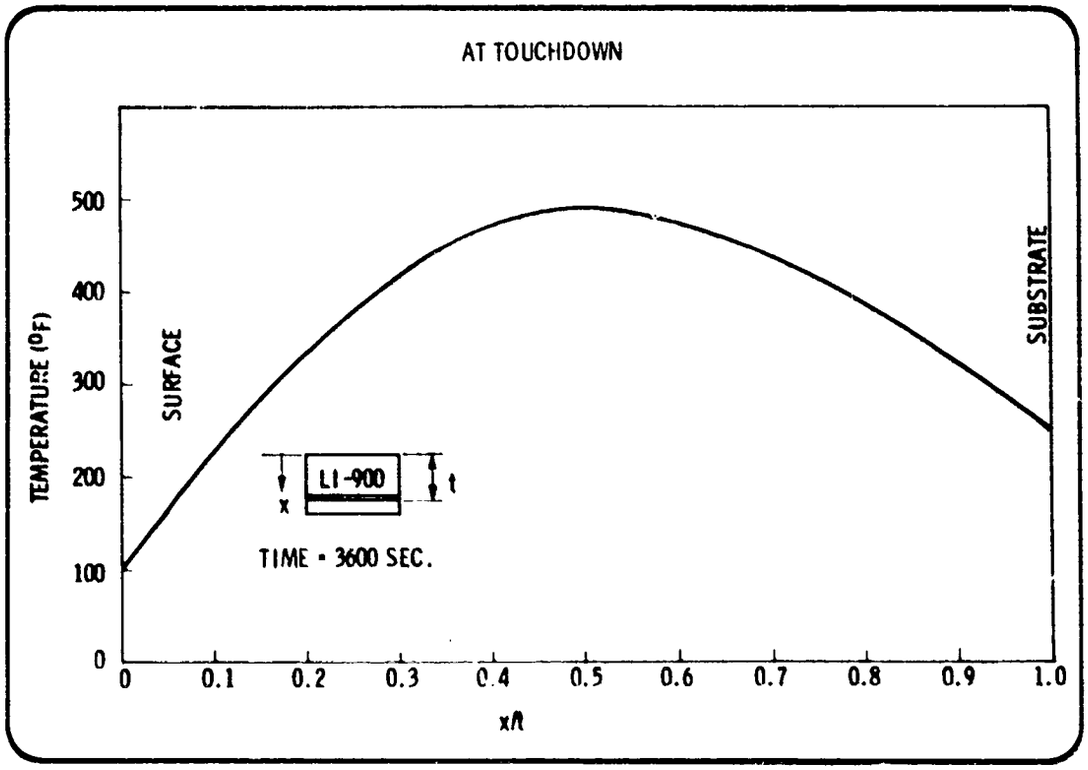

Fig. 2.3-4 Temperature Profile—Area 2P

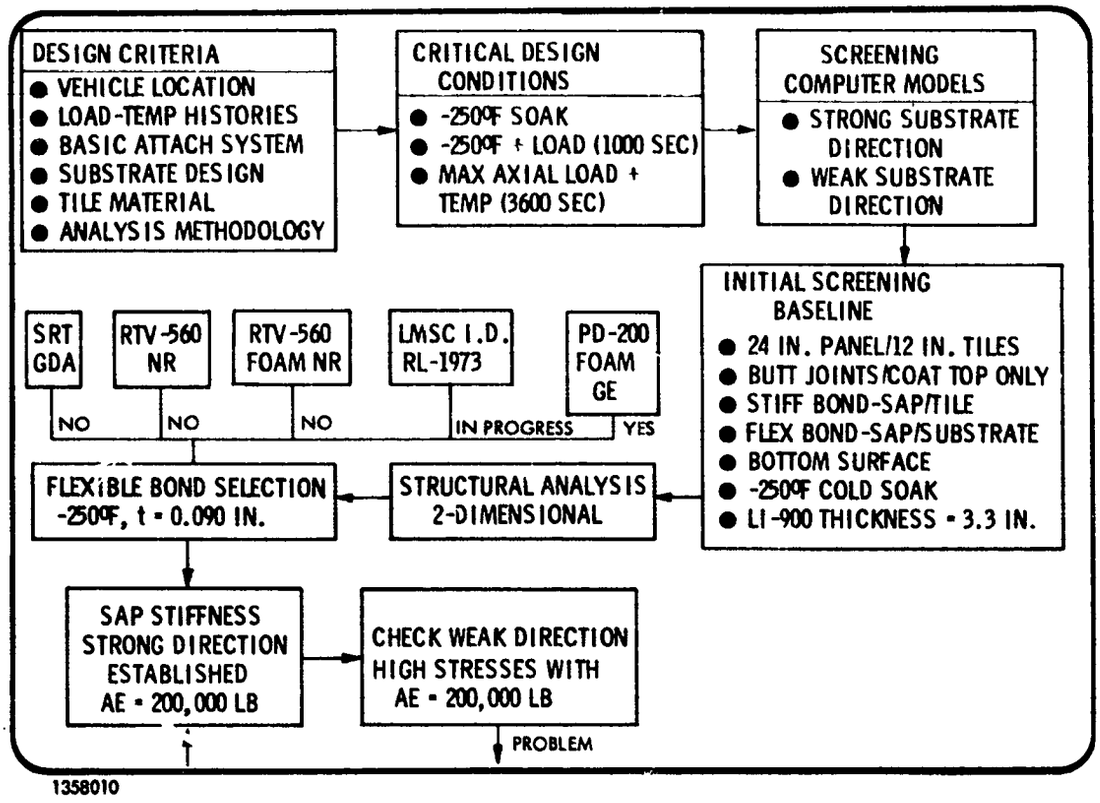

Fig. 2.3-5 Logic Sequence – Structural Screening

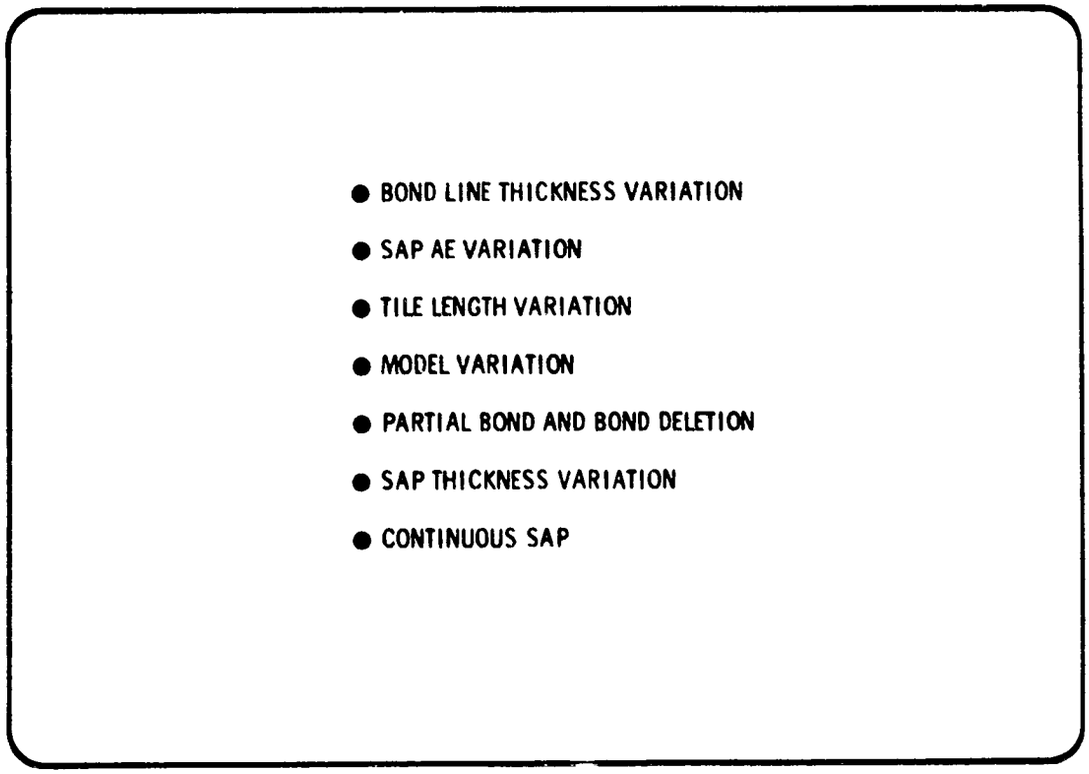

Fig. 2.3-6 Screening Studies – Weak Direction

Analytical activities to arrive at an acceptable design for the weak substrate plane are shown in Fig. 2.3-6. At various points in the activities, changes in the design were checked against the strong direction to verify compatibilities. A design compatible with requirements in both planes resulted from this effort.

The results from each activity are presented subsequently.

Following establishment of the lower baseline design, various sensitivity studies were performed as shown in Fig. 2.3-7.

2.3-4 Structural Screening Studies for Bottom Location (Area 2P)

The NR RTV-560 data at -250°F were used to assess the use of RTV-560 for this application. A modulus of 700,000 psi was used in the analysis. Plotting maximum LI-900 stress versus SAP extensional stiffness has shown that stiffness greater than 500,000 psi would be required for use of this bonding system. As can be seen from Fig. 2.3-8, increasing the stiffness results in lower stresses, but positive margins were never achieved. Therefore, RTV-560 was dropped from the analytical matrix.

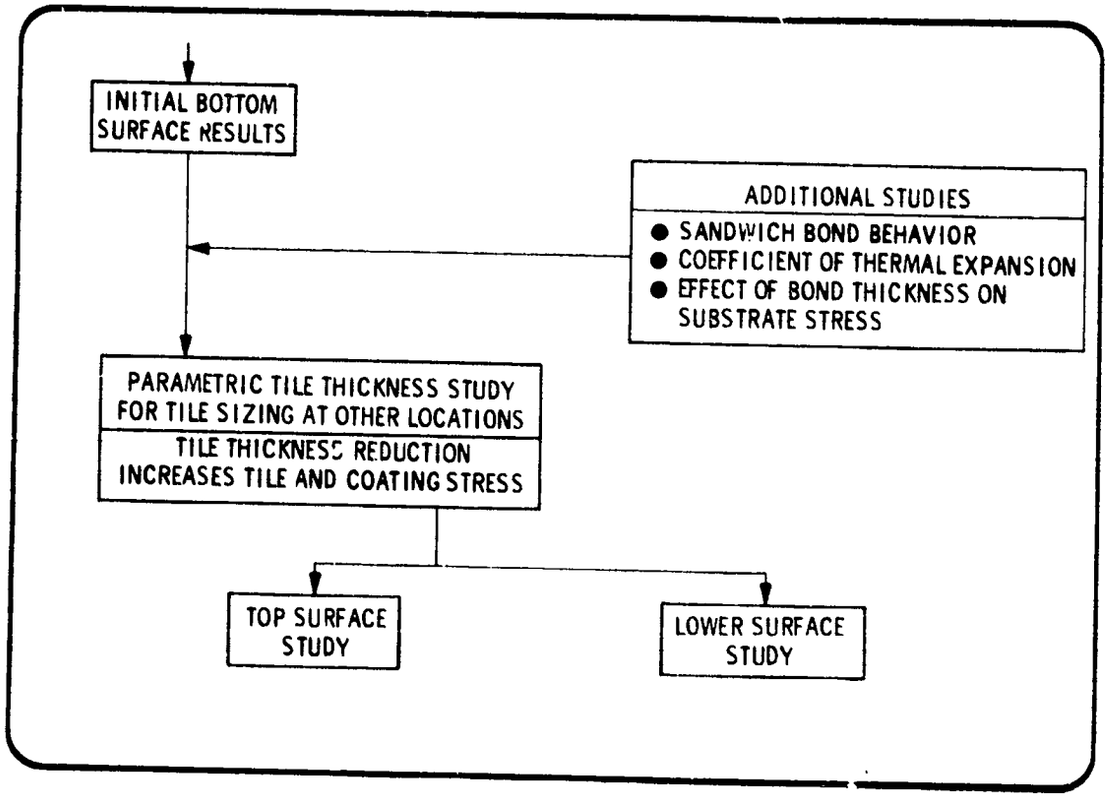

Fig. 2.3-7 Logic Sequence – Structural Sizing

NR data were also used to evaluate the use of RTV-560 foam. A modulus of 113,000 was used for the -250°F condition. As with basic RTV-560, it can be seen from Fig. 2.3-9 that SAP stiffnesses above 300,000 would be required to achieve positive margins. Therefore, this system was also dropped from the analytical matrix.

The GE-PD-200 foam bond system was also evaluated. A modulus of 12,000 psi was used for the -250°F condition.

As shown in Fig. 2.3-10, the SAP stiffness required with this system is much less than previously shown. Positive margins are shown for critical stresses with a SAP stiffness of 150,000 and above. Therefore, considering the available data, PD-200 was selected as the baseline attachment system for the screening analysis. A SAP extensional stiffness of 200,000 was selected for the tradeoff studies.

A SAP stiffness requirement of 200,000 lb was established for the strong direction, with the parameters shown in Table 2.3-1. Stress levels are well within design allowables. However, a check of the stresses in the weak direction showed this design to be inadequate. The design drivers, normal tension and shear stresses, both increased substantially.

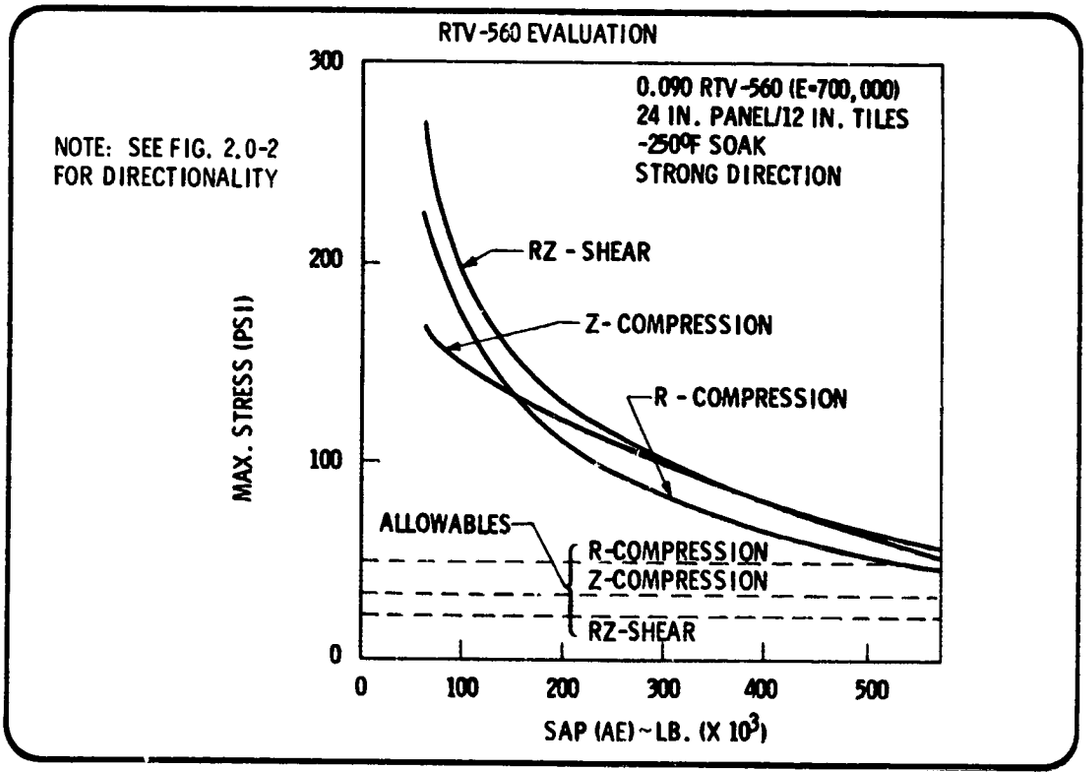

Fig. 2.3-8 LI-900 Stress Vs SAP Stiffness

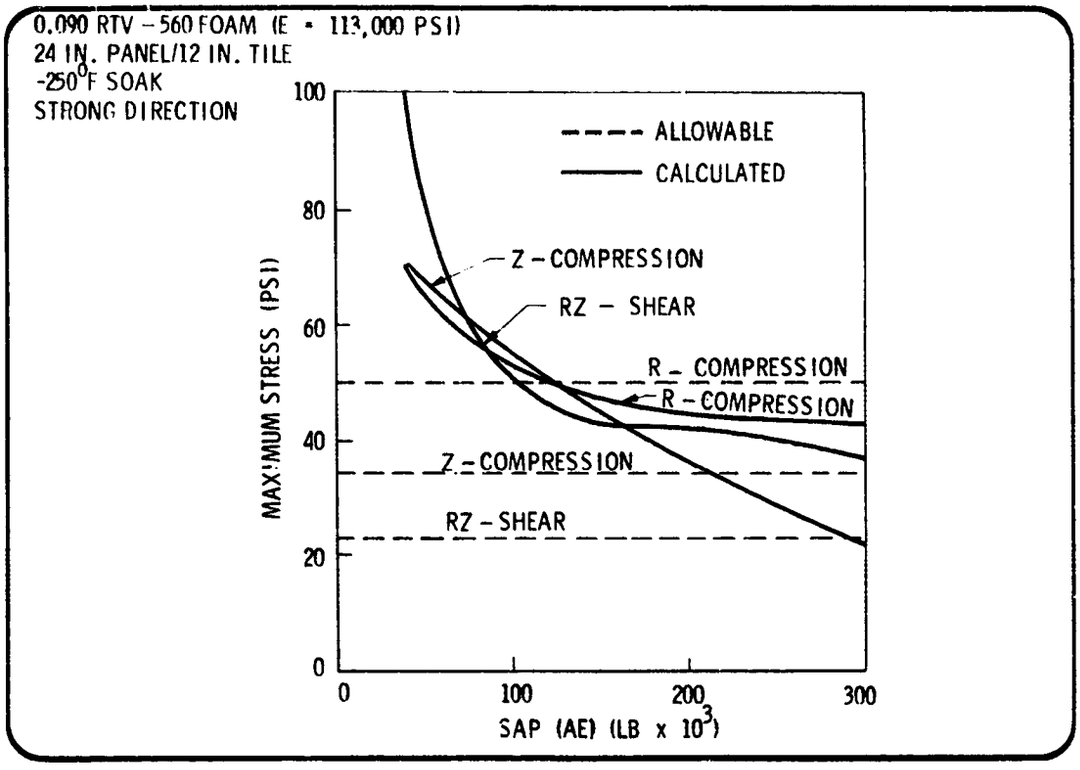

Fig. 2.3-9 LI-900 Stress Vs SAP Stiffness (RTV-560 Foam Bond)

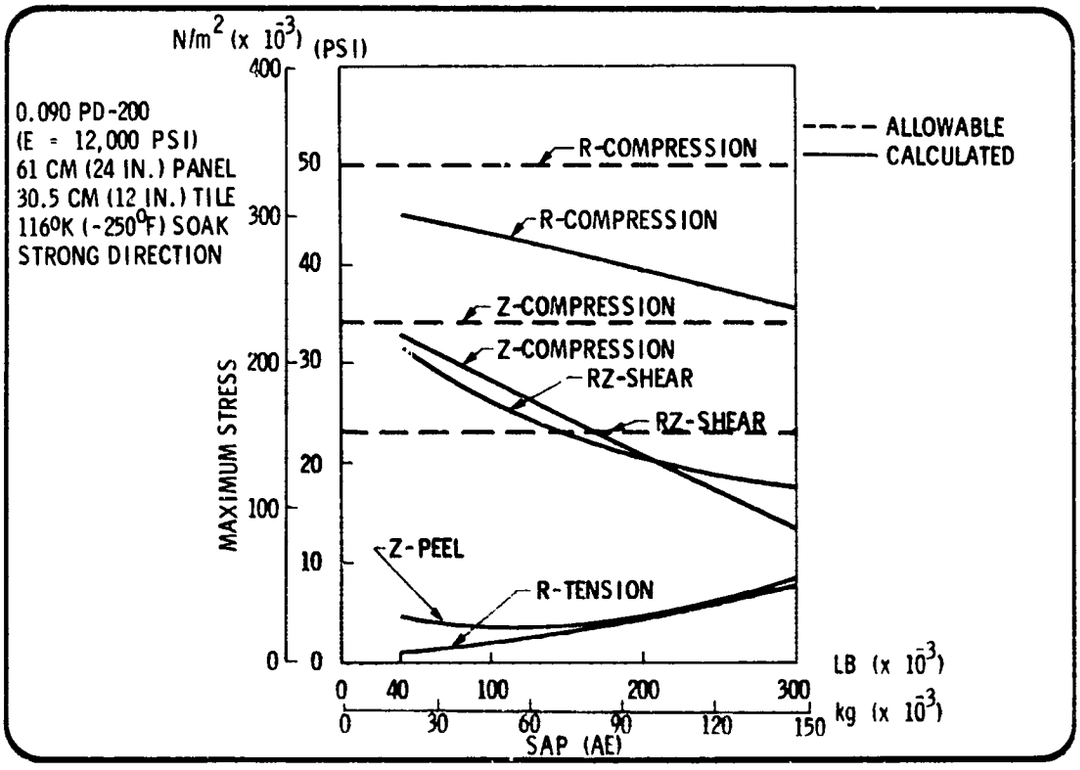

Fig. 2.3-10 LI-900 Stress Vs SAP Stiffness (PD-200 Foam Bond)

Table 2.3-1

FIRST DESIGN -- MAX LI-900 STRESSES

TILE LENGTH : 12 IN.
PD-200 FOAM BOND SYSTEM THICKNESS : 0.090 IN.
STRAIN ARRESTOR PLATE EXTENSIONAL STIFFNESS: 200,000 LB
STRAIN ARRESTOR PLATE THICKNESS : 0.012 IN.
TILE THICKNESS : 3.30 IN.

	STRONG	WEAK	ALLOWABLE
LONGITUDINAL TENSION (PSI) -	5	17	45
LONGITUDINAL COMPRESSION (PSI) -	-40	-33	50
NORMAL TENSION (PSI) -	5	55	12
NORMAL COMPRESSION (PSI) -	21	-9	34
SHEAR (PSI) -	21	30	23

The solution to this problem involved many studies. The effects of each potential modification were evaluated for the strong direction also prior to design change.

The desirability of decreasing the bond thickness was investigated in the strong direction. It was determined that LI-900 stresses were relatively insensitive to bond thickness as shown in Fig. 2.3-11.

The effect of varying bond line thickness in the weak direction was studied with the results shown in Fig. 2.3-12. This study indicated the desirability of decreasing the bondline thickness. It was expected that the bondline should be increased instead. The phenomena is attributed to the stiffness of the bond at -250°F, where additional material with a high coefficient of expansion in the composite increases the total deformation.

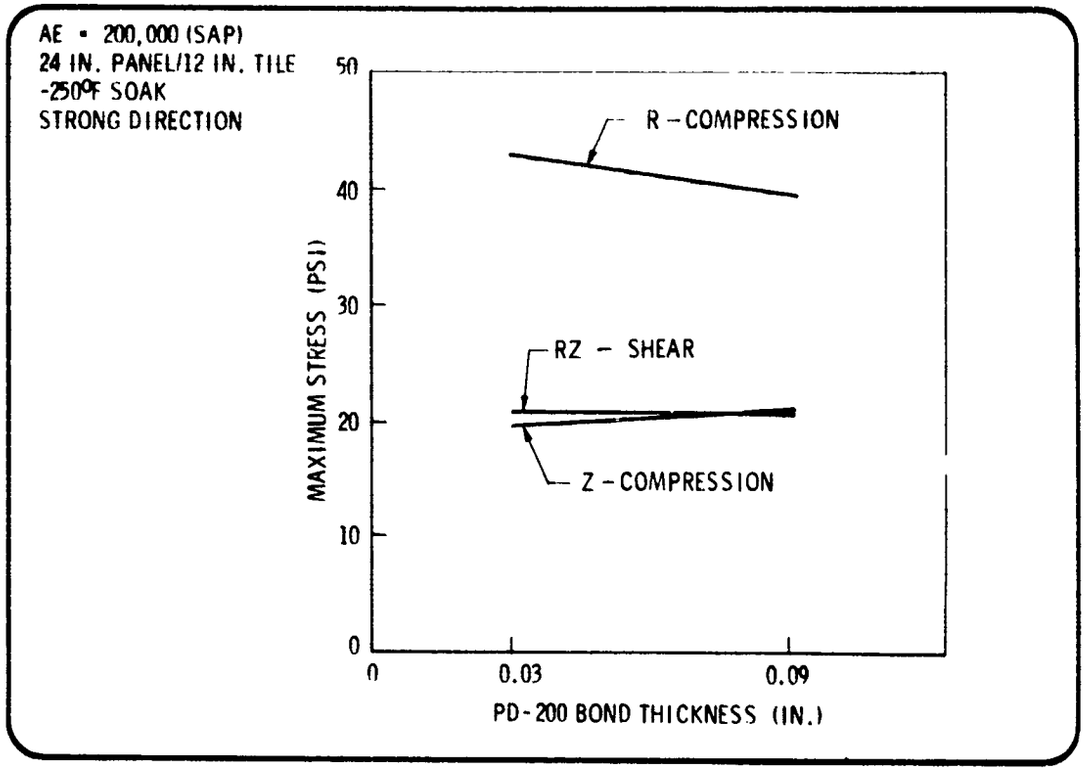

Fig. 2.3-11 LI-900 Stress Vs Bond Thickness (Strong)

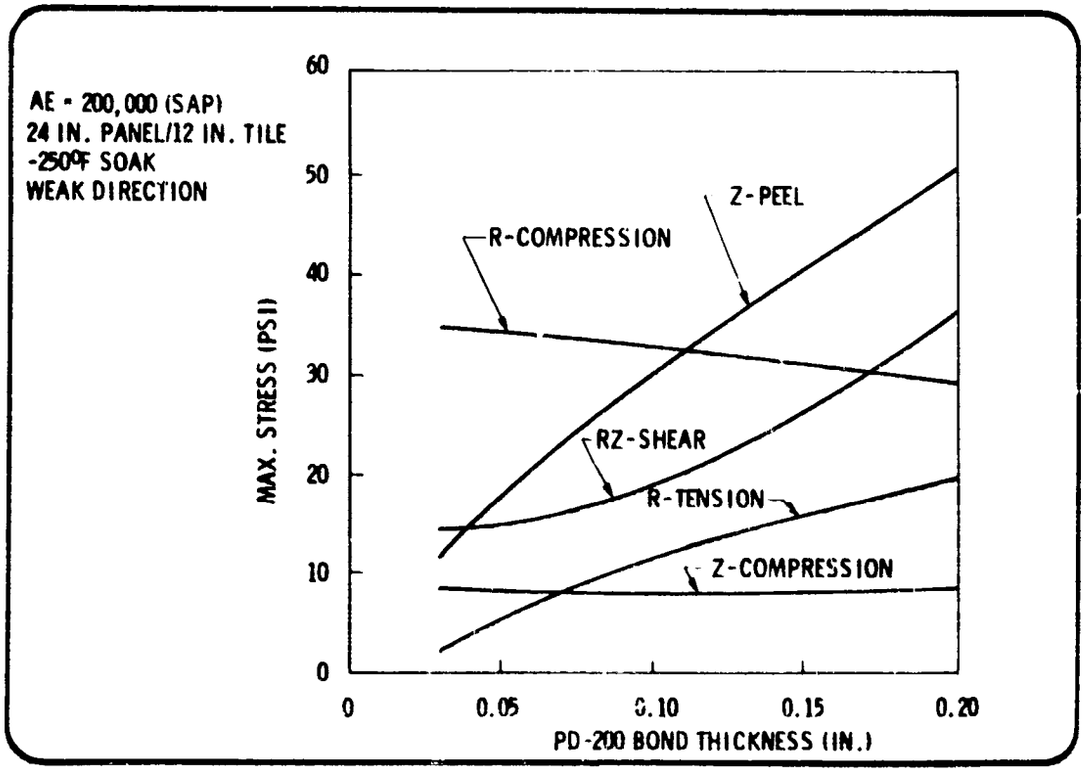

Fig. 2.3-12 LI-900 Stress Vs Bond Thickness (Weak)

The desirability of increasing the SAP stiffness in the weak direction was studied. As shown in Fig. 2.3-13, it was found that LI-900 stresses increased with increasing SAP stiffness. This trend opposes the strong direction trends, but indicates that an optimum stiffness can be determined and that the use of an orthotropic stiffness should be investigated.

The opposing trends of the LI-900 critical stresses versus SAP stiffness are compared in Fig. 2.3-14. The following two charts illustrate the mechanics involved in the composite at the -250° soak condition.

The composite is fabricated and assembled at room temperature. As shown in Fig. 2.3-15, the reduction in temperature has little effect on the LI-900 and SAP because of their low coefficients of thermal expansion. The aluminum substrate (and bond), however, contracts a significant amount because of relatively high coefficient of expansion. This contraction gives rise to high shear stresses, forcing compatibility at layer interfaces of the composite. These shear stresses result in bending of the components and, therefore, induce stresses in the LI-900.

The amount of bending in the tile-SAP combination is primarily dependent on the extensional SAP stiffness (AE); the bending in the substrate is dependent on the substrate bending stiffness (EI).

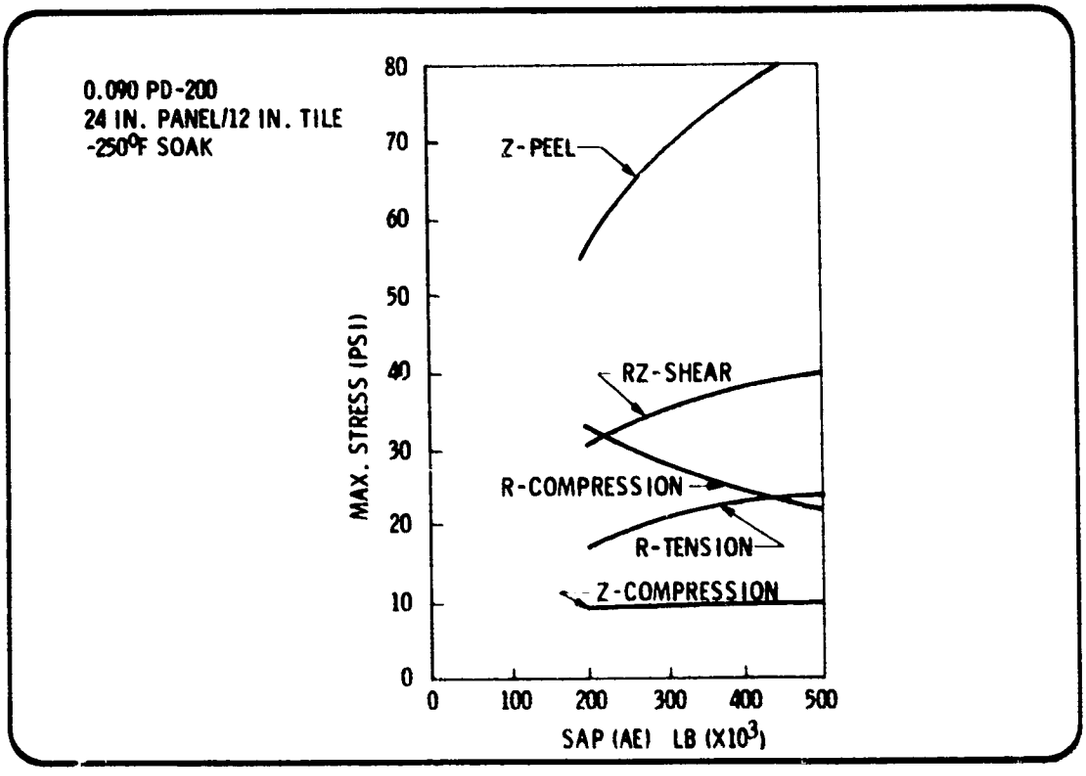

Fig. 2.3-13 LI-900 Stress Vs Sap Stiffness – Weak Direction

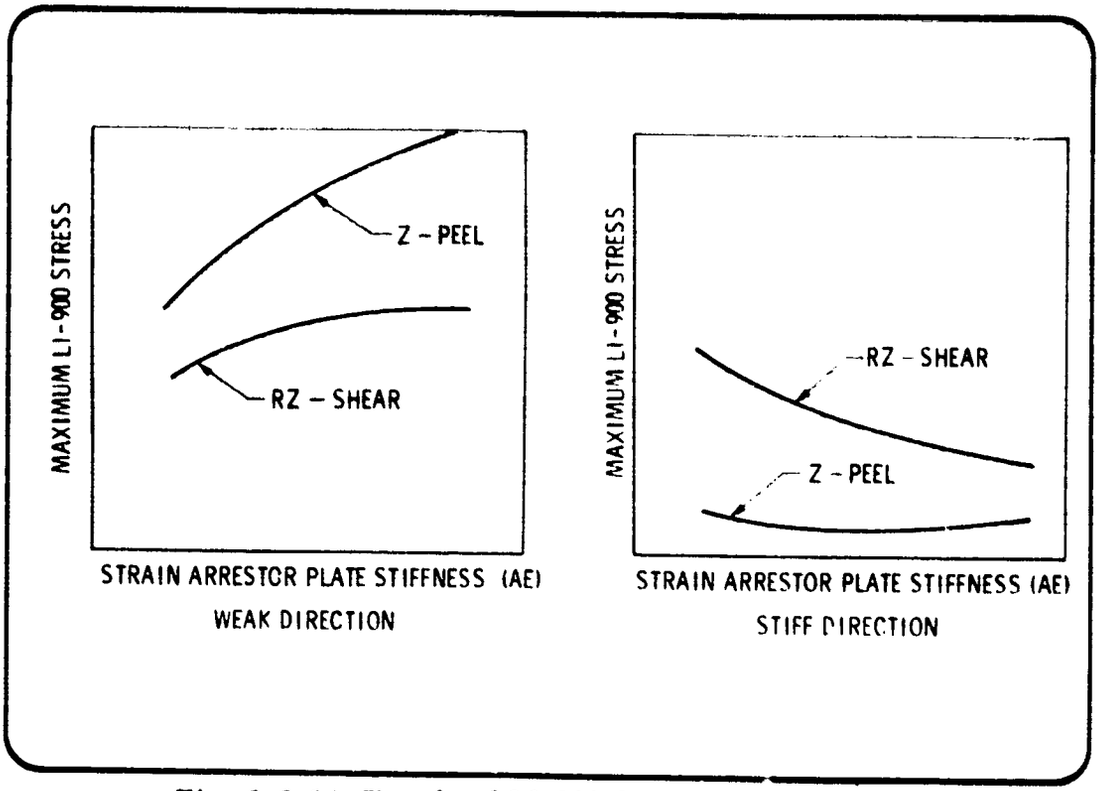

Fig. 2.3-14 Trends of LI-900 Stress Vs Stiffness For Stiff and Weak Substrates

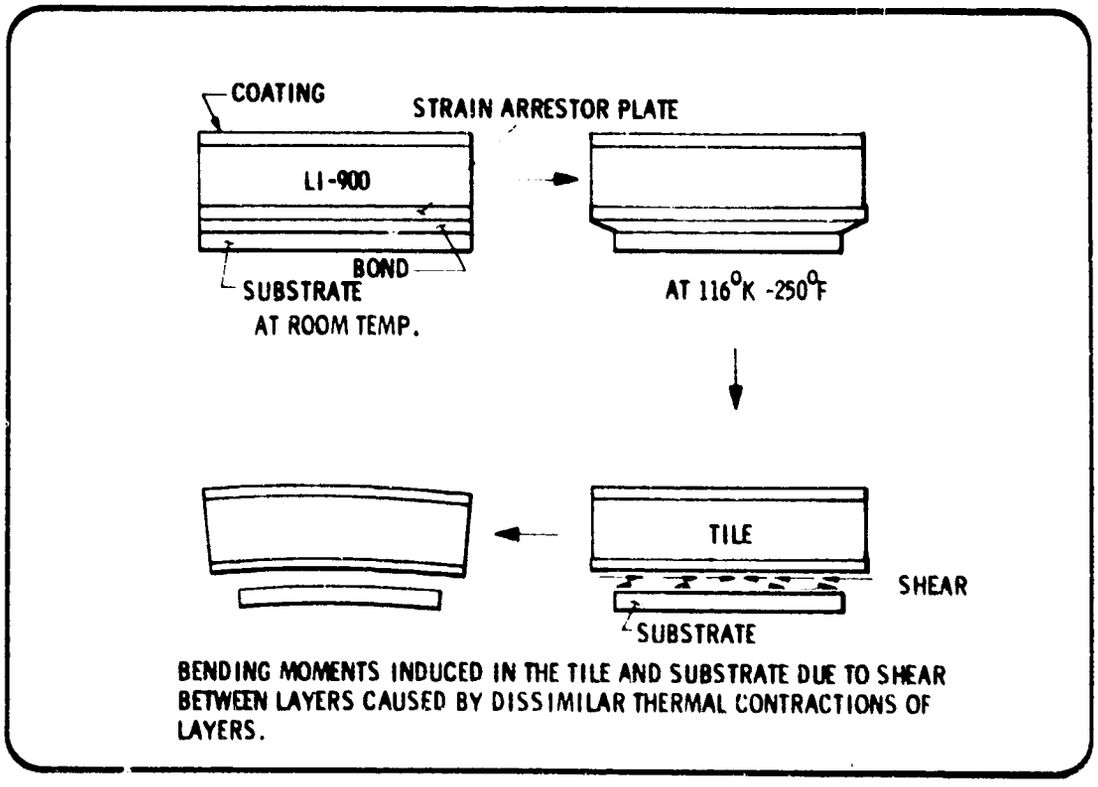

Fig. 2.3-15 Cold Soak Mechanics – Induced Bending

In the weak direction, the imposed shear loads easily bend the substrate, as shown in Fig. 2.3-16 (1) and (2). A low AE SAP is also easily bent to conform to a large radius. The large radius of curvature results in moderate stresses at the tile edge. Hence, a low AE SAP is desirable (Fig. 2.3-16 (1)).

With a high AE (Fig. 2.3-16 (2)) and weak substrate, the low shear stresses near the center of the tile have little effect on the SAP and all compatibility is forced abruptly near the edge. This gives rise to high loads in the LI-900 tile.

In the stiff direction, the shear stresses again easily deform a low stiffness SAP (Fig. 2.3-16 (3)) but cannot bend the stiff substrate (high EI). This results in high compression stress at the edge of the tile. A high AE SAP in conjunction with the stiff substrate (Fig. 2.3-16(4)) results in little bending of either component, since compatibility at the tile edge is easily achieved. Very low peel stresses result. Hence, a high AE SAP is desirable.

The tile length in the weak direction was varied to assess the possibility of varying the dimensions. As shown in Fig. 2.3-17, the shear stress level was found to be a minimum at approximately 13 inches. The peel stress, however, continues to decrease with increasing tile length. This study indicates the possibility of increasing tile length to decrease overall stress levels in the LI-900.

As shown in Fig. 2.3-18, the LI-900 stresses continue to increase with increasing tile length in the strong direction. Again, opposite trends have been established. Based on this study, the decision was made to limit the tile length to 12 inches.

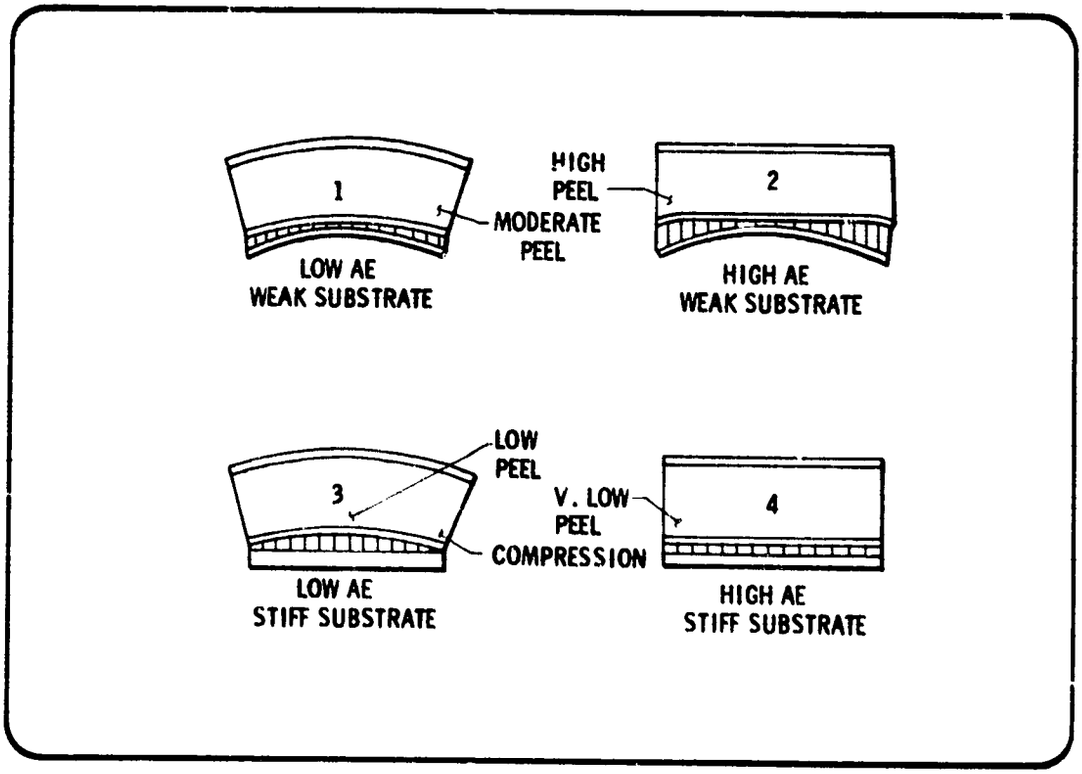

Fig. 2.3-16 Cold Soak Mechanics – Max Stress

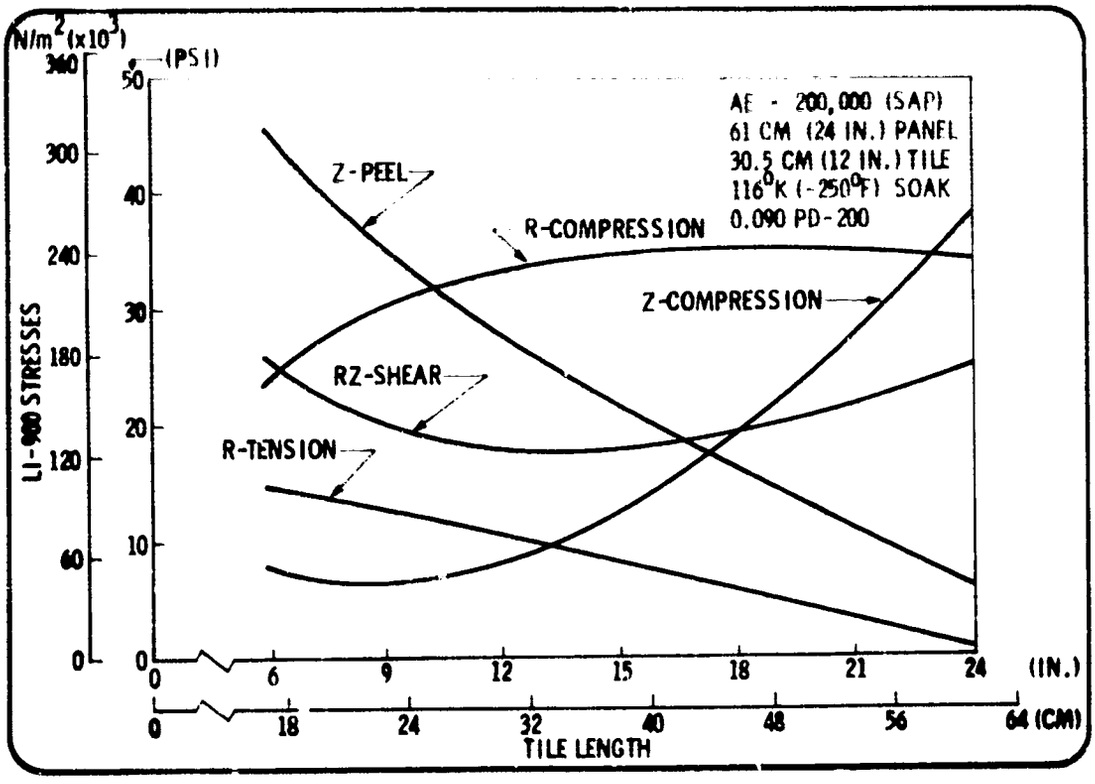

Fig. 2.3-17 LI-900 Stress Vs Tile Length – Weak Direction

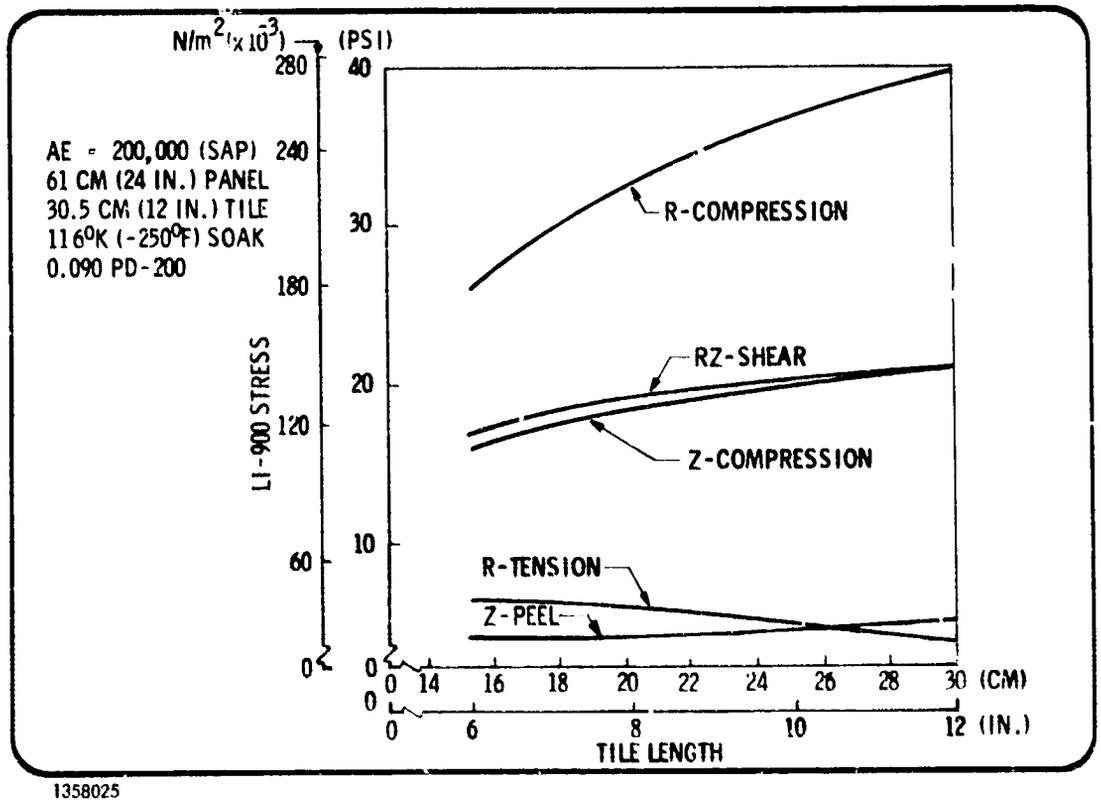

1358025

Fig. 2.3-18 LI-900 Stress Vs Tile Length– Stiff Direction

At this stage in the screening analysis, investigations to reduce weak direction tile stresses had considered (1) variable bond thickness, (2) variable SAP stiffness, and (3) variable tile length. The bond thickness was reduced to 0.030 inch. The two latter investigations revealed opposite trends in the two directions.

Analytical modeling of the orbiter primary structure is restricted in the tile analysis because of relative geometries. Accuracy is greatly reduced when increasing the dimensions of the substrate and including more tiles. A section of a continuous shell structure was modeled as a discrete width panel, which results in good simulation in the stiffener direction but poor simulation in the weak direction. The continuous thin shell cannot deflect in application in the same manner as a free edge in the model; some restraint would exist at any boundary taken.

To simulate this restraint, the model was pinned in the vertical direction which more closely represents a supported plate rather than a beam. In modifying the model, the design of the 24 by 24-in. prototype panel required under the contract was considered. Stiffer edge stiffeners will be designed to provide this restraint.

Use of this modeling device reduced the critical stresses by approximately 50 percent, as can be seen in Table 2.3-2. This model has subsequently been used for the weak direction studies.

Table 2.3-2

COMPARISON OF LI-900 STRESS IN PANELS

WITH AND WITHOUT END SUPPORT

	MAXIMUM LI-900 STRESSES	
	WITHOUT END SUPPORT	WITH END SUPPORT
R - TENSION	17	10.3
R - COMPRESSION	-33	-33
Z - TENSION	55	27.5
Z - COMPRESSION	-9	-8
RZ - SHEAR	30	17.8

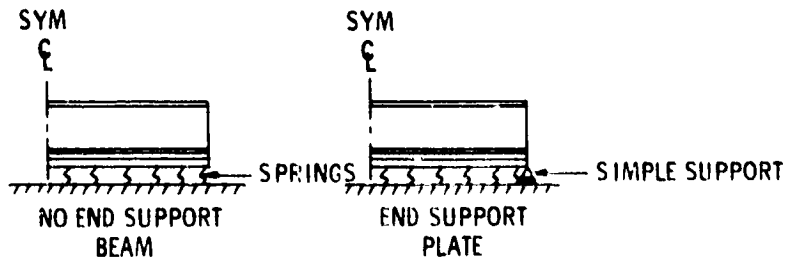

Deletion of the bond (SAP to substrate) was considered to reduce weak direction stresses. Although peel stresses were reduced for a small percentage bond deletion, shear stresses increased, as shown in Fig. 2.3-19. With more than 10-percent deletion, both critical stresses increased. Based on this study, deletion of bond from the SAP edges does not appear to relieve critical stresses.

The effect of partial bonding of the SAP to the structure was investigated. One-inch areas were placed at various locations. Except with bonding at the center point only, critical stresses increased, as indicated in Table 2.3-3. Bonding at the center greatly reduced all stresses in each material of the composite. This application was considered as a boundary condition only and does not appear rational for vehicle design. With such a small area, reliability would be reduced and conditions such as vibration could become critical. It appears that partial bonding is feasible for reducing stresses but cannot be baselined at this time.

The effect of varying SAP thickness while retaining the same extensional stiffness was investigated for the bottom surface. An increase in thickness increases the bending stiffness (EI). In the weak direction both peel and shear stresses increased with thickness, as shown in Fig. 2.3-20. Therefore, the thinnest possible SAP consistent with the 200,000-lb extensional stiffness is desirable for reducing weak direction LI-900 stresses.

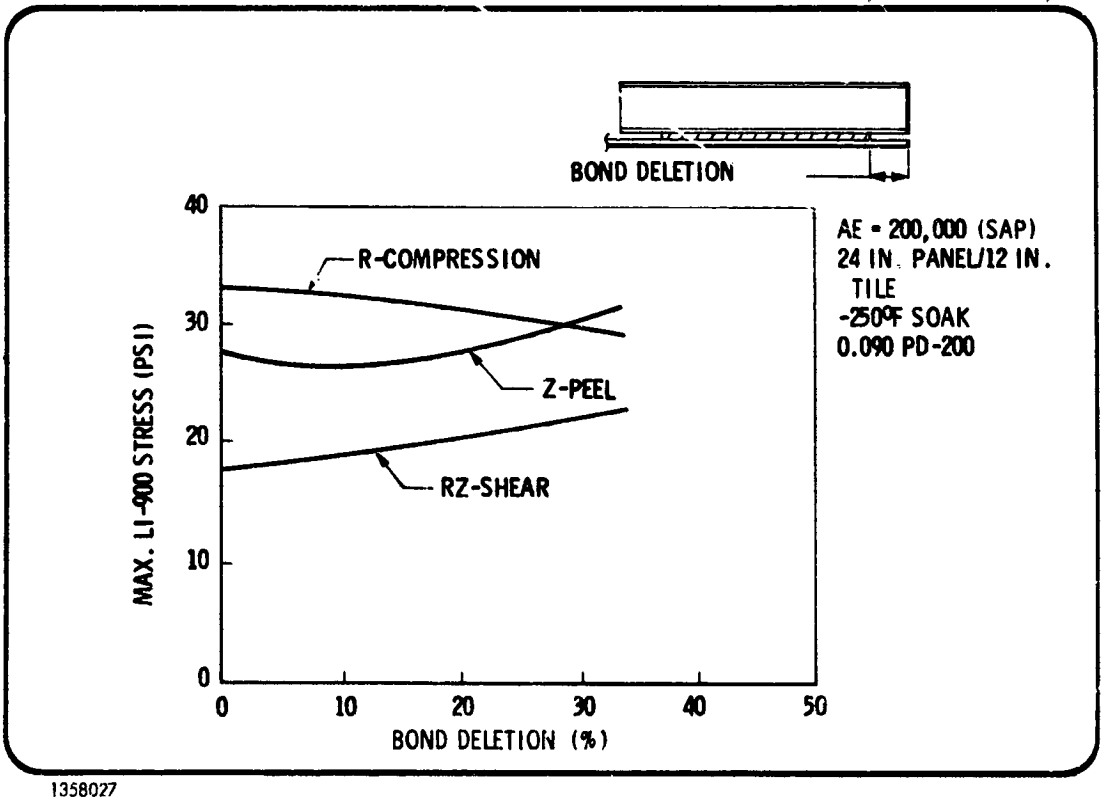

Fig. 2.3-19 LI-900 Stress Vs Percent Bond Deletion– Weak Direction

Table 2.3-3
PARTIAL BOND STUDY -- WEAK DIRECTION

AE = 200,000 (SAP)
24 IN. PANEL/12 IN. TILE
-250°F SOAK, 0.090 PD-200

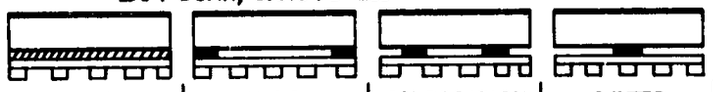

	FULL LENGTH	ENDS	1/4 POSITION	CENTER
COATING				
PRINC TENSION	995	1,073	856	13
PRINC COMPRES	-20	-33	0	-2
PRINC SHEAR	498	536	428	7
LI-900				
R-TENSION	10.3	23.3	7.4	2.2
R-COMPRESSION	-33	-27.6	-21.1	-1.9
Z-TENSION	27.5	75.0	38.2	6.4
Z-COMPRESSION	-8	-46.1	-36.1	-4.7
RZ-SHEAR	17.8	39.9	25.1	5.8
PD-200				
PRINC TENSION	527	623	560	419
PRINC COMPRES	-212	-321	-163	-19
PRINC SHEAR	350	440	361	219

1358030

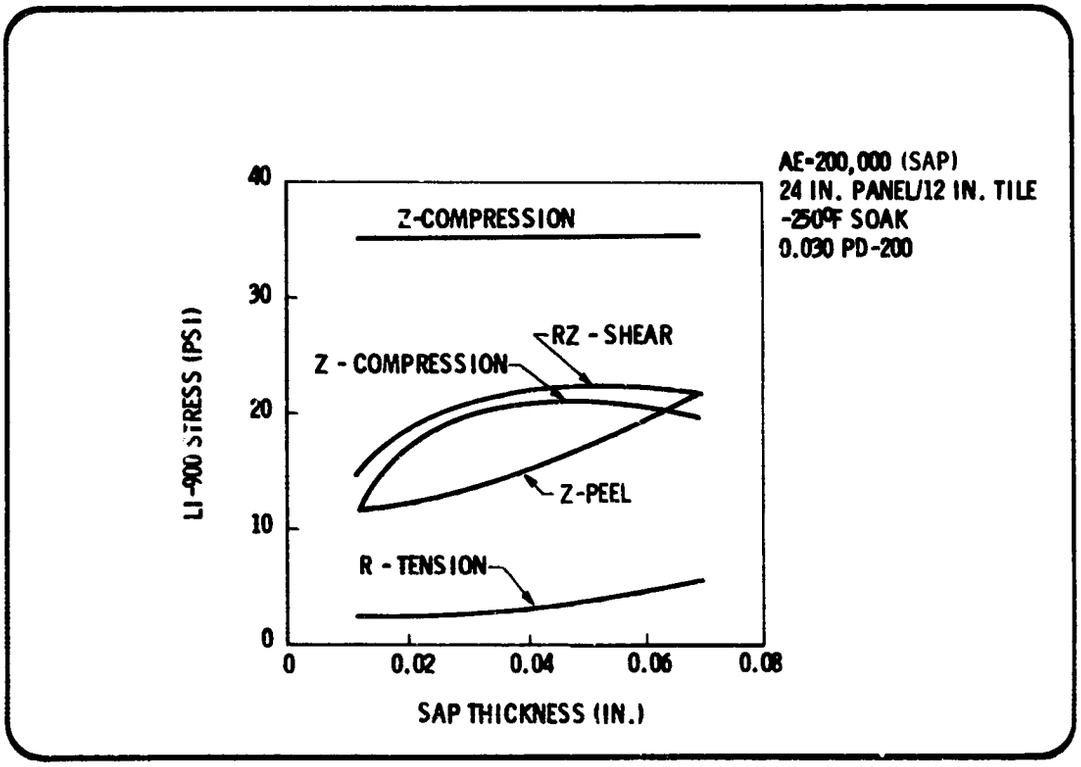

1358003

Fig. 2.3-20 LI-900 Stress Vs Sap Thickness– Weak Direction

The effect on SAP stresses as a function of stiffness and thickness was investigated. As shown in Fig. 2.3-21, SAP stresses increase rapidly at small plate thicknesses. It is therefore necessary to consider the thickness of the plate so that the allowable stresses are not exceeded.

The effect of increasing the SAP dimensions to include more than one tile was investigated, with the results shown in Table 2.3-4. Although normal tension decreased in this study, shear increased to unacceptable levels. Therefore, it appears impractical to extend the SAP beyond the individual tile edges.

Sensitivity of the coefficient of thermal expansion for the SAP composites considered was investigated, with the results shown in Fig. 2.3-22. For the GY-70 graphite baselined in this study, data reflecting a negative coefficient have been reported. For an AE of 200,000 lb, very little difference in LI-900 stresses results when the actual value of the SAP coefficient is changed to that of LI-900. Calculations of this value for the composite to be fabricated under this contract indicate the coefficients will be equal.

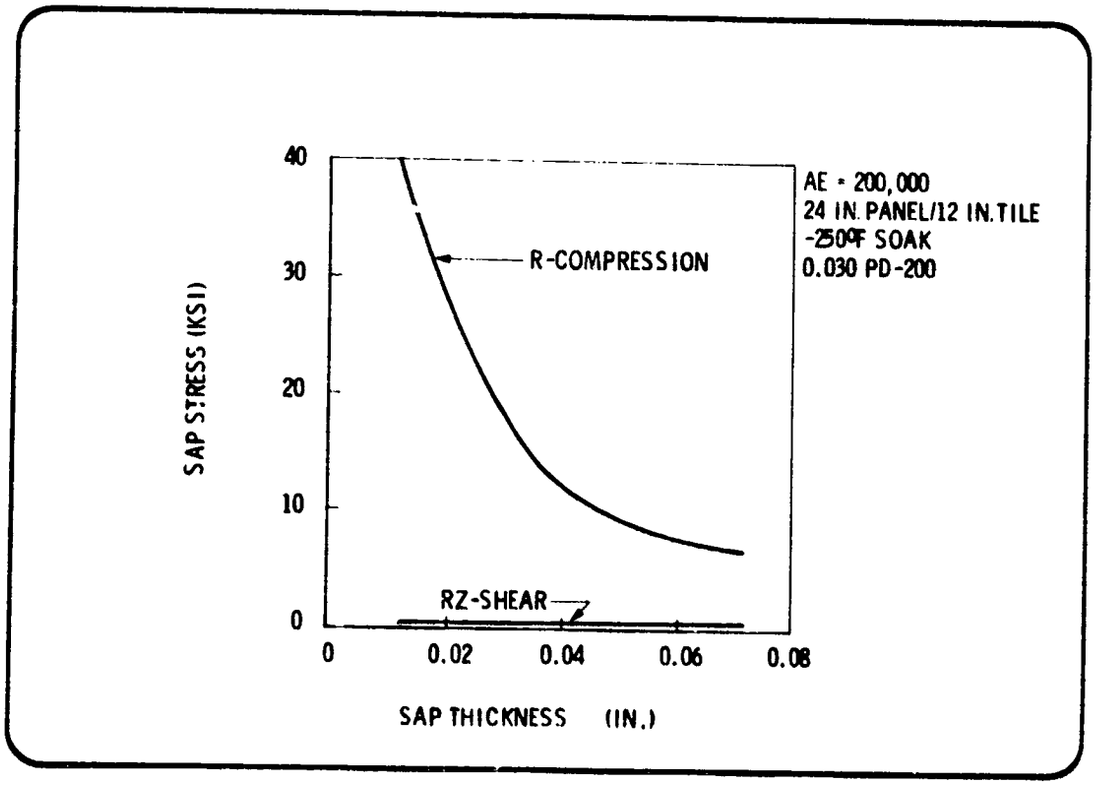

Fig. 2.3-21 SAP Stress Vs SAP Thickness

Table 2.3-4
CONTINUOUS SAP VS INDIVIDUAL TILE SAP

AE = 200,000
SAP t = 0.012
24 IN. PANEL/12 IN. TILE
0.090 PD-200
-250°F SOAK
WEAK DIRECTION

STRESS (PSI)	12 IN. SAP	24 IN. SAP
LONGITUDINAL TENSION	10	4
LONGITUDINAL COMPRESSION	-33	-41
NORMAL TENSION	28	8
NORMAL COMPRESSION	-8	-36
SHEAR	18	64

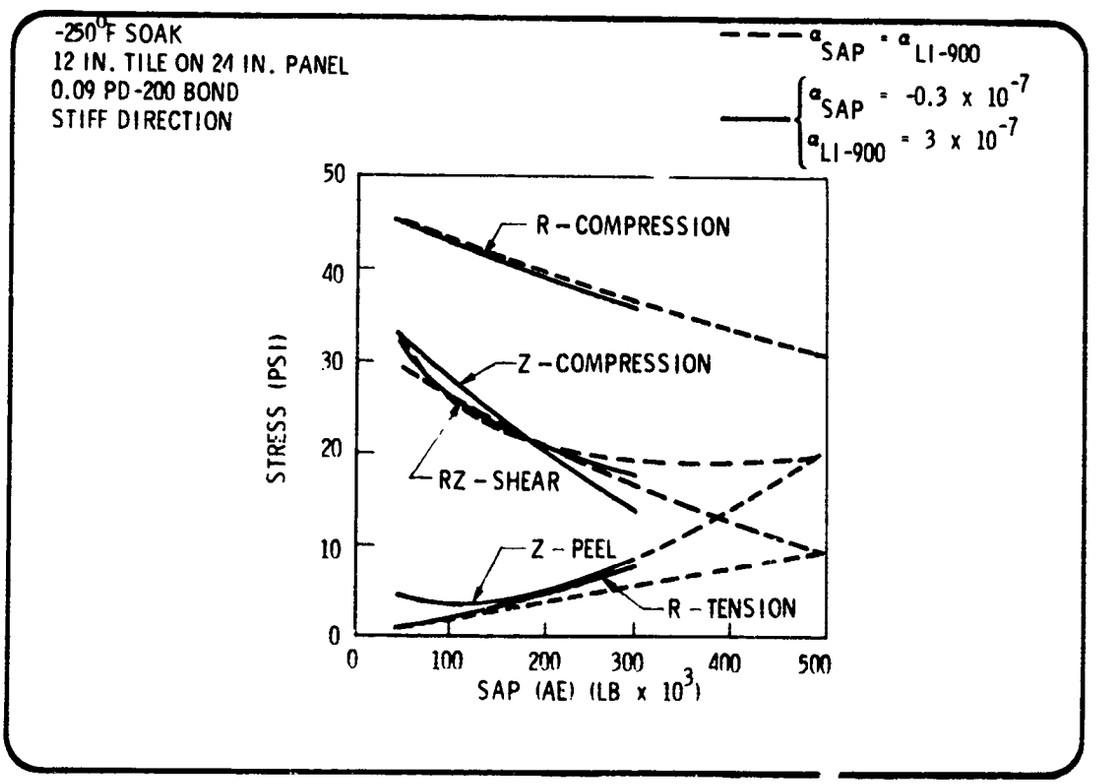

Fig. 2.3-22 LI-900 Stress Vs Strain Arrestor Plate Stiffness

As previously shown, the primary stresses in the LI-900 at the -250°F soak condition are a result of the differential contractions of the attachment and aluminum substrate. Although effects are minor in the substrate for the stiff direction, the weak direction aluminum stresses are substantial because of the thin, unstiffened face sheet. Shown in Fig. 2.3-23 as a function of bond thickness, the composite tends to restrain the aluminum from contracting, resulting in tensile stresses. As the bond thickness is reduced, the high modulus SAP has a greater effect. The stresses also increase with increasing SAP extensional stiffness.

As a result of the various screening studies, a large amount of data has been accumulated. A preliminary design has been established for the bottom (Area 2P) design conditions. The properties used in the analysis were:

Material Properties	E (psi)	G (psi)		α(in./in./°F)
Coating	9.1×10^6	3.99×10^6	0.17	0.4×10^{-6}
LI-900	(15,900) (2448)	3317	0.30	0.4×10^{-6}
Strain Arrestor Plate	16.7×10^6	6.34×10^6	0.32	-0.3×10^{-6}
PD-200 Foam Bond System	12,000	4800	0.25	111.0×10^{-6}
Substrate	11.4×10^6	4.30×10^6	0.30	13.1×10^{-6}

The stress levels shown in Table 2.3-5 are compatible with the LI-900 properties. As stated earlier, the -250°F cold soak condition imposes stresses as severe as the t = 1000 second condition when mechanical loading is present and heating of the bondline begins. The maximum substrate temperature/load condition at touchdown is much less severe than the cold soak.

The data generated in the lower surface study are valuable in establishing a preliminary design. Major relationships previously established generally hold true. The effects on LI-900 stresses of decreasing LI-900 thickness are to increase the shear stress and generally not to effect the peel stress. This is shown in Fig. 2.3-24. Note that the Area 2P design and critical condition (-250°F) are used here.

The effect on coating stresses of decreasing the LI-900 thickness is to greatly increase the compression and shear stresses as shown in Fig. 2.3-25. Again, the Area 2P design and critical condition (-250°F) are used.

2.3.5 Structural Screening for Side and Top Locations

A preliminary design has been established for the side surface. The tile dimensions were decreased from 12-in. square to 6-in. square. The bond thickness increased to 0.090 in. Only the cold soak condition was checked for this screening exercise. The results are shown in Table 2.3-6.

The preliminary design for the top surface is the same as for the side: 6-in. tiles with 0.090 in. bond. Again, only the cold soak condition was considered in screening, with the results shown in Table 2.3-7.

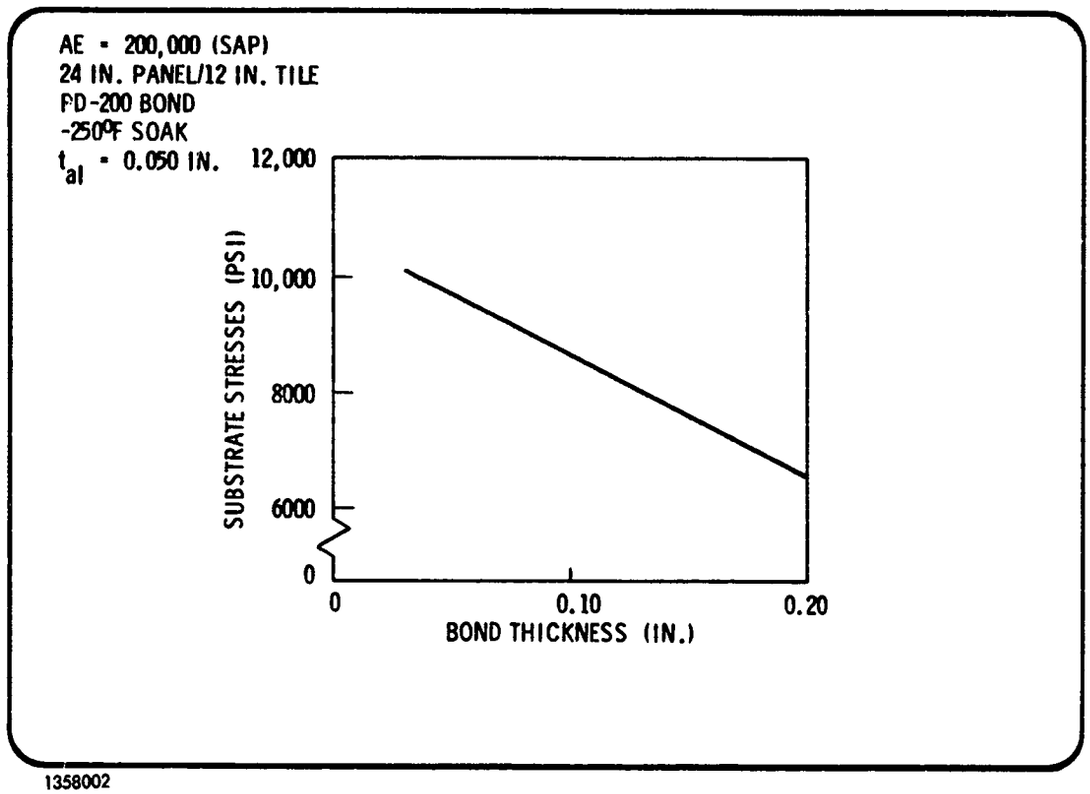

1358002

Fig. 2.3-23 Substrate Stress Vs Bond Thickness – Weak Direction

Table 2.3-5

SCREENING STUDIES

INITIAL RESULTS FOR ORBITER BOTTOM SURFACE (AREA 2P)

TILE LENGTH: 12 IN.
PD-200 FOAM BOND SYSTEM THICKNESS: 0.03 IN.
PANEL LENGTH: 24 IN.
STRAIN ARRESTOR PLATE EXTENSIONAL STIFFNESS: 200,000 IN.
STRAIN ARRESTOR PLATE THICKNESS: 0.012 IN. (BASED ON GY-70/X-904 PROPERTIES)
TILE THICKNESS: 3.45 IN.

LOADING CONDITIONS		AXIAL LOAD OR STRESS	0	0	750 PPI TENSION (t = 1000 SEC)	-450 PPI COMP (t = 1000 SEC)	0 (t = 10,000 SEC)	60,000 PSI TENSION (t = 3600 SEC)
TEMPERATURE		SURFACE (°F)	-250	-250	2,086	2,086	2,086	100
		BACKFACE (°F)	-250	-250	-250	-250	-250	250
SUBSTRATE DIRECTION			STRONG	WEAK	STRONG	STRONG	WEAK	STRONG
MAXIMUM STRESSES (PSI)	COATING	PRIN TENSION	1,102	821	127	405	161	8
		PRIN COMP	-2	-6	-91	-82	-93	-276
		SHEAR	551	411	64	203	80	138
	LI-900	LONG TENSION	1	2	3	4	3	12
		LONG COMPR	-43	-35	-36	-47	-35	-3
		NORMAL TENSION	6	11	2	4	10	2
		NORMAL COMPR	-20	-9	-20	-26	-9	-7
		SHEAR	21	15	18	23	14	6
	STRAIN ARRESTOR	LONG TENSION	-	-	-	-	-	14,031
		LONG COMP	-48,066	-39,296	-40,115	-52,491	-39,221	-
		SHEAR	398	320	334	438	322	43
	PD-200	PRIN TENSION	724	685	653	762	684	61
		PRIN COMP	-446	-401	-358	-505	-407	-59
		SHEAR	573	543	496	620	545	60
	SUBSTRATE STRESS	LONG TENSION	2,282	10,000	7,974	-	9,975	60,157
		LONG COMPR	-	-	-	-4,387	-	-

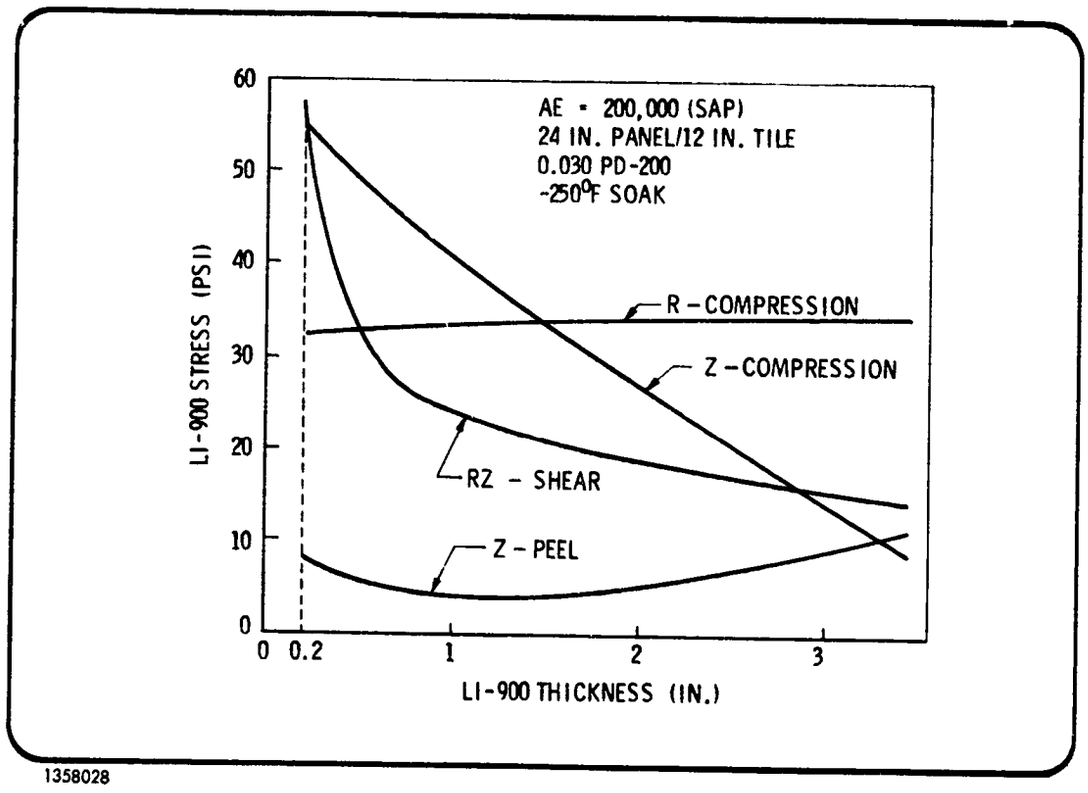

Fig. 2.3-24 LI-900 Stress Vs LI-900 Thickness – Weak Direction

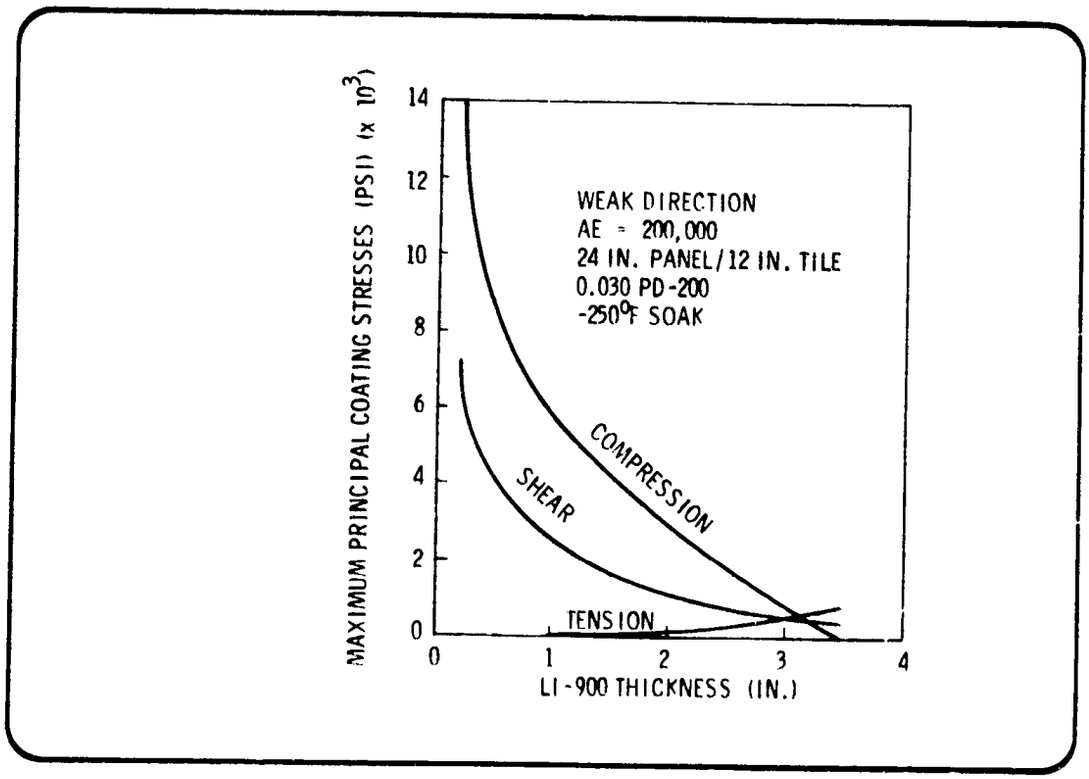

Fig. 2.3-25 Principal Coating Stress Vs LI-900 Thickness

Table 2.3-6

SCREENING STUDIES

INITIAL RESULTS FOR ORBITER SIDE SURFACE

TILE LENGTH	: 6 IN.
PD-200 FOAM BOND SYSTEM THICKNESS	: 0.090 IN.
PANEL LENGTH	: 24 IN.
STRAIN ARRESTOR PLATE EXTENSIONAL STIFFNESS	: 200,000 LB
STRAIN ARRESTOR PLATE THICKNESS	: 0.012 IN.
TILE THICKNESS	: 0.538 IN.

LOADING CONDITIONS		AXIAL LOAD OR STRESS	0	0
TEMPERATURE		SURFACE (°F) BACKFACE (°F)	-250 -250	-250 -250
SUBSTRATE DIRECTION			STRONG	WEAK
MAXIMUM STRESSES (PSI)	COATING	PRIN TENSION PRIN COMP SHEAR	1 -1,700 850	2,471 -2 1,235
	LI-900	LONG. TENSION LONG. COMP NORMAL TENSION NORMAL COMP SHEAR	6 -25 4 -21 17	15 -22 40 -8 21
	STRAIN ARRESTOR	LONG. TENSION LONG. COMP SHEAR	- -29,361 350	- -24,993 308
	PD-200	PRIN TENSION PRIN COMP SHEAR	531 -234 356	509 -182 329
	SUBSTRATE STRESS	LONG. TENSION LONG. COMP	1,373 -469	5,007 -58

Table 2.3-7

SCREENING STUDIES

INITIAL RESULTS FOR ORBITER TOP SURFACE

TILE LENGTH	: 6 IN.
PD-200 FOAM BOND SYSTEM THICKNESS	: 0.09 IN.
PANEL LENGTH	: 24.0 IN.
STRAIN ARRESTOR PLATE EXTENSIONAL STIFFNESS	: 200,000 LB
STRAIN ARRESTOR PLATE THICKNESS	: 0.012 IN. (BASED ON GY-70/X-904 PROPERTIES)
TILE THICKNESS	: 0.20 IN.

LOADING CONDITIONS		AXIAL LOAD OR STRESS	0	0
TEMPERATURE		SURFACE (°F) BACKFACE (°F)	-250 -250	-250 -250
SUBSTRATE DIRECTION			STRONG	WEAK
MAXIMUM STRESSES (PSI)	COATING	PRIN TENSION PRIN COMP SHEAR	3 -4,950 2,475	1,769 -43 884
	LI-900	LONG. TENSION LONG. COMP NORMAL TENSION NORMAL COMP SHEAR	5 -24 3 -22 31	10 -19 20 -7 19
	STRAIN ARRESTOR	LONG. TENSION LONG. COMP SHEAR	- -28,072 367	- -22,975 323
	PD-200	PRIN TENSION PRIN COMP SHEAR	535 -248 3 3	505 -207 338
	SUBSTRATE STRESS	LONG. TENSION LONG. COMP	1,420 -482	4,770 -49

2.4 DETAIL DESIGN STUDIES

As a result of the strain arrestor system screening studies described in Subsections 2.2 and 2.3, a specific strain arrestor system was selected. This is described in detail in Subsection 2.5, Prototype Panel Design Analysis. Using this system, detail design analyses have been performed for three locations on the orbiter vehicle – bottom, side, and top. These analyses are discussed in this subsection under the following topics.

- Design conditions
- Material properties
- Configuration and analysis models
- Analysis cases
- Results of detail design analyses

2.4.1 Design Conditions

Design conditions applicable to the detail design analyses were discussed in Subsection 2.1. These included reentry heating (Figs. 2.1-1 and 2.1-2), limit substrate differential pressure (Fig. 2.1-3), and bond line temperatures and load histories for the three locations (Figs. 2.1-4 through 2.1-6).

The point design requirements have been specified by NASA/MSC.* LMSC has complied with these requirements in the design effort.

Structural Design Requirements

Ultimate Factor-of-Safety:	1.5
Combined Loading:	Summation of ratio of the allowable load to combined limit loads $\geq$ 1.35
Panel Flutter:	Flutter-free for 1.5 times local dynamic pressures at any flight Mach number

Thermal Design Requirements

Design factors of safety are not applied to the heating rates for the specified vehicle areas shown in Fig. 2.5-1. The heating rate for Area 2 has been perturbed to result in a maximum surface temperature of 1533°K (2300°F), as shown on Fig. 2.5-2. Adiabatic conditions have been assumed for the panels in insulation sizing efforts.

2.4.2 Material Properties

Material properties used in the detail design analyses are those presented in Tables 2.1-2 and 2.5-3 through 2.5-5, the same properties used in the prototype panel design analysis described in Subsection 2.5. These properties are somewhat different from

*D. J. Tillian, NASA/MSC, to R. D. Buttram, LMSC, "Point Design Requirements for Two Orbiter Design Areas-Reusable Surface Insulation TPS Development, Phase 2", U. S. Government Two-Way Memo, 21 July 1971

those used for screening studies, since they represent the most recent test data. Also reflected in the detail design analysis are the following changes:

- Construction of the strain arrestor plate has been changed from a quasi-isotropic layup to a layup whose properties are directional. This was done to relieve adverse effects of the directionally-stiffened primary structure (Phase II, Area 2P construction). The details of the strain arrestor plane construction can be found in Section 2.5, Prototype Panel Design.
- The PD-200 foam bond system has been replaced by RM RL-1973/RTV-560 bond system to improve strain isolation at -250°F.

2.4.3 Configuration and Analysis Models

The configurations analyzed in the detail design studies were modeled with the Wilson code finite element code grids shown in Fig. 2.4-1. The key dimensions are listed in Table 2.4-1.

Table 2.4-1

DIMENSIONS OF DETAIL DESIGN CONFIGURATIONS (IN.)

	Bottom	Side	Top
Coating Thickness	0.012	0.012	0.012
Tile Length	12	6	6
Tile thickness	3.00	0.53	0.175
Strain arrestor plate thickness	0.028	0.028	0.028
Bond system thickness	0.073	0.073	0.073

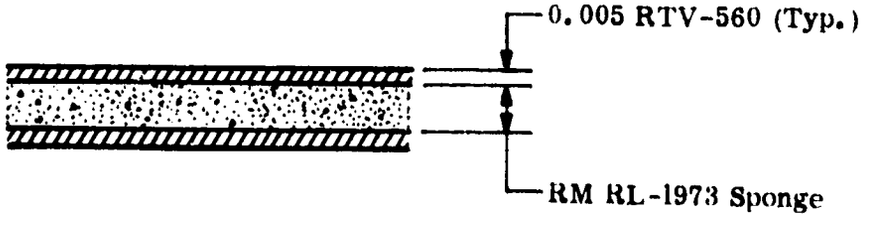

Bond System Geometry at the SAP - Primary Structure Interface

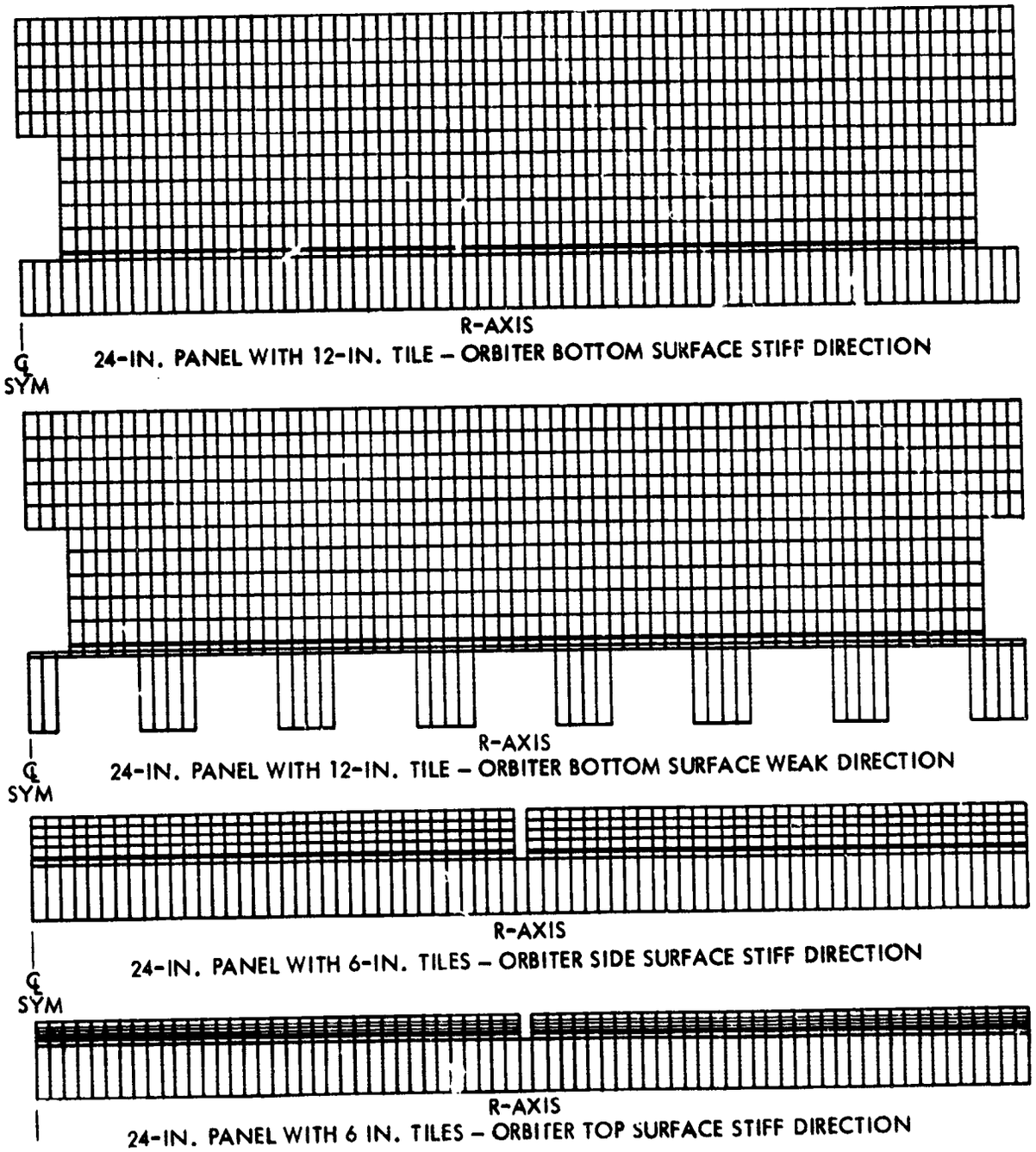

Fig. 2.4-1 Finite Element Models Used for Detail Design

The primary differences between the models used for the screening studies and the detail design models are:

- All screening configurations had butt joints, whereas the detail design studies utilized the proposed joint designs for each surface. A typical joint design for the bottom surface of the orbiter is shown in Fig. 2.4-1. Presently, butt joints are being used for the top and the side surface areas.
- All models for the detail design incorporated the proposed coating schemes. For the bottom surface tiles the 0042 coating is extended down to the mid-point of the thickness of the tiles. The coating covers all five exposed sides of the tiles for the top and side surface configurations. The screening study configurations had coating on the top of the tiles only for all tiles.
- The bond model used for the detail design analysis has three layers, representing each layer of the bond system individually. In the screening studies only one layer of bond with corresponding effective material properties was used.

2.4.4 Analysis Cases

The analysis cases shown in Table 2.4-2 have been chosen to satisfy the present contract requirements that TPS panels shall be designed to withstand loads and temperatures encountered during ascent, orbit, entry, cruise, touchdown, and after touchdown (when applicable).

Ascent. Phase II efforts (NAS 9-12083) indicated that the most critical loading condition during ascent for the TPS system at Area 2P occurs at 60 seconds from launch, when the pressure loads peak to 4.0 psi limit (6.00 ultimate) at room temperature. Simultaneously, the panel is exposed to 1500 lb/in. limit (2250 lb/in. ultimate) compression line load. This critical load condition has been applied to panels at three orbiter locations.

Orbit. One of the present contract requirements dictates that the TPS system shall be designed to -250°F soak condition during orbit. This condition is critical because the strain isolation capability of the bond system at the primary structure interface is reduced considerably at this extreme low temperature.

The -250°F soak condition has been applied to panels at three locations. Because of directional properties of the primary structure (stiffened skin configuration), it was necessary to perform the analysis twice for each panel, covering the strong and weak directions.

Descent. During descent the tiles at the bottom surface experience high initial surface temperatures and gradients. The steepest temperature gradient through the tile occurs at around 500 seconds from reentry. At this time the surface (coating) of the tile is at 2300°F while the substrate is still at -250°F. This condition has been checked in Subsection 2.5.

Table 2.4-2

DETAIL DESIGN STUDY: ANALYSIS CASES

	Case No.	Location	Substrate Model	Initial Temp. °F	Time Sec	Bond Line Temp. °F	Surface Temp. °F	Nx lb/in.	ΔP Psi	Remarks
Ascent	10BS	Bottom	Strong	75	60	75	75	-2250	6.75 Coll.	
	8SS	Side	Strong	75	60	75	75	-2250	6.75 Coll.	
	7TS	Top	Strong	75	60	75	75	-2250	6.75 Coll.	Maximum
	11BW	Bottom	Weak	75	60	75	75	0	6.75 Coll.	Pressure
	9SW	Side	Weak	75	60	75	75	0	6.75 Coll.	
	8TW	Top	Weak	75	60	75	75	0	6.75 Coll.	
Orbit	2BS	Bottom	Strong	-250		-250	-250	0	0	
	2SS	Side	Strong	-250		-250	-250	0	0	Orbit,
	2TS	Top	Strong	-250	–	-250	-250	0	0	Maximum
	1BW	Bottom	Weak	-250		-250	-250	0	0	Cold Soak
	1SW	Side	Weak	-250		-250	-250	0	0	
	1TW	Top	Weak	-250		-250	-250	0	0	
Descent	3BS	Bottom	Strong	-250	1000	-248	2130	-389	0	Steepest Temp. Gradient
	4BW	Bottom	Weak	-250	1000	-248	2130	0	0	Steepest Temp. Gradient
	5BS	Bottom	Strong	-250	2700	-128	400	-2170	.75 Burst	High Substrate Strain
	6BS	Bottom	Strong	70	3600	228	100	-3000	.75 Burst	High Substrate Strain
	7BS	Bottom	Strong	-250	3600	-31	100	6000	3 Coll.	High Substrate Strain
	8BW	Bottom	Weak	70	6000	304	100	0	0	Max. Substrate Temp.
	9BS	Bottom	Strong	70	6000	304	100	0	0	Max. Substrate Temp.
	3SS	Side	Strong	-250	700	-120	1020	-389	0	Steepest Temp. Gradient
	4SS	Side	Strong	70	1800	292	100	4050	3 Coll.	Max. Substrate Temp.
	5SW	Side	Weak	70	1800	292	100	0	3 Coll.	Max. Substrate Temp.
	6SS	Side	Strong	70	2400	260	100	6000	3 Coll.	Max. Substrate Strain
	3TS	Top	Strong	70	700	212	588	778	0	
	4TW	Top	Weak	70	1300	304	303	0	0	Max. Substrate Temp.
	5TS	Top	Strong	70	1800	256	100	4050	3 Coll.	
	6TS	Top	Strong	70	2400	188	100	6000	3 Coll.	Max. Substrate Strain

Other reentry conditions are based on the bond line temperature/line load history curves for the bottom, side and top surfaces represented by Fig. 2.1-4, 2.1-5 and 2.1-6 and the pressure history curve given by Fig. 2.1-3. Note that temperature/load curves include two initial reentry temperatures, -250°F and 70°F, respectively. The critical conditions have been chosen to reflect the maximum strain at the substrate (mechanical and thermal combined) along with pressures that increase the expected curvature of the panel resulting from thermal loading. Also note that these figures represent limit loads and pressures. Ultimate values (1.5 x limit) have been used for the analysis.

Temperature profiles (through the thickness) corresponding to cases other than the soak conditions are given in Figs. 2.4-2 through 2.4.7. These temperature values, along with the corresponding material properties (shown in Tables 2.1-2 through 2.5-5) have been incorporated in the calculations.

Analyses were performed for both substrate directions when the temperature at the bond line (substrate) was the dominant factor in producing high substrate strains.

2.4.5 Results of Detail Design Analyses

The results of the detail design analyses performed for the cases listed in Table 2.4-2 are summarized in Table 2.4-3 which contains values of maximum stresses (tension denoted as +, compression as -), determined for each of the materials in the analysis models. Critical stresses for each case are listed in Table 2.4-4 in comparison with allowable values. Note from this table that the maximum transverse stresses in the LI-900 are predominately compressive and are much below compression strength allowables from LMSC test data. However, if the Mueller Hypothesis (which asserts that the usable compressive strength of the LI material does not exceed the tensile strength, see Appendix A1) is used, then negative margins are indicated in relation to average tensile strengths for two cases (cases 10BS and 4 BW) and for several other cases in relation to minimum values. This results from the fact that the limited LI-900 test data currently available indicates a "notch" in transverse tensile strength at room temperature, e.g., the values are lower than those for either lower temperatures (-250°F) or higher temperatures (400°F and higher). Also note that Table 2.4-4 does not include the comparison of critical stresses for the bond system with the allowable values. This is mainly because of the lack of allowable data for the bond system present. Likewise, the linear analysis technique used in the calculations does not reflect the true behavior of the bond system, such as the non-linear relaxation phenomena peculiar to these flexible systems. The linear analysis approach, however, is proven to be a conservative approach by tests.

The locations of maximum stresses for each of the analysis configurations are indicated in Figs. 2.4-8a, b, and c, and plots of stress histories versus allowables (using the Mueller hypothesis that the compressive strength allowables are the same as tensile allowables for LI-900) are presented in Figs. 2.4-9 through 2.4-11.

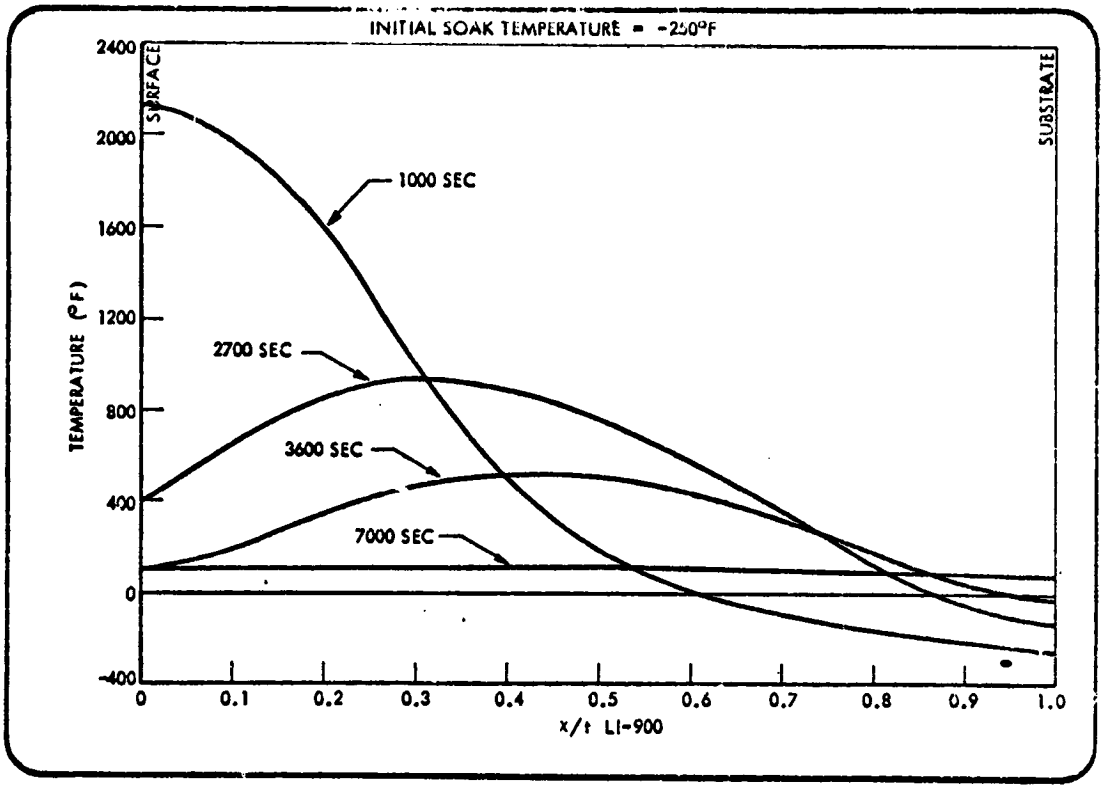

Fig. 2.4-2 LI-900 Temperature Distribution, Orbiter Lower Surface, Initial Soak Temperature = -250°F

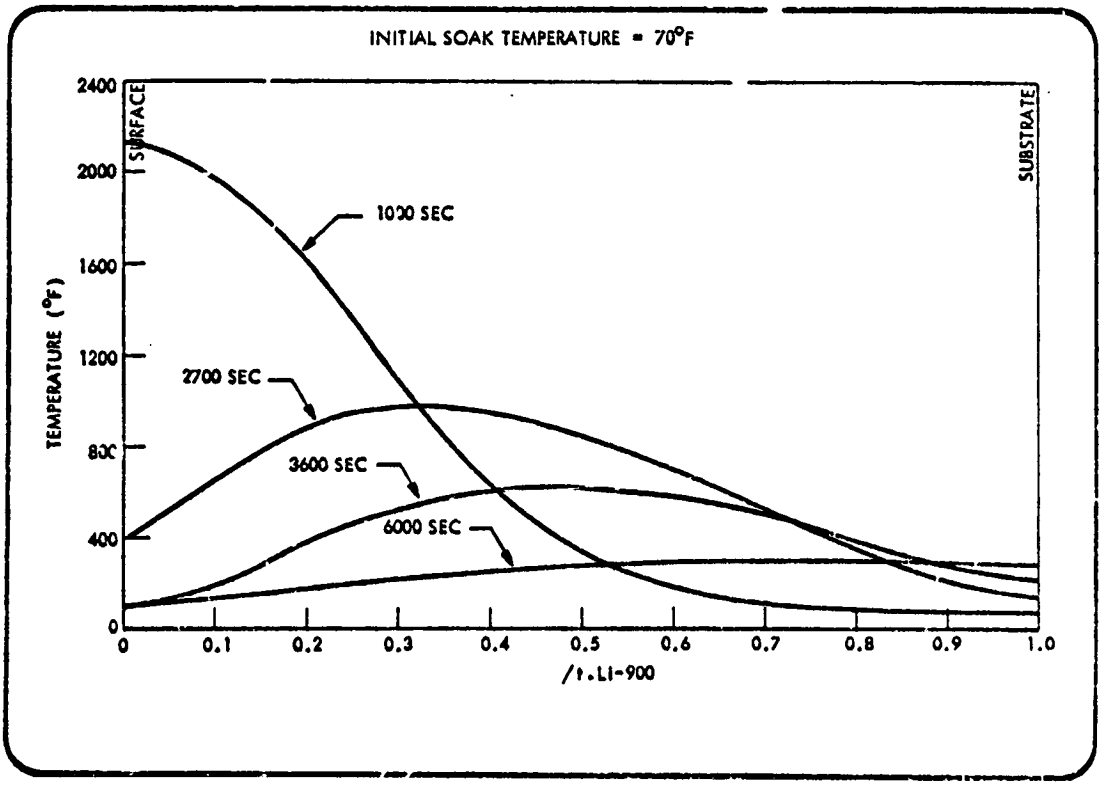

Fig. 2.4-3 LI-900 Temperature Distribution, Orbiter Lower Surface, Initial Soak Temperature = 70°F

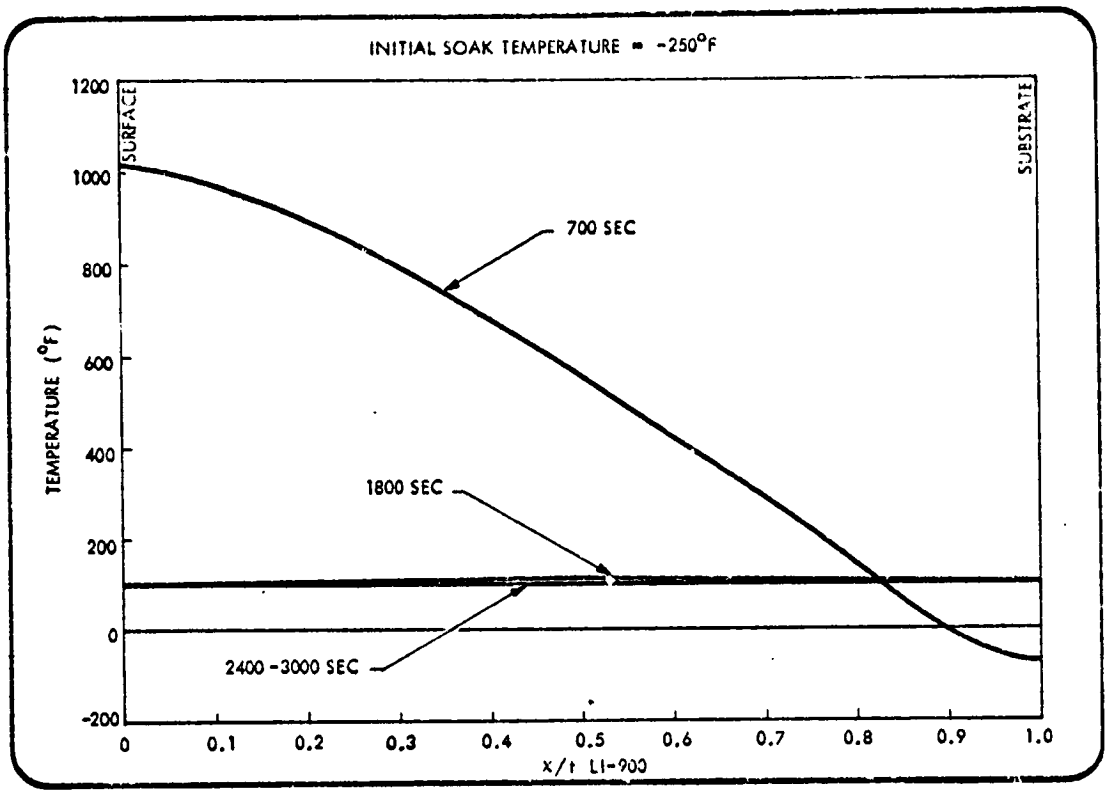

Fig. 2.4-4 LI-900 Temperature Distribution, Orbiter Side Surface, Initial Soak Temperature = -250°F

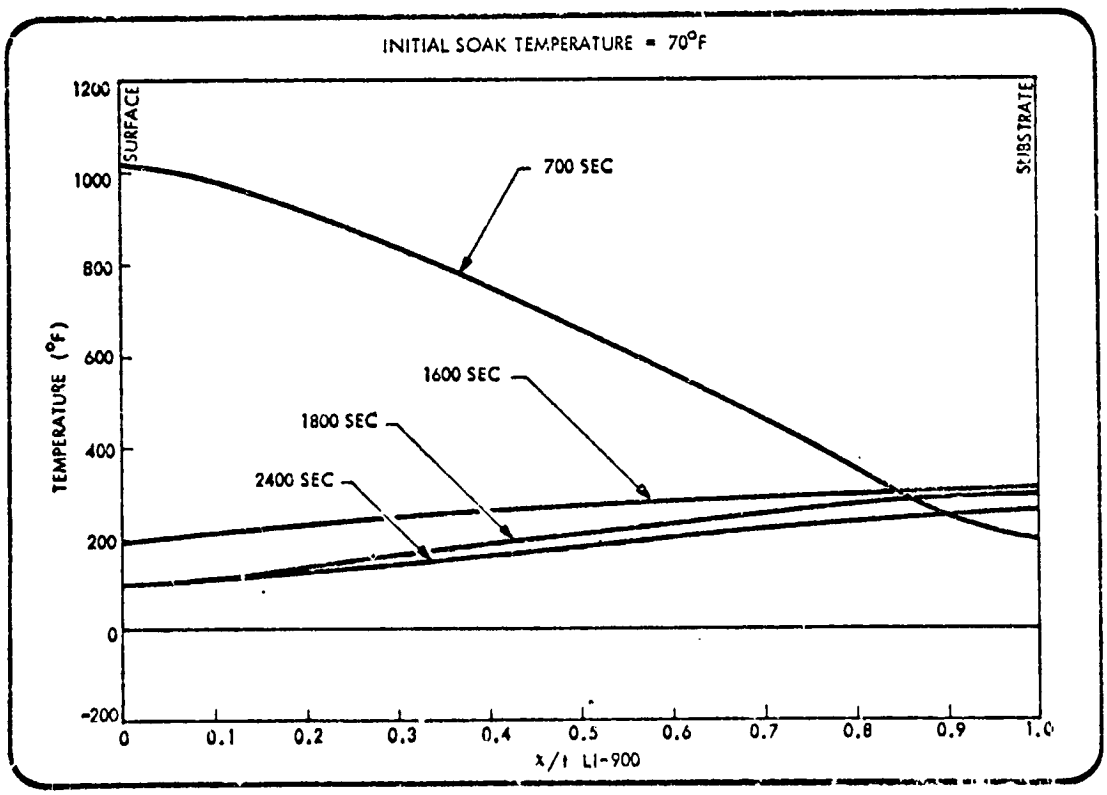

Fig. 2.4-5 LI-900 Temperature Distribution, Orbiter Side Surface, Initial Soak Temperature = 70°F

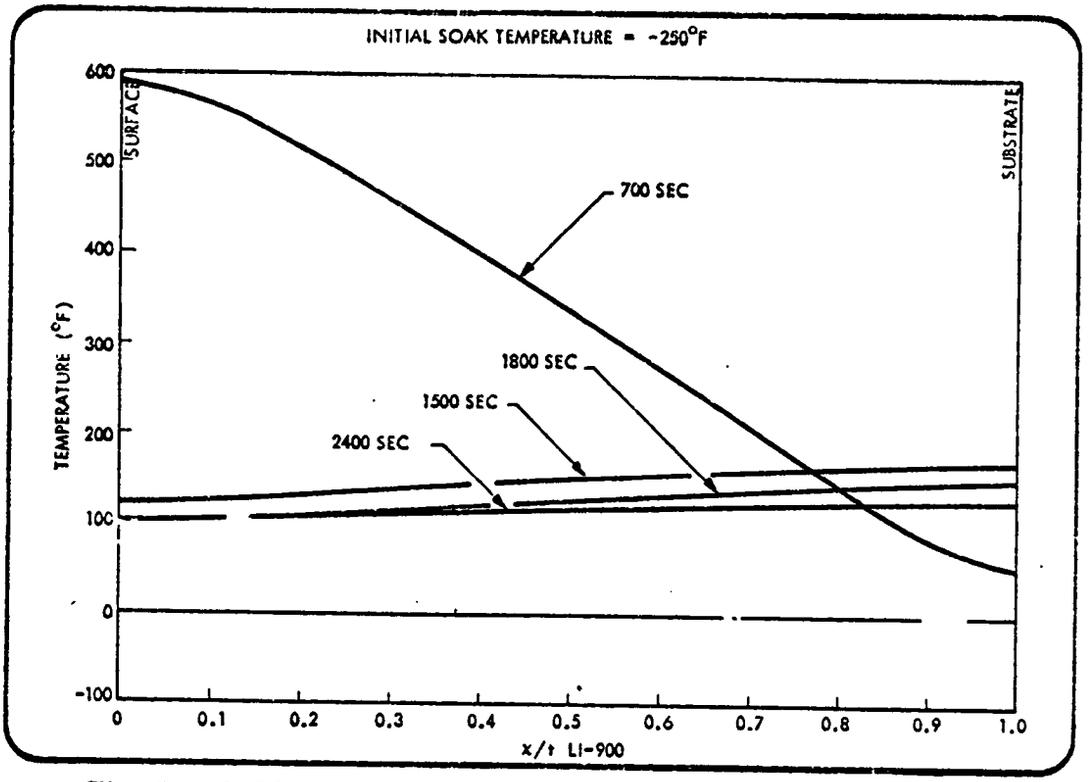

Fig. 2.4-6 LI-900 Temperature Distribution, Orbiter Top Surface, Initial Soak Temperature = -250°F

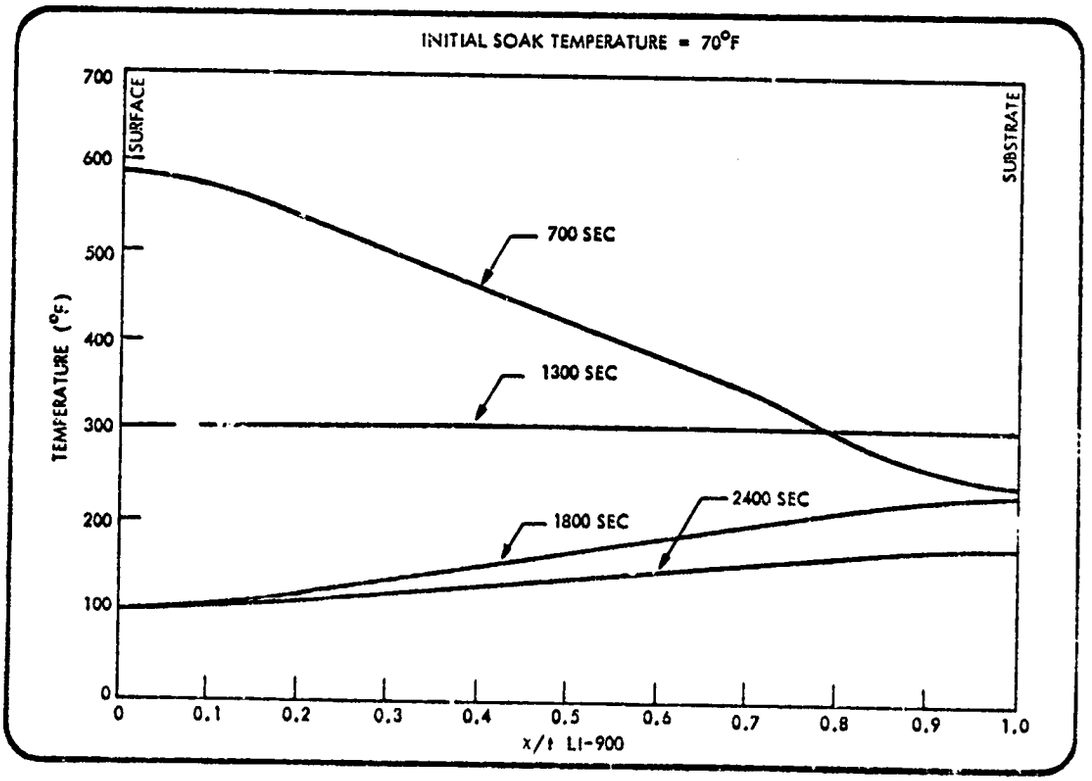

Fig. 2.4-7 LI-900 Temperature Distribution, Orbiter Top Surface, Initial Soak Temperature = 70°F

Table 2.4-3

STRESS RESULTS, ASCENT CONDITIONS, T = 75° F

(All stress values are psi)

Material	Location Case Stress/Model	Bottom 10BS	Side 8SS	Top 7TS	Bottom 11BW	Side 9SW	Top 8TW
		Strong Dir.			Weak Dir.		
Coating	Princ. Tension	155	151	102	237	165	145
	Princ. Compr.	-486	-488	-580	-103	-208	-378
	Princ. Shear	240	240	287	122	109	186
LI-900	R-Tension	2.1	2.0	1.1	1.8	2.0	1.5
	R-Compr.	-3.9	-2.7	-3.0	-3.6	-1.8	-2.2
	Z-Tension		–	–	–	–	–
	Z-Compr.	-19.1	-13.3	-10.3	-11.3	-14.4	-11.4
	RZ-Shear	4.7	-4.0	-4.1	3.9	3.8	5.0
SAP	R-Tension	147	149	167	26.2	110	170
	R-Compr.	-29.8	-24.8	-23.7	-28.7	-14.5	-32
	RZ-Shear	-4.7	-22.2	-14.1	3.4	-22.9	-14
RTV	Princ. Tension	–	–	–	–	–	–
	Princ. Compr.	-22.4	-12.5	-10.7	-10.8	-11.8	-10.3
	Princ. Shear	7.3	3.9	3.5	3.1	3.4	2.9
RM/RL	Princ. Tension	–	–	–	–	–	–
	Princ. Compr.	-20.1	-11.1	-9.5	-10.6	-11.5	-10.0
	Princ. Shear	8.2	4.5	3.9	4.2	4.5	4.0
Aluminum	Princ. Tension	146.8	146.8	146.8	65.3	51.3	52.8
	Princ. Compr.	-22,994	-22,994	-22,994	-70.0	-54.3	-56.1
	Princ. Shear	11,497	11,491	11,492	67.3	52.3	54.3

Table 2.4-4

STRESS RESULTS, ORBIT CONDITIONS, ORBIT COLD SOAK, T = -250°F
(All stress values are psi)

Material	Location / Case / Model/Stress	Bottom 2 BS	Side 2 SS	Top 2 TS	Bottom 1 BW	Side 1 SW	Top 1 TW
		Strong Dir			Weak Dir		
Coating	I Rinc Tension	1,068	204.0	139.0	788.0	394.0	599
	Princ Compr	-107	-483	-2,201	-119	-514	-3,863
	Princ Shear	534	242	1,100	394	257	1,931
LI-900	R-Tension	8.1	9.1	7.4	2.3	-	-
	R-Compr	-32.0	-17.5	-16.7	-42.9	-35.2	-31.6
	Z-Tension	12.2	14.2	1.5	11.0	12.8	5.9
	Z-Compr	-9.6	-20.8	-15.3	-17.0	-13.9	-25.3
	RZ Shear	-11.6	8.3	-17.7	25.1	14.5	31.6
SAP	R-Tension	—	—	—	—	—	—
	R-Compr	-22,559	-13,339	-12,886	-6,559	-5,024	-4,244
	RZ-Shear	345	291	305	203	-169	-203
RTV	Princ Tension	4,695	4,722	4,713	4,578	4,613	4,599
	Princ Compr	-206	-181	-193	-159	-130	-160
	Princ Shear	2,323	2,336	2,332	2,250	2,265	2,257
RM/RL	Princ Tension	765	736	737	685	681	681
	Princ Compr	-201	-161	-173	-108	-75	-106
	Princ Shear	440	410	413	352	336	348
Aluminum	Princ Tension	3,683	2,072	2,112	2,937	1,490	1,733
	Princ Compr	-2,085	-1,228	-1,256	-573	-627	-662
	Princ Shear	1,840	1,030	1,050	1,465	745	865

Table 2.4-5

STRESS RESULTS, DESCENT, BOTTOM SURFACE
(all stress values are psi)

Case		3 BS	4 BW	5 BS	6 BS	7 BS	8 BW	9 BS
Entry Temp (°F)		-250	-250	-250	70	-250	70	70
Time (sec)		1000	1000	2700	3600	3600	6000	6000
Coating	Princ Tension	171	161	236	81.8	206	11.2	14.5
	Princ Compr	-221	-237	-49.7	-192	-21.6	-192	-6.9
	Princ Shear	112	119	118	94.5	103	96	7.3
LI-900	R-Tension	9.9	9.9	3.7	1.1	1.2	13.0	0.23
	R-Compr	-34.5	-42.4	-3.6	-4.1	-1.8	-0.57	-3.1
	Z-Tension	5.5	6.1	6.1	3.1	0.29	2.7	1.3
	Z-Compr	-16.6	-26.7	0.5	-13.6	-0.62	-3.3	-1.7
	RZ-Shear	12.3	27.0	2.3	-4.2	1.4	-9.0	-2.9
SAP	R-Tension	–	–	–	1,289	–	–	527
	R-Compr	-24,465	-6,535	-844		-517	-54.3	–
	RZ-Shear	369	212	7.0	-6.5	3.2	-7.0	2.7
RTV	Princ Tension	4,696	4,591	19.7	2.4	9.7	4.3	2.1
	Princ Compr	-229	-173	-12.9	-23.5	-4.2	-10.7	-13.0
	Princ Shear	2,328	2,257	16.0	11.3	6.8	6.9	7.2
RM/RL	Princ Tension	787	695	31.1	4.2	9.1		3.2
	Princ Compr	-233	-122	-3.4	-17.1	-2.6	-2.9	-6.3
	Princ Shear	465	363	15.8	10.2	5.4	3.6	4.6
Aluminum	Princ Tension	1,200	2,864	67.9	50,501	67.9	15.8	27.4
	Princ Compr	-5,666	-570	-17,430	-275	-24,624	-234	-61.4
	Princ Shear	2,833	1,427	8,715	25,250	12,312	116	30.7

Table 2.4-6

STRESS RESULTS, DESCENT, SIDE SURFACE

(All stress values are psi)

Case		3SS	4SS	5SW	6SS
Entry Temp. (^{o}F)		-250	70	70	70
Time, Sec.		700	1800	1800	2400
Coating	Princ. Tension	139	86.2	125	89.3
	Princ. Compr.	-544	-331	-79.3	-327
	Princ. Shear	272	164	76.4	162
LI-900	R-Tension	6.3	0.84	13.9	0.9
	R-Compr.	–	-3.6	-0.36	-3.1
	Z-Tension	1.2	–	–	–
	Z-Compr.	-4.7	-9.0	-5.1	-9.2
	RZ-Shear	3.0	-2.8	9.1	-2.7
SAP	R-Tension	32.3	438	–	474
	R-Compr.	-54.4	–	-58.8	–
	RZ-Shear	10.0	-14.1	-6.4	-14.0
RTV	Princ. Tension	8.6	–	–	0.87
	Princ. Compr.	-9.0	-16.8	-12.4	-16.3
	Princ. Shear	7.8	7.4	5.3	7.6
RM/RL	Princ. Tension	18.9	1.4	0.14	2.6
	Princ. Compr.	-4.5	-9.4	-5.4	-9.9
	Princ. Shear	10.6	5.0	2.1	5.9
Aluminum	Princ. Tension	1.2	34,498	18.1	50,499
	Princ. Compr.	-3,158	-276	-87.5	-276
	Princ. Shear	1,579	17,249	45.0	25,250

Table 2.4-7

STRESS RESULTS, DESCENT, TOP SURFACE

(All stress values are psi)

Case		3TS	4TW	5TS	6TS
Entry Temp (^{o}F)		70	70	70	70
Time, sec		700	1300	1800	2400
Coating	Princ. Tension	109	819	85.9	84.6
	Princ. Compr.	-793	-15.9	-443	-392
	Princ. Shear	396	409	220	194
LI-900	R-Tension	3.3	13.8	0.70	0.79
	R-Compr.	-2.3	-	-2.5	-1.8
	Z-Tension	0.77	3.1	-	-
	Z-Compr.	-4.3	-0.71	-7.0	-6.8
	RZ-Shear	5.0	-7.1	-3.1	-2.7
SAP	R-Tension	454	-	431	429
	R-Compr.	-	-290	-	-
	RZ-Shear	-10.8	-5.3	-9.2	-8.5
RTV	Princ. Tension	0.64	4.3	-	1.9
	Princ. Compr.	-9.2	-10.7	-13.4	-11.7
	Princ. Shear	3.9	6.4	6.1	5.8
RM/RL	Princ. Tension	0.87	4.3	1.6	2.6
	Princ. Compr.	-4.1	-3.5	-7.9	-7.9
	Princ. Shear	2.0	3.3	4.5	5.0
Aluminum	Princ. Tension	6,226	16.8	34,899	50,500
	Princ. Compr.	-1.9	-96.7	-276	-276
	Princ. Shear	3,113	47.7	17,449	25,250

Table 2.4-8

CRITICAL STRESSES

	Case No.	Location	Substrate Model	Coating – Tension			LI-900 In-Plane			LI-900 Transverse			LI-900 Shear		
					Allowable			Allowable			Allowable			Allowable	
				Stress	Avg	Min	Stress	Avg	Min	Stress	Avg	Min	Stress	Avg	Min
ASCENT	10BS	Bottom	Strong	155	2100	1140	-4	51	47	-19	16	9	5	32	27
	8SS	Side	Strong	151	2100	1140	-3	51	47	-13	16	9	4	32	27
	7TS	Top	Strong	102	2100	1140	-3	51	47	-10	16	9	4	32	27
	11BW	Bottom	Weak	237	2100	1140	-4	51	47	-11	(-47)*	(-43)*	4	32	27
	9SW	Side	Weak	165	2100	1140	2	51	47	-14	(-47)*	(-43)*	4	32	27
	8TW	Top	Weak	145	2100	1140	-2	51	47	-11	(-47)*	(-43)*	5	32	27
ORBIT	2BS	Bottom	Strong	1068	2000	1180	-32	67	49	12	28	20	12	39	35
	2SS	Side	Strong	204	2000	1180	-18	67	49	-21	28	20	8	39	35
	2TS	Top	Strong	139	2000	1180	-17	67	49	-15	28	20	18	39	35
	1BW	Bottom	Weak	788	2000	1180	-43	67	49	-17	(-47)*	(-43)*	25	39	35
	1SW	Side	Weak	394	2000	1180	-35	67	49	-14	(-47)*	(-43)*	15	39	35
	1TW	Top	Weak	599	2000	1180	-32	67	49	-25	(-47)*	(-43)*	32	39	35
ESCENT	3BS	Bottom	Strong	171	2000	1360	-35	67	48	-17	25	19	12	32	27
	4BW	Bottom	Weak	161	2000	1360	-42	67	48	-27	(-47)*	(-43)*	27	32	27
	5BS	Bottom	Strong	236	2075	1187	4	70	62	3	24	20	2	32	27
	6BS	Bottom	Strong	82	2100	1140	-4	51	47	-14	16	9	4	32	27
	7BS	Bottom	Strong	206	2100	1140	-2	51	47	3	16	9	1	32	27
	8BW	Bottom	Weak	11	2100	1140	13	51	47	-3	(-47)*	(-43)*	9	32	27
	9BS	Bottom	Strong	15	2100	1140	-3	51	47	-2	(-47)*	(-43)*	3	32	27
	3SS	Side	Strong	139	2029	1302	6	59	48	-5	23	17	3	32	27
	4SS	Side	Strong	86	2100	1140	-4	51	47	-9	16	9	3	32	27
	5SW	Side	Weak	125	2100	1140	14	51	47	-5	16	9	9	32	27
	6SS	Side	Strong	89	2100	1140	-3	51	47	-9	16	9	3	32	27
	3TS	Top	Strong	109	2079	1187	3	70	62	-4	24	20	5	32	27
	4TW	Top	Weak	819	2079	1187	14	70	62	3	24	20	7	32	27
	5TS	Top	Strong	86	2100	1140	-3	51	47	-7	16	9	3	32	27
	6TS	Top	Strong	85	2100	1140	-2	51	47	-7	16	9	3	32	27

*Compressive Strength Values (see pp. B2-36 and B2-37).

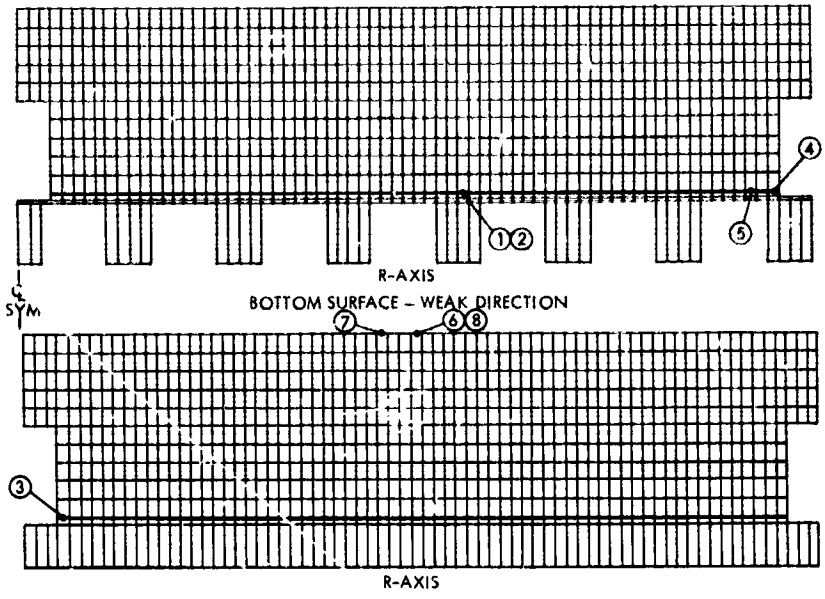

LOCATION	MAX. LI-900 STRESS (PSI)		TIME
1	R – TENSION	13	6000 SEC, REENTRY, MAX. SUBSTRATE TEMP
2	R – COMPRESSION	-43	-250°F COLD SOAK
	Z – TENSION	12	-250°F COLD SOAK
4	Z – COMPRESSION	-27	1000 SEC, REENTRY, STEEP TEMP. GRADIENT
5	RZ – SHEAR	27	1000 SEC, REENTRY, STEEP TEMP. GRADIENT
	MAX. COATING STRESS (PSI)		
6	PRINCIPLE TENSION	1068	-250°F COLD SOAK
7	PRINCIPLE COMPR	-486	ASCENT
8	PRINCIPLE SHEAR	534	-250°F COLD SOAK

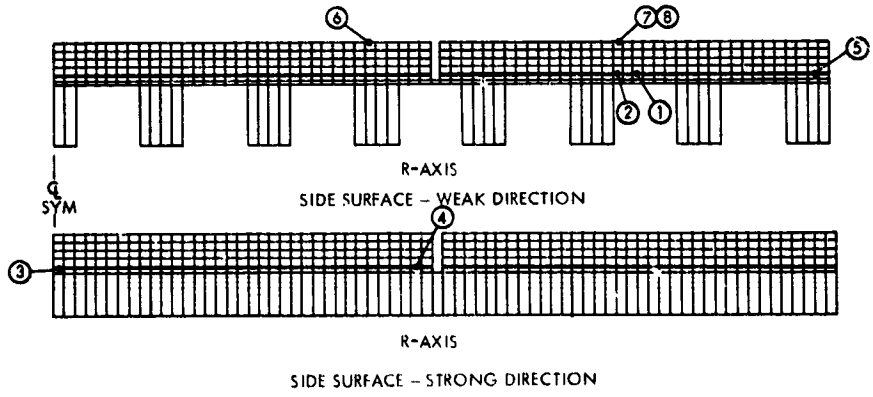

LOCATION	MAX. LI-900 STRESS (PSI)		TIME
1	R – TENSION	14	1800 SEC, REENTRY, MAX. SUBSTRATE TEMP.
2	R – COMPRESSION	-35	-250°F COLD SOAK
3	Z – TENSION	14	-250°F COLD SOAK
4	Z – COMPRESSION	-21	-250°F COLD SOAK
5	RZ – SHEAR	15	-250°F COLD SOAK
	MAX. COATING STRESS (PSI)		
6	PRINCIPLE TENSION	394	-250°F COLD SOAK
7	PRINCIPLE COMPR.	-544	700 SEC, REENTRY, MAX. COATING TEMP.
8	PRINCIPLE SHEAR	272	700 SEC, REENTRY, MAX. COATING TEMP.

Fig. 2.4-8 Location of Critical Stress Elements

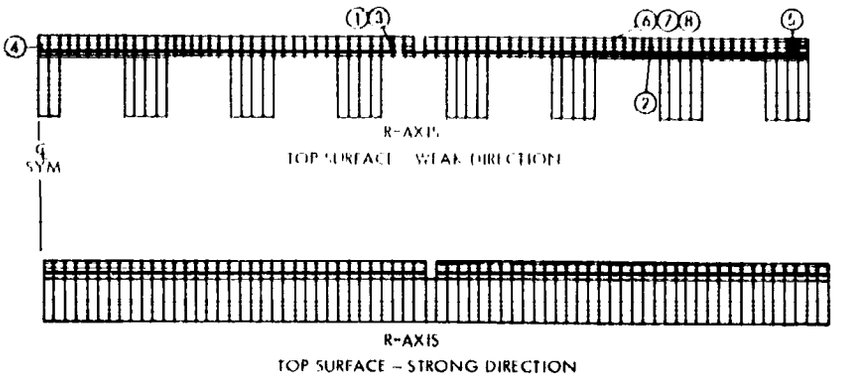

LOCATION	MAX. LI-900 STRESS (PSI)		TIME
1	h – TENSION	14	1300 SEC, REENTRY, MAX. SUBSTRATE TEMP.
2	R – COMPRESSION	-32	-250°F COLD SOAK
3	Z – TENSION	6	-250°F COLD SOAK
4	Z – COMPRESSION	-25	-250°F COLD SOAK
5	RZ – SHEAR	32	-250°F COLD SOAK
	MAX. COATING STRESS (PSI)		
6	PRINCIPLE TENSION	819	1300 SEC, REENTRY, MAX. SUBSTRATE TEMP.
7	PRINCIPLE COMPR.	-3863	-250° F COLD SOAK
8	PRINCIPLE SHEAR	1931	-250°F COLD SOAK

Fig. 2.4-8 Location of Critical Stress Elements (Cont'd)

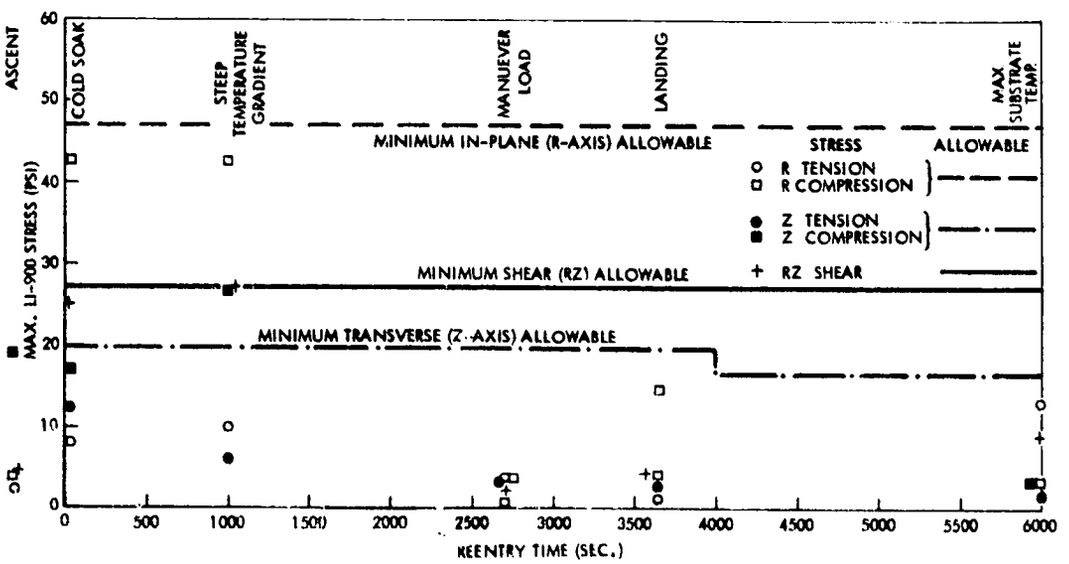

Fig. 2.4-9 LI-900 Stress History During Reentry – Orbiter Side Surface

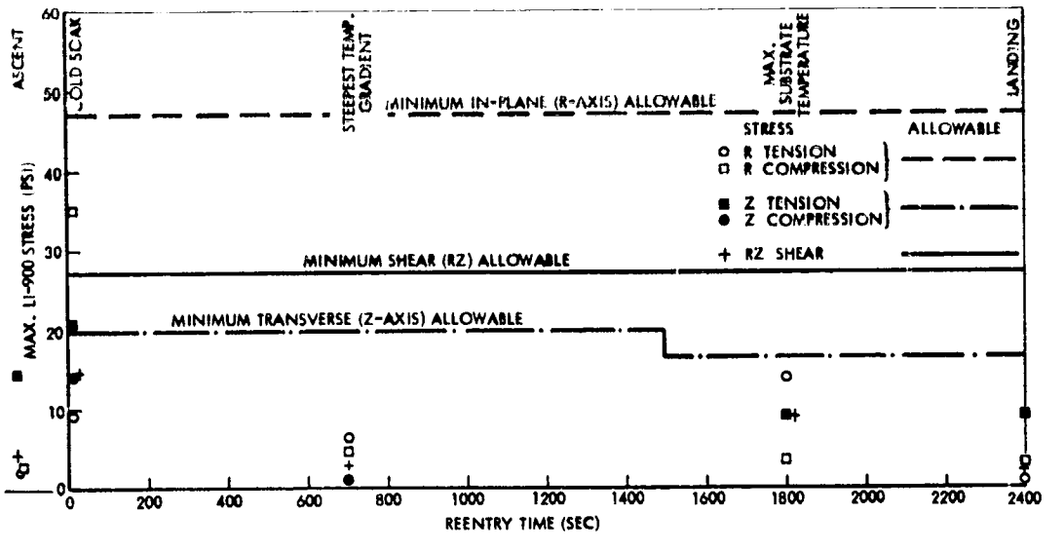

Fig. 2.4-10 LI-900 Stress History During Reentry – Orbiter Side Surface

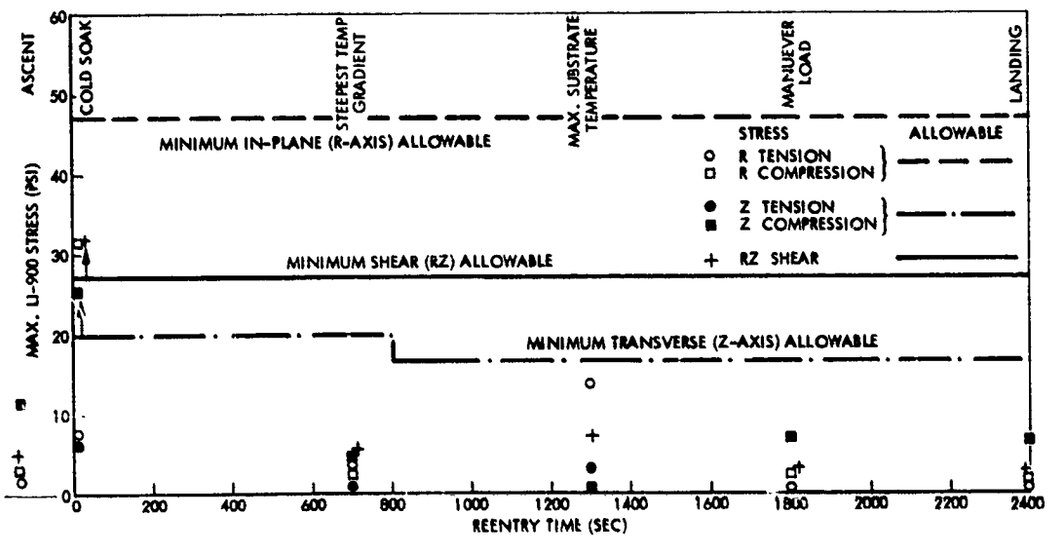

Fig. 2.4-11 LI-900 History During Reentry – Orbiter Top Surface

2.5 PROTOTYPE PANEL DESIGN ANALYSIS

One prototype panel is to be designed, analyzed, fabricated, and delivered to NASA/MSC under this program. The panel is to meet the design requirements specified by NASA/MSC and listed herein in Par. 2.5.1.

The panel is representative of the orbiter Area 2P structure and is identical in cross-sectional detail to that of Aluminum Panel No. 2 of Phase II contract NAS9-12082. The panel has been lengthened to 1.25 m (49.20 in.) to fit NASA/MSC test fixtures and to assure more even strain distribution in the substrate and less stress concentration in the RSI tiles. The 0.305 m (12 in.) LI-900 tiles are bonded to a graphite-epoxy strain arrestor plate riding on a layer of low-density, low modulus, strain-isolating sponge.

The prototype panel test plan is detailed in a separate document, LMSC-D159811, and shown in summary in Table 2.5-1. In addition to the thermal and loading conditions of the Phase II contract, the 116°K (-250°F) cold soak condition is to be met. For re-entry stress calculations, a starting soak temperature of both 116°K (-250°F) and room temperature was used as shown in Fig. 2.5-1.

For the prototype panel, a strain arrestor plate was specifically designed having optimum stiffness in the stiffened and unstiffened substrate directions to result in lowest LI-900 stresses. Parametric curves from subsection 2.3 were used to optimize design thicknesses and dimensions to ensure lowest possible LI-900 and coating stresses.

The prototype panel substrate was designed to have positive margins of safety with ultimate applied loads and with the material properties reduced by high temperature. The coating and LI-900 tiles were designed with positive margins of safety using minimum strength allowables obtained from tests.

2.5.1 Prototype Panel Design Conditions

The point design requirements for the prototype panels have been specified by NASA/MSC*. LMSC has complied with these requirements in the design effort.

Structural Design Requirements

Ultimate Factor-of-Safety:	1.5
Combined Loading:	Summation of ratio of the allowable load to combined limit loads ≥1.35
Panel Flutter:	Flutter-free for 1.5 times local dynamic pressures at any flight Mach number

*D. J. Tillian, NASA/MSC, to R. D. Buttram, LMSC, "Point Design Requirements for Two Orbiter Design Areas-Reusable Surface Insulation TPS Development, Phase 2," U.S. Government Two-Way Memo, 21 July 1971

Table 2.5-1

LI-900 PROTOTYPE PANEL TEST SEQUENCE

Test No.	No. of Cycles	Test
1	1	5.1.1 Axial Load Test
2	1	5.1.2 Radiant Heat Test (1700°F, Atmospheric Pressure)
3	1	5.1.3 Radiant Heat Test (2300°F, Atmospheric Pressure)
4	1	5.1.4 Radiant Heat Test (2300°F, Atmospheric Pressure and Axial Load, Maximum Bondline Temperature Condition)
5	1	5.1.5 Orbit Cooldown Cycle (Atmospheric Pressure)
6	5	5.1.6 Radiant Heat Test (2300°F, Reduced Pressure)
7	1	5.1.7 Acoustic Test
8	10	5.2.1 Radiant Heat Test (2300°F, Reduced Pressure)
9	1	5.2.2 Acoustic Test
10	10	5.2.3 Radiant Heat Test (2300°F, Reduced Pressure)
11	1	5.2.4 Acoustic Test
12	1	5.2.5 Orbit Cooldown Cycle (Atmospheric Pressure)
13	1	5.2.6 Radiant Heat Test (2300°F, Atmospheric Pressure and Axial Load, Maximum Bondline Temperature Condition)

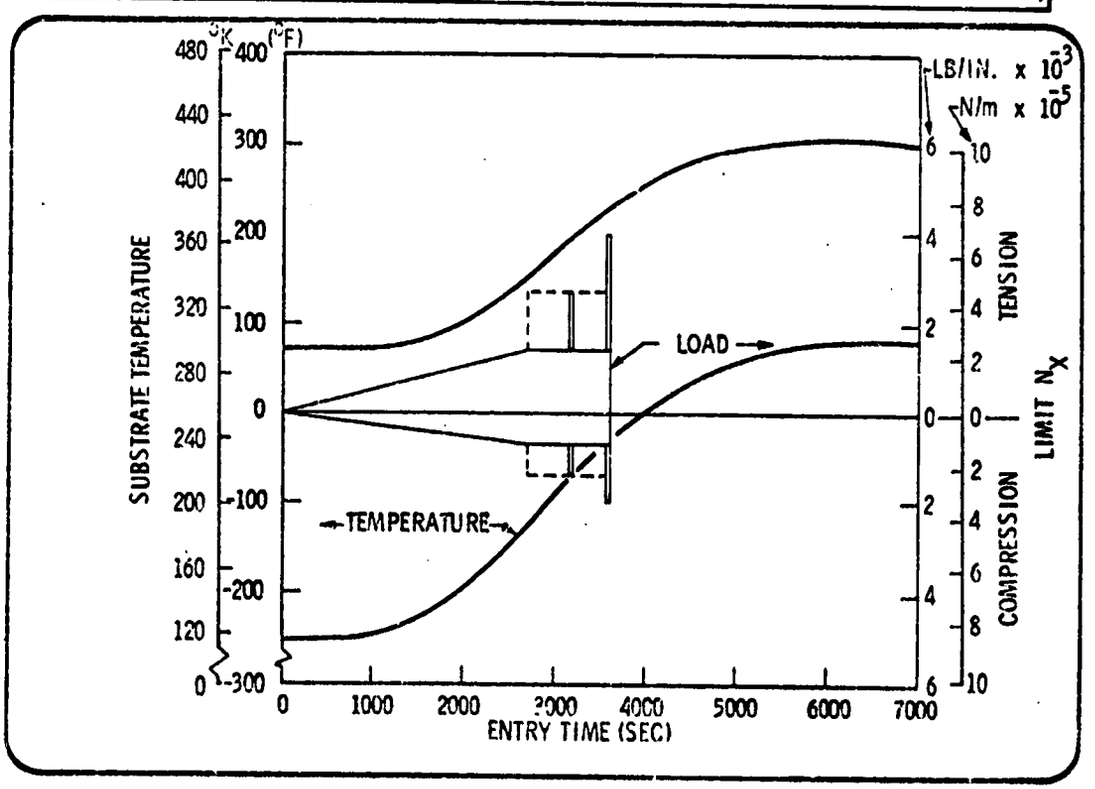

Fig. 2.5-1 Area 2P Temperature/Load History

Thermal Design Requirements

Design factors of safety are not applied to the heating rates for the specified vehicle areas shown in Fig. 2.5-2. The heating rate for Area 2 has been perturbed to result in a maximum surface temperature of 1533°K (2300°F), as shown in Fig. 2.5-3. Adiabatic conditions have been assumed for the panels in insulation sizing efforts.

Environments

The combination of conditions considered and the critical design conditions are summarized in Table 2.5-2.

2.5.2 System Design Properties

The mechanical and thermal properties of the materials used in the prototype panel are summarized in Tables 2.5-3 through 2.5-5 and 2.1-2 and 2.1-3. The following materials are listed: 0042 coating; LI-900; HMS/X-904; RTV-560; RM/RL-1973; and 2024-T86 aluminum.

Both minimum and average strength values are listed for LI-900 and the coating as determined from LMSC testing. Property variation with temperature is included.

Strain arrestor plate properties were deduced by analysis using supplier-published properties for unidirectional lamina. A LMSC-developed computer code called LAMINATE was used to ascertain the overall elastic, thermal and strength properties of orthotropic laminates.

RTV-560 and RM/RL-1973 properties were obtained from test results published by General Dynamics Convair Aerospace Division in support of a NASA contract on RSI adhesive characterization,and properties at 116°K (-250°F) were obtained from LMSC in-house testing.

2.5.3 Design and Analysis of Prototype Panel Substrate

The prototype panel substrate is identical to that of the aluminum panel No. 2, Area 2P, of the Phase II contract NAS9-12083 except for the alloy and the edge stiffeners. The panel was optimally designed to meet requirements set forth by NASA/MSC, as summarized in Table 2.5-2. The alloy was changed from 7075-T6 to 2024-T86 to correspond to the proposed North American shuttle orbiter material. The 2024-T86 alloy has higher strength properties at high temperature 422°K (300°F) and therefore increases the margin of safety of the panel.

The panel end fittings were redesigned to comply with NASA/MSC instructions on panel length and test fixture compatibility (see Fig. 2.5-4). Margins of safety on the panel end fittings were raised and finger-plates added to allow more gradual load transfer into the panel. The increased panel length assures more uniform strain distribution in the test section and avoids stress concentrations arising in the RSI tiles. The edge stiffeners were increased in stiffness to more closely resemble the support provided to a true panel by an orbiter structural longeron or bulkhead (see Fig. 2.5-5). The previous configuration provided little additional support at the edges and the result

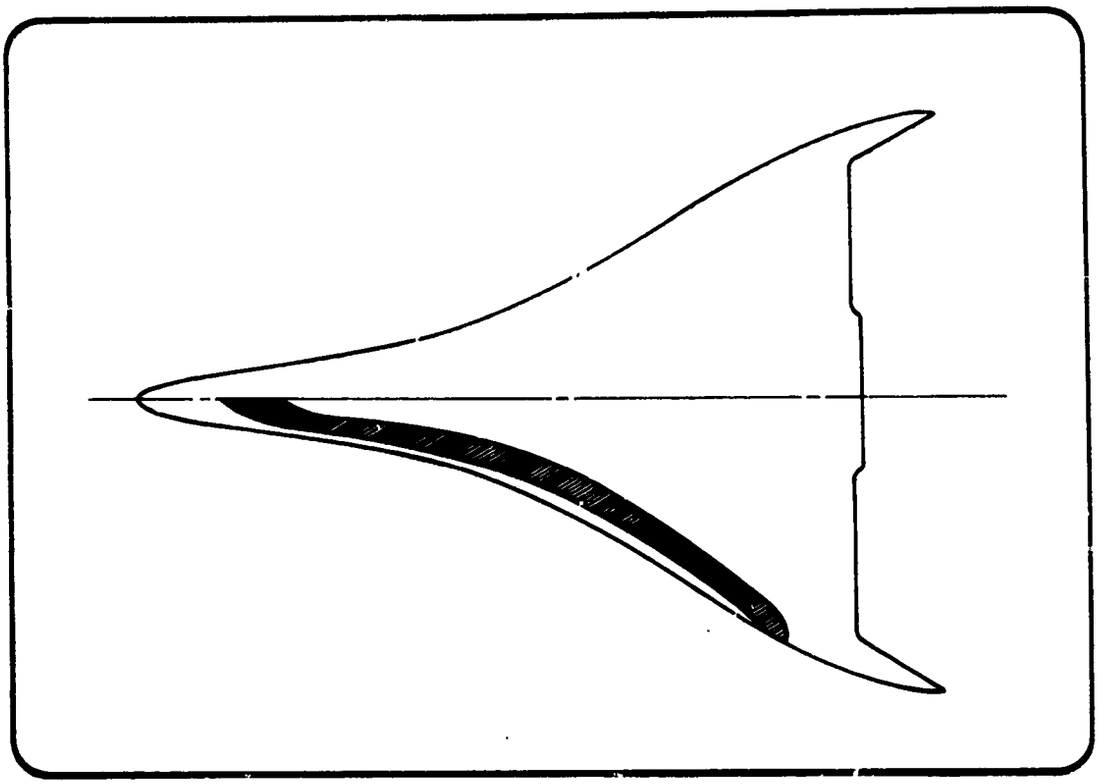

Fig. 2.5-2 TPS Design Area for Orbiter Lower Surface

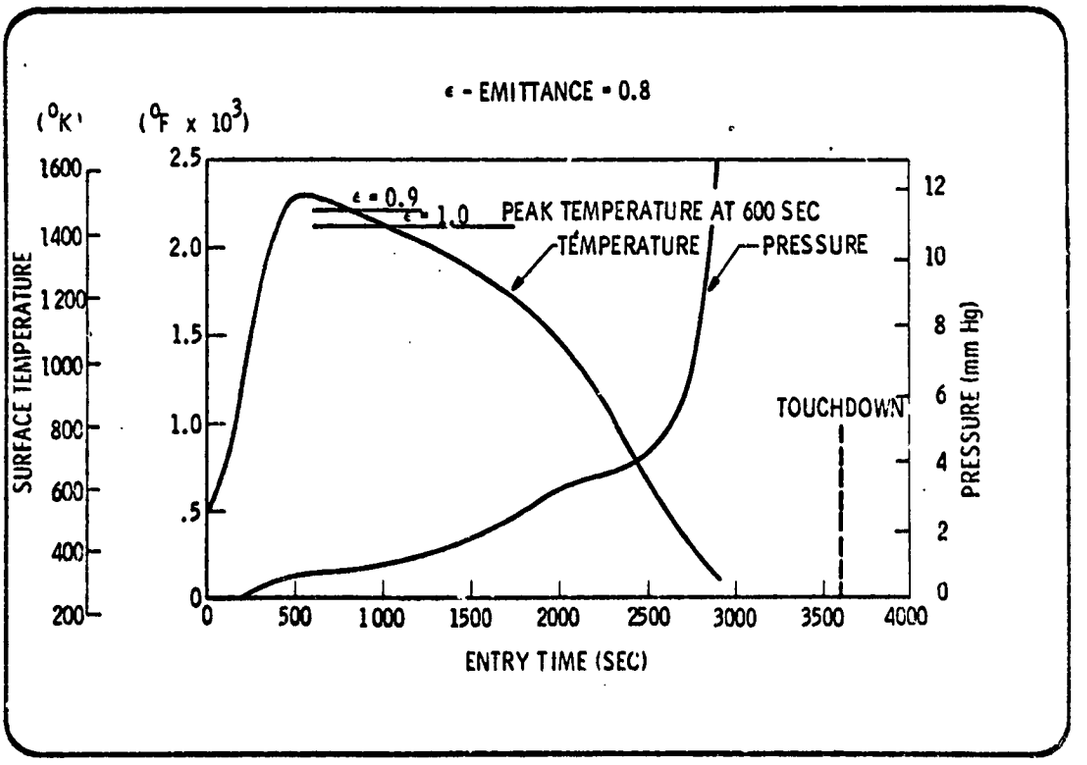

Fig. 2.5-3 Reentry Temp. and Press. Histories – Area 2

Table 2.5-2

ORBITER SHELL DESIGN CONDITIONS

Operation	Elapsed Time	Differential Pressure (Limit) (PSI)		In-Plane Load (Limit) (PPI)		SPL (dB)	Max Surface Temp (°F)	Maximum Backface Temp (Ambient) (°F)
		Collapse	Burst	Tension	Comp.			Aluminum
Launch	–	–	–	–	–	160	–	R.T.
Ascent	60 sec 67 sec 75 sec	+4.0 – +1.8	-3.0 – -1.9	+2300 – +2700	-1500 – -2000	150 161 155	≈200 – –	R.T. R.T. R.T.
Entry	10 min 25-45 min	+0.1 +1.5	-0.0 -0.5	+300 +1400	-200 -700	– 141	2300 1850-400	-250 <300
Post-Entry Cruise	45-60 min	+2.0	-0.5	+2700	-1400	124	≈100	<300
Landing	60 min	+0.5	-0.5	+4000	-2000	124	≈100	<300
Dead Stop	>60 min	–	–	–	–	–	≈100	300

- Plus pressure is collapse (venting allowance included)
- Plus in-plane load is tension
- Factor-of-safety between limit and ultimate is 1.5

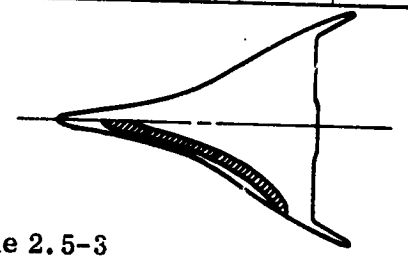

Table 2.5-3

MATERIAL PROPERTIES – PROTOTYPE PANEL

2024-T86 Aluminum

Temperature	116°K (-250°F)	297°K (R.T.)	422°K (300°F)
Elastic Modulus (N/M^2) (PSI)	79.4×10^9 (11.5×10^6)	72.4×10^9 (10.5×10^6)	69×10^9 (10.0×10^6)
Shear Modulus (N/M^2) (PSI)	30.4×10^9 (4.4×10^6)	27.6×10^9 (4.0×10^6)	26.2×10^9 (3.8×10^6)
Poisson's Ratio	0.33	0.33	0.33
Thermal Expansion ($M/M/^oK$) (in./in./°F)	14.8×10^{-6} (8.2×10^{-6})	22.2×10^{-6} (12.3×10^{-6})	23.6×10^{-6} (13.1×10^{-6})
Tension (N/M^2) (ULT) (PSI)	496×10^6 (72,000)	496×10^6 (72,000)	427×10^6 (72,000)
Compression (N/M^2) (Yield) (PSI)	407×10^6 (59,000)	407×10^6 (59,000)	366×10^6 (53,000)
Shear (N/M^2) (ULT) (PSI)	276×10^6 (40,000)	276×10^6 (40,000)	248×10^6 (36,000)
Bearing (N/M^2) (ULT) (PSI)	876×10^6 (127,000)	876×10^6 (127,000)	794×10^6 (115,000)

Table 2.5-4

MATERIAL PROPERTIES – PROTOTYPE PANEL

HMS/X-904 Graphite-Epoxy

	Undirectional	Laminate
Temperature	All	All
Elastic Modls (S) (N/M^2) (PSI)	155×10^9 (22.4×10^6)	88.7×10^9 (12.86×10^6)
Elastic Modls (W) (N/M^2) (PSI)	5.52×10^9 ($.8 \times 10^6$)	30.4×10^9 (4.4×10^6)
Shear Modls (SZ) (N/M^2) (PSI)	4.14×10^9 ($.6 \times 10^6$)	3.38×10^9 ($.49 \times 10^6$)
Shear Modls (ZW) (N/M^2) (PSI)	2.07×10^9 ($.3 \times 10^6$)	2.54×10^9 ($.368 \times 10^6$)
Poisson's Ratio (SZ)	.45	.311
Poisson's Ratio (ZW)	.33	.321
Thermal Expansion (S) (In./In./°F)	$-.9 \times 10^{-6}$ (-0.5×10^{-6})	$-.514 \times 10^{-6}$ ($-.285 \times 10^{-6}$)
Thermal Expansion (W) (In./In./°F)	36×10^{-6} (20×10^{-6})	4.07×10^{-6} (2.26×10^{-6})
Thermal Expansion (Z) (In./In./°F)	36×10^{-6} (20×10^{-6})	36×10^{-6} (20×10^{-6})
Tension (S) (N/M^2) (PSI)	409×10^6 (59,200)	242×10^6 (35,000)
Tension (W) (N/M^2) (PSI)	18×10^6 (2,600)	69×10^6 (10,000)
Compression (S) (N/M^2) (PSI)	610×10^6 (88,300)	345×10^6 (50,000)
Compression (N) (N/M^2) (PSI)	124×10^6 (18,000)	138×10^6 (20,000)
Shear (In-Plane) (N/M^2) (PSI)	67×10^6 (9,700)	131×10^6 (18,974

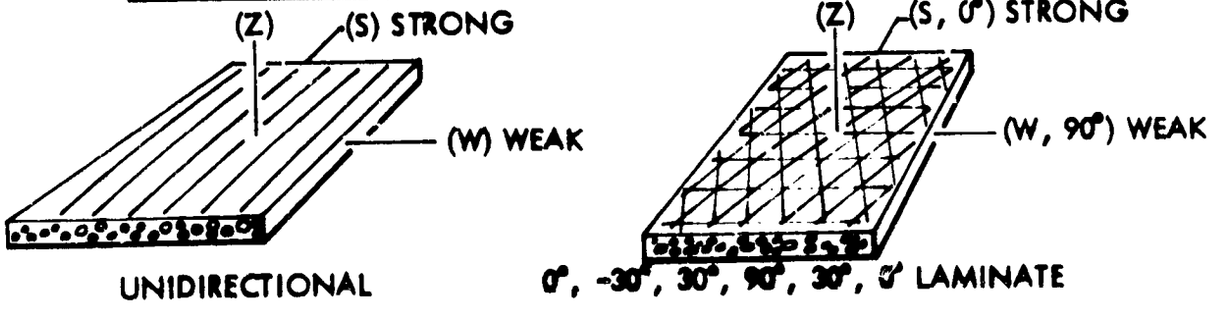

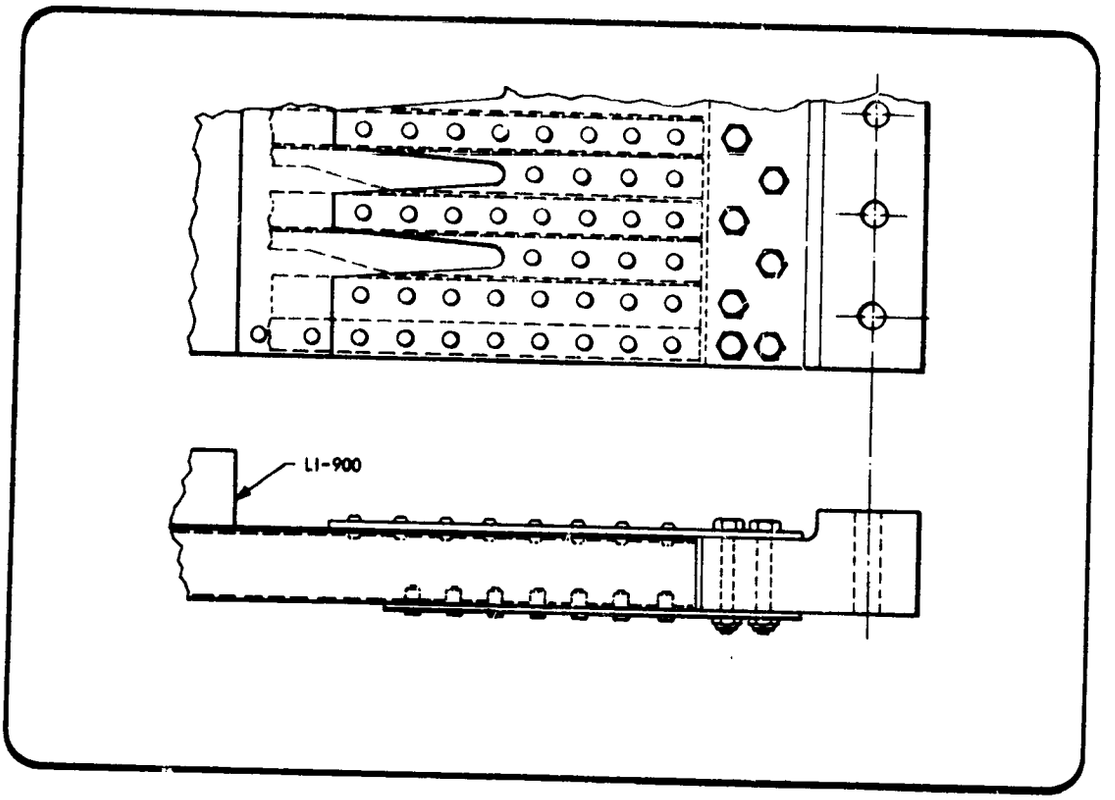

Fig. 2.5-4 Panel End Geometry

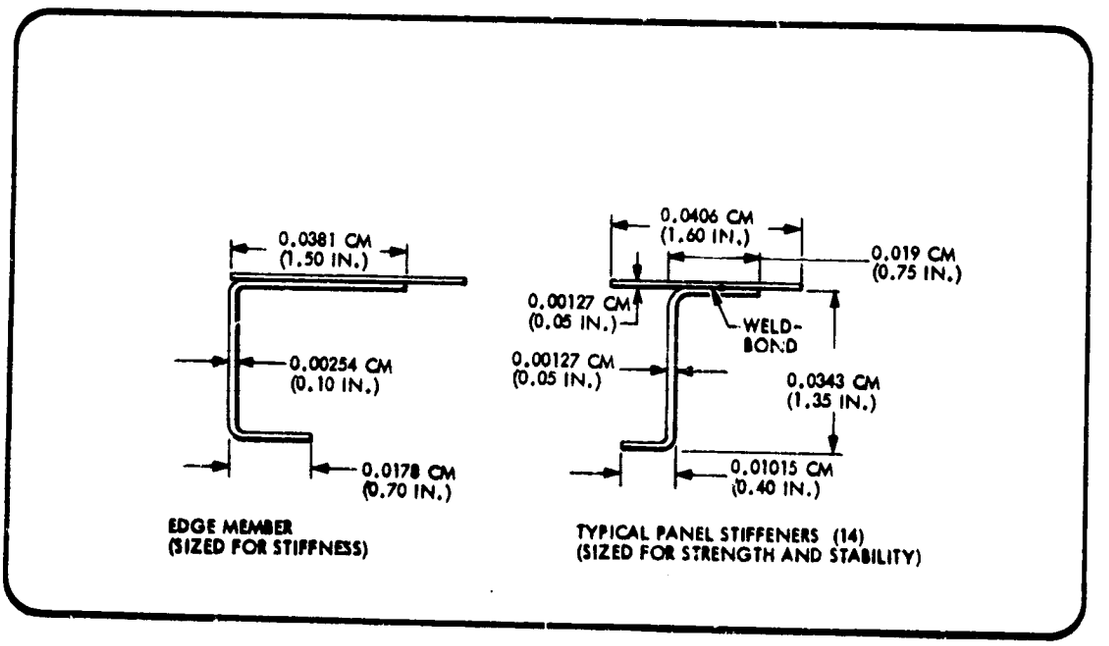

Fig. 2.5-5 Basic Panel Section

Table 2.5-5

MATERIAL PROPERTIES
RTV 560 AND RM-RL 1973

RTV-560					RM-RL 1973			
(1) Bond T °F	(2) E PSI	(3) G PSI	(4) μ	(5) α 1/°F	(6) E PSI	(7) G PSI	(8) μ	(9) α 1/°F
300	430	155	0.5	108^{-06}	145	18	0.25	94^{-06}
200	410	150	0.5	108^{-06}	135	18	0.25	94^{-06}
70	340	135	0.5	108^{-06}	135	18	0.25	94^{-06}
-65	290	110	0.5	106^{-06}	160	17	0.25	480^{-06}
-90	310	111	0.5	106^{-06}	210	19	0.25	450^{-06}
-100	315	112	0.5	106^{-06}	240	20.5	0.25	437^{-06}
-120	340	125	0.5	106^{-06}	330	27	0.25	410^{-06}
-150	450	180	0.5	106^{-06}	630	52	0.25	375^{-06}
-244	140,000	54,000	0.3	93^{-06}	7400	2900	0.25	277^{-06}
-250	150,000	57,700	0.3	92.3^{-06}	7400	2900	0.25	271^{-06}

more closely resembled a beam than a panel. The amount of additional edge support was limited by the area added to the panel cross-section, since this reduces the total strain in the panel under load. Appendix A2 includes an analysis of the edge stiffener.

Appendix A2 also includes the end fittings analysis. The basic panel analysis as found in LMSC-D152738 Vol. II of contract NAS9-12083 has been revised to include the 2024-T81 aluminum alloy and is included in Appendix A2.

Margins of safety for the panel substrate are presented in Table 2.5-6. They are based on ultimate test loads using high temperature material properties. The basic panel was designed for loads and pressures found in Table 2.5-2.

2.5.4 RSI Tile Analysis

This section summarizes the final design of tile size, bond, and strain arrestor plate selection for the deliverable prototype panel.

With the metallic substrate designed, the RSI tile must be tailored to fit that substrate. It must be emphasized that since the substrate stiffness properties play a large part in the behavior of the overall TPS system, and therefore influence the RSI tile design, the design presented is uniquely analyzed for this substrate and no other.

Table 2.5-6

PANEL MARGINS OF SAFETY (ULTIMATE)

BASIC PANEL SECTION

- COMPRESSION + PRESSURE – CRIPPLING ——— 0.12
- TENSION + PRESSURE – TENSION ——— 0.13
- TENSION ONLY ——— 0.30
- TENSION ONLY – LOAD MISALIGNED ——— 0.10

END PLATES AND FITTING

- JO-BOLTS, SKIN, BEARING ——— 0.81
- JO-BOLTS, STIFFENER TOP, BEARING ——— 0.29
- JO-BOLTS, STIFFENER BOTTOM, BEARING ——— 0.32
- UPPER FINGER PLATE, TENSION ——— 1.02
- LOWER FINGER PLATE, TENSION ——— 1.48

The WILSON two-dimensional, linear finite-element computer code was used for the analysis, and panel cross-sections were examined that were parallel to the substrate stiffeners (strong direction) and perpendicular to the stiffeners (weak direction). In the weak direction, the support afforded to the panel by bending stiffness of the stiffeners supported between frames was included in the analysis by using simulated springs or soft columns in the computer model. (See Figs. 2.5-6 and -7.) The column modulus was selected such that the spring deflection under load is equal to that of the center of the stiffener under the same load. The results of subsection 2.3, Design Curves, were used as guidelines in selecting geometric parameters to initiate the prototype panel analysis. The results indicated that for the lowest possible LI-900 stresses a .305m (12 in.) tile with minimum sponge thickness was desirable. A strain arrestor plate having an extensional stiffness (area x modulus) of 890,000 N (200,000 lb) was found to be optimum, assuming the plate consisted of six layers of unidirectional lamina laid up at 60 deg to each other in-plane and symmetrical through the thickness. This produced a plate having equal elastic properties at any direction in the plane. However, the structural behavior of the TPS system in the strong and weak directions indicated that a strain arrestor plate having different elastic properties in the two directions would lead to a more optimal design. The material selected for use in the prototype panel is HMS/X-904 graphite/epoxy due to its availability in suitable lamina thicknesses and its high elastic modulus or stiffness.

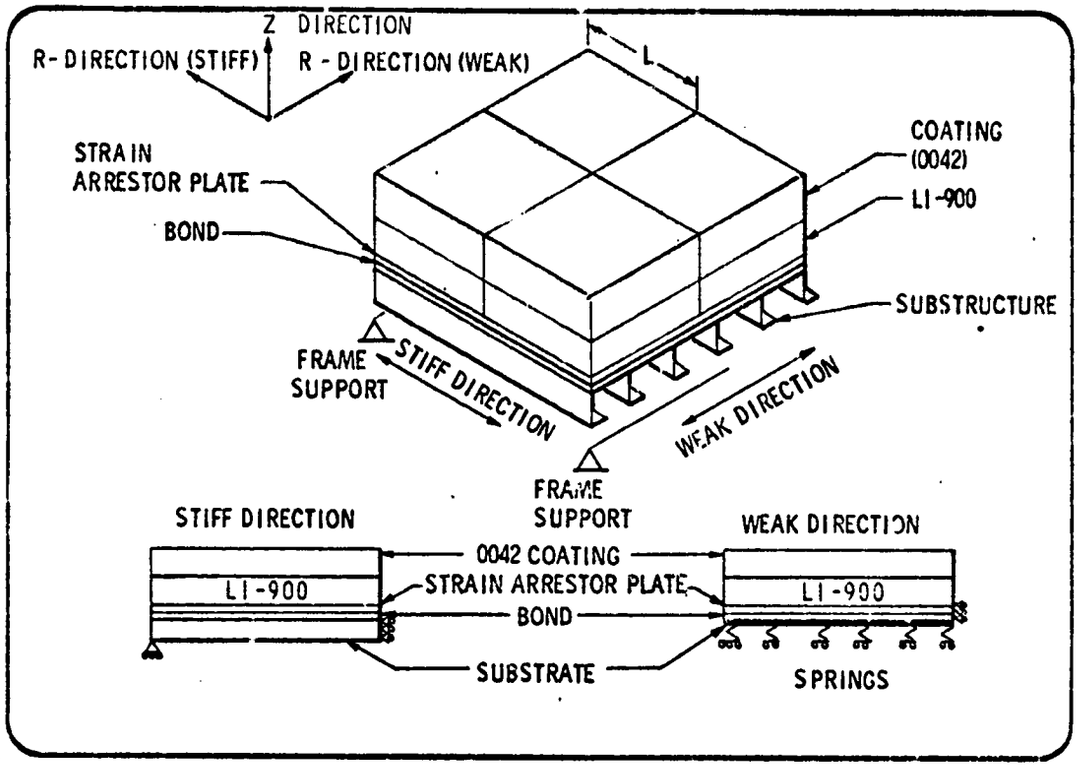

Fig. 2.5-6 Computer Modeling

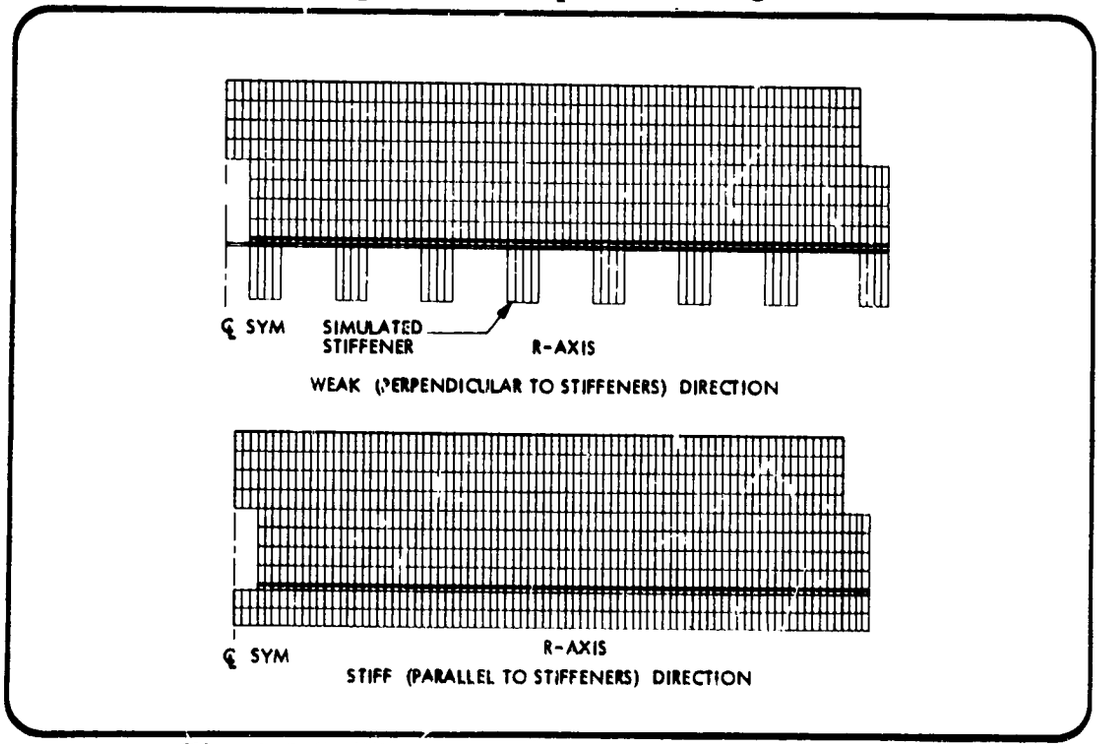

Fig. 2.5-7 Wilson Finite Element Computer Models

Figure 2.5-8 shows curves of LI-900 stresses vs strain arrestor plate stiffness for the weak direction. These curves indicate that an optimal strain arrestor plate stiffness of about 445,000 N (100,000 lb) exists for the weak direction. In addition, curves had shown that in the strong direction a high plate stiffness would result in low LI-900 stresses. Using the LAMINATE computer code, a number of different layups were studied to find one having the desired stiffness in all directions. The selected layup has two outer layers at 0 deg, two layers at -30 deg and at 30 deg, and one central layer at 90 deg, the 0 deg direction being aligned with the strong direction and the 90 deg direction with the weak. The resulting stiffness distribution is approximately elliptical in the plane and has desirable values at all angles. (See Fig. 2.5-9). The strong direction extensional stiffness is 1,600,000 N (360,000 lb) and in the weak direction is 546,000 (123,000 lb). The seven layers are .004 in. thick each and have 50 percent fiber volume after layup. The strength envelope shown for the plate is based on initial failure in the epoxy and is highly conservative as the fibers would still be capable of resisting much higher stresses. However, predicted stresses are within the envelope shown in Fig. 2.5-10.

The minimum commercially available thickness of RM/RL-1973 sponge at this time is .00159 m (.0625 in.). RM/RL-1973 was found to have a lower elastic modulus at 116°K (-250°F) than PD-200, offering better strain isolation. A layer of .00127 m (.005 in.) RTV-560 is used on either side of the sponge as a bond.

Since the LI-900 material was found to be most critical in terms of stress, the design was aimed at keeping these stresses to a minimum, with attention also being paid to the coating stresses. It was found that the most severe stress conditions in the LI-900 occur during the 116°K (-250°F) cold soak due to dissimilar coefficients of expansion and during landing at 3600 sec after start of reentry when a 1050×10^3 N/M (6000 ppi) line load exists in the substrate. Stress results are shown in Table 2.5-7. High thermal gradients were once again not found to be critical in the LI-900 due to its low coefficient of expansion 1533°K (2300°F), even at t = 500 sec into reentry when a thermal gradient exists such that the surface temperature is 1533°K (2300°F) and the substrate temperature is 116°K (-250°F). See Fig. 2.5-13.

Maximum coating stresses occur at the center of the top surface of the tile, whereas critical LI-900 stresses occur at the tile edges just above the strain arrestor plate, and previous three-dimensional analyses have shown that the highest edge stresses occur at the tile corners. These critical stresses are peel tension, compression, and shear. Highest in-plane stresses occur at the tile center just above the strain arrestor plate. (See Table 2.5-8.) RSI margins of safety are found in Table 2.5-9.

No allowance was made for bond creep or relaxation, as insufficient data were available at the time. However, testing at General Dynamics has shown that as much as 85 percent stress relaxation occurs in RM/RL 1973 at the glass-transition temperature and, for the 116°K (-250°F) cold soak condition, the stress results tabulated here are considered highly conservative.

The t = 3600 sec analysis includes the ultimate line load of 1050×10^3 N/M (6000 ppi) although the test load will be 700×10^3 N/M (4000 ppi) limit load. Pressure was not included, as it is excluded from the test plan. Temperature profiles at 3600 sec are shown in Figs. 2.5-11 and -12.

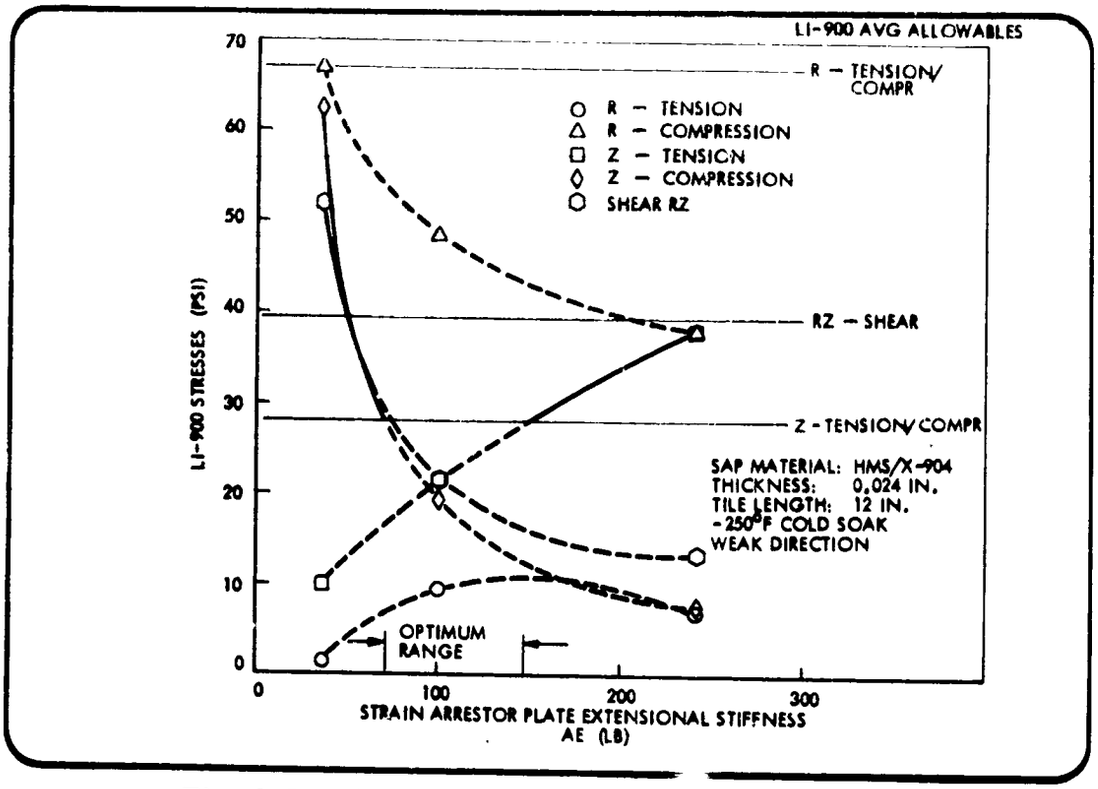

Fig. 2.5-8 LI-900 Stress Vs Strain Arrestor Plate Extensional Stiffness

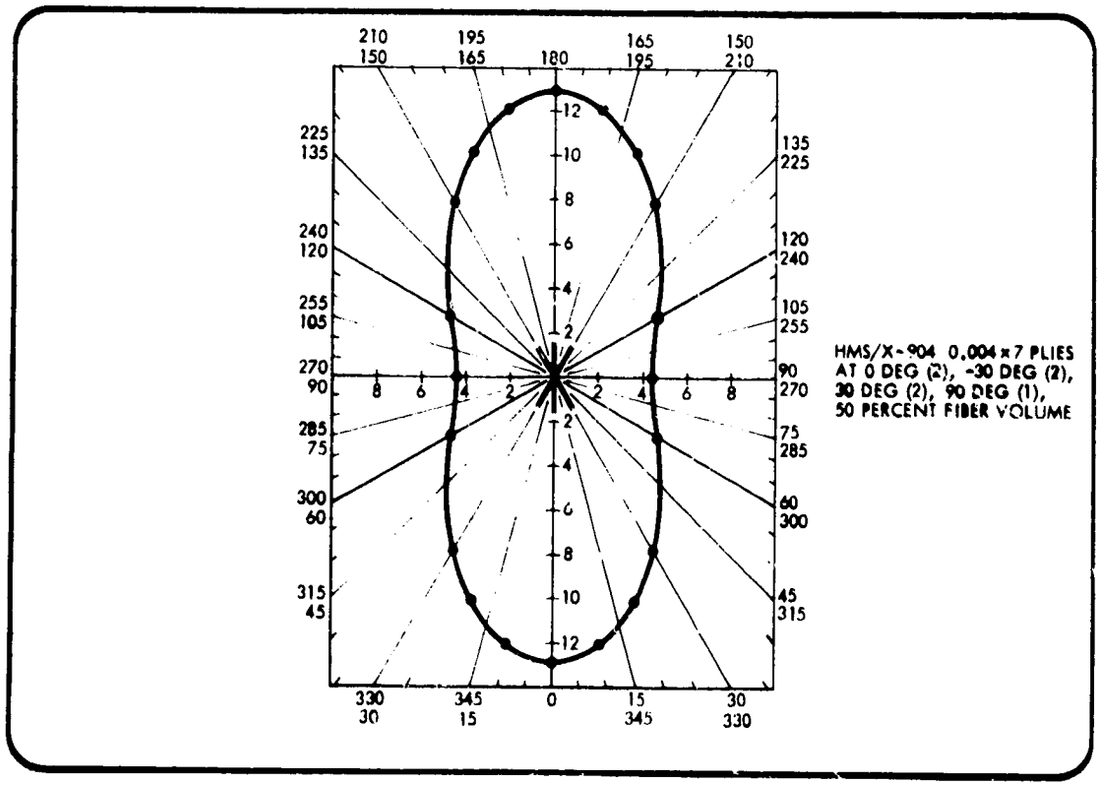

Fig. 2.5-9 Strain Arrestor Plate Elastic Modulus, E (X 10^6 PSI) Vs Ply Direction

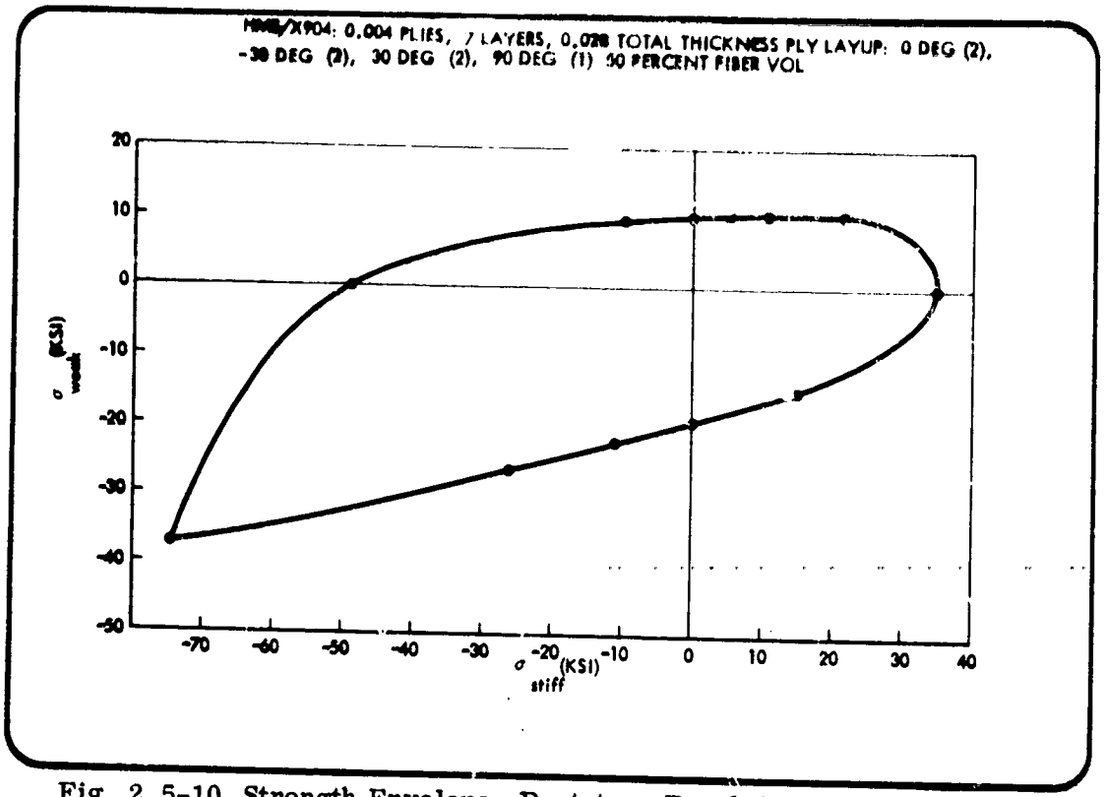

Fig. 2.5-10 Strength Envelope, Prototype Panel Strain Arrestor Plate

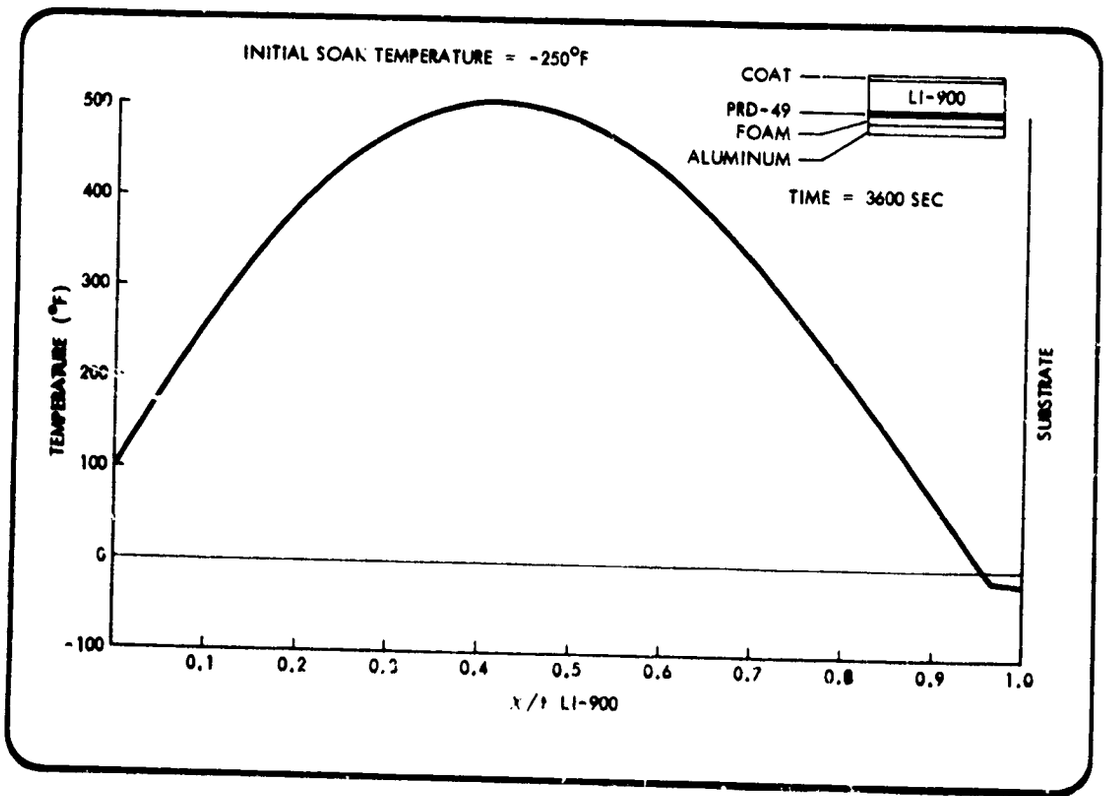

Fig. 2.5-11 Prototype Panel – Initial Soak Temp. -250°F

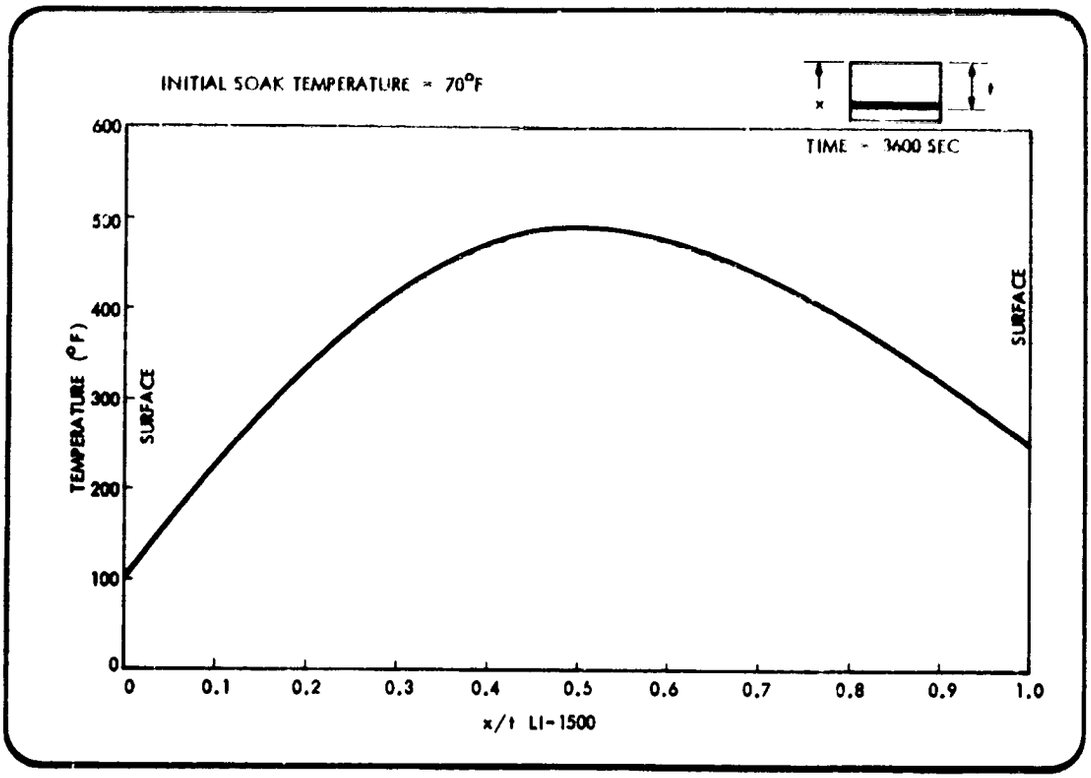

Fig. 2.5-12 Prototype Panel – Initial Soak Temp. 70°F

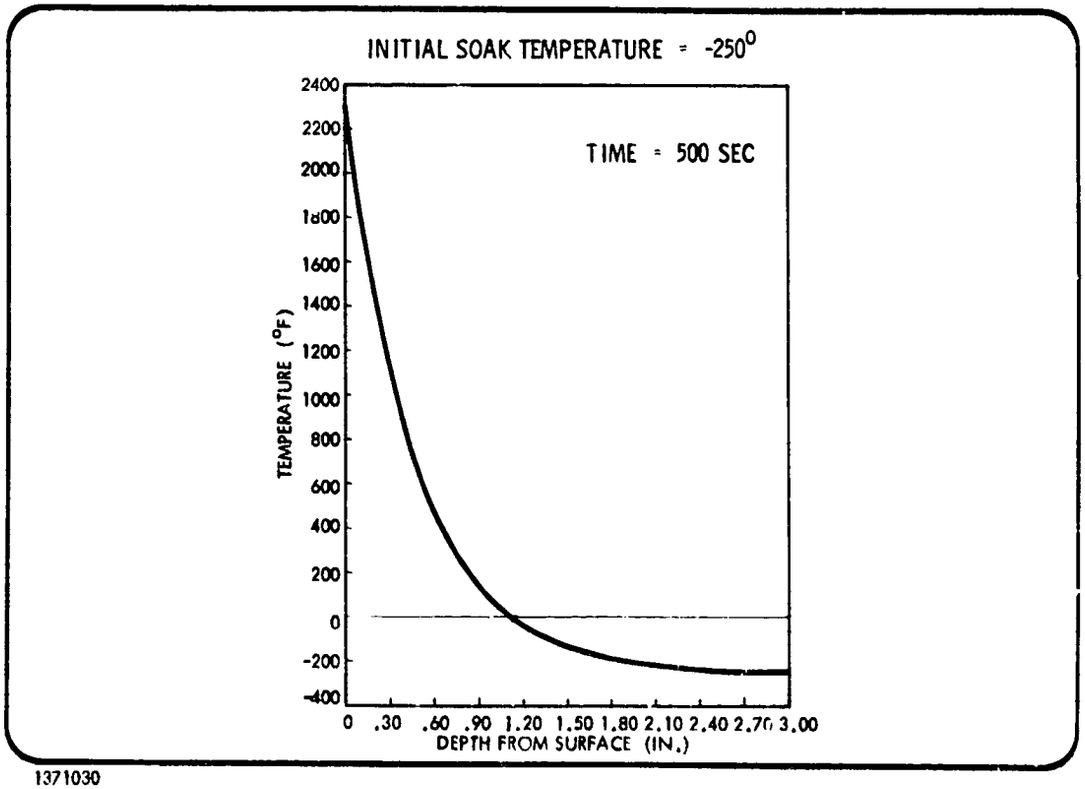

1371030

Fig. 2.5-13 Temp. Profile, LI-900, t = 500 Sec, -250°F Reentry Start

Table 2.5-7

PROTOTYPE PANEL TILE DESIGN STRESSES
(12 Inch Tile)

Thicknesses	
Coat:	.012
LI-900:	3.00
S.A.P:	.028
Foam:	.0625
RTV-560:	.005

S.A.P.	
Mat'l:	HMS/X-904
No. of Plies:	7 (.004 ea)
Orientation:	0^{o}, $\pm 30^{o}$, 90^{o} (1)
Stiff AE:	360,000 lb
Weak AE:	123,000 lb
50% Fiber Vol.	

Tile Length:	12"
Panel Length:	24"
Panel Width:	24"

	-250^{o}F Stiff	-250^{o}F Weak	t = 3600 Sec 70^{o}F Start	t = 3600 Sec -250^{o}F Start	t = 500 Sec t_{coat} = 2300^{o}F	Strength Allowables Min.	Strength Allowables Ave.
Coating							
Princ. Tension	1,171	763	107	141	349	1266	2134
Princ. Compr.	-201	-188	-19	-27	-781		
Princ. Shear	585	381	53	70	390		
LI-900							
R-Tension	9	2	1	2	12	47	67
R-Compr.	-33	-43	-4	-3	-32	-47	-67
Z-Tension	18	12	2	2	11	20	28
Z-Compr.	-10	-19	-5	-2	-16	-20	-28
RZ-Shear	16	24	5	1	15	35	39
Strain Arr. Plate							
R-Tension/Compr.	-23,229	-6,639	1,393	574	-23,000		
RZ-Shear	357	247	7	4	356		
RM/RL-1973 Sponge							
Princ. Tension	767	686	11	8	765		
Princ. Shear	444	350	12	6	445		
Aluminum							
R-Tension/Compr.	2,327	3,002	18,023	18,913	2,452		
Criteria A* (LI-900 only)	1.04 (0.579)	1.53 (0.993)	0.14	0.025	0.75		

Criteria A $= \frac{\sigma_R^2}{F_{tR}^2} + \frac{\sigma_Z^2}{F_{tZ}^2} + \frac{\gamma_{RZ}^2}{F_{sRZ}^2}$

R in-plane axis

Z transverse axis

F_t tension allowable

F_s shear allowable

*Min. LI-900 allowables used. Ave. LI-900 allowables used in parentheses.

Table 2.5-8

PROTOTYPE PANEL TILE DESIGN

(Max. Stress Locations – 12 Inch Tile)

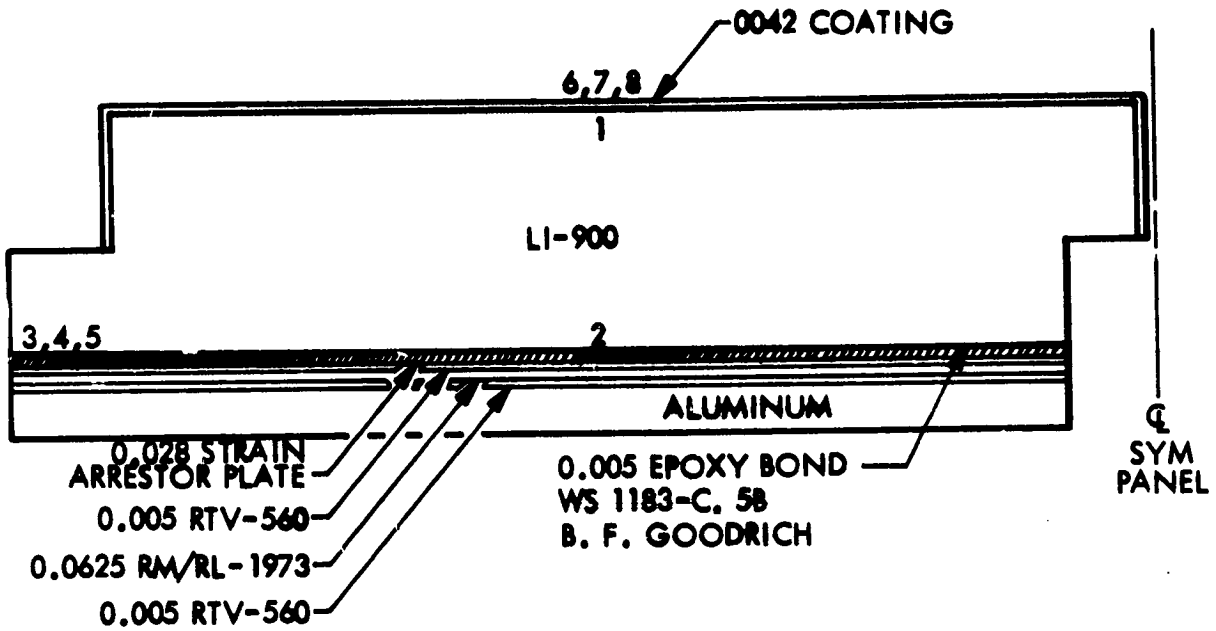

Location	Maximum Stress – LI-900			
1	R-Tension	=	12 PSI	(t = 500 sec from -250°F cold start)
2	R-Compr.	=	-43 PSI	(-250°F cold soak, weak direction)
3	Z-Tension	=	18 PSI	(-250°F cold soak, stiff direction)
4	Z-Compr.	=	-19 PSI	(-250°F cold soak, weak direction)
5	RZ-Shear	=	24 PSI	(-250°F cold soak, weak direction)

	aximum Stress – Coating			
	rinc. Tens.	=	1171 PSI	(-250°F cold soak, stiff direction)
	inc. Compr.	=	-781 PSI	(t = 500 sec from -250°F cold start)
8	rinc. Shear	=	585 PSI	(-250°F cold soak, stiff direction)

Table 2.5-9

RSI MINIMUM MARGINS OF SAFETY

Location	Stress	M.S. Avg Properties	M.S. Min Properties
1	R-Tension	4.67	2.92
3	Z-Tension	0.55	0.11
5	RZ-Shear	0.62	0.46
6	Coating Tension	0.82	0.08

It was stipulated by the contract that the prototype panel design meet all requirements of an area 2P orbiter panel design. This is assured in the detail design studies of subsection 2.4, as the orbiter bottom surface tile design used there is identical to that of the prototype panel.

The stress analysis results show that predicted stresses in the LI-900 and coating during prototype panel testing will be below the minimum strength values of the materials obtained from testing.

Stress results in Table 2.5-10 show that a .15 m (6 in.) tile is also feasible with the orthotropic strain arrestor plate. The .30 m (12 in.) tile length was chosen for ease of manufacture. .15 m (6 in.), .20 m (8 in.) and .30 m (12 in.) tiles may be used interchangeably on this panel.

2.5.5 Prototype Panels

One prototype panel has been designed and fabricated in accordance with contract requirements to point design conditions specified by NASA/MSC.

The panel consists of a .61 m (24 in.) by .61 m (24 in.) test section of aluminum substrate supporting four .305 m (12 in.) by .305 m (12 in.) tiles with an extended length of substrate on each side of the test section with fittings and shear-plates for installation in the NASA/MSC tensile test fixture. The test fixture mounting holes on each end are 1.25 m (49.20 in.) apart and match holes in steel channels loaned by NASA/MSC to be used in the test fixture.

The four tiles are cut back .0127 m (1/2 in.) on the outer edges to accommodate an insulating blanket that surrounds the test section during the radiant heat test. Each tile is separated by a joint containing a .0254 m (1 in.) wide strip of coated FI-600 filler made of loosely packed silica fibers bonded to the aluminum substrate with RTV-560.

The graphite/epoxy strain arrestor plates are oriented in such a way that the 0 deg ply direction is parallel to the substrate stiffeners.

Table 2.5-10

PROTOTYPE PANEL TILE DESIGN STRESSES
(6 Inch Tile)

Thicknesses	
Coat:	.012
LI-900:	3.00
S.A.P.:	.028
Foam:	.0625
RTV-560:	.005

S.A.P.	
Mat'l:	HMS/X-904
No. of Plies:	7 (.004 ea)
Orientation:	0°, $\pm 30^\circ$, 90° (1)
Stiff AE:	360,000 lb
Weak AE:	123,900 lb
50% Fiber Vol.	

Tile Length:	6"
Panel Length:	24"
Panel Width:	24"

	-250°F Stiff	-250°F Weak	t = 3600 Sec 70°F Start	t = 500 Sec $t_{coat} = 2300^\circ$F	Strength Allowables Min.	Strength Allowables Ave.
Coating						
Princ. Tension	169	355	49	349	1266	2134
Princ. Compr.	-102	-149	-19	-692		
Princ. Shear	84	178	25	346		
LI-900						
R-Tension	9	4	1	11	47	67
R-Compr.	-16	-36	-3	-16	-47	-67
Z-Tension	15	21	2	14	20	28
Z-Compr.	-10	-4	-3	-12	35	39
RZ-Shear	15	17	4	15	35	39
Strain Arr. Plate						
R-Tension/Compr.	-12,121	-4,947	372	-12,141		
R-Z Shear	314		3	314		
RM/RL-1973 Sponge						
Princ. Tension	736	686	5	735		
Princ. Shear	404	334	6	405		
Aluminum						
R-Tension/Compr.	1,083	1,436	48,006	1,092		
Criteria A* (LI-900 only)	.799	1.110 (.546)	.054	.73		

Criteria A = $\frac{\sigma_R^2}{F_{tR}^2} + \frac{\sigma_Z^2}{F_{tZ}^2} + \frac{\gamma_{RZ}^2}{F_{sRZ}^2}$

R = in-plane axis

Z = transverse axis

F_t = tension allowable

F_s = shear allowable

*Min. LI-900 allowables used. Ave. allowables in parentheses.

Minimum gaps between tiles are such that at 116°K (-250°F) contraction of the aluminum base will not cause butting of one tile against another.

Detail drawing no. SKW-111672 sheets 1, 2, and 3, and drawing no. SKW-111772, show the panel details and assembly (see section 6).

References:

Prototype Panel Test Plan, LMSC-D159811

Section 3

PROPERTY CHARACTERIZATION – TASK B

3.1 INTRODUCTION

The objective of this task was to obtain mechanical and thermophysical properties of LI-900 and the 0042 surface coating. The test program followed the Property Test Plan (LMSC-D282611) approved by NASA/MSC and this final report documents the results.

LI-900 has been tested in both the as-fabricated condition and after 20 radiant heat cycles according to the test matrix of Table 3.1-1. Detailed discussion of test techniques as well as the radiant cycling are given first, followed by a presentation and interpretation of the data obtained.

A similar test matrix is being performed on LI-900 and the 0042 coating for comparison by Battelle under NASA direction, with the exception that mechanical testing will be limited to room temperature, 800°F, and 1600°F. Concurrently, NASA/Ames is also conducting the test program of Table 3.1-1, using LI-1500 instead of LI-900.

Table 3.1-1
TEST MATRIX

	TEMPERATURES (°F)								
	-320	-250	RT	400	800	1200	1600	1800	2200
AS RECEIVED:									
COATING TENSION		X	X	X	X	X	X		
LI-900 IN-PLANE TENSION		X	X***	X	X	X	X		
LI-900 TRANSVERSE TENSION		X	X***	X	X	X	X		
LI-900 TRANSVERSE SHEAR**		X	X	X	X	X	X		
COATING THERMAL EXPANSION	←								→
LI-900 THERMAL EXPANSION	←								→
LI-900 THERMAL CONDUCTIVITY		←						→	
RADIANTLY CYCLED:									
LI-900 IN-PLANE TENSION			X	X	X	X	X		
LI-900/COATING TRANSVERSE TENSION			X	X	X				
LI-900 TRANSVERSE SHEAR**			X	X	X	X	X		
LI-900 THERMAL EXPANSION	←								→
LI-900 THERMAL CONDUCTIVITY		←						→	

*TEN DATA POINTS OBTAINED FOR EACH MECHANICAL TEST CONDITION, THREE SPECIMENS FOR EACH THERMOPHYSICAL TEST CONDITION.
**DESIGNATED AS "IN-PLANE" SHEAR IN CONTRACT.
***POISSON'S RATIOS ALSO DETERMINED.

3.2 TEST TECHNIQUES

3.2.1 Specimen Configurations

Thermophysical test specimen dimensions are shown in Fig. 3.2.1-1. Two sizes of thermal conductivity specimens are necessary since two different test devices are needed to obtain data over the entire temperature range indicated in Table 3.1-1. Thermal conductivity measurements were also performed for heat conduction in-plane and the specimen was similar to the 7-in. diameter disc; however, it was fabricated from several pieces of LI-900, of course cut at 90 deg to the specimen shown in the figure.

Mechanical test specimens originally planned for this effort appear in Fig. 3.2.1-2. As will be described in Par. 3.2.2.1, no adequate means of bonding specimens was found to work over the entire range of test temperatures of Table 3.1-1. Hence, mechanical means of gripping LI-900 were devised necessitating additional specimen configurations. The specimens of Fig. 3.2.1-2 were used but only for the following temperatures:

Transverse tension In-plane tension	-250^{o}F,RT
Transverse shear	RT

To complete the test matrix, the specimens of Fig. 3.2.1-3 were added. Two general types of tension "dogbones" as shown were necessary to obtain strength and modulus, as neither specimen type could adequately provide both pieces of data due to limitations on specimen length and size. The in-plane tension ultimate "I" was used for tests on "as-fabricated" LI-900 at 400^{o}F and 800^{o}F only; otherwise, all other in-plane elevated temperature tests were performed using the "II" specimen with a smaller cross section. Some problems of grip slippage at the highest temperature levels necessitated this change during the test effort, as elaborated upon in Par. 3.2.3.2.

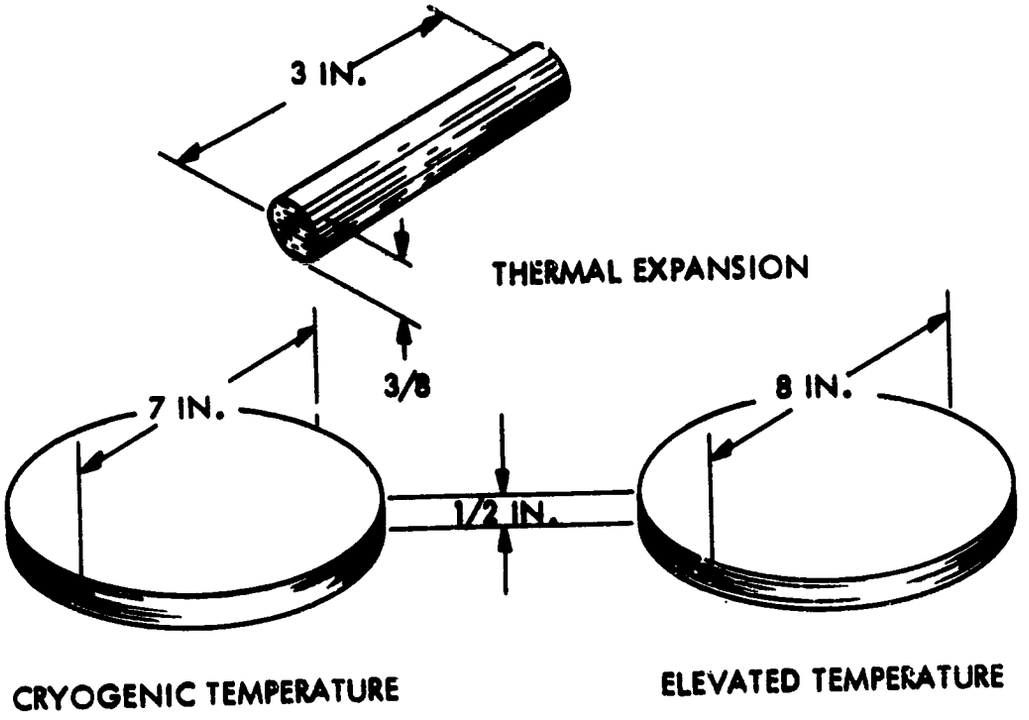

Fig. 3.2.1-1 Thermophysical Test Specimens

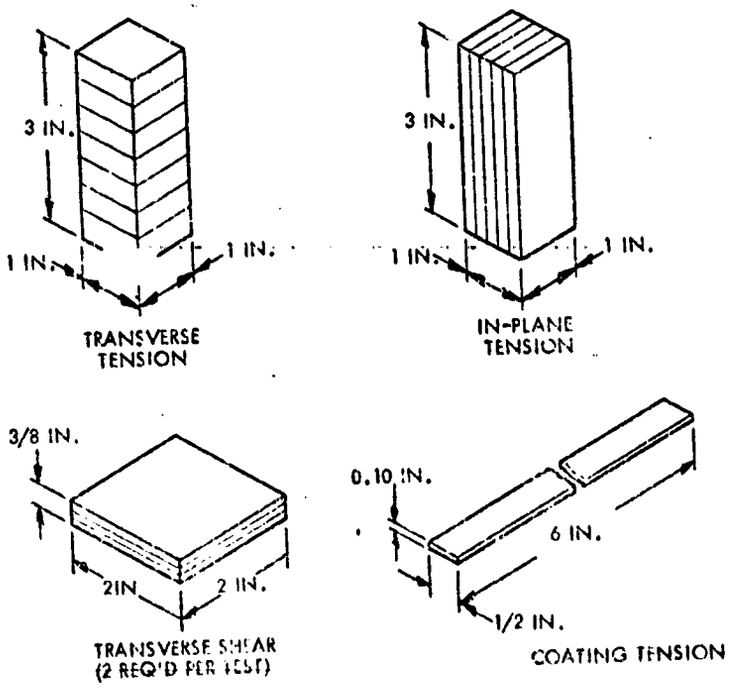

Fig. 3.2.1-2 Mechanical Test Specimens Originally Planned

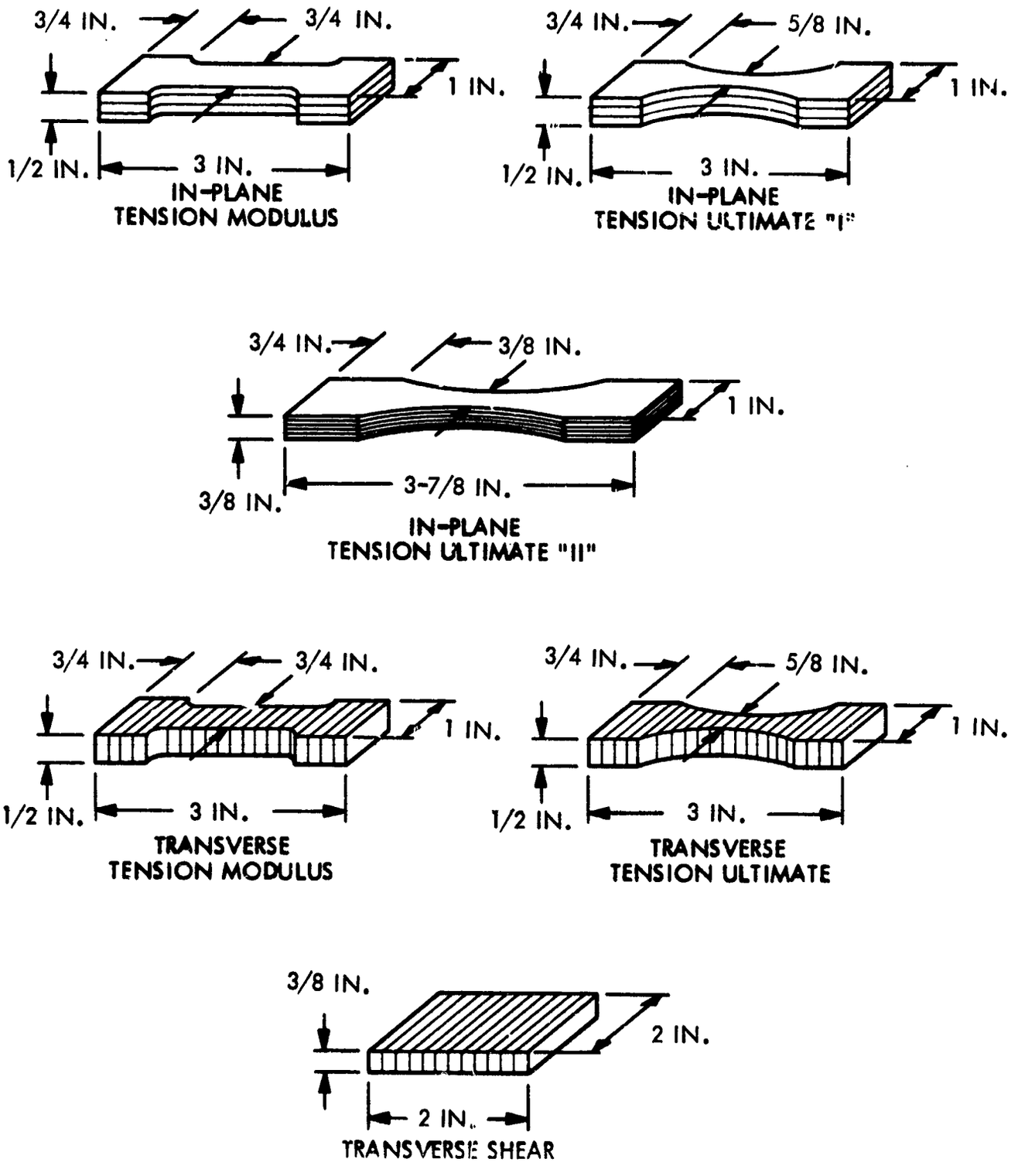

Fig. 3.2.1-3 Additional Mechanical Test Specimen Configurations Developed Under Contract

3.2.2 Thermophysical Test Fixtures and Procedures

The following sections describe the means whereby the thermal expansion and thermal conductivity characteristics of LI-900 and the 0042 coating have been determined for the test conditions outlined in Table 3.1-1.

3.2.2.1 Thermal Expansion. Linear thermal expansion measurements were performed over the temperature range of 77° to 1497°K (-320° to 2200°F) using three pushrod type dilatometers. Fused silica dilatometers were used for the 77° to 297°K (-320° to 75°F) and the 297° to 1200°K (75° to 1700°F) temperature ranges, and an alumina dilatometer was employed from 1088° to 1497°K (1500° to 2200°F). Measurements were performed on LI-900 before and after thermal cycling and on the 0042 coating material before cycling. In all cases the specimen geometry was a cylindrical bar nominally 0.95-cm by 7.6 cm (3/8-in. diameter by 3-in.) long. The apparatus and test procedures are described in the following subsections.

Experimental Apparatus. The pushrod-type of dilatometer measures the difference in length change between the sample and a reference material which forms the sample support means. Thus, the thermal expansion characteristics and temperature of the reference material, over the sample length, must be accurately known. Fused silica is a very stable low thermal expansion material for temperatures to 1200°K (1700°F) and is used extensively in dilatometric measurements. At higher temperatures fused silica does not maintain the excellent stability of the expansion property, and other materials must be used for the dilatometer. For the testing to 1390°K (2500°F) in air LMSC uses an alumina system which has excellent stability. However, it has one disadvantage in that its expansion characteristics are clearly an order of magnitude greater than fused silica. Consequently, the measurement uncertainty is greater with this system when applied to very low thermal expansion materials.

The fused silica and alumina dilatometers used for this study are essentially of the same type of construction as shown in Fig. 3.2.2-1. The basic differences in apparatus are in the heating method and instrumentation for measurement of specimen length change. The outer tube-pushrod assemblies for the two fused silica systems are the same; the outer tube being 45.8 cm (18-in.) long. Hemispherical ends are formed at the lower ends of the outer tube and the pushrod so that the specimen contacts are spherical surfaces to minimize misalignment errors. In each case, the silica pushrod weighs 33 gms. The alumina system is 12-in. long and has a pushrod weighing 18 gms. The total load on the specimen is the sum of the pushrod weight and the force imposed on the pushrod by the dial gage (10 gm) or the linear variable displacement transducer (LVDT) (<1 gm).

For the low-temperature dilatometer system the fused silica outer tube and pushrod assembly are suspended in a silica tube which is immersed in a cryogen dewar. A copper sheath with heater windings is located between the specimen and outer tubes for control of sample temperature. The sample space is filled with helium and the outer chamber evacuated during operation. The motion of the pushrod is measured on a dial gage having a sensitivity of 1×10^{-5} in.

The intermediate temperature fused silica dilatometer assembly is placed into an alumina tube furnace for programmed specimen heating. The furnace is controlled to heat the specimen at $\approx 1^{o}$K (1.5 to 2^{o}F) per min. by a proportional-type controller having a continuously variable set point input and a 2-KW SCR power supply. The pushrod assembly is suspended from an Invar bracket which serves as the mounting for the LVDT, which measures pushrod motion. This LVDT has full-scale ranges of 5.1×10^{-2} and 1×10^{-2} cm (2×10^{-2} in. and 4×10^{-3} in.) with a sensitivity of 1×10^{-6} in. The LVDT control unit output signal is recorded continuously together with the specimen thermocouple output with an x-y plotter.

The alumina dilatometer assembly is supported from a thermostated brass block onto which the dial gage used for motion measurement is mounted (sensitivity of 1×10^{-5} in.). This assembly is suspended from the upper end of a graphite tube furnace. Separate purge gas systems are provided for the dilatometer and the furnace. Specimen temperature is determined using an optical pyrometer which is sighted onto the outer alumina tube at each test temperature level (steady state).

The fused silica dilatometers are calibrated prior to each test series, using a National Bureau of Standards fused silica standard, SRM 739. This procedure serves to verify both the accuracy of the dilatometer material thermal expansion properties and the

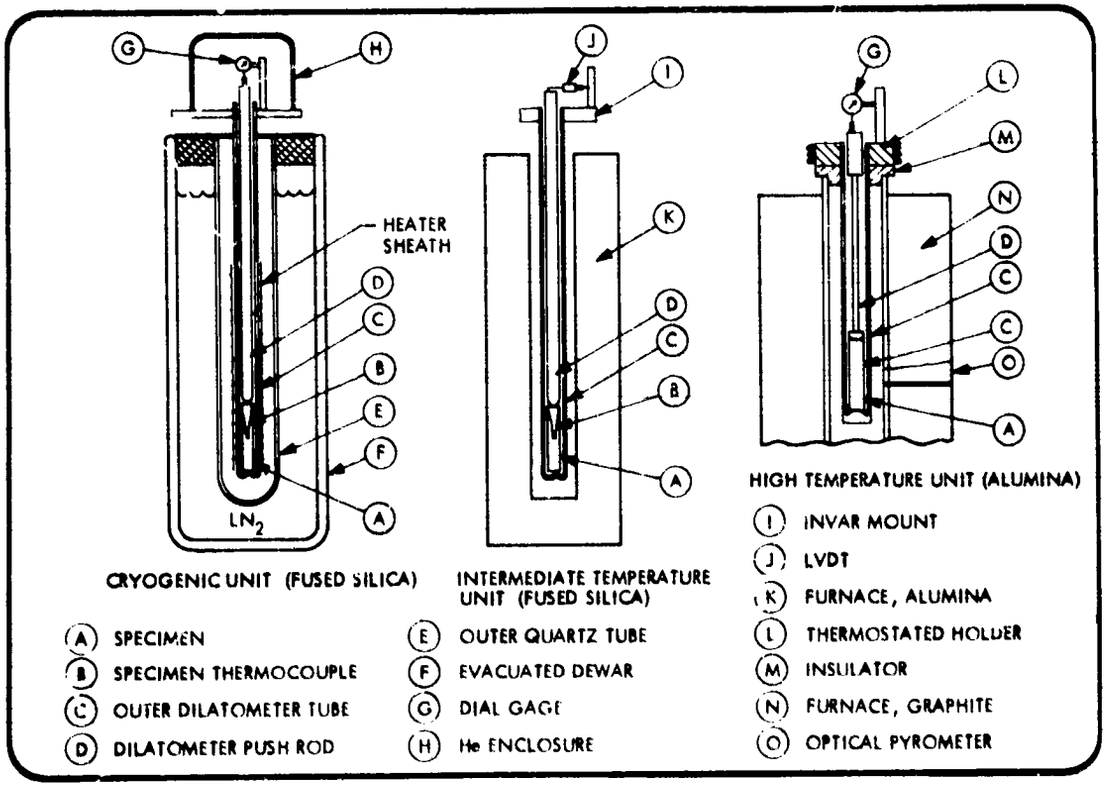

Fig. 3.2.2-1 Dilatometer Construction

temperature and dimensional change measuring systems. The alumina dilatometer is calibrated at lower temperature against SRM 739 and at higher temperatures against a sapphire rod which was initially compared against gold, platinum, and alumina standard specimens supplied under an AGARD round robin test program.* The transducer and dial gages are also periodically checked for absolute accuracy using Measurement Standards Laboratory gage blocks. The overall accuracy of measurement of pushrod motion is calculated to be 3 by 10^{-6} in. for the intermediate temperature system, 1×10^{-5} in. for the cryogenic unit, and 3×10^{-5} for the high temperature assembly.

Experimental Procedure. Sample preparation consists of cutting each bar to a nominal length of 7.6 cm (3 in.); finishing the ends so that they are flat and parallel; measuring length, diameter, and weight of specimen; and installation of a 3-mil diameter chromel-constantan thermocouple in the center of each bar (except for the high-temperature tests), the junction being cemented to the specimen with a small bead of refractory cement. Post-test measurements are made of specimen overall length and diameter.

For the low-temperature apparatus, the inner and outer quartz tube assemblies, with the specimen installed, are evacuated; the cryogen reservoir then filled with LN_2; and the evacuated spaces back-filled with helium. After the specimen temperature equilibrates with that of the LN_2 reservoir, the outer gas space is evacuated while maintaining a GHe purge in the inner space, and the dial gage reading is recorded. Electrical power is then applied to the copper heater sheath to raise the specimen to the next desired temperature level. After steady-state temperature conditions are achieved, dilatometer and specimen temperatures and dial gage readings are recorded. Heater power is increased, and this procedure is repeated until room temperature is reached.

Testing in the intermediate temperature range dilatometer is accomplished by placing the dilatometer assembly with the specimen into the tube furnace-holder unit. The transducer gain is set and checked with gage blocks and its output, together with that of the specimen thermocouple connected to the x-y plotter. The temperature programmer-control unit is activated, and a continuous record of transducer and thermocouple outputs is produced during the entire heating cycle to the maximum test. The temperature transducer also has a digital output, and this is noted on the plotter chart at intervals to serve as a check of the trace accuracy.

The high-temperature dilatometer is operated in a point-by-point fashion similar to the cryogenic unit. The dilatometer unit is placed into the furnace, and the gage reading recorded at room temperature. Furnace temperature is then increased to approximately $1088^{\circ}K$ ($1500^{\circ}F$), and after dilatometer temperature and dial gage readings have stabilized, they are recorded. Temperature is raised in successive intervals and this procedure is repeated until the desired maximum temperature is reached. When material shrinkage occurs, dial gage readings are made at 1 min. intervals until a $\approx 12 \times 10^{-2}$ cm (5×10^{-2} in.) shrinkage is observed, and the test is then terminated. Further shrinkage may occur because of the slow cooling cycle in this furnace, and post-test length measurements do not necessarily reflect the final dial gage reading.

---

*E. Fitzer, "Cooperative Thermal Expansion Measurements, Final Report on Project TX44, Project Section 1A," AGARD Structures and Materials Panel, 1971

Thermal expansion, $\Delta L/L_o$, is calculated from the recorded dimensional change, ΔL, (from dial gage or from transducer output voltage times calibration factor of mils per volt) and the dimensional change of the dilatometer over the specimen length by the following:

$$\Delta L/L_o = \Delta L_g/L_o + \Delta L_d/L_o$$

where L_o is the initial specimen length, ΔL_g is the pushrod motion, and ΔL_d is the dilatometer expansion from calibration data.

For the very low thermal expansion materials, such as the silica systems, the maximum uncertainty in the computed value of $\Delta L/L_o$ is due principally to the uncertainty in the dimensional change measurement and the value of the dilatometer material expansion. In the case of the intermediate temperature system, the estimated maximum uncertainty for the LI-900 and coating specimens is a maximum 15 percent near room temperature, and decreases to 2 percent at the upper end of the temperature range. Maximum uncertainty for the cryogenic dilatometer is 15 to 25 percent over the test temperature range (because of the dial gage accuracy). With the high-temperature unit, the uncertainty is due principally to the uncertainty in the alumina expansion relative to the very low thermal expansion silica materials. For this apparatus the estimated maximum uncertainty in $\Delta L/L_o$ is 10 percent from 1500 to 2300°F.

3.2.2.2 Thermal Conductivity. The thermal conductivity measurements performed on the LI-900 specimens were made using the guarded hot plate (Americans Society for Testing Materials C177) facilities. A 7-in. dia. unit, Fig. 3.2.2-2, was employed for the 117° to 478°K (-250° to 400°F) range, and the 8-in. dia. apparatus, Fig. 3.2.2-3, covered the temperature range of 533° to 1310°K (500° to 1900°F).

? t Apparatus. Both guarded hot plates are of a similar design, the principal differences being in constructional materials for the various temperature ranges and guard size (the 8-in. apparatus is suitable for materials up to 1-1/4 in. thick whereas, the 7-in. unit has a maximum thickness capability of 3/4-in.). Both units have a 4-in. diameter measuring area, and they are configured for operation in vacuum or air to 1 atmosphere pressure. The 7-in. units utilize blackened copper surface plates for main and guard heaters and heat sink surfaces, and oxidized stainless steel plates are used in the 8-in. apparatus.

Chromel-alumel thermocouples are located in the surface plates of the 7-in. unit, whereas, the 8-in. unit uses platinum-platinum/10 percent rhodium thermocouples. Guard-to-main heater temperature balance is achieved using series-connected, electrically-insulated differential thermocouples located in both main and guard heaters, and their outputs control the guard power supply. Temperatures of the sink plates and outer guard ring are automatically controlled with SCR-type controllers. Main heater power is from a regulated, manually-controlled dc supply. Each unit is installed in a vacuum chamber having both oil diffusion and mechanical pumping systems with LN_2 cold traps. Intermediate pressures above 10^{-2} torr are achieved using a controlled leak into the chamber. Pressures are measured using Bourdon-type gages, as well as thermocouple and ionization gages located in the chamber base plate.

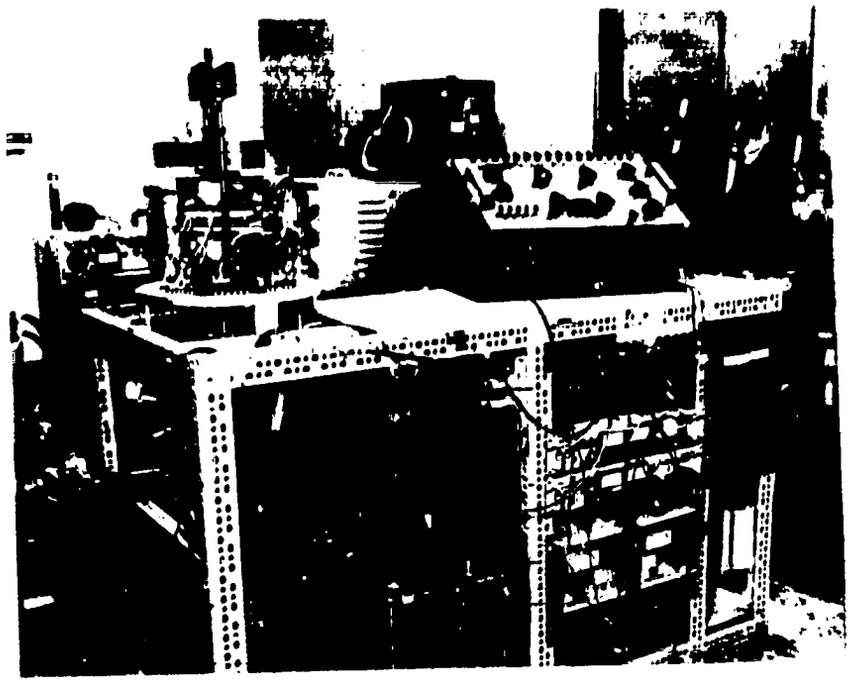

Fig. 3.2.2-2 Seven-In. Diameter Guarded Hot Plate

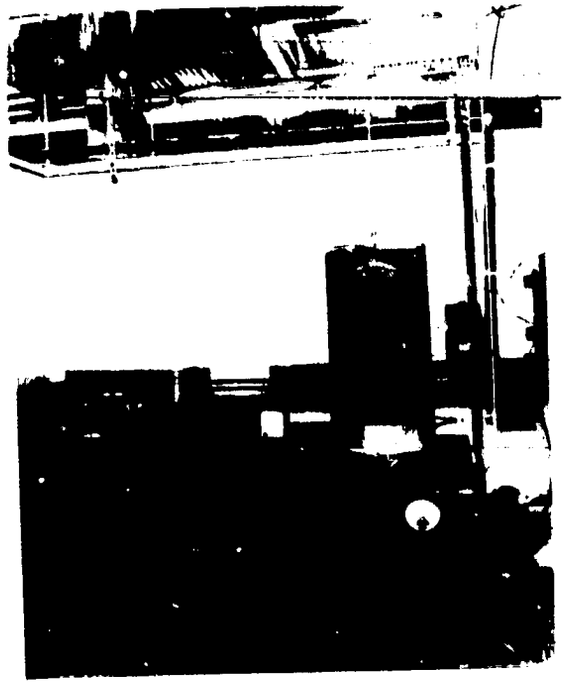

Fig. 3.2.2-3 Eight-In. Diameter Guarded Hot Plate

General arrangement of the specimen heat-sink stack is shown in Fig. 3.2.2-4. A compressive load is applied to the stack through the upper sink mounting plate, the force originating from the compression of a coil spring. To achieve uniform thermal conductance at each surface plate-to-specimen interface, a layer of silica fiber paper is placed at each surface.

Experimental Procedure. Each specimen (two per test) is instrumented with six thermocouples, two in the measuring and one in the guard areas on each side. Chromel-alumel (5-mil dia.) thermocouples are used for the 7-in. system and platinum-platinum/10-percent rhodium (5 mil) are used for the 8-in. tests. Each thermocouple is installed in a 1/16-in. deep groove cut into the surface and attached in place with a refractory cement. Specimens are then dimensioned and installed in the apparatus. The stack for the 7-in. apparatus is insulated with approximately 1-in. of fibrous glass batt insulation, and a chopped fiber approximately 4-in. thick, is used for the 8-in. unit.

Testing is started at the lowest temperature in vacuum. Ambient pressure is then raised to the desired levels at one temperature condition. This sequence is repeated until the maximum temperature is reached. Each test condition is maintained until steady-state is achieved, as reflected by three successive sets of thermocouple readings (at one-half hour intervals) which do not vary by more than $2^{\circ}F$. Thermal conductivity is computed from

$$k = \frac{E \times I \times t}{2A \times \Delta T}$$

where E is voltage drop across the main heater, I is current, t is specimen thickness between hot and cold face thermocouples, A is measuring heater surface plate area, and ΔT is the average temperature difference between hot and cold face thermocouples. Estimated maximum uncertainties in thermal conductivity for the LI-900 materials are 7 percent and 10 percent for the 7-in. and 8-in. units, respectively.

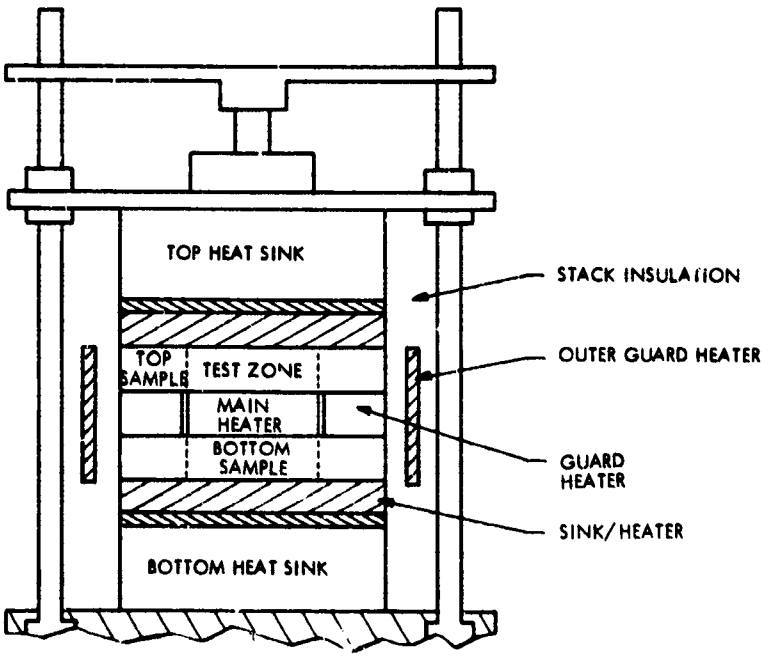

Fig. 3.2.2-4 Guarded Hot Plate Test Stack

3.2.3 Mechanical Test Fixtures and Procedures

3.2.3.1 Preliminary Investigations. At the start of the testing program it was assumed that it would be possible to bond the LI-900 to "attachment blocks" which could then be connected to the testing machine by conventional means. Much of the effort in the early stages of the program centered around finding a suitable cement for bonding the LI-900 to the attachment blocks. Unfortunately, a cement usable above 800°F was never found.

There are several available cements allegedly usable to 2000°F (and even higher). First, it is evident from working with these cements that they possess almost no strength at the higher temperatures. This is not necessarily a reflection on the honesty of the manufacturer's claims. In most applications (described in their catalogs) these "cements" are used as potting compounds and sealing materials, in places where the loads to be carried are very small, or in "confined compression." In all such cases the cement can perform its function at low stress levels and where the stress is mainly compressive.

Despite the low strength of the cements tried, most of the failures observed were in the LI-900 immediately adjacent to the cement line. It was found that most of the basic constituents of high-temperature cements contain compounds which are chemically incompatible with LI-900 at temperatures over 1000°F. The offending compounds are alkali metals, phosphates, sulphates, and oxi-sulphates. The full chemical explanation for this is not within the domain of this report. Of the six Sauereisen cements tried (Nos. 1, 9, 29, 30, DW30, and 75) none were found suitable for use with LI-900. They all displayed substantial strength at room temperature and no strength at 1600°F, with the failure occurring in the LI-900 adjacent to the bond (not in the cement line). Sauereisen No. 29 reputedly contains zircon and only very small quantities of sodium silicate. This cement proved adequate for bonding the coatings to attachment blocks. In this case, the failure loads of the coating specimens (which are very thin) were low, the area of the bonded surfaces relatively large and acting in shear, and the joint and attachment blocks out of the heated zone (though still experiencing an appreciable rise in temperature – not exceeding 1000°F). This cement did not work for the tension tests and showed the same type of failures as the other cements in tension tests at 1600°F.

The search then shifted to the establishment of a suitable method for clamping the LI-900 in the testing machine. The problem here is that the bearing or compressive stress field of the clamping can undermine the tensile or shear strength of the LI-900 at the boundary of the clamped zone. While this might have been overcome by having oversize specimen ends so that clamping pressures and tensile stresses in the clamped zone could be low, this solution was not employable because the specimen sizes had been permanently established early in the program, based on a tight compromise involving material availability and the minimum acceptable size for a bonded specimen.

While the primary goal of the testing program was to establish the mechanical strength characteristics of the LI-900 (and its coating), a secondary but equally vital goal turned out to be establishing a realistic and economically feasible test. The difficulties encountered, the solutions devised and their relative successes, will be discussed in the test procedures subsection for each test type. In some cases, a certain type of test had to be performed in different ways at different temperatures. When this was

necessary, and where possible, tests at one of the temperatures were run using both methods for comparison. However, even when this was done all questions were not fully answered because batch variations were often a factor. It is apparent that variations in properties exist from one batch to the next. Even within a given batch, where the numbering is indicative of the position within a slab from which the batch was cut, the properties appear to vary gradually with the specimen number. Where a batch change occurs, a reference to it will be made in the tables.

3.2.3.2 Tension Tests. If a suitable cement for use at 1600°F had been found, the plan was to use a 1 by 1 by 3-in. prismatic specimen with the 1-in. square faces bonded to attachment plates. At room temperature this has proven to be a satisfactory test configuration, using an epoxy to bond the LI-900 to the aluminum end block. (For elevated temperatures and at −250°F, quartz attachment blocks are used to match the expansion coefficient of the block to that of the LI-900.) Since the specimen has a uniform cross-section, and since the modulus of the end attachment blocks is so much greater than that of the LI-900, the modulus of the LI-900 can be obtained with very little error by measuring the relative motion of the attachment blocks. This is done with a pair of differential transformers, one at each side of the specimen to average out any bending that may occur.

Figure 3.2.3.2-1 shows a 1 by 1 by 3-in. specimen bonded to two aluminum blocks. The blocks, in turn, are attached by screws to a bracket which holds the differential transformer on a "shelf" on which the probe of the differential transformer rests (labelled "front"). This same bracket, at each end, is part of a combination clevis and universal joint. Having these U-joints at each end of the specimen improves alignment under tension and minimizes bending moments. One of the differential transformers is visible in the center of the picture. Two differential transformers visible on either side of the specimen were used to measure the lateral contraction of the specimen under load (i.e., Poisson's Ratio). The side differential transformers have their probes lightly spring loaded toward the specimen by pieces of shimstock bent into a loop. The axial differential transformer probe travels downward (as the specimen extends) by gravity alone. A small wad of sealing putty is visible on the probe shelf; this is used to hold the probe in its true vertical position during setup.

At -250°F, quartz blocks replace the aluminum attachment blocks, and a specially-slotted jaw is used to attach the quartz to the clevis and testing machine (see Fig. 3.2.3.2-2). The differential transformers have been replaced by "clip gage" extensometers because frost causes the core of the differential transformer to stick in the coil unit. A "clip gage" is a small arch made of shimstock bent to the correct proportions and strain gaged at its apex. The arch span is purposely slightly oversize so that it must be cambered closed a small amount to fit into special slots machined on the attachment block holders. This causes it to be highly spring-loaded against the holder blocks. Any change in position of the holder blocks (due to elongation of the specimen) causes a change in strain in the arch. This is measured by the strain gages. The clip gage signal must be greatly amplified, since the arch is basically a strain "demagnifier." The clip gages are calibrated at -250°F by a special calibration fixture which replaces the specimen and attachment blocks, and is made to move (without appreciable stress in the pull rods) by the same drive mechanism that applies force to the specimen during

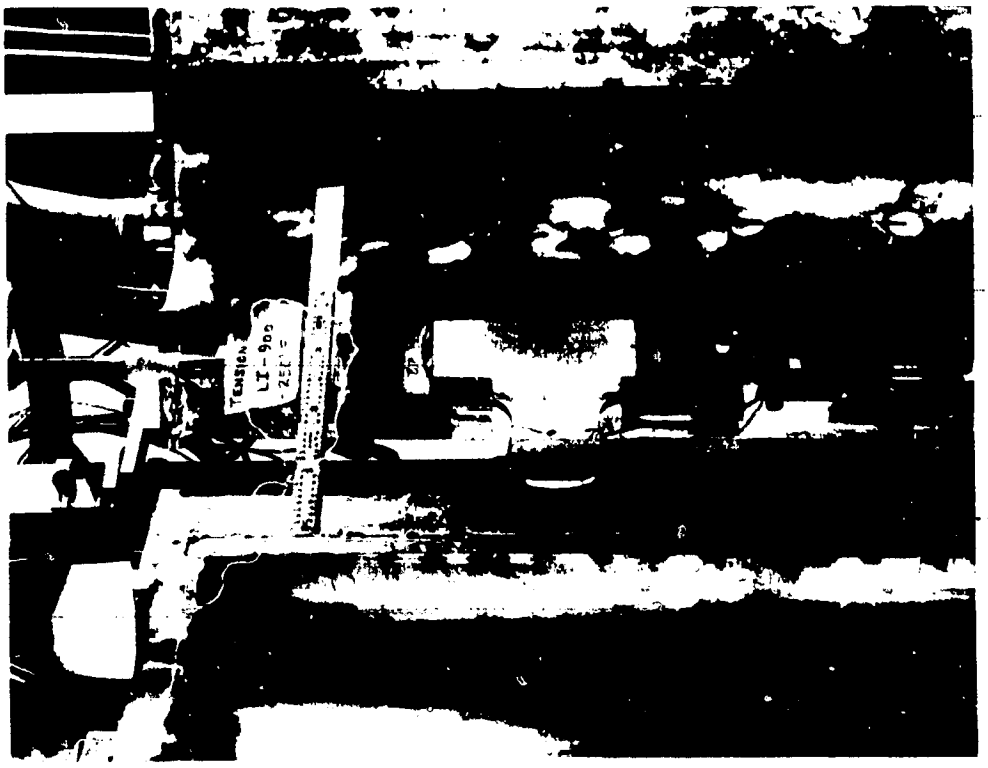

Fig. 3.2.3.2-2 Tension Tests on 1 by 1 by 3-in. Specimens at -250°F

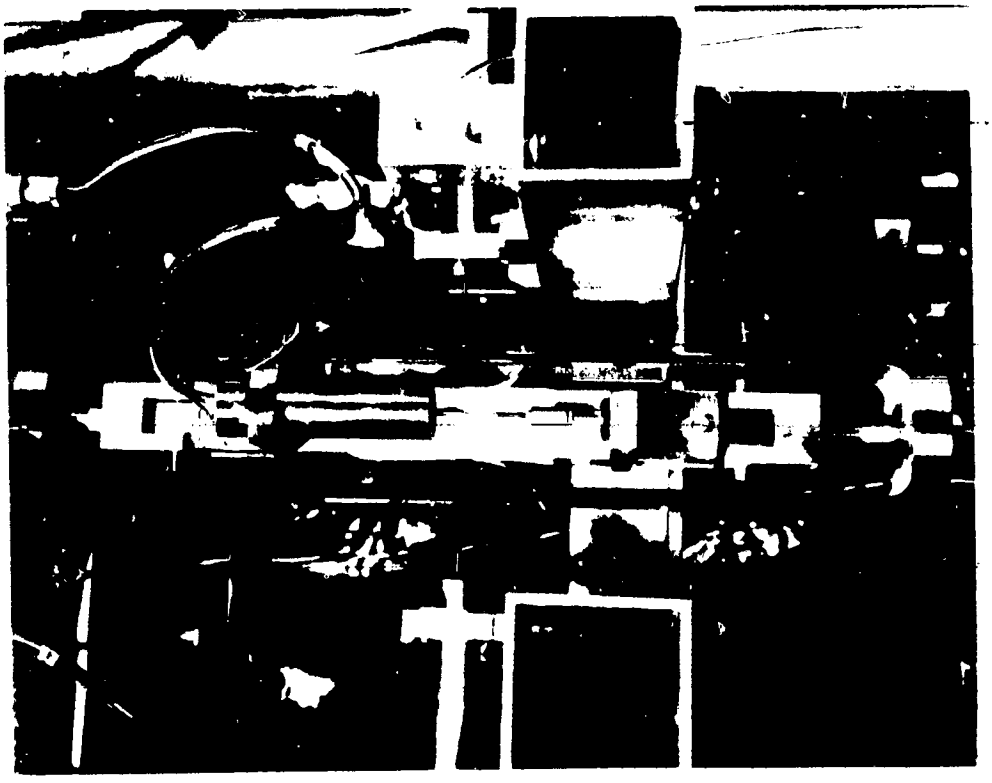

Fig. 3.2.3.2-1 Tension Tests on 1 by 1 by 3 Specimens at Room Temperature

actual tests. A dial gage outside the cold chamber monitors the motion applied to the calibrator

The cold tests are performed inside a triple-walled cold chamber which opens into two halves (as shown in Fig. 3.2.3.2-2) for specimen installation. The cavity formed by the two outer walls is filled with liquid nitrogen. The boiloff gas circulates down a second (inner) cavity formed by the two inner walls and is then released into the central test chamber, from which it leaks into the atmosphere through the two end openings. A positive pressure is thus maintained in the chamber. The intermediate cavity serves to minimize a "cold spot" formed by the LN_2 in the partially-filled outer chamber. The latter chamber acts as a heat barrier as well as the source of cold gas. The central chamber temperature is controlled by the level of LN_2 in the outermost cavity. The temperature response of the system is quite sluggish, so that uniform temperature is easily maintained during a test of a few minutes duration. The tolerance on temperature control is $\pm 15^{o}F$. Most of this uncertainty arises out of the thermocouple placement.

An iron-constantan thermocouple was pressed lightly against the surface of the LI-900 (visible in Fig. 3.2.3.2-3). In a practice run it was found that an external thermocouple read within five degrees of a thermocouple embedded to the specimen's centerline if the rate of change of temperature on both thermocouples had become very small. This meant that it was not necessary to embed the thermocouple in the test specimens and risk causing a stress concentration and premature failure of the specimen.

At all elevated test temperatures (400, 800, 1200 and $1600^{o}F$), a specimen clamping fixture had to be used because no cements were satisfactory (see Par. 3.1). The device is shown in Fig. 3.2.3.2-3 and consists of two large serrated plates which sandwich the specimen at each end. The plates in each pair are drawn together by four screws which fall just outside the flared ends of the specimen "dog-bone" outline. The surface clamped by each large plate is 0.75 in. by 0.75 in. In addition, two smaller plates clamped the smaller side faces of the flared end. These side plates are drawn against the specimen by two screws (each) threaded into the layer plates. The contact area of each of these side plates is 0.50 in. by 0.75 in. These side plates were soon dropped because they were found to be unneeded.

Various types of serrations were tried. The first type was a saw-tooth pattern (0.125-in. pitch, 0.020-in. depth). The saw teeth are visible on the side plates of Fig. 3.2.3.2-3 and in Fig. 3.2.3.2-4 at the left of the picture. The pattern was temporarily dropped in favor of a snake-skin pattern (center of Fig. 3.2.3.2-4), created by cutting 0.0625-in. radius grooves at 0.0625-in. pitch in two directions at 45^{o} to the direction of tension. This worked better than the saw-tooth pattern because the latter had a tendency to cut the specimen severely at the first tooth, causing failure in this region. While failures continued to occur at the edge of the grip with the snake-skin pattern, they occurred only occasionally. The snake-skin pattern worked satisfactorily in the $400^{o}F$ and $800^{o}F$ tests, but slippage started in tests at $1200^{o}F$. The slippage was due to the expansion of the stainless steel saws used to clamp the plates together. Since the LI-900 has a near-zero expansion coefficient (compared to 6 by 10^{-6} per ^{o}F for the stainless steel), the expansion of the bolts was relieving the clamping pressure.

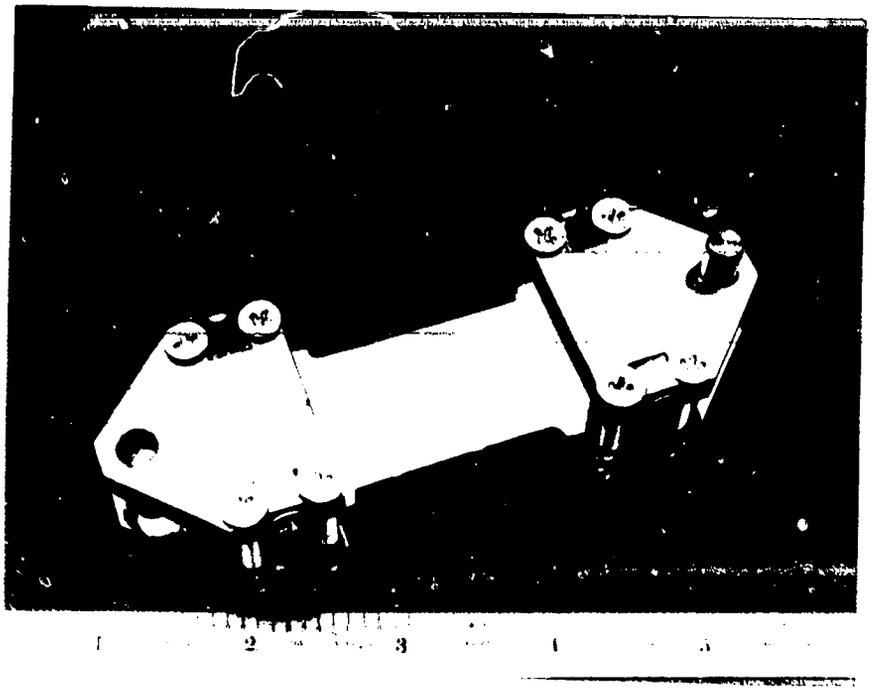

Fig. 3.2.3.2-3 Tension Test Fixture for Elevated Temperature Tests

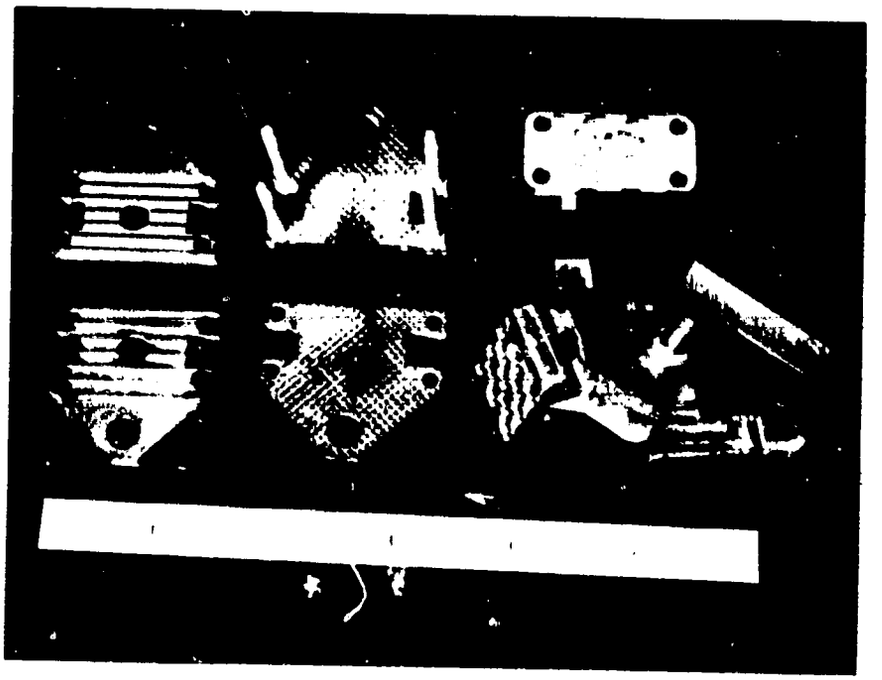

Fig. 3.2.4.2-4 Serrated Face Styles for Tension Tests

This problem was temporarily remedied by using tungsten screws (ground from tungsten welding rod stock). However, this solution proved too expensive when it was found that the tungsten screws (at $160 a set) lasted an average of two tests. (The oxidation of tungsten in air increases drastically around 1200°F, and the oxide is a fine powder which flakes off easily, permitting the oxidation to continue steadily).

A satisfactory solution was arrived at by returning to the stainless screws and the saw-tooth face, and using the expedient of opening the furnace after soaking at the test temperature, tightening the screws once more, reclosing the furnace, and allowing the specimen to return to its test temperature before initiating the tension test. Opening the furnace in mid-test (once slipping was observed), tightening, and continuing the test after a return to test temperature, was a procedure also used successfully. In tests at 1600°F, it takes over an hour to return to test temperature, even if the furnace is opened only momentarily, so that the furnace opening procedure leaves a lot to be desired.

A new fixture was made, based on the relative success of a principle used in the shear tests at elevated temperature. This device, which is shown at the right-hand side of Fig. 3.2.3.2-4, uses an ice-tong principle to supply clamping force to the specimen, thus eliminating the need for tightened screws. The four screws are still used to apply initial clamping and indentation. This indentation is needed to generate the initial axial force which creates the clamping through the ice-tongs (see Fig. 3 2.3.2-5). The serrations were also changed to a "snow-tire-tread" pattern, achieved by using an 0.25-in. diameter end boring mill at 0.313-in. pitch in the direction of pull and 0.375-in. pitch in the other direction. The overlapping 0.250-in. diameter holes are bored to a depth of 0.030 in. (see Fig. 3.2.3.2-6). The result is a series of approximately rectangular protrusions 0.030 in. high. When these grips are used, the screws are tightened until the protrusions are almost completely embedded (this is easily visible at the edges). In this configuration of grip, only 8 percent of the grip touches the specimen. The remaining 92 percent remains undamaged and appears better able to transfer the stress than when the entire surface is "crushed" by the grip (albeit a much lower level of crushing stress). In all other grip face styles, a small torque wrench was used to establish a repeatable level of tightness in the clamping. The torque levels used ranged from 12 to 24 in.-oz with 16 in.-oz proving to be the most satisfactory for the snake-skin pattern. If the torque is too light, the specimen slips; if it is too high, the specimen becomes crushed in the grip and fails in the crushed region. Some specimens proved to be more sensitive to crushing damage than others. This will be discussed elsewhere.

The furnace used in elevated temperature tests was a split-muffle furnace, in which the two halves (normally hinged) had been separated 0.50 in. by a sheet of transite. Gaps in the transite sheet left a slot through which extensometer probes penetrated to the specimen. The furnace was mounted on a sliding frame (with linear ball bushings), which allowed it to slide vertically. A cable, pulley, and counterweight made it very easy to move the 80-lb furnace up, exposing the test frame and specimen (see Fig. 3.2.3.2-7). In its raised position, the furnace remained at its full heating level, so as to minimize the time required for warm-up after specimen installation. The furnace temperature was manually controlled. Temperature monitoring on the specimen itself

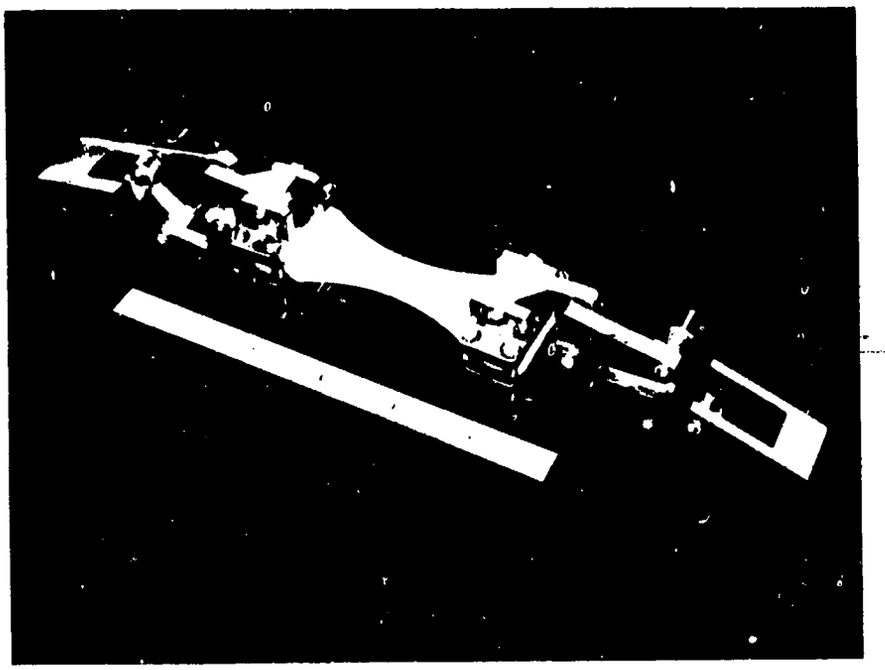

Fig. 3.2.3.2-5 Ice-Tong Tension Grip

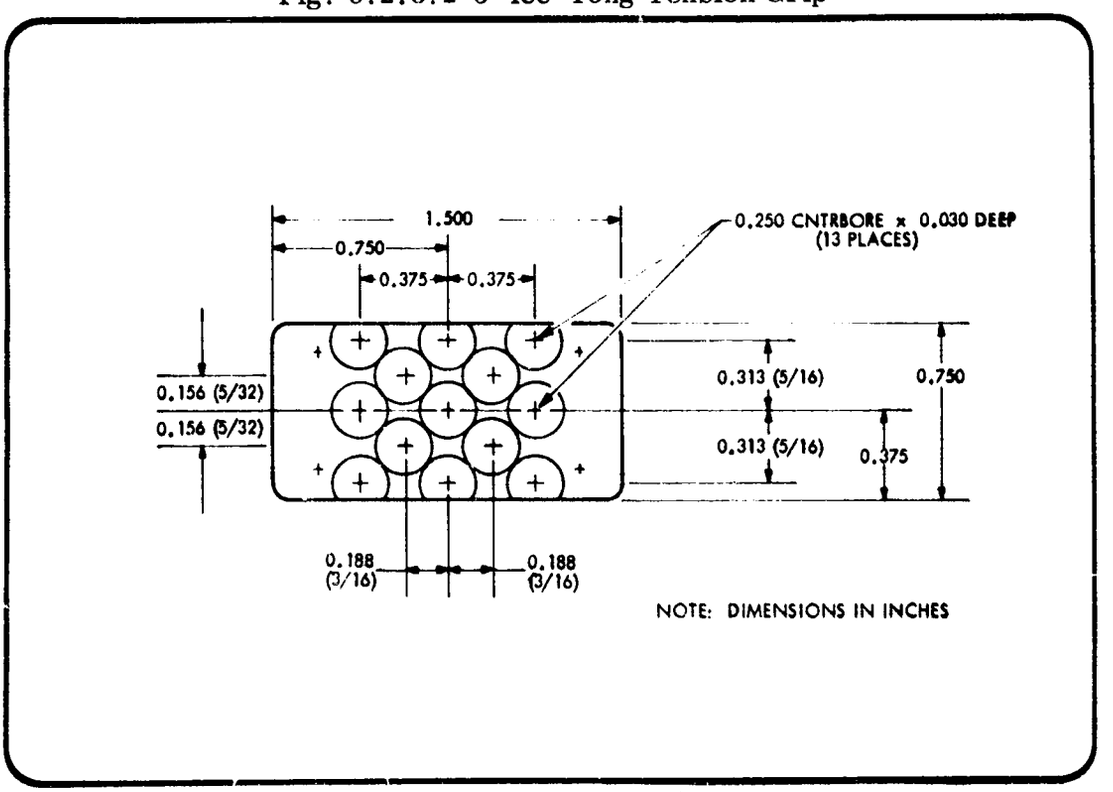

Fig. 3.2.3.2-6 Snow-Tread Grip Pattern

was by means of an iron-constantan thermocouple. As in the case of tests at -250°F, an exploratory test with embedded thermocouples showed that a surface thermocouple was a reliable index of specimen temperature once a temperature plateau had been reached and held for about five minutes.

In all tensile tests, load was applied to the specimen by a pull-rod connecting the U-joint (at the specimen) to a 40-lb load-cell. This load cell, in turn, was connected to a small screw-jack driven by a dc motor. The testing rate was controlled by the dc voltage to the motor, and was set at approximately 0.5 percent (strain) per minute. The load was reached by a small stainless steel frame milled from a 2.5-in. diameter stainless steel billet (Fig. 3.2.3.2-8). This made it possible to immerse the entire load reaction frame inside the cold chamber, or the 3-in. (internal) diameter of the furnace.

At elevated temperatures, strain was measured directly on the specimen by a pair of extensometers whose probes penetrated the furnace wall (through special slots) at right angles to the axis of tensile stress (see Fig. 3.2.3.2-9). In this figure, the furnace is raised but the slot for the extensometer is visible on its base surface.

The extensometers used a differential transformer as the sensing element. It was placed well outside the furnace where, shielded from the radiation by a piece of foil, it operated at room temperature. The motion of two points on the specimen was transferred to the differential transformer coil and core by two levers operating in seesaw fashion, pivoted at approximately their mid-point on crossed invar flexures. The cool end of the lever was machined from an invar billet, and this included an integral crossed flexure and center reference (fixed ground) block. Both levers were, in fact, integral with the center reference block, the whole device being machined out of a single invar billet. The hot end of each lever was a 0.25-in. diameter alumina rod (7 in. long) potted into the remaining invar half. Figure 3.2.3.2-10 shows the left and right-hand extensometers on a special calibration fixture. The tips of the alumina probes each have a 45-deg. conical tip, 0.040 in. high. This tip was lightly pressed into the LI-900 (see Fig. 3.2.3.2-11). The amount of pressure was adjusted and gaged by having the extensometer mounted on a pair of flexured linkages. The extensometer and linkage assembly were mounted on a micrometer stage, which permitted a precise motion in a direction perpendicular to the loading axis of the specimen. A fixed piece of heavy shimstock (see Fig. 3.2.3.2-9) acted as a reference point when the whole assembly was translated toward the specimen. When the probes made contact, the extensometer translated backward relative to the micrometer stage (on the flexured linkages). When they had translated backward about 0.050 in. and made contact with the heavy shimstock reference, the contact pressure was approximately 15 grams and penetration of the cone point approximately 0.030 in. The above figures were found by trial and error to be optimum. Other adjustments were included in the extensometer base to ensure that both probes advanced to the same depth. Penetration was made in small, roughly equal, and consecutive steps from the left and right side of the specimen so that the penetration force would not push the specimen out of alignment.

Alignment adjustments were made with the furnace "up" and penetration was only initiated after the specimen had reached the test temperature. This procedure was necessary, since the thermal expansion of the load reactior frame caused the entire specimen

Fig. 3.2.3.2-8 Load Reaction Frame With Tensile Specimen in Place

Fig. 3.2.3.2-7 Tensile Tests at Elevated Temperature (Furnace in Raised Position)

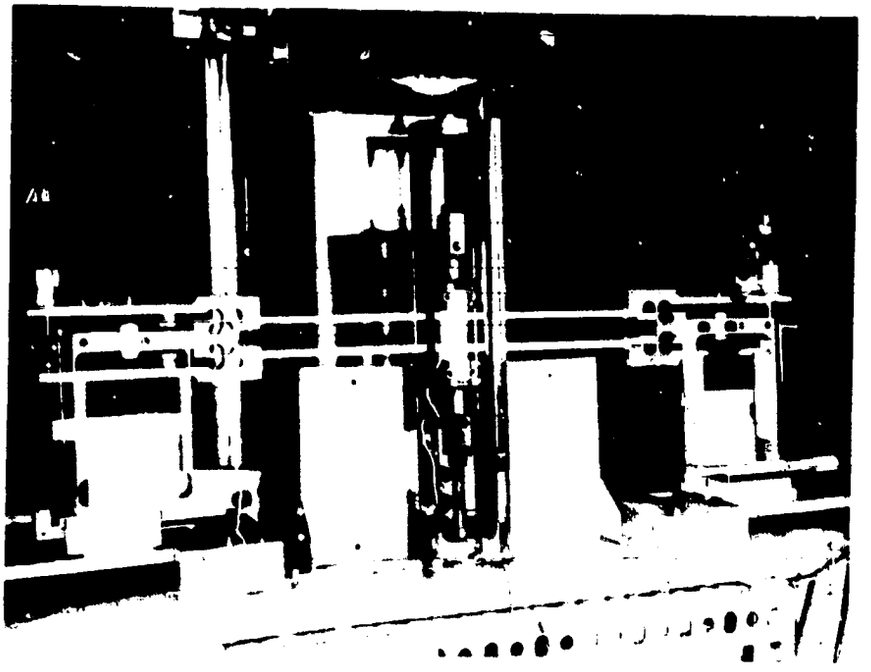

Fig. 3.2.3.2-9 Extensometer for Tests at Elevated Temperature

Fig. 3.2.3.2-10 High Temperature Extensometer on Calibration Fixture

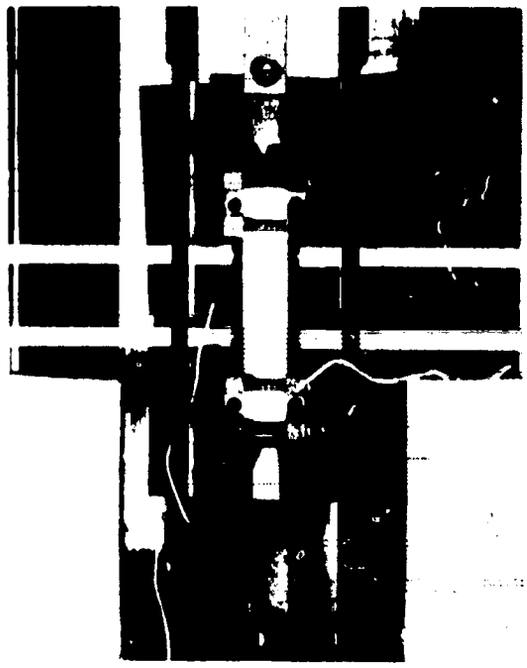

Fig. 3.2.3.2-11 Extensometer Tips Before Penetration

to rise about 0.10 in. (at 1600°F), and this amount exceeded the usable range of measurable motion. Since the strain-to-failure of LI-900 is on the order of 0.25 percent and the gap length used was 1.00 in., the relative motion being measured was 0.0025 in. The system magnification was nominally 2000 (5 in. on the recording chart for 0.0025 in. of relative motion on the specimen), and system accuracy is estimated to be between two and three percent. The actual resolution was better than 25 microinches.

The extensometers are calibrated on a Templin calibrator. This device (see Fig. 3.2.3.2-10) can apply a motion of 0.002 in. with an accuracy of ±0.000002 in., so that the reference standard is not a significant source of error. Blocks of LI-900 were bonded to the jaws of the calibrator, and the repeatability of measurements was studied as a function of tip penetration in the LI-900. It was determined that with approximately 0.030 in. of tip penetration the repeatability of the calibration was better than plus/minus one percent if a new penetration(in virgin material) was made for each trial excursion. The return-to-zero and repeatability on successive cycles (without relocation of the tip) was only plus/minus five percent. Since actual tests are single (one way) cycle events, it is felt that one percent repeatability (based on penetration into virgin material) is a justifiable claim.

Elastic modulus had to be measured on specimens different from those used to determine the ultimate strength. This situation arose out of the inability to bond specimens.

Three inches of overall length was budgeted for the bonded specimens (which were to be 1 by 1 by 3 in.). When it became necessary to resort to clamping grips, the specimen had to have a dog-bone outline. Since one inch of gage length was the minimum acceptable for the extensometer, very little length was left for a radius and transition between the gage length section and the wider ends, (the gage length section obviously requires a constant cross-section) so modulus specimens were made with a 0.125 in. radius at the transition. It was evident that all specimens would fail at this transition zone, and most probably at a stress less than it would fail at if the failure occurred in a region devoid of any stress concentration. For this reason, specimens with no straight section, but with a large radius and very gradual change in cross-section, were used for determination of the ultimate strength. Strain was not measured on these specimens (see Fig. 3.2.1-3). A review of the test data shows that for the weak direction specimens, the failure loads for the modulus specimens was very nearly the same as for the ultimate specimens (at all temperatures above room temperature). For the strong direction specimens, the ultimate specimens produced higher values than for the modulus specimens. This implies a certain insensitivity to stress concentrations when the stress is in the weak direction.

3.2.3.3 Shear Tests on LI-900. As in the case of the tension tests, the fact that specimens could not be bonded to attachment bars forced devising a radically different test method from the one originally planned. The original method involved a torsion fixture and two specimens being tested simultaneously in shear at opposite ends of a diametral set of bars. One bar was rotated relative to the other by the torsion fixture. The shearing stress on the specimen could be calculated from the measured torque. (This device is described more fully later in the text.)

The substitute device was a short beam bend test, in which the two ends of the beam as well as a fairly wide central zone were rigidly clamped to prevent rotation. This fixity of the ends and center reduces the bending moments and minimizes the unwanted bending stresses in the specimen. The fixture is shown in Fig. 3.2.3.3-1. In the upper right, the fixture is shown fully assembled with a specimen in place and with a clip gage attached to the fixture.

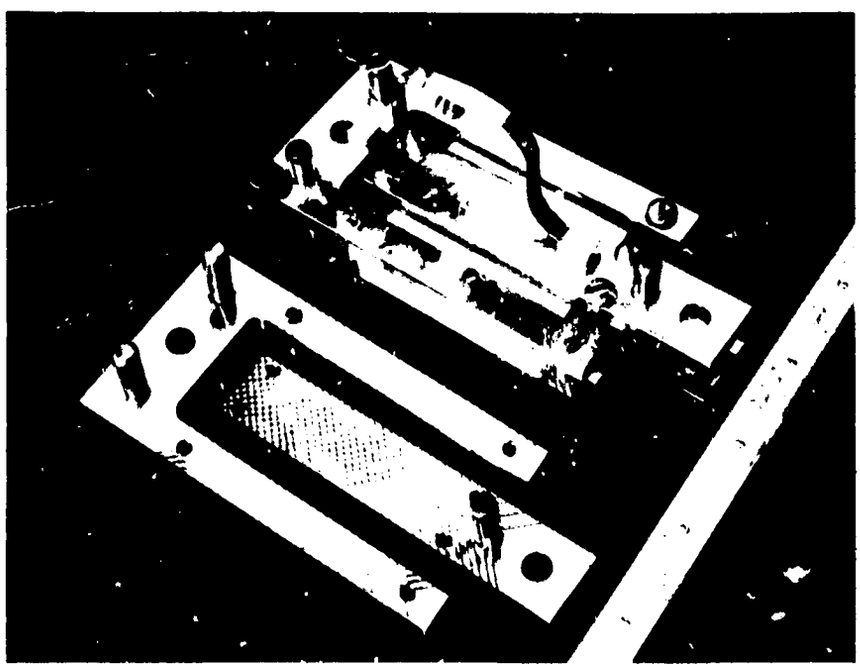

Fig. 3.2.3.3-1 Shear Test Fixture (-250°F and Room Temperature)

The gripping face shown has the snake-skin (see par. 3.2.3.2) pattern, and this was used on all -250°F and most of the room temperature tests. The specimen is 2-in. square by 3/8-in. thick. The center zone clamped by the I-bracket is 0.75 in. wide, and the two edge clamping strips (the verticals of the U-shaped piece) are 0.375 in. wide. This leaves a clear span of 0.25 in. between the U-bracket and the I-bracket.

The area under shear stress is 0.375 in. by 2.00 in. on each side of the I-bracket. Some controversy exists as to whether a parabolic stress distribution applies (as in the case of a beam with a rectangular cross-section), and whether a 1.5 factor should then be applied to obtain the peak stress rather than the average stress. To be on the conservative side, the 1.5 factor was not applied, and the values reported are the average stress.

In an effort to establish the magnitude of slippage in the grips (which would affect the calculated shear modulus), grips with gaps other than 0.25 in. were tried. At room temperature, 10 tests were run with a 0.25-in. gap, 10 tests with a 0.125-in. gap, and 10 tests were run with a 0.345-in. gap. Varying the gap resulted in some change in the width of the clamped zone, but it was hoped that the effect of the clamping width would be negligible. Since slippage represents a smaller precentage of the total deformation measured as the span, or gage length, becomes greater, the shear modulus in tests with the largest gap was obviously higher than that obtained with the smaller gaps. In the test with larger gaps however, the bending deflection ceases to be negligible. Various schemes using simultaneous solutions of equations involving the shear modulus and slippage are presented in Appendix B-3. The data values reported in Appendix B-3 however, are for the 0.250-in. gap.

As in the tension tests, a torque wrench was used to apply 16-in.-oz. of torque to each of the four clamping screws. Figure 3.2.3.3-2 shows the shear test fixture in the load reaction frame (which is the same as the one used in tension tests). In this figure, the extensometers are not installed (see Fig. 3.2.3.3-1 for a typical clip gage installation). Figure 3.2.3.3-3 is a close-up of the first shear fixture tried, which used a saw-tooth face. This pattern of serrations was discarded after preliminary tests showed that it damaged the specimen excessively, causing low failure stress values and failures originating in the tooth marks. Also, the horizontal teeth did not inhibit rotation of the clamped zone of the specimen as well as did the snake-skin pattern eventually used.

The clip gage extensometer used in tests at -250°F and at room temperature spanned between the U-bracket and the I-bracket, measuring the gross relative motion of the two parts. The calculation of modulus has to assume that these two parts act as rigid bodies and that they experience negligible strain compared to the deformation of the specimen.

While the shear tests were in progress, difficulties were already being encountered with slippage in tension tests at the higher test temperatures (due to the expansion of the clamping screws). In anticipation of this, an ice-tong shear grip was made. It was first tried and found to be more successful than the snake-skin pattern. The ice-tong shear fixture is shown in Fig. 3.2.3.3-4 and 3.2.3.3-5. In Fig. 3.2.3.3-6 the

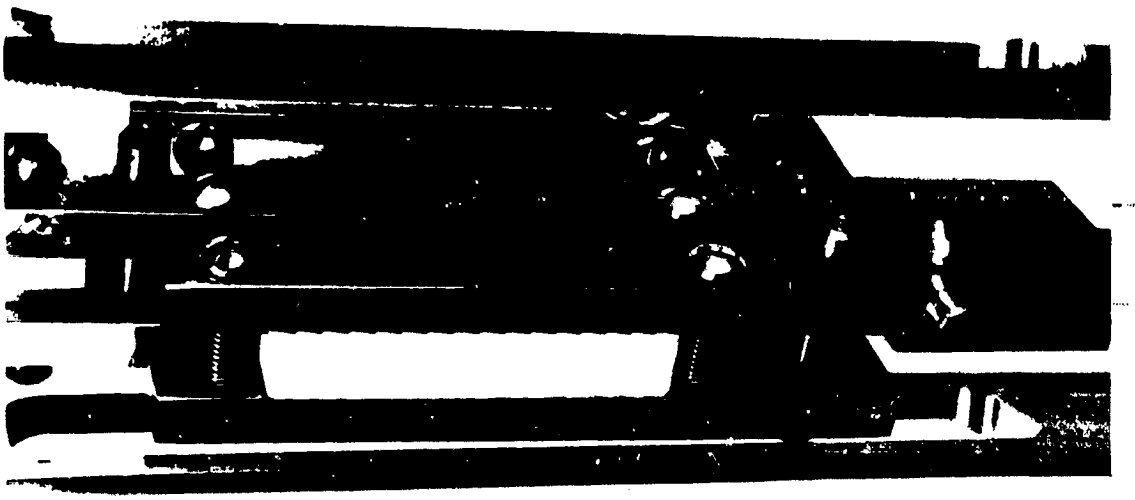

Fig. 3.2.3.3-3 Shear Test Fixture – Saw-Tooth Pattern

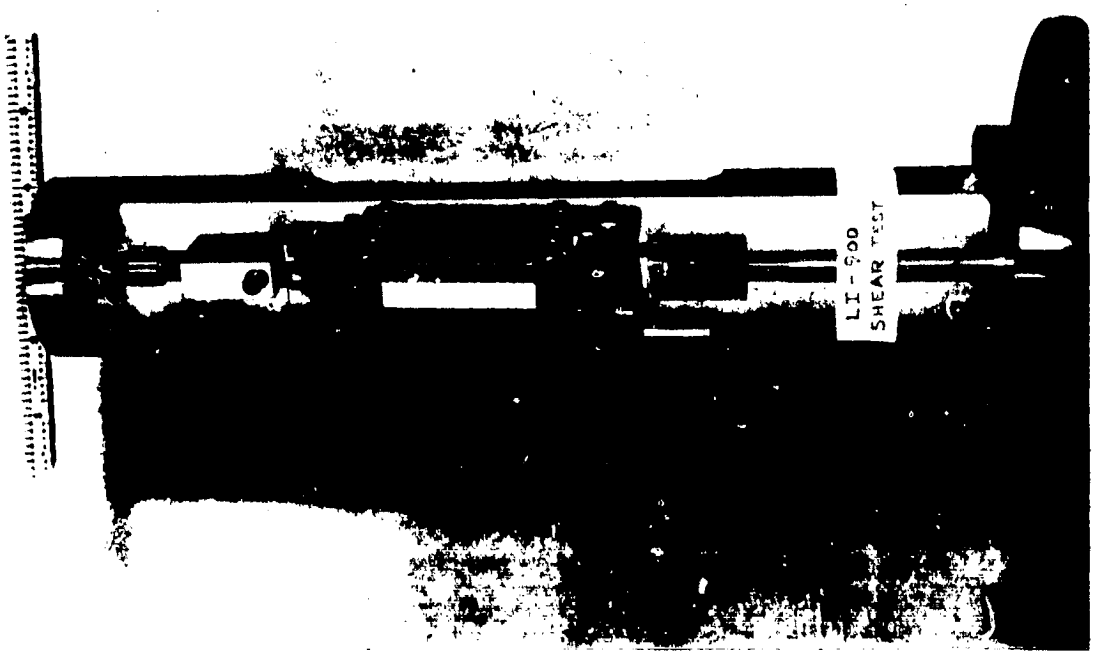

Fig. 3.2.3.3-2 Shear Test Fixture in Reaction Frame

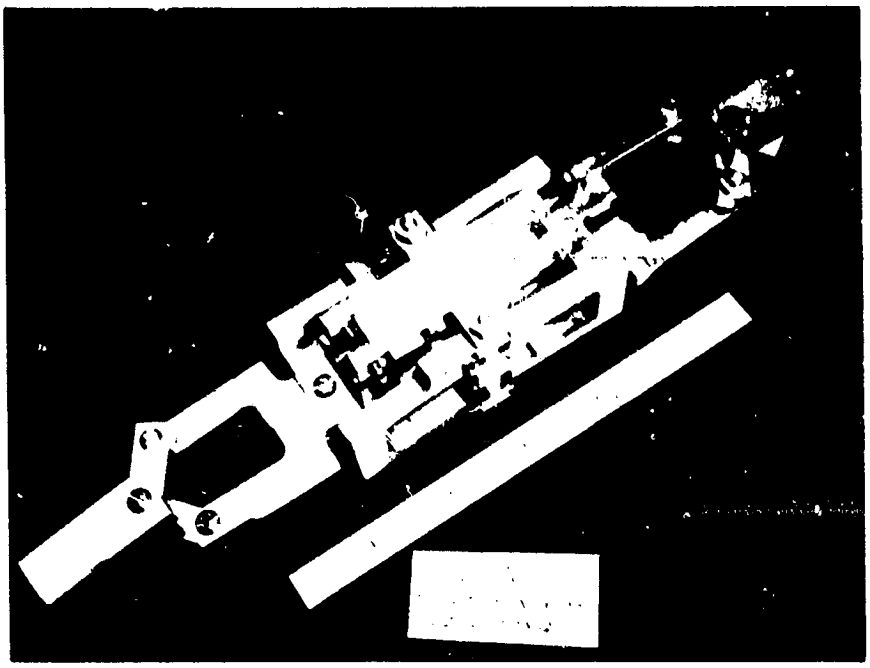

Fig. 3.2.3.3-4 Shear Test Fixture – Ice Tong

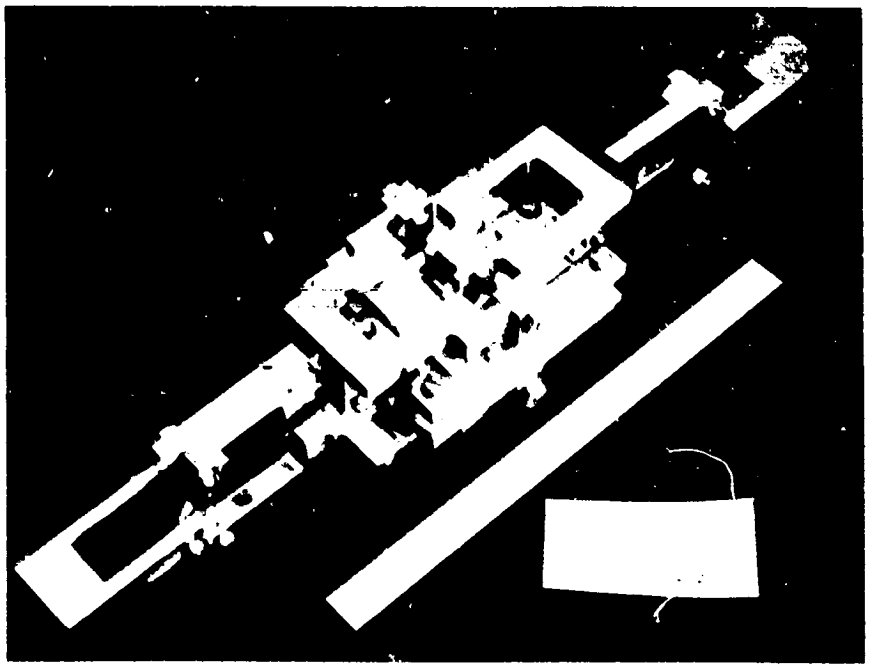

Fig. 3.2.3.3-5 Shear Test Fixture – Ice Tong

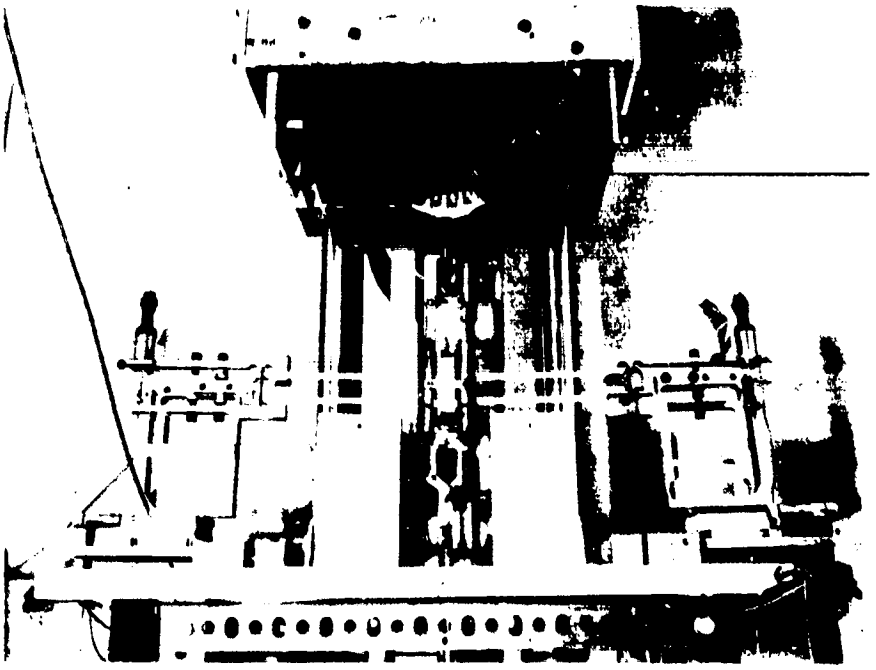

Fig. 3.2.3.3-6 Ice-Tong Shear Fixture in High-Temperature Test Frame

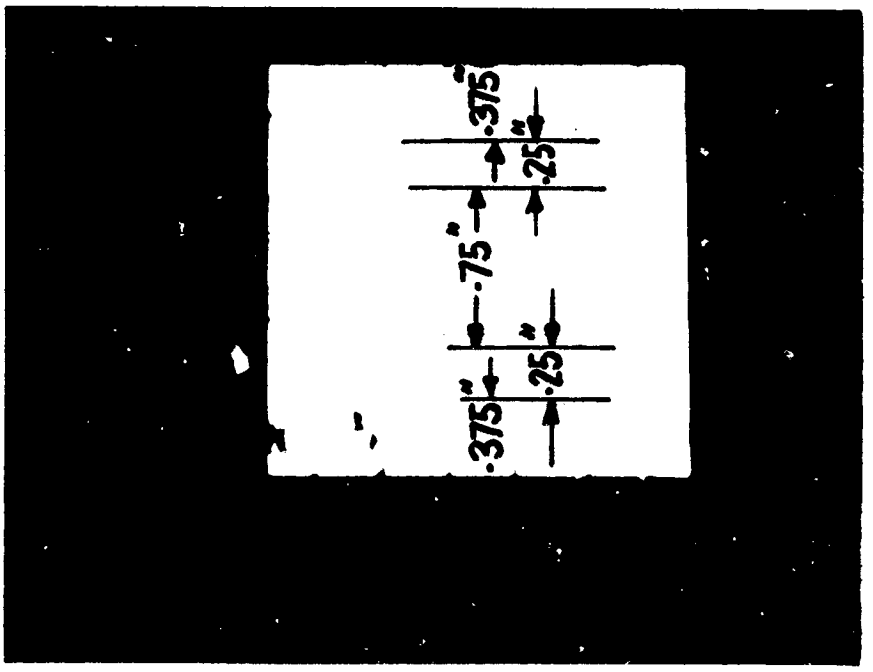

Fig. 3.2.3.3-7 Indentation Pattern of Ice-Tong Shear Fixture

fixture is shown installed in the high temperature test frame. The indentation pattern of this fixture is shown in 3.2.3.3-7. The clear span, or gage length, on this test configuration is 0.25 in. (as marked on the photograph), and the clamped zones are the same width as on the standard snake-skin pattern fixture. Careful scrutiny of this indentation pattern will show that total fixity can not occur right at the boundary of the 0.25-in. gage length, since only about 15 percent of the axial length is actually clamped at this boundary. This means that the gage length is effectively greater than 0.25 in., but how much more is difficult to ascertain.

Lockheed, who designed the grips and supervised their use, is inclined to take a value between 0.35 and 0.40 in., but without more rigorous investigation there is no sound basis for using these, rather than the nominal value of 0.25 in., which is quite satisfactory for comparative purposes (i.e., change of modulus with temperature). A more thorough investigation would require a set of fixtures having different gage length spans, but this will also require a variation in specimen size, since the snow-tire-tread pattern cannot be changed, at least not near the gage length boundary, or else new variables will be introduced.

The snow-tread-tire pattern requires that the protrusions be completely embedded, and this is gaged visually and by feel when the initial clamping screws are tightened, rather than with a torque-wrench, as in the case of the snake-skin pattern. At room temperature and moderate temperatures (up to 800°F) virtually no slipping occurred (a small amount just prior to failure is not uncommon). In the 1200 and 1600°F test considerable slippage was experienced, even at low loads. However, after slippage, the loading process resumes and after several repetitions of slippage and loading resumption, failure is eventually reached. It is felt that this slippage is not truly slipping (as was encountered in the snake-skin grips) because careful examination of the specimen surface shows a clean imprint (shown in Fig. 3.2.3.3-1), and that what appears to be slippage is just a local and sudden crushing at one of the protrusions of the pattern. After this crushing has occurred, some consolidation at the crushing site allows the load to build up again. Eventually, crushing starts at another of the protrusions, with its resultant momentary drop in load. The tendency to crush locally, then, appears to increase markedly in the 1200 and 1600°F tests. The reason why this consolidation or compaction leaves no tear marks is that it happens on a microscopic scale. The slip or discontinuity in the stress strain curve usually amounts to one-half a mil (0.0005 in.), hardly a recognizable increment on a rough fibrous surface. Since the segments of stress-strain curve between slips are fairly uniform in slope, the "slippage" (or consolidation steps) are not detrimental to obtaining a shear modulus.

In the elevated temperature shear tests, strain was measured with the same extensometers as those used in the elevated temperature tensile tests, the only difference being that the probes rested on special "sills" machined onto the I-brackets and U-brackets. (In the ice-tong fixture the U-bracket is more properly an H-bracket because it was more convenient to have the cross-bar some distance away from the ends of the two side clamping bars.)

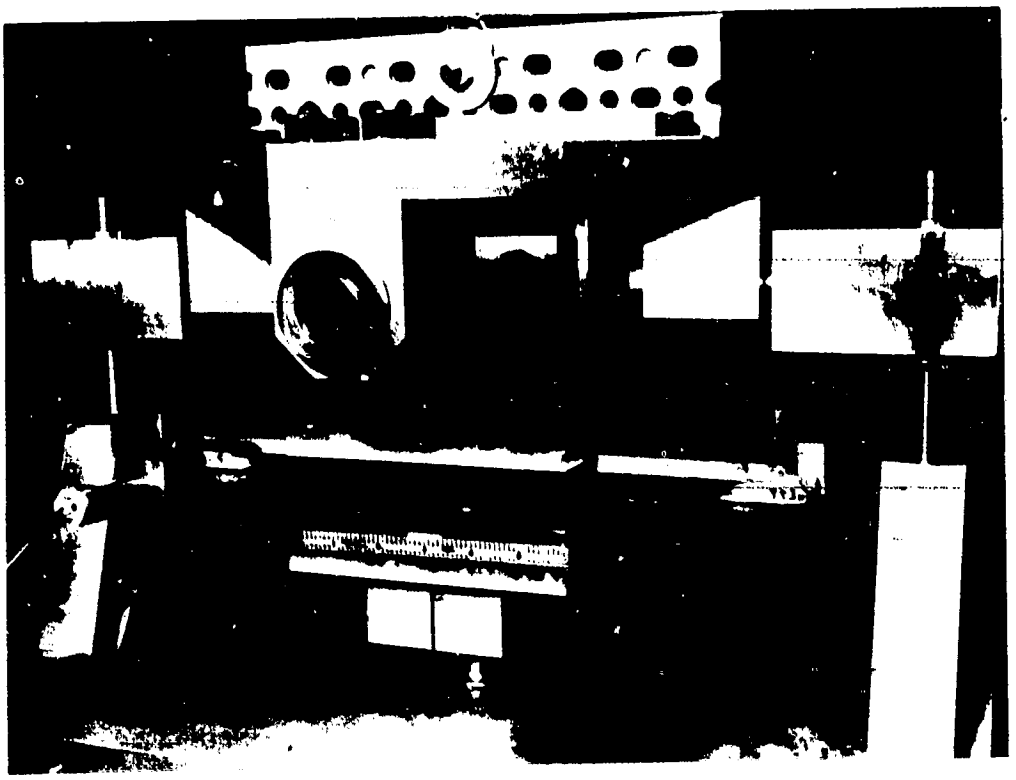

Fig. 3.2.3.3-8 Torsion Test Fixture

As a cross-check on the performance of the short beam shear tests (both the snake-skin and the later ice-tong devices), a series of shear tests was performed on LI-900 at room temperature only using the torsion tester which had been used on all shear tests prior to this contract. The device is shown in Fig. 3.2.3.3-8 and consists of a torque generator (not visible) and a five-degrees-of-freedom reaction head, visible in the upper half of the figure. This reaction head replaces the more usual fixed clamping system to hold the nonrotated end of a specimen under torsion. The drawback to the conventional clamped end is that it applies moments, lateral shear or thrust to the specimen when the clamping is applied (unless everything is in perfect alignment). The five-degrees-of-freedom head holds the specimen against the applied torsion, but is free to rotate (or pivot) about two axes perpendicular to the axis of torsion, and also to translate freely along these two axes. In addition, the reaction head is free to translate along the axis of torsion (permitting the specimen to shorten during the torsion test, and to make its initial length a noncritical item in the test). This is achieved with linear ball bushings and a gimbal arrangement in which the bearings are replaced by the linear ball bushings.

The specimen is prepared by bonding a pair of 2-in. square by 0.375-in. thick specimens to two elongated aluminum plates. The specimens are bonded at each end of the plates and between the two plates. (In the photograph, 2-in. diameter disc specimens are shown instead of 2-in. square specimens. This only changes a coefficient in the data-reduction formula.)

One of the plates is bolted to the torque generator and the other to the five-degrees-of-freedom reaction head. The application of torque to the lower plate places the specimen primarily in shear. To those who argue that this is a better test than the short beam shear, it should be pointed out that in both cases there is, in fact, bending stress as well as shear stress. The beam "axis" in the case of the torsion tester, is parallel to the axis to torsion. The two ends of the beam are translated without rotation of the beam ends being permitted. This leads to zero moment at the center and a moment at each end equal to $P \times L/2$, where P is the shearing force (at each of the two specimens) and L is the gage length of the specimen, in this case 0.375 in. The same formula applies to the short beam test (if each span is considered individually), except that the span L is 0.250 in. In the case of the torsion tester, the section modulus ($1/6\ bh^2$) is 1.33 $in.^3$, whereas in the short beam test it is only 0.124 $in.^3$. Taking into consideration the difference in span of the two types of tests, the bending stress in the short beam test is 7.15 times greater than in the torsion test. This may not be a very significant item, since the peak shear stress does not occur in the same spot as the peak bending stress. Still, if the material has a very low bending (tensile stress) it is obviously more prone to failing in bending if the short beam test is used.

In the torsion tester, twisting of the aluminum bars is a factor which causes an apparent shear deflection less than the true shear deflection. This subject is discussed more fully in Appendix B-4. The following two other points must be raised in connection with the torsion test device:

- Is the shear stress distribution in the specimen (arising out of the twisting of the plates) such that the specimen is favored or penalized?

- Bonding of the specimen causes an effective shortening of the specimen, since the glue is absorbed into the specimen to some degree of depth. (This partially impregnated layer may also strengthen the specimen by "keying" together the jagged profiles of the bonded layers on each face.)

The only shear test which comes substantially closer to perfection (in stress-distribution) is a torsion test on a fairly large diameter thin-walled specimen. Such a specimen was not feasible within the scope of this program, but would certainly put to rest a lot of questions as to the real value of the shear modulus and the shear strength.

3.2.3.4 Coating Tension Tests. Elastic modulus, peak stress, and peak strain were determined for the LI-42 coating at the temperature levels indicated in Table 3.3-1. As in the case with tests upon LI-900, a number of problems were encountered which had to be resolved to ensure that reliable data were being generated. Even so, batch to batch variation in the coatings introduced a factor which makes it difficult to interpret the temperature dependence of the material.

Specimens were delivered deposited on about 1/4-inch thick slabs of RSI which was in the range of 15 to 18 pcf density. This was removed by sanding the specimen on a coarse wood file with light finger pressure. It was found that as much of the relatively soft LI-900 as desired could be removed from the specimen if normal care was exercised. It should be emphasized that the coating consisted of two components. The outermost portion is an approximately 12-mil thick layer of the add-on high emittance layer. This outer layer thickness, it is important to note, appears to remain constant for specimens fabricated from material manufactured at different times. The second layer of material – densified silica – acts as an interface between the RSI and the outer coating layer. This material is softer (lower elastic modulus) than the true coating and, most important, exhibited variations in thickness of from 3- to 12-mils, depending upon the material batch from which it was taken. In all cases, the thickness of the coating specimen used for calculations (and as otherwise referenced) is the total thickness of these two layers, and the term coating is used to describe this composite material. An analysis devised to separate the properties of the two components is described in the section on test results.

Test Fixture and Instrumentation. An overview of the test fixture is shown in Fig. 3.2.3.4-1. Load is applied with a 400-pound screw jack driven by a small dc variable speed motor. A load cell and displacement transducer (DCDT) are incorporated in the load-displacement path and their analog outputs are recorded as permanent X-Y plots. Load path alignment is improved by the use of universal joints and clevises as shown in Fig. 3.2.3.4-2. Cross-head motion is measured by a transducer attached to a by-pass bracket (the upper portion is shown in Fig. 3.2.3.4-2 fixed just at the clevis) and this quantity necessarily – but unfortunately – includes extraneous displacement path motions, such as pin seating and glue deformation. Identification of these quantities was approximated by testing several "zero gage length" specimens. These were specimens made with as short as possible clear span. They were then tested in the same manner as a normal coating and their deflection was considered the sum of all extraneous motion. This factor could then be removed from the actual data. This procedure was applied at all test temperatures and for all end tab configurations as applicable.

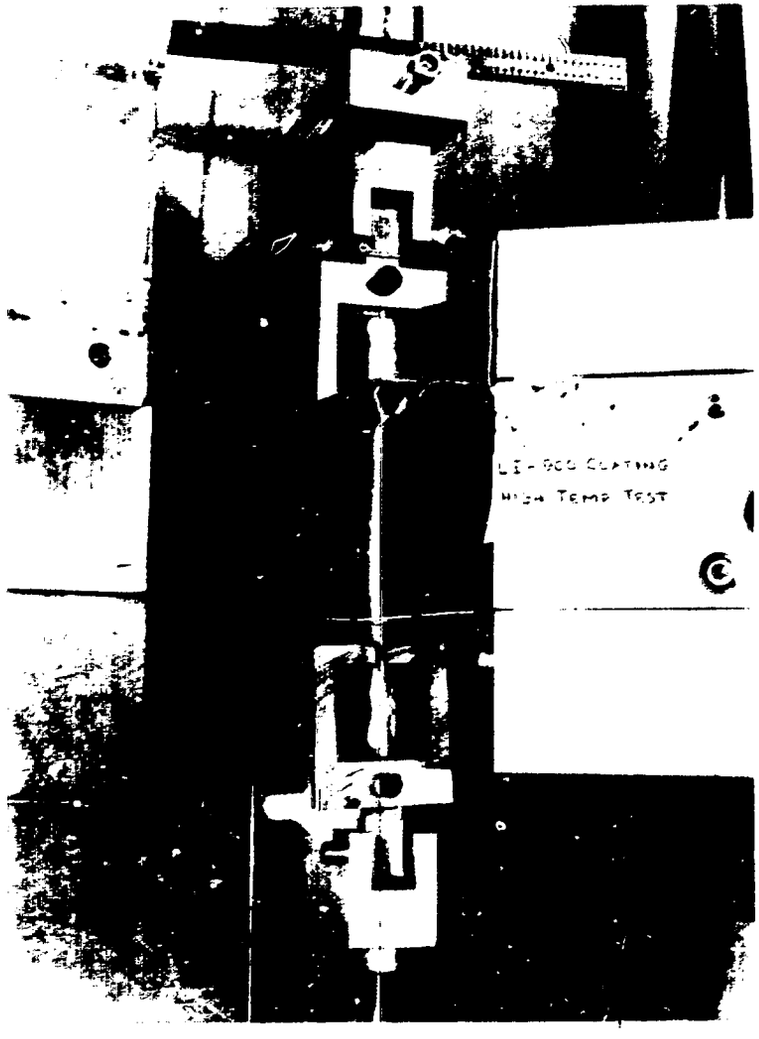

Fig. 3.2.3.4-1 A Coating Specimen in the Test Fixture Prior to an Elevated Temperature Test

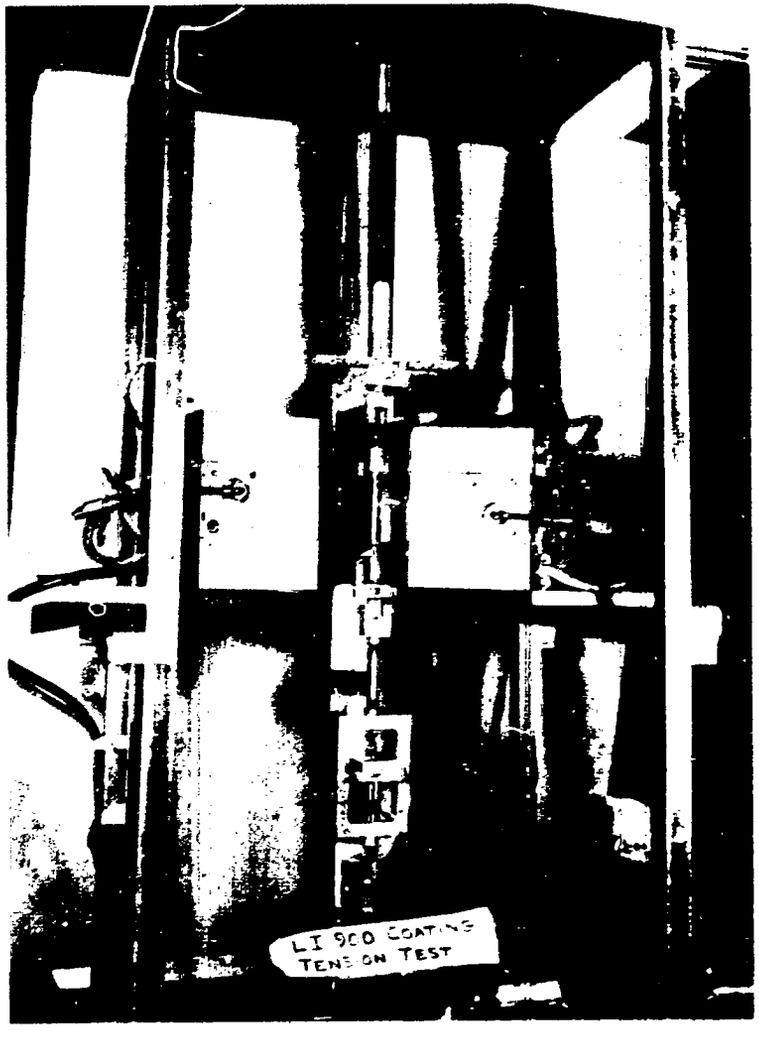

Fig. 3.2.3.4-2 Coating Test Frame in Elevated and/or Room Temperature Test Configuration

Specimen Preparation. Specimen preparation began by removing LI-900 from the coating. The entire coating test program was one of test technique evolution. Procedures were attempted and discarded both in test procedure and specimen preparation and a chronological sequence will be related.

Room Temperature and Cryogenic Specimens. The first specimens produced had aluminum tabs bonded to the ends. These tabs sandwiched the coating at either end and had concentric holes predrilled to receive a clevis pin for test frame attachment. ALL RSI was removed from the coating by the "filing" process in these early tests, and the tabs were bonded on using Hysol epoxy for room temperature tests. The -250°F configuration was the same, except that the end tabs used were stainless steel and the epoxy was replaced by Sauereisen No. 29 low-expansion cement. The tests were successful but there were several drawbacks. Figure 3.2.3.4-3 shows one of these – specimen curvature – very clearly. When all the RSI is removed from a piece of coating of normal specimen length, stress relief causes the curvature which is clearly evident in this photograph. The problem was not a serious one for tests at room temperature, but special and cumbersome procedures were necessary for successful -250°F testing. It was necessary to apply and maintain sufficient room temperature preload to straighten the specimen and keep it straight until the cryogenic test temperature was reached. Many specimens were inadvertently broken during this test phase.

Elevated Temperature Specimens. Two changes were incorporated for the elevated temperature tests. It was found that stainless steel end tabs were unsuitable for even the 400°F test temperature. It was necessary to match the extremely low expansion properties exhibited by both the coating and the Sauereisen cement. Our solution to the problem is shown in Fig. 3.2.3.4-4. Quartz blocks were bonded to the specimen which then is placed in the specially fabricated stainless steel grips. Figures 3.2.3.4-1 and 3.2.3.4-2 show these universal temperature specimen assemblies in the test frame.

Care must be taken in bonding these quartz blocks to the specimen to avoid undesired bending moments during testing. A special specimen preparation jig was devised for this purpose and can be seen in Figs. 3.2.3.4-5 and 3.2.3.4-6. Careful machining and the clamping action of the conical tip screws forces precise side-to-side alignment of the loading edge faces (the interior faces) of the blocks as they are bonded. Figure 3.2.3.4-6 shows several of the finished specimens just before removal from the jig.

The second change was incorporated at about the same time. It had been found from the start that removal of all the RSI from a coating produced an extremely fragile specimen. This was not a serious drawback for specimens with early style aluminum end tabs, but the relatively heavy quartz blocks soon produced an extremely high breakage rate during the normal amounts of specimen handling. I was found that 30 or 40 mils of RSI, when left on the coating during preparation, solved this problem and also eliminated the undesired curvature resulting from a bare specimen. Early tests had shown by this time that there were several orders of magnitude difference between the coating and the RSI in their modulus and ultimate strength values. Thus, the advantage gained in having increased specimen lateral stiffness (which is directly

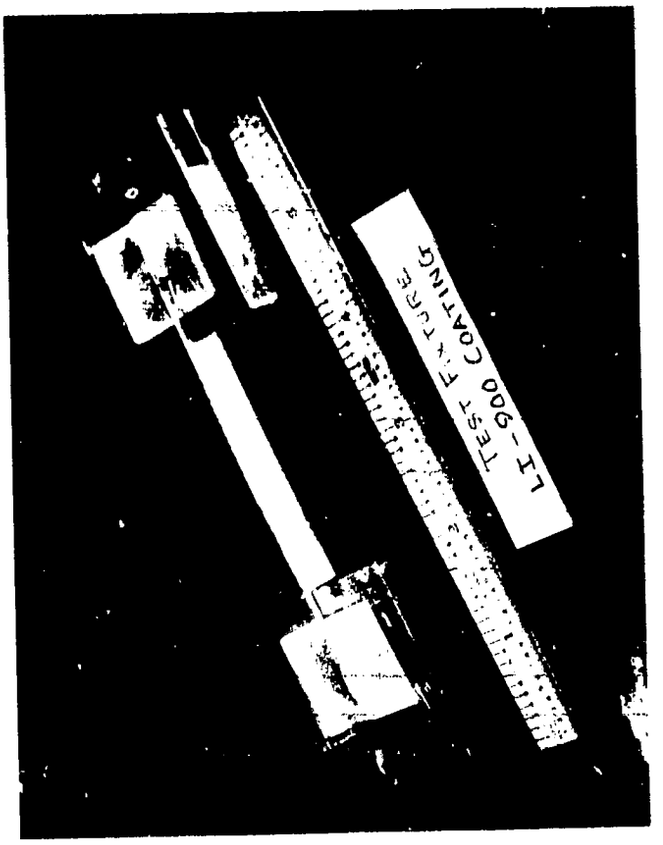

Fig. 3.2.3.4-4 Elevated Temperature Coating Specimen in its Grip Fixture

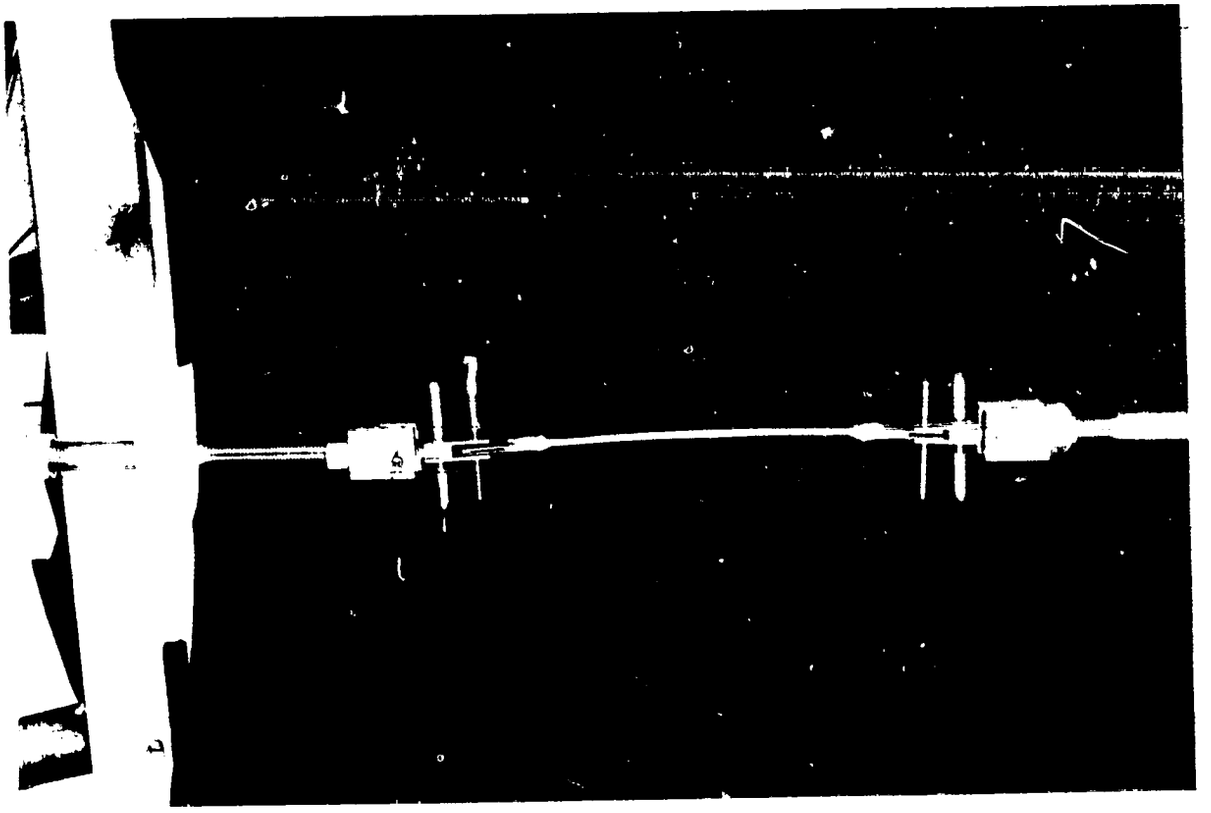

Fig. 3.2.3.4-3 Room Temperature Coating Specimen Mounted in the Test Fixture

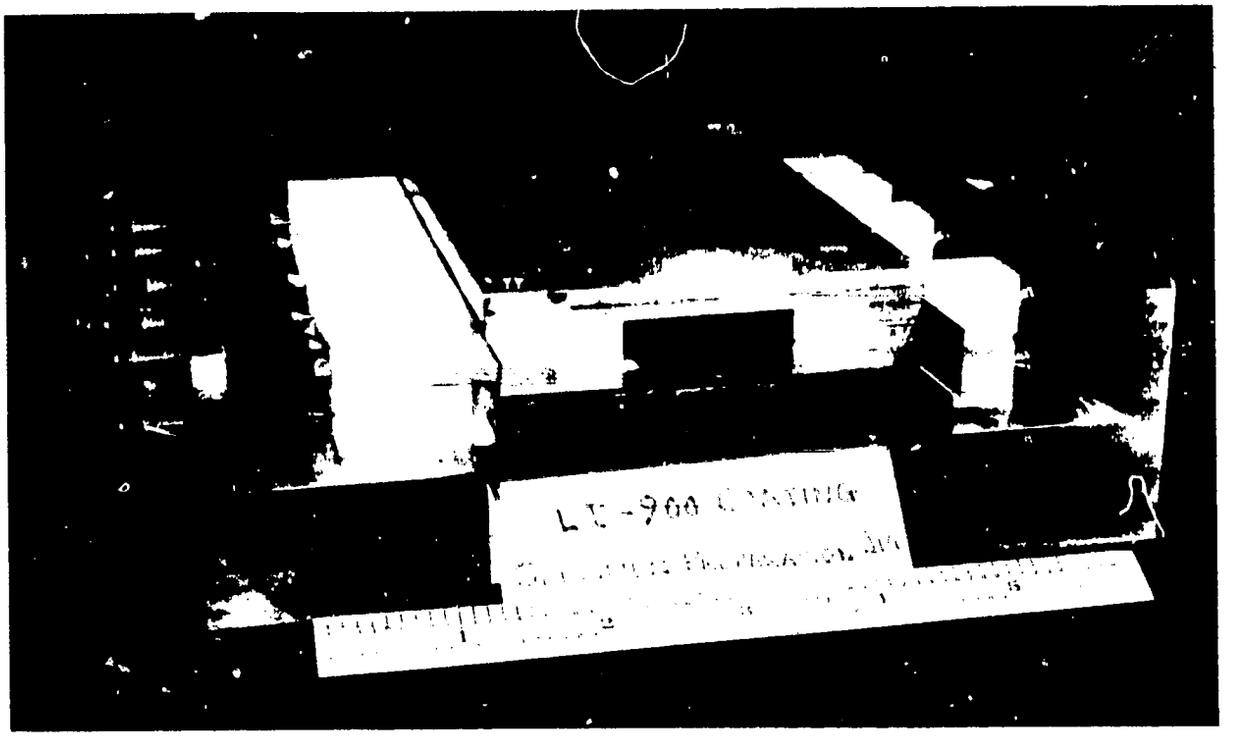

Fig. 3.2.3.4-5 Complete Coating Specimen Preparation Jig

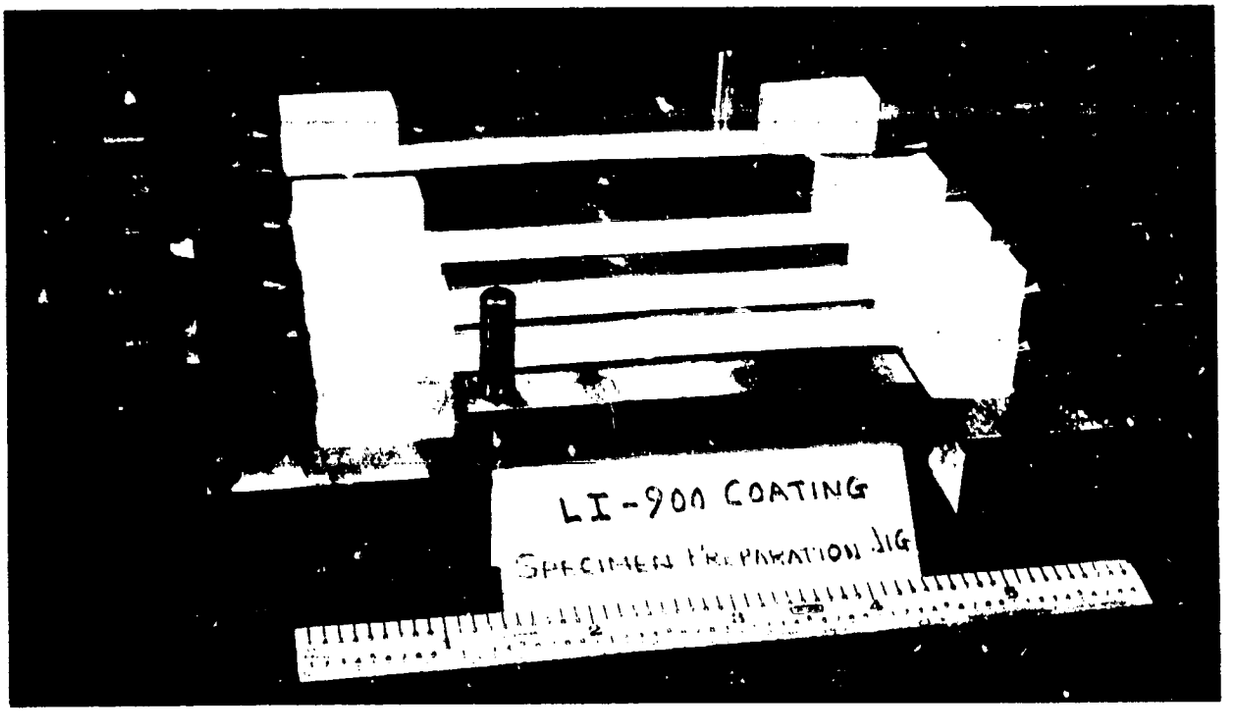

Fig. 3.2.3.4-6 Coating Specimen Preparation Jig Just Prior to Removal of Finished Specimens

proportional to the cube of its thickness) far surpasses any small, probably unidentifiable errors introduced by this procedure. Several 1200°F and 1600°F tested specimens are shown in Fig. 3.2.3.4-7. Results of these tests are reported in Section 3.3.1.

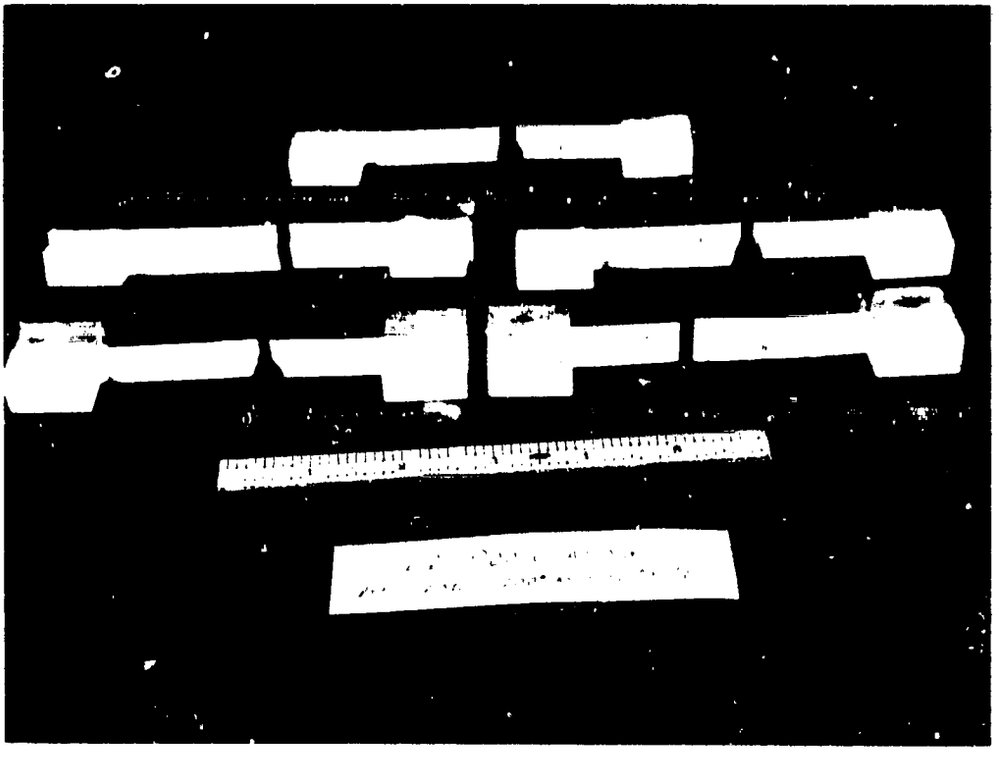

Fig. 3.2.3.4-7 Elevated Temperature Specimens After Testing

3.2.3.5 Accuracy Measurements. The following comments apply to all tests described in sections 3.2.3.2, 3.2.3.3, and 3.2.3.4.

Load cells were calibrated using dead weights accurate to 0.25 percent. The system accuracy, taking into account possible random errors in calibration, as well as in actual measurements, is slightly better than ±2 percent to a certainty level of 99 percent. In elevated temperature tests, the load cell remained at ambient temperature and there was no friction or seal at the point where the pull-rod penetrated the furnace or cold chamber, so that the accuracy is the same as at room temperature.

Deflection and Strain Measurements. Accuracy of the clip gages is ±4 percent. The basic accuracy is the same as that of the load cell, except that an allowance of about 2 percent must be made for non-repeatability of measurements arising out of the seating of the clip gage. At -250°F, a further allowance must be made for slight changes in calibration that are believed to be attributable to variations in the moisture "held" by a coating that protects the strain gage. We estimate the final accuracy (to the 99 percent certainty level) to be ±6 percent, i.e., it is felt that there is a 99 percent probability that the measurements fall within ±6 percent of the values reported.

On the differential transformers used in all elevated tension and shear tests, and in the 1 x 1 x 3 tension tests at -250°F and room temperature, and in all the coating tests the accuracy is the same as for the load cell, i.e., ±2 percent to a 99-percent certainty level. In all tests at other than ambient temperature, the differential transformer was never exposed to anything but ambient temperature, so the accuracy remains unchanged. In the coating test, corrections were made for the compliance of linkages included in the strain measurement "loop", and since this involves an additional set of measurements, the accuracy is decreased by a factor of 1.4 percent, so the final figure is ±3 percent (rounded off upwards from 2.8 percent). The extra set of measurements is described in the paragraph on coating tests, 3.2.3.4, in which specimens of zero gage length are used to calibrate out the deformation of the bond line and linkages in series with the specimen.

3.2.3.6 Cyclic Radiant Heat Tests. Twenty thermal cycling tests were performed on coated LI-900 RSI material to test its performance under an Area 2P heat pulse, with the primary structure at an initial temperature of -250°F. The basic purpose of such tests was to provide sufficient material for evaluation of LI-900 mechanical and thermophysical properties after the equivalent of twenty reentries. A description of the RADVAC facility in which the tests were carried out is given in Appendix B1, as well as a comprehensive summary of the tests. A general view of the setup and the four 12 by 12 by 3-in. coated blocks prior to the start of the thirteenth cycle is shown in Fig. 3.2.3.6-1.

The maximum temperature measured through the LI-900 material are shown in Fig. 3.2.3.6-2, with the temperautre data band encompassing temperature measurements taken over the 20 cyclic tests. To evaluate the material's thermal performance, temperature predictions were made for the material assuming the first and last thermocouple measurements (0.14 in. and 2.45 in. depth) as boundary conditions for the thermal model. Maximum temperatures predicted in depth (specifically for cycle No. 10) are included in Fig. 3.2.3.6-2. The test temperatures are in good agreement

with the predicted values and indicate that LI-900 thermal conductivity values do not differ significantly from that of LI-1500 (the predictions assume that the LI-900 conductivity is equal to the LI-1500 conductivity). In depth temperature predictions and test measurements for cycle No. 10 are shown in Fig. 3.2.3.6-3 as a function of test time.

Also shown in Fig. 3.2.3.6-2 are the general locations from which mechanical test specimens were cut. The basic philosophy behind the cutting scheme was that specimens would be tested at the temperature level the material would experience during the cyclic radiant heat pulse. This plan could be followed for all the in-plane tensile tests. However, because of redesign of the transverse shear specimen it was not possible to restrict the temperature to a narrowband as was desired. The best that could be done was to conduct high-temperature tests on specimens located nearest the heated surface and low temperature tests nearest the colder backface.

General cutting diagrams for all of the radiantly cycled specimens are shown in Figs. 3.2.3.6-4, 3.2.3.6-5, and 3.2.3.6-6. Identification of the specimen configuration is depicted in the figures; however, the following should be referred to for clarity.

Specimen	Test
J	Room Temperature In-Plane Tension
K	Elevated Temperature In-Plane Modulus
L	Elevated Temperature In-Plane Ultimate Strength
M	Transverse Shear
N	Transverse Tension
P	Thermal Conductivity
Q	Thermal Expansion

The material block shown in Fig. 3.2.3.6-6 suffered some coating damage during the twelfth heat cycle because of inadvertent water ingestion before the beginning of the heat cycle. A full discussion is given in Appendix B1.

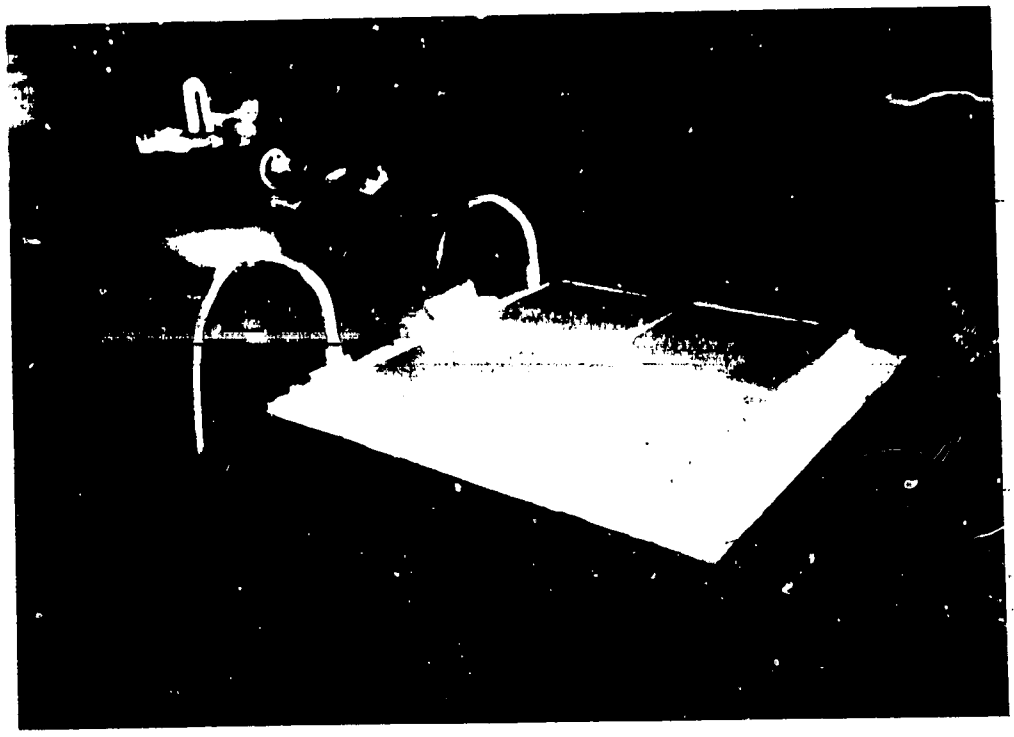

Fig. 3.2.3.6-1 Cyclic Radiant Heat Test Setup

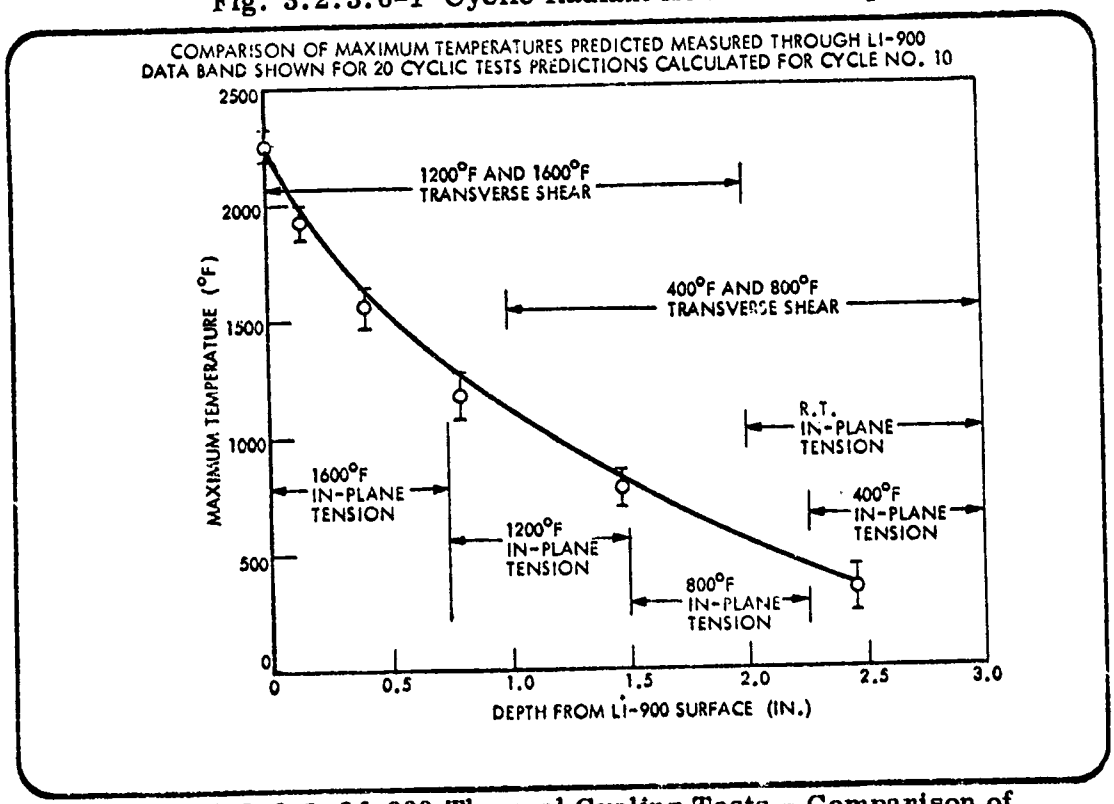

Fig. 3.2.3.6-2 LI-900 Thermal Cycling Tests – Comparison of Max. Temperatures Predicted Measured Through LI-900

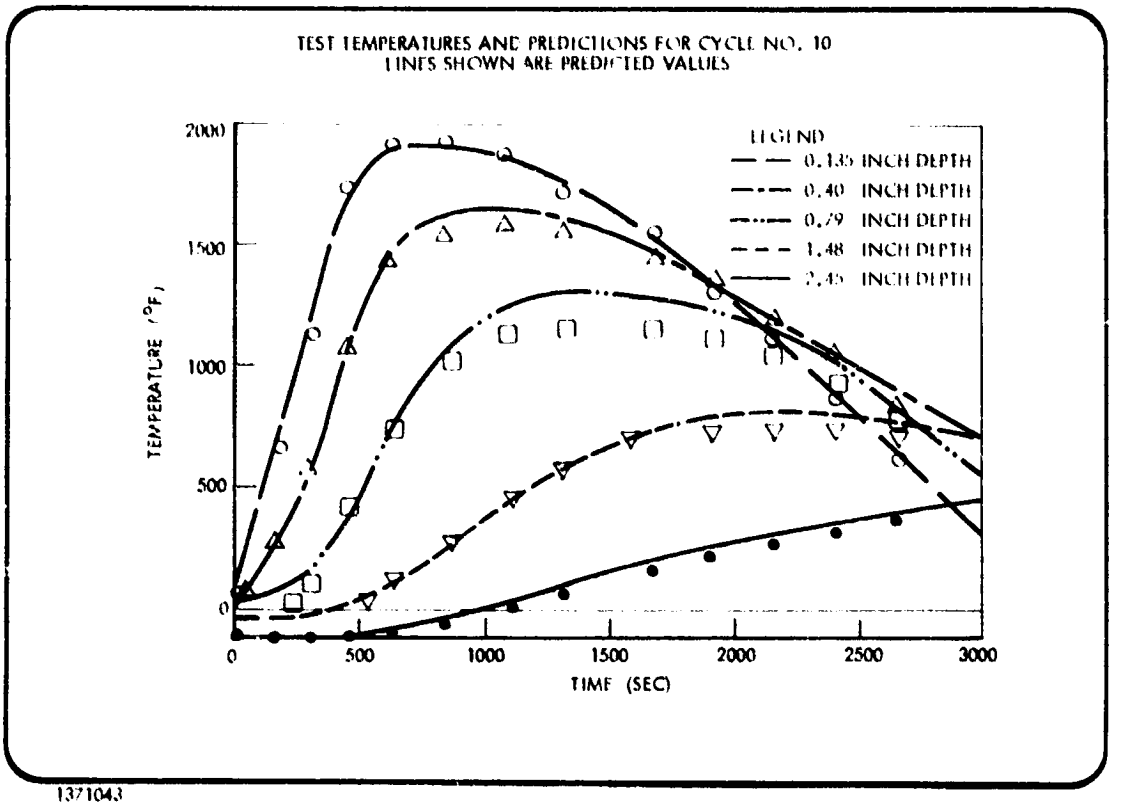

Fig. 3.2.3.6-3 Thermal Cycle Tests, Temperature and Predictions

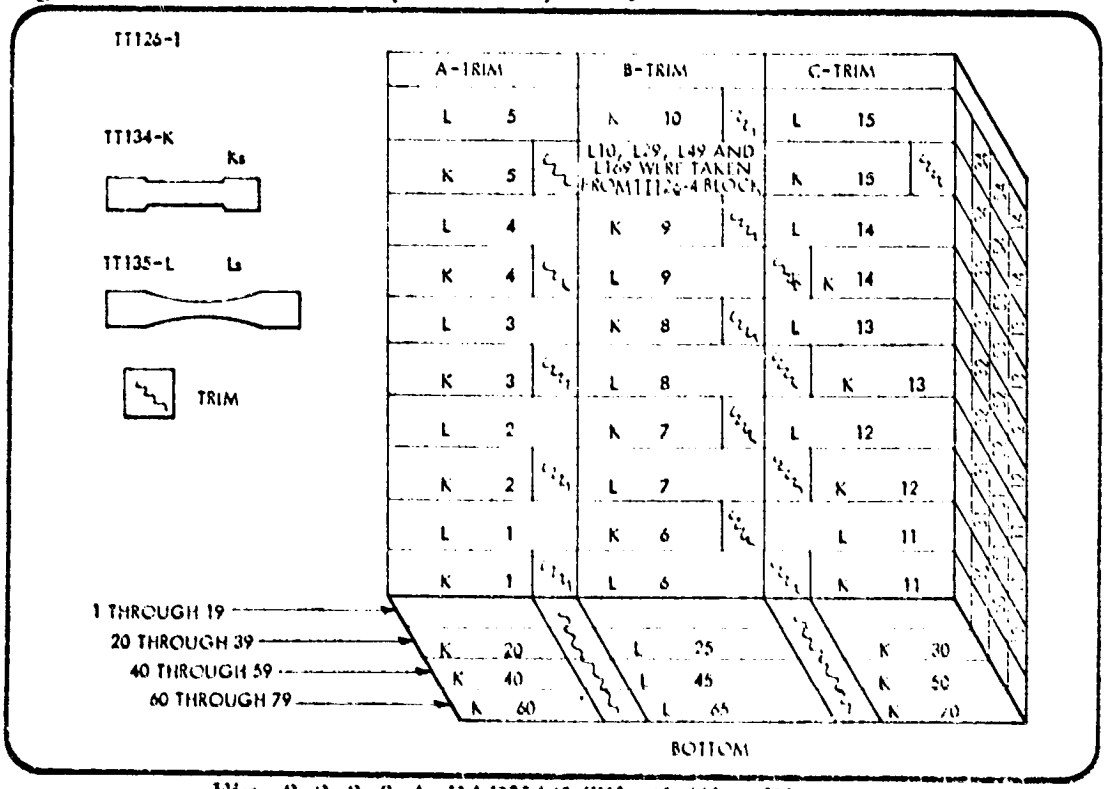

Fig. 3.2.3.6-4 RADVAC Tile Cutting Diagram

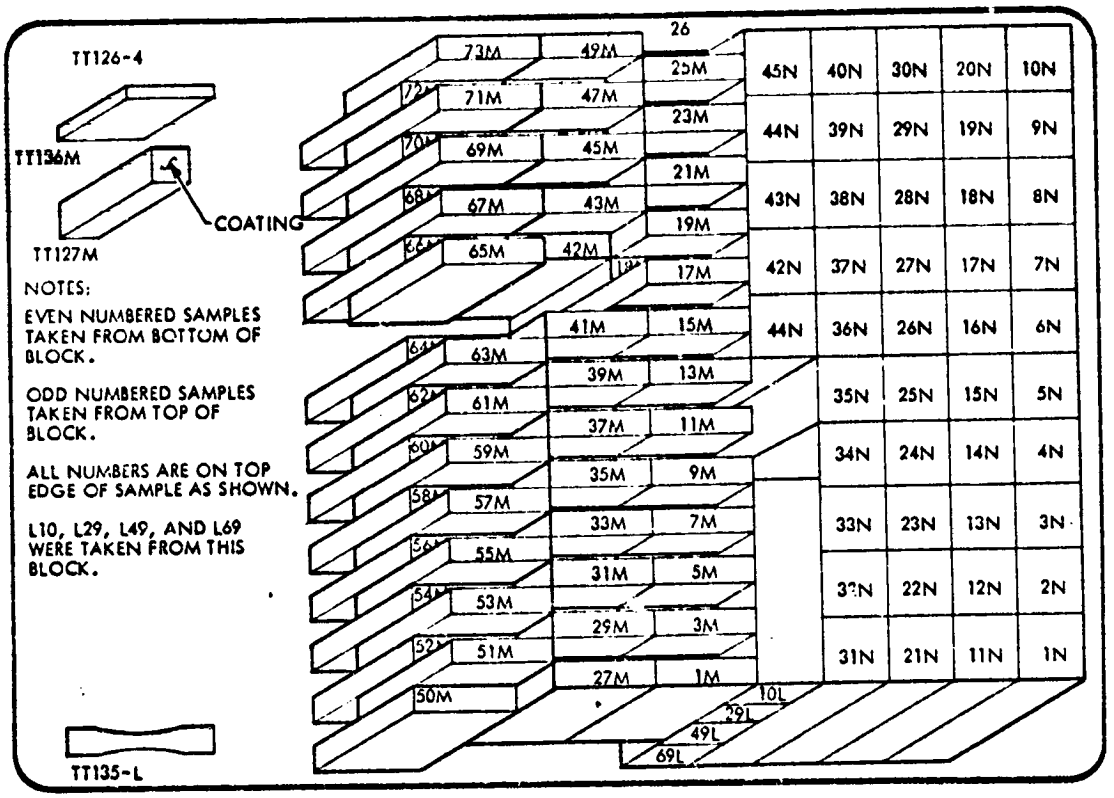

Fig. 3.2.3.6-5 RADVAC Tile-Cutting Diagram

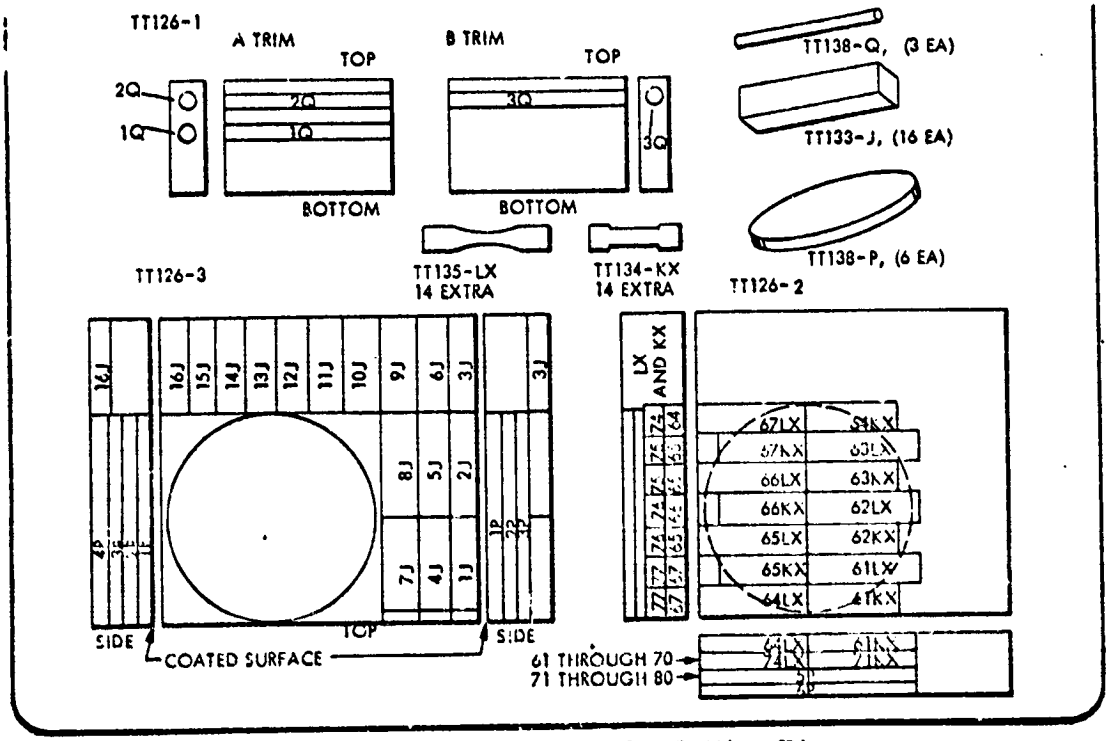

Fig. 3.2.3.6-6 RADVAC Tile-Cutting Diagram

3.3 TEST RESULTS

3.3.1 Thermophysical Properties

3.3.1.1 Thermal Expansion. Thermal expansion measurements were performed on three specimens each of LI-900 (both as-fabricated condition and after thermal cycling) in a direction normal to the tile thickness direction and on the 0042 coating material over the temperature range of -320° to 2200°F. Experimental apparatus and procedures have been described in Par 3.2.2. The experimental results are presented in the following subsections.

LI-900. The thermal expansion behavior of this material as a function of temperature is shown in Fig. 3.3.1-1, and the experimental data are tabulated in Appendix B-2. For the intermediate temperature dilatometer (70° to 1700°F) the data were taken from the continuous record of ΔL versus temperature, whereas the other data are discrete points. The spread in the data from the three specimens ranges from one to three times the estimated maximum uncertainty for a single set of data.

Thermal expansion characteristics of the three radiantly-cycled specimens are shown in Fig. 3.3.1-2 , and the raw data presented in Appendix B-2. No data were measured below 70°F for this case.

Thermal expansion of the 0042 coating material is presented in Fig. 3.3.1-3 , with the data given in Appendix B-2. The test specimens were cast bars of coating material rather than specimens of coating applied to LI-900. This method of sample preparation was chosen for two reasons. First, previous experience had shown that it is extremely difficult to totally remove the densified LI-900 layer from the coating while maintaining an uncracked specimen of the dimensions required for these measurements. Testing on this type of specimen would not be representative of only the coating material because of the presence of some of the surface LI-900 interface layer. Second, to obtain a specimen of sufficient cross-section to resist bending under the loads imposed by the dilatometer it is necessary to laminate a series of thicknesses of the coating and secure them in such a manner that a rigid column is achieved. For the regular expansion materials any shippage occurring between layers could result in an excessive error in the ΔL measurement. For the coating material the data spread between individual specimens is again one to three times the estimated maximum uncertainty for a single specimen.

A comparison of the linear expansion behavior of the 0042 coating and the LI-900 is shown in Fig. 3.3.1-4. The curves represent the average values for each set of three specimens. The thermal expansion of fused silica (data supplied by WBS for SRM 739) is also shown for comparison with the fibrous and cast materials. It should be noted that the discontinuities in the curves in the 1600°F region are due to the two different dilatometers used for the experiments.

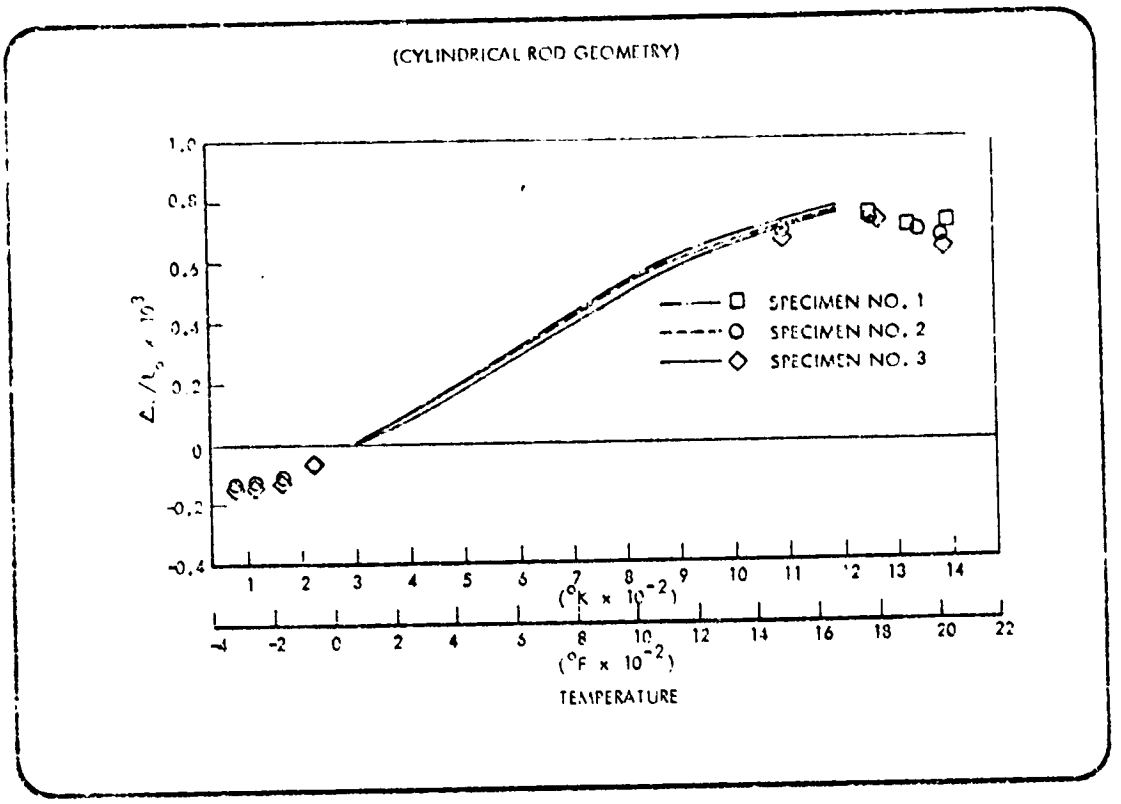

Fig. 3.3.1-1 Thermal Expansion of LI-900 As Fabricated (In-Plane Direction)

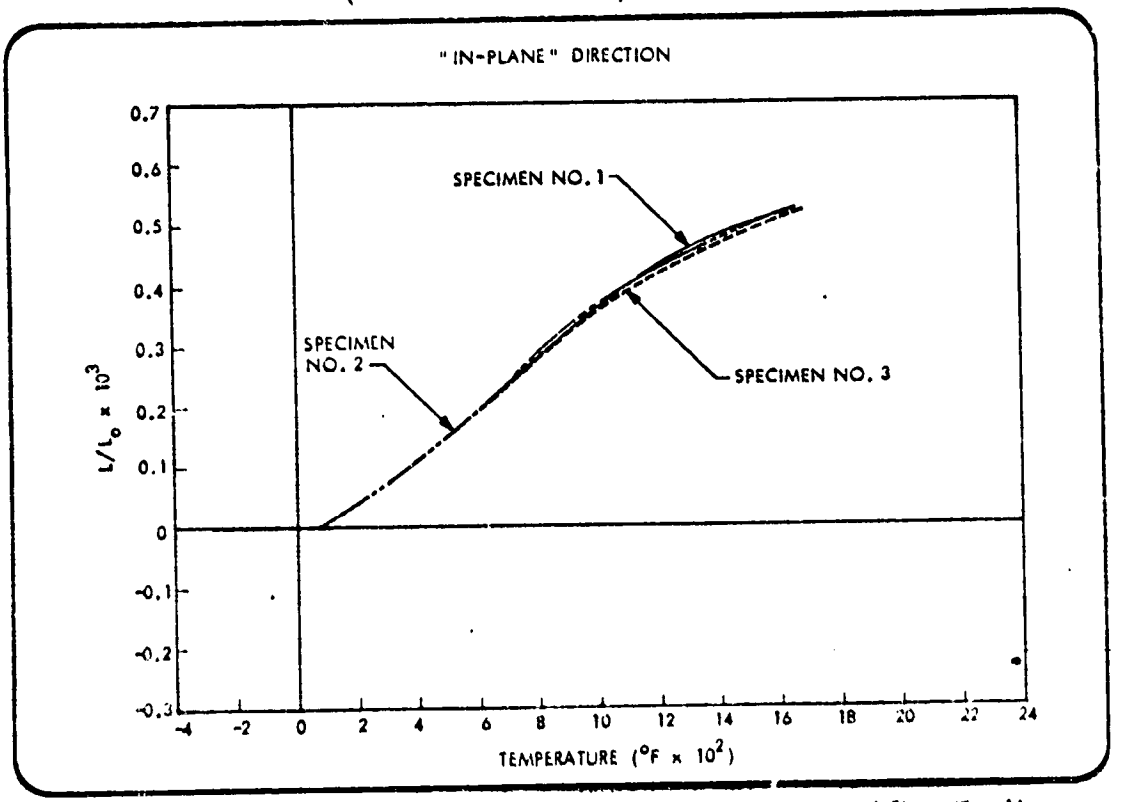

Fig. 3.3.1-2 Linear Thermal Expansion of LI-900 After Cycling

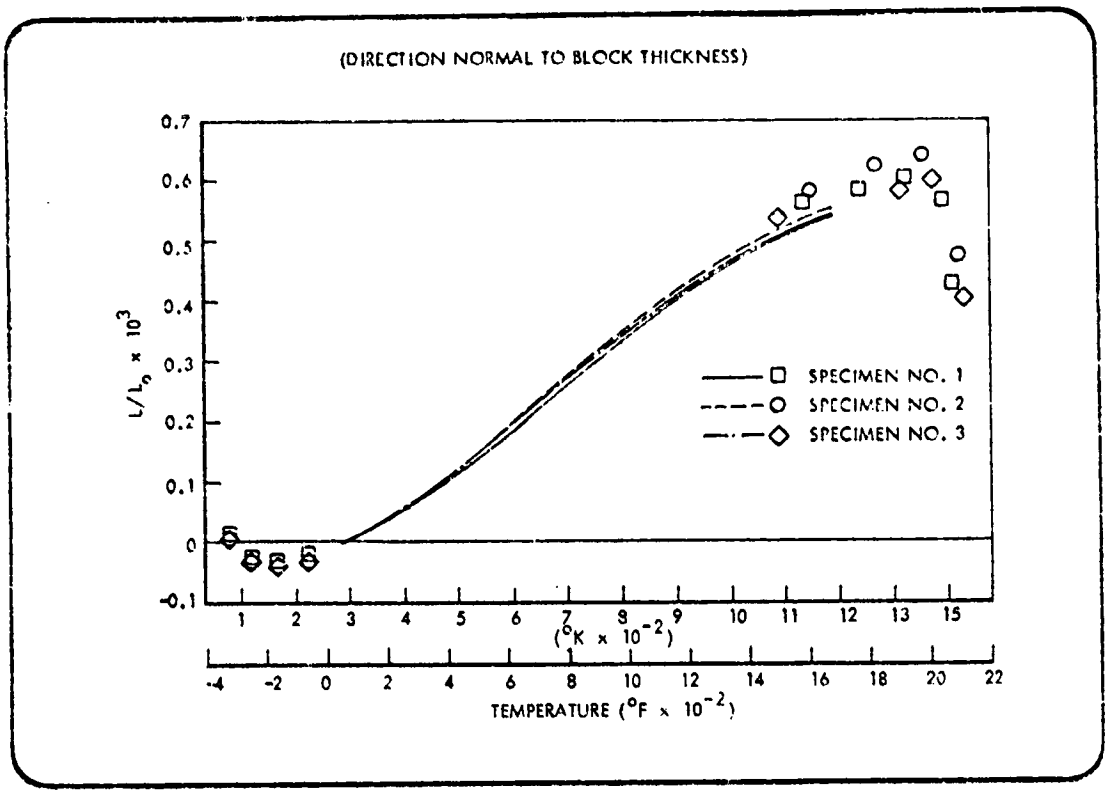

Fig. 3.3.1-3 Thermal Expansion of 0042 Coating As Fabricated (Cylindrical Rod Geometry)

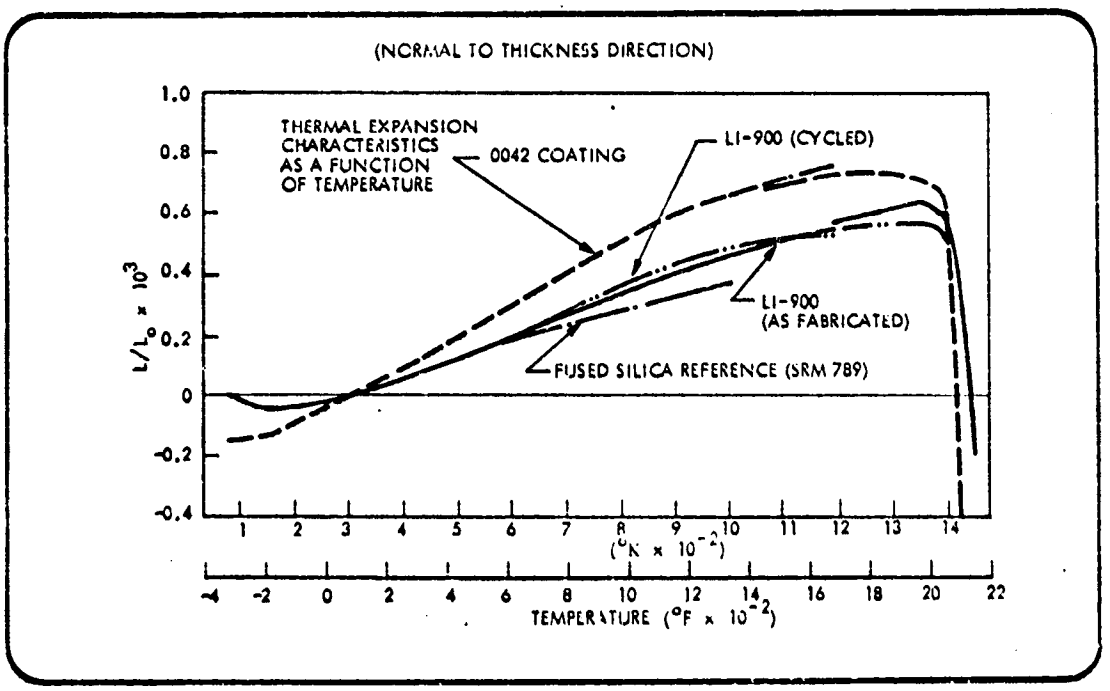

Fig. 3.3.1-4 Comparison of 0042 and LI-900 (In-Plane Direction)

The LI-900 material shows a smooth function of $\Delta L/L_O$ with temperature to approximately 2000°F. At this temperature an apparent shrinkage occurs. From 2000° to 2100°F there is some question as to whether this is truly shrinkage or is due in part to a deformation of the LI-900 from the load imposed by the dilatometer on the spherical surfaces contacting the specimen ends with a resultant indentation of the surface. This would be a possibility if the material compressive strength decreases in this temperature range.

From 2100° to 2200°F the decrease in ΔL appears to be attributable to real shrinkage, as evidenced by the permanent percent decrease in specimen length from post-test measurements. The coating material also exhibits a shrinkage at approximately 2000°F, with a more pronounced shrinkage at 2100°F than LI-900. The questions of contact deformation may also be raised for this material in the region of its softening point.

3.3.1.2 LI-900 Thermal Conductivity. Thermal conductivity measurements were performed on the LI-900 material in the transverse (through-the-thickness) direction over the temperature range of -190° to 1890°F (mean temperature) and at air pressures from one atmosphere to vacuum (10^{-4} torr). The 7-in. diameter guarded hot plate was used for temperatures to 400°F, and the 8-in. apparatus was employed for the higher temperature testing. All specimens were in the form of disks 1/2-in. thick. Lower temperature thermal conductivity measurements were also made for the in-plane direction using the 7-in. apparatus.

The experimental effective thermal conductivity for the transverse direction is shown in Fig. 3.3.1-5, and tabulated in Appendix B-2. Figure 3.3.1-5 shows the effect of

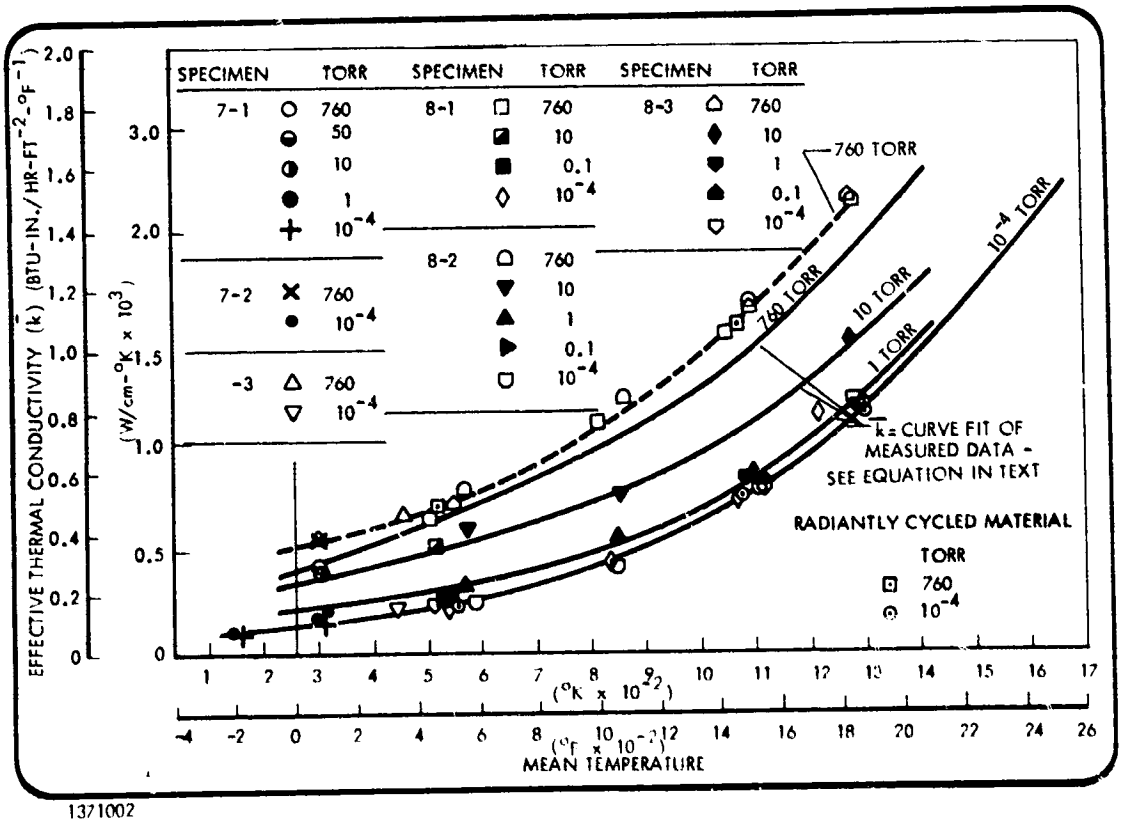

Fig. 3.3.1-5 L1-900 Thermal Conductivity for Transverse Direction

mean temperature and gas pressure on the effective thermal conductivity of the LI-900. The solid lines of Fig. 3.3.1-5 represent the equation

$$\bar{k} = 1.2 \times 10^{-2}(T_m)^{1/3} + 2.96 \times 10^{-2}\sigma(T_m)^3 + \frac{3.90 \times 10^{-7}(T_m)0.71}{\frac{3.03 \times 10^{-6}(T_m)^{1.185}}{P} + 2.14 \times 10^{-3}}$$

where T_m is the mean temperature, σ is the Stefan-Boltzmann constant and P is the ambient air pressure in Torr. This equation is in the form of additive heat transport mechanisms for solid phase conduction, radiation, and gas phase conduction; and it should be noted that this is representative of the small ΔT test data for which T_m is a reasonable approximation of the temperature field.

The coefficients of the first and second terms on the right side of the equality sign were evaluated from the experimental data under vacuum conditions. The first term represents the solid conduction where $T^{1/3}$ is an approximation of the temperature - dependance of the thermal conductivity of fused silicon in the form $k(T) \propto$ at m. The coefficient 1.2×10^{-2} includes both the thermal and geometric properties of fiber-to-fiber contact areas and fiber lengths and diameters. The coefficient 2.96, of the second term is $4\,n^2/3\beta$ where n is the effective refractive index of the fiber-void system and β is the material extinction coefficient. Both coefficients were evaluated from the experimental data by the form

$$\frac{\bar{k}_{vac}}{(T_m)^{1/3}} = A + B\,\sigma\,(T_m)^{2.67}$$

with simultaneous solutions for A and B.

The third term on the right side of the equation represents the heat transfer due to the presence of an interstitial gas, which for these data is air. The form used to approximate the gas phase contribution to the effective thermal conductivity is

$$k_g = \bar{\alpha}\, k_{go} \frac{L}{L + \lambda}$$

where $\bar{\alpha}$ is the accommodation coefficient (taken as 1 for air), k_{go} is the thermal conductivity of air at a given temperature, L is a characteristic void dimension, and λ is the mean free path at a given temperature and pressure. The gas thermal conductivity can be approximated reasonably well from 100° to 2000°F by the form $a(T)^n$ where n = 0.71 for air. The mean freepath is

$$a\left(\frac{\mu}{p}\right)\left(\frac{T}{n}\right)^{1/2}$$

where p is the viscosity, and μ is the molecular weight of the gas. As μ is a function of temperature, this was substituted into the preceding equation to yield

$\lambda = \frac{a(T)^n}{P}$ where n is 1.185 (0.685 μ). The constant 2.14×10^{-3} represents a characteristic void dimension from L = 0.78 Df/ s where Df is an average fiber diameter (1.26) and s is the solid portion.

The equation developed from the data is a reasonable representation of the experimental points from vacuum to the 10-ton pressure conditions. At atmospheric pressure the equation under predicts the data. One possible explanation for this behavior may be the presence of some free connection at this high pressure. If one assumes the vertical cell dimensions are on the order of the specimen thickness (not a closed cell type of structure) for ΔT's of 100^{o} to 200^{o}F the Groshoff number varies from 10 to 10^4 and some corrective transport would be expected for $N_{Gr} \geq 10^3$. This problem is under study at this time.

The thermal conductivity of the LI-900 material in the in-plane direction is shown in Fig. 3.3.1-6 and compared with the transverse direction values. The increased conductivity appears to be due to an increase in solid conduction of approximately 40 percent which is probably due to an anisotropic fiber orientation in the tile.

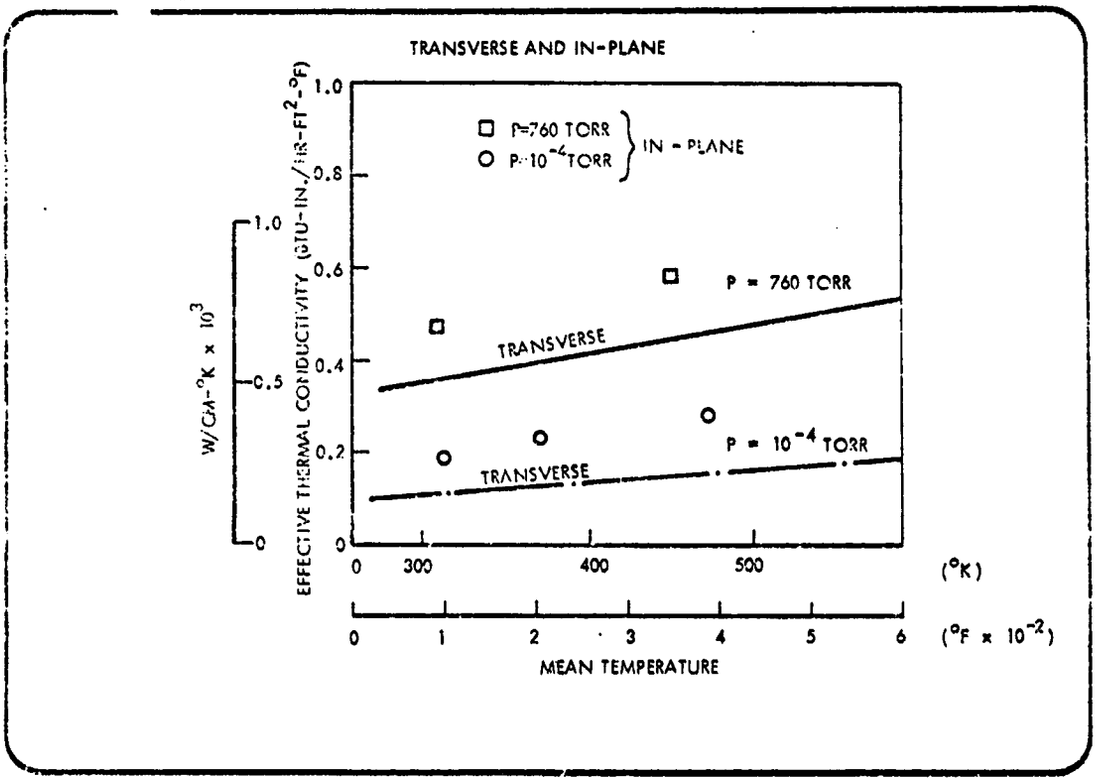

Fig. 3.3.1-6 Comparison of LI-900 Transverse and In-Plane Effective Thermal Conductivities

The thermal conductivity in the transverse direction for one radiantly cycled specimen is shown in Fig. 3.3.1-5, in which no change is seen from the as-fabricated condition.

3.3.2 Mechanical Properties

All data generated under this task are tabulated in Appendix B2 where average, maximum and minimum values are reported for each variable measured under each test condition. Standard deviation is also reported for all strength data. Included in the appendix are sample load-deflection (stress-strain) curves for many of the test conditions.

In Table 3.3.2-1 are shown average values for strength and moduli for the 0042 high emittance coating and LI-900 for all test conditions required by Table 3.1-1. The number appearing just above and to the left of each set of results is the number of specimens represented by the average values. In some cases values taken for design purposes in Task A may differ somewhat from those reported here because design work was proceeding while data were still being accumulated.

3.3.2.1 Coating Tension. As discussed in Section 3.2.3.4, coating specimens consisted of a layer of densified silica as well as the high emittance coating of primary interest. An analysis designed to separate the mechanical properties of each constituent of the composite coating is therefore given in Appendix B4 and the results for the high emittance layer are shown in Figs. 3.3.2-1 and 3.3.2-2. The dramatic dip in the curves is the result of a batch of material used to obtain the 400°F data only. It is evident that this material has been influenced by an unknown parameter. Otherwise, ultimate strength seems to exhibit a relatively constant value with temperature, while Young's modulus decreases with increasing temperature.*

Under the LMSC independent development program the compressive strength of the 0042 coating was obtained at room temperature using specimens cut from the thermal expansion bars. The average value for three tests was 12,633 psi as compared with 2438 psi in tension(individual compressive data points are given in Appendix B2). The large difference in tensile and compressive strengths is typical of glassy materials.

3.3.2.2 LI-900 Tension. Figures 3.3.2-3 through 3.3.2-6 summarize the results for both weak direction (transverse) and strong direction (in-plane) tension in both the as-fabricated and in the radiantly cycled conditions. The figures exhibit increased strength at -250°F over that at room temperature, which latter condition generally seems to be the low point of the strength curve. These curves show no marked trend as temperature is increased but do show the relative insensitivity of the material to radiant cycling by comparing Figs. 3.3.2-3 and 3.3.2-4.

Elastic moduli of LI-900 appear to increase with temperature up to a softening point, as seen from Figs. 3.3.2-5 and 3.3.2-6. These curves also demonstrate that radiant cycling has no effect on the strong direction modulus.

Poisson ration measurements were made during the room temperature tests. To describe the results, a coordinate system and subscript convention must be defined.

*The composite coating analysis is only valid for average moduli; hence no maximum or minimum values are given in Fig. 3.3.2-2.

If x and y are any orthogonal directions in the plane of a tile, z is the transverse coordinate, and, the strain-stress relations are written

$$\epsilon_x = \frac{1}{E_x}(\sigma_x - \nu_{xy}\,\sigma_y - \nu_{xz}\,\sigma_z)$$

$$\epsilon_y = \frac{1}{E_y}(-\nu_{yx}\,\sigma_x + \sigma_y - \nu_{yz}\,\sigma_z)$$

$$\epsilon_z = \frac{1}{E_z}(-\nu_{zx}\,\sigma_x - \nu_{zy}\,\sigma_y + \sigma_z)$$

then average values are

$$\nu_{xy} = \nu_{yx} = 0.115$$

$$\nu_{xz} = \nu_{yz} = 0.153$$

$$\nu_{zx} = \nu_{zy} = 0.043$$

Since LI-900 is transversely isotropic with respect to an axis perpendicular to a tile, a value of the strong direction shear modulus can be computed from ν_{xy} using the well known relation

$$G_{xy} = E_x/2(1 + \nu_{xy})$$

The result is 10,142 psi on the average.

Compressive strengths for LI-900 in both the weak and strong directions were also obtained under the LMSC independent development program. Average values for six specimens were:

Weak Compression – 47.5 psi

Strong Compression – 62.6 psi

3.3.2.3 LI-900 Weak Shear. Difficulties encountered in shear testing have been discussed in Section 3.2.3.4 and a further account is given in Appendix B3. A more reliable and analytically tractable shear test specimen is required, namely large-diameter torsion cyclinders, in order to adequately quantify shear moduli and strength.

Nevertheless, the results of this effort can be used to infer the effect of temperature and/or radiant cycling on the weak direction shear properties. Figure 3.3.2-7 shows increased strength at -250°F over room temperature properties but that the strength at elevated temperature is essentially constant above 400°F. Room temperature data shown are, unfortunately, for specimens taken from different batches of material. Essentially, the same trend in seen in Fig. 3.3.2-8 for the radiantly cycled material, except that the strength level has decreased. Modulus data reported in Figs. 3.3.2-9 and 3.3.2-10 show essentially the same trends.

Comparative results of the different tests conducted in shear are shown in Table 3.3.2-1 to indicate some of the disparity. As pointed out in Appendix B3, variations in specimens within a given batch, as well as batch to batch variations, color the results and emphasize the need for a definitive shear test. The shear values in Table 3.3.2-1 may be compared with shear test results obtained by Pilot Plant personnel evaluating physical properties of blocks of LI-900, utilizing screening test techniques (described in the final report, NAS 9-12137, "Improvement of Reusable Insulation Material," LMSC-D266204, 1 Mar 1972). Pilot plant shear values were:

Room Temperature Average, *As Fabricated, First Batch – 27.1 psi

Room Temperature Average, As Fabricated, Second Batch -- 35.6 psi

Room Temperature Average, Radiantly Cycled – 28.0 psi

*2 or 3 specimens

FOLDOUT FRAME

FOLDOUT FR

1

2

Table 3.3.2

SUMMARY OF AVERAGE VALUES OF STRENGTH AND MO

		As Fabricated			
Temperature →		-250°F	R.T.	400°F	800
High Emittance Coating Tension		[10] 2134 11.45×10^6	[11] 2438 6.21×10^6	[10] 1761 1.35×10^6	[10] 2 9.01
LI-900 Weak Tension	1 in. x 1 in. x 3 in.	[10] 28.0 5,795	[10] 16.0 5,775		
	Coated 1 in. x 1 in. x 3 in.				
	Modulus Dogbones			[10] 6,765	[10] 7,
	Ultimate Dogbones			[10] 23.5	[10] 2
LI-900 Strong Tension	1 in. x 1 in. x 3 in.	[10] 66.9 19,705	[10] 50.7 23,545		
	Modulus Dogbones			[10] 35,440	[10] 35,
	Ultimate Dogbones			[10] 69.5	[10] 7
LI-900 Weak Shear	Torsion Fixture		[9] 31.5 3,598		
	"Snow Tire Tread" Grip 0.250 in. Gage Length		[10] 29.1 3,295	[10] 21.6 1,790	[10] 2 1,
	"Snake Skin" File Grip 0.250 in. Gage Length	[10] 39.4 1,620	[8] 23.7 2,191		
	"Snake Skin" File Grip 0.125 in. Gage Length	[4] 38.3 975	[7] 24.3 1,476		
	"Snake Skin" File Grip 0.345 Gage Length	[4] 36.1 1,852	[7] 19.5 2,153		

Note: All Values in PSI

3.3.2-1

D MODULI OF LI-900 AND HIGH EMITTANCE COATING

ated			Radiantly Cycled				
800°F	1200°F	1600°F	R.T.	400°F	800°F	1200°F	1600°F
10 2608 9.01×10^6	10 2627 5.37×10^6	10 2215 3.54×10^6					
			10 15.0	10 14.3	10 15.0		
10 7,885	10 8,329	10 8,146					
10 22.2	10 22.8	10 24.7					
			10 56.3 27,401				
10 35,625	10 39,030	11 36,118		10 32,655	10 38,860	10 40,500	10 38,110
10 74.8	10 58.6	10 66.6		10 65.3	10 59.7	10 58.4	10 80.5
10 22.2 1,594	10 19.3 1,790	10 20.3 1,661	10 21.4 2,320	10 15.9 1,781	10 14.4 1,221	10 13.8 1,015	10 15.0 993

PRECEDING PAGE BLANK NOT FILMED

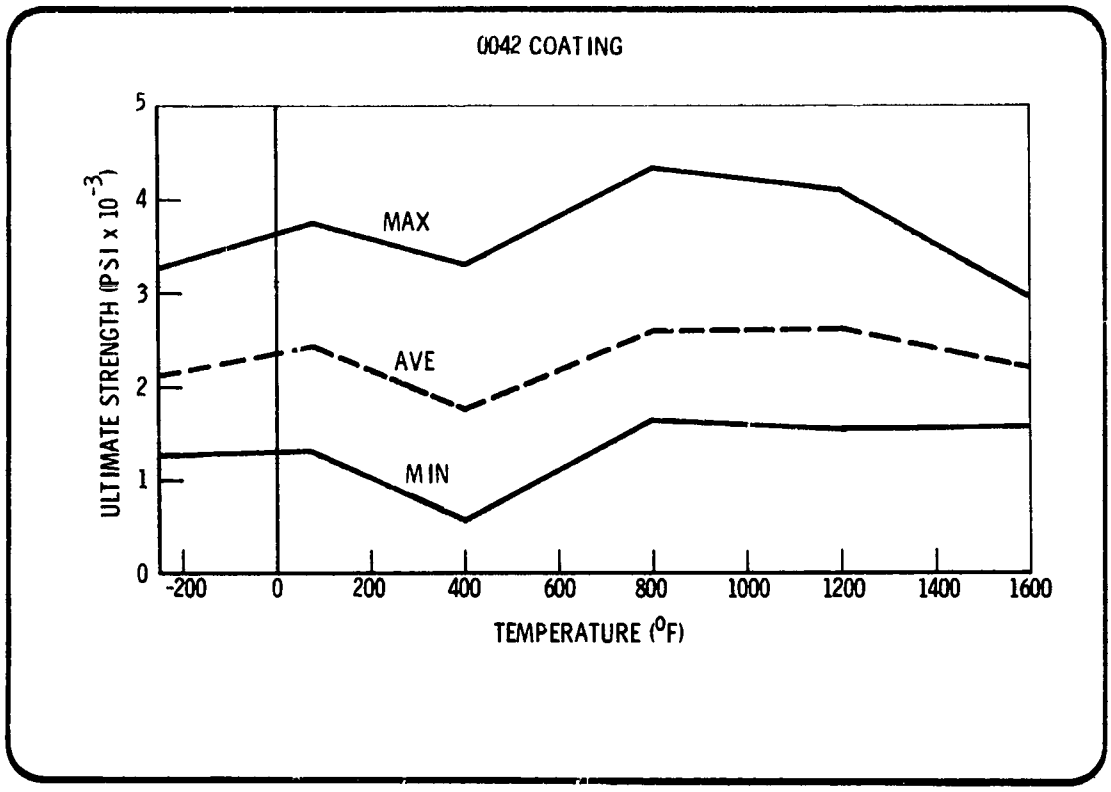

Fig. 3.3.2-1 0042 Coating, Ultimate Tensile Strength Vs Temperature

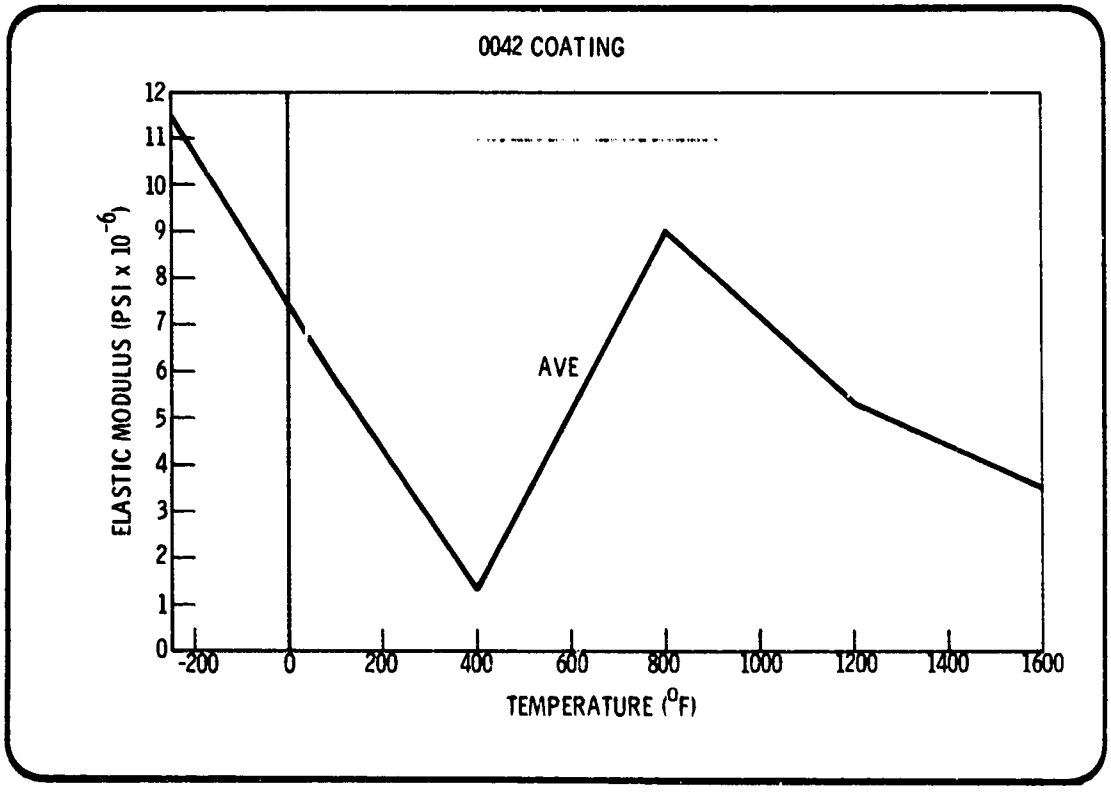

Fig. 3.3.2-2 0042 Coating, Elastic Modulus Vs Temperature

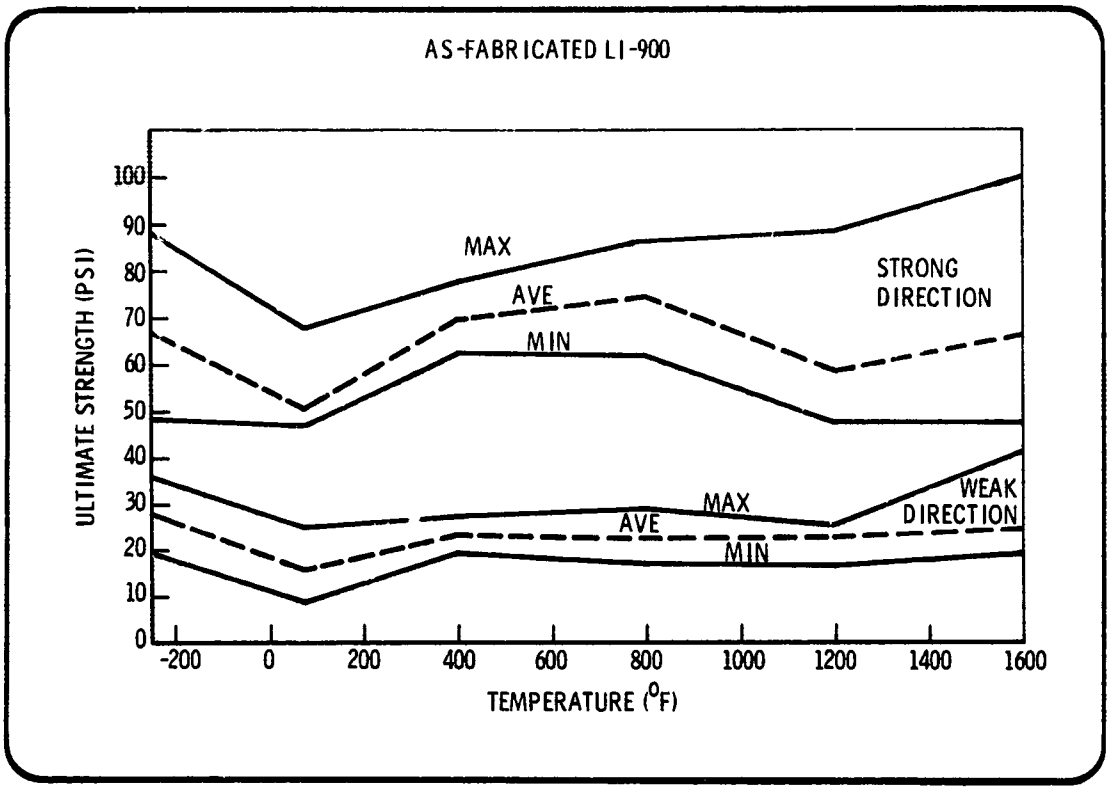

Fig. 3.3.2-3 As-Fabricated LI-900 Tensile Strength Properties Vs Temperature

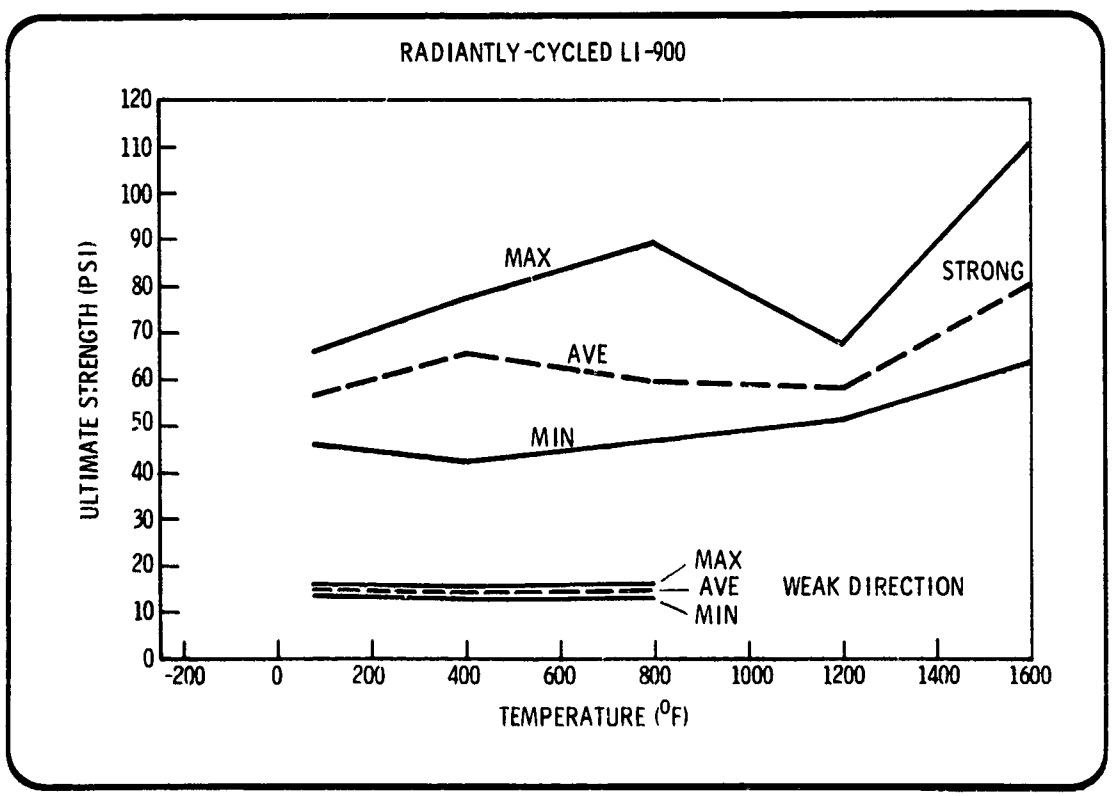

Fig. 3.3.2-4 Radiantly-Cycled LI-900 Tensile Strength Allowables Vs Temperature

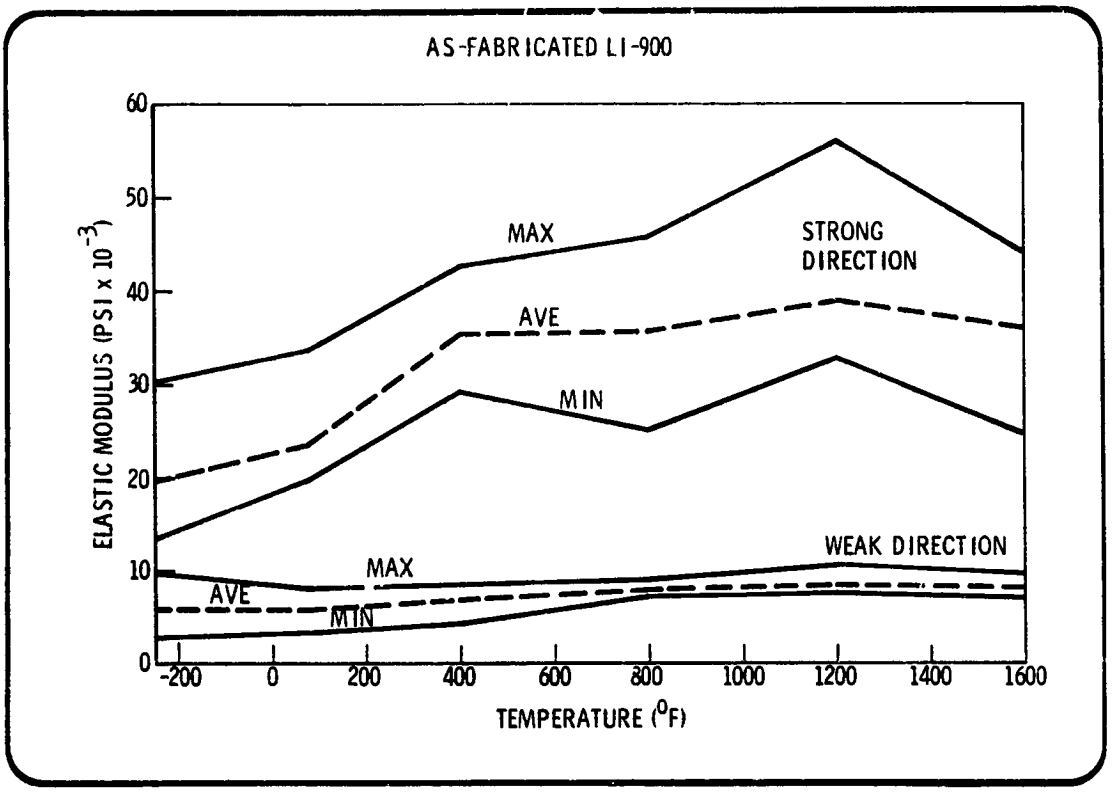

Fig. 3.3.2-5 As-Fabricated LI-900 Elastic Modulus Vs Temperature

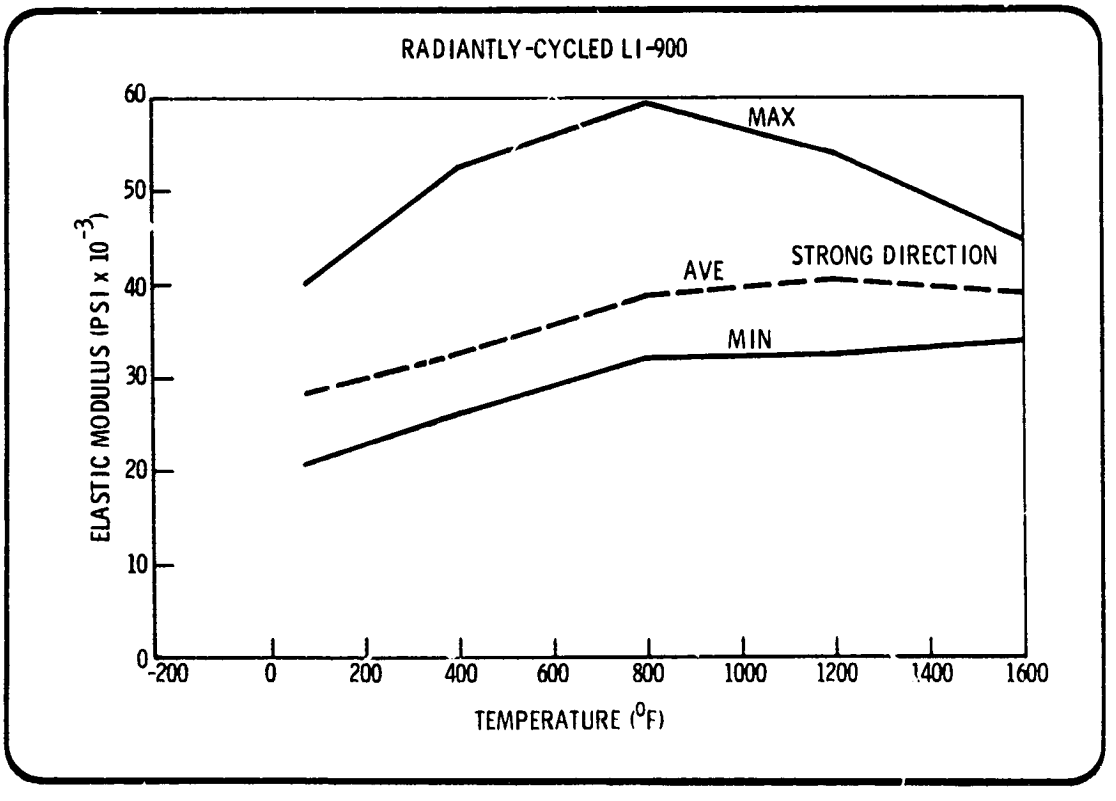

Fig. 3.3.2-6 Radiantly-Cycled LI-900 Elastic Modulus Vs Temperature

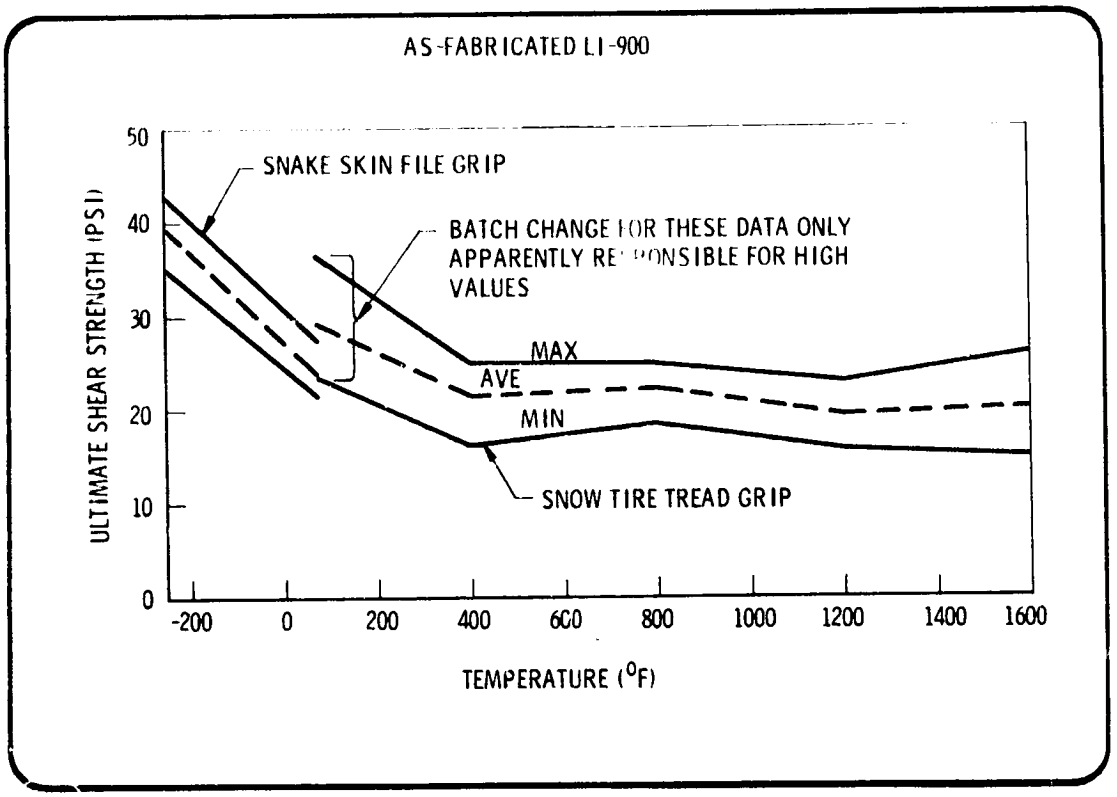

Fig. 3.3.2-7 As-Fabricated LI-900 Weak Shear Strength Vs Temperature

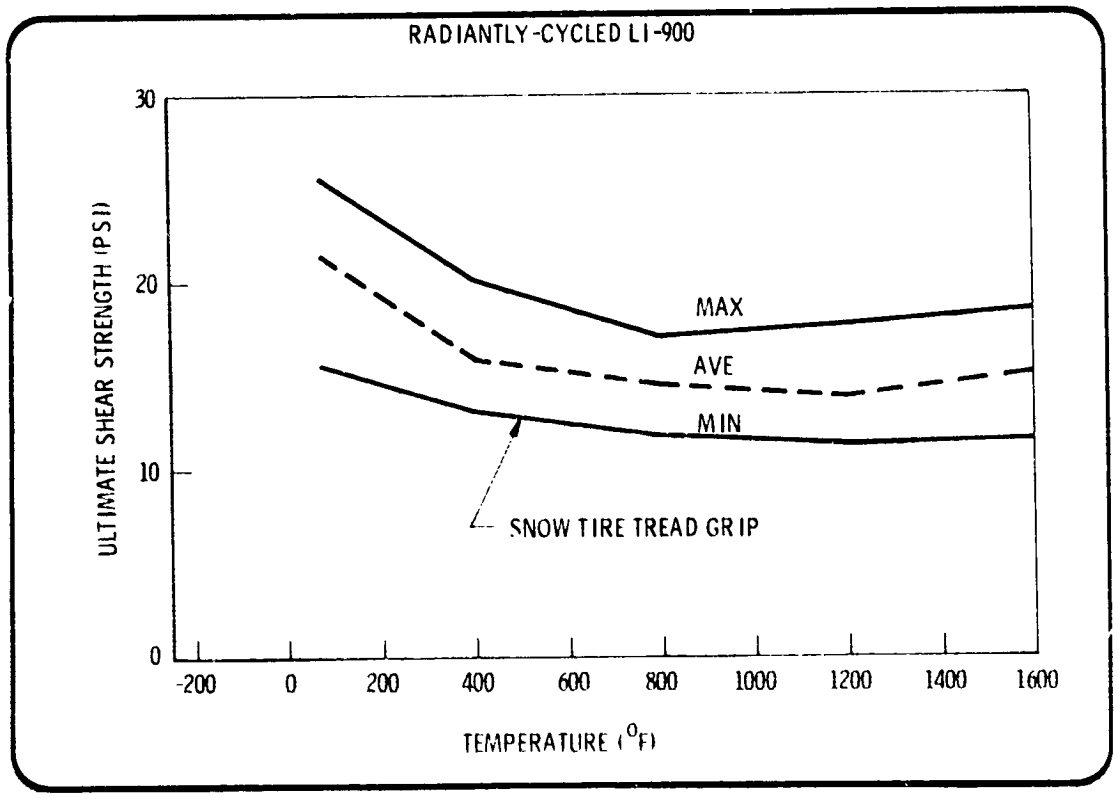

Fig. 3.3.2-8 Radiantly-Cycled LI-900 Weak Shear Strength Vs Temperature

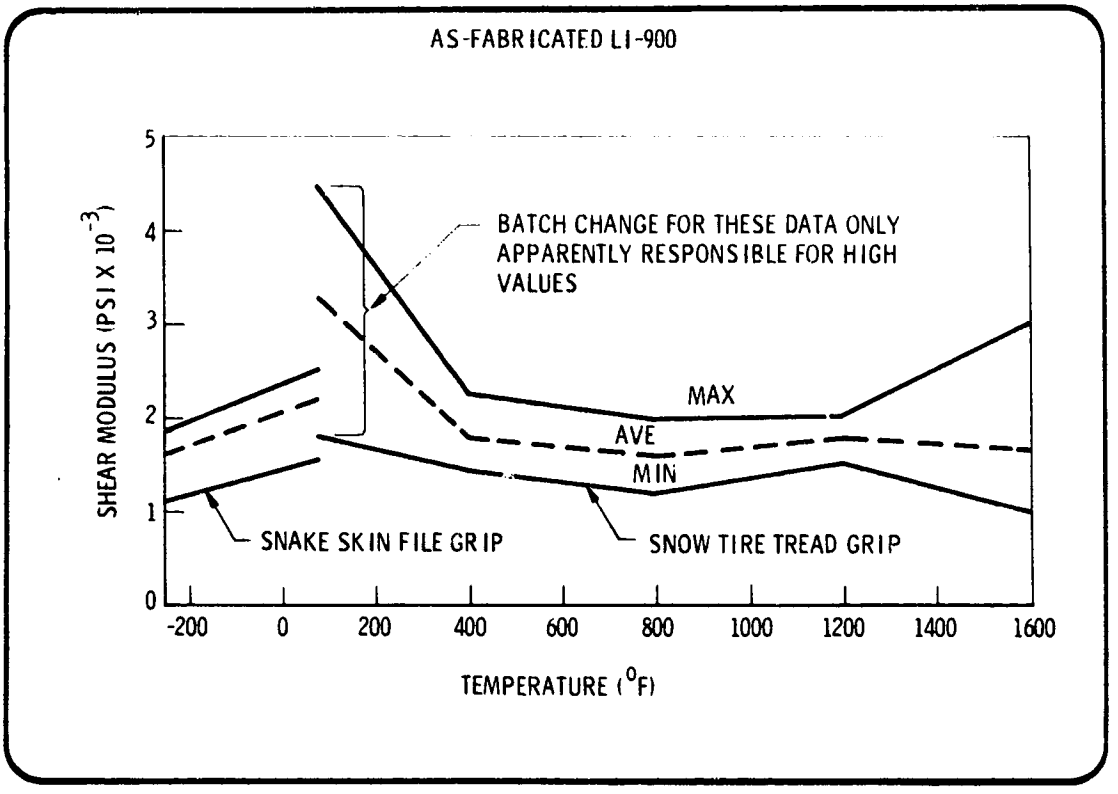

Fig. 3.3.2-9 As-Fabricated LI-900 Weak Shear Modulus Vs Temperature

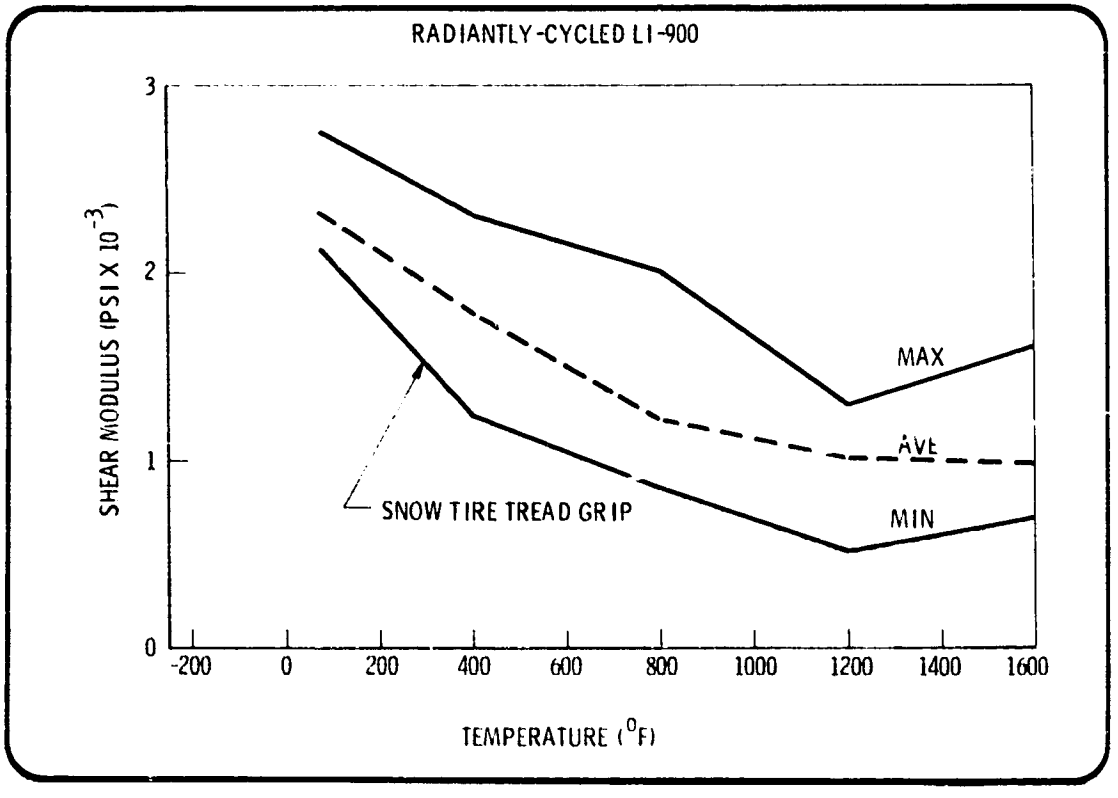

Fig. 3.3.2-10 Radiantly-Cycled LI-900 Weak Shear Modulus Vs Temperature

Section 4

CONTRACTOR ENVIRONMENTAL TEST DESIGN DEVELOPMENT – TASK C

A test program, containing a series of four tests, was defined under this task to simulate critical environments and conditions. Because LI-900 is a relatively new variation of the all-silica RSI, a variety of performance data are needed, particularly as a result of corrective testing. Tests planned were:

- Thermal Response Tests (C-1) to simulate the critical environments that will be encountered by the orbiter during various mission phases that influence the TPS attachment design.
- Turbulent Duct Tests (C-2) to determine the effects of the orbiter flight turbulent heating environment on the LI-900 material over a portion of the service life of the thermal protection system.
- Convective Cycling Tests (C-3) to determine the cumulative effects of the orbiter flight convective heating environment on the LI-900 material over
- Chemical Tolerance Tests (C-4) to determine the susceptibility of LI-900 RSI material to inadvertent or accidental exposure to common reactive chemicals.

LMSC has designed and fabricated test models and submitted test plans for all four series and has conducted tests C-1 and C-4. The conduct of tests C-2 and C-3 were the responsibility of NASA/ARC and NASA/MSC respectively, although the analyses were accomplished by LMSC. All test models incorporated the strain arrestor plate (SAP) concept except those for C-4, the chemical tolerance tests.

4.1 THERMAL RESPONSE

4.1.1 Task C-1 Response Tests

A series of tests were performed utilizing the LMSC SK 62034B environmental test model to evaluate the thermal performance of the LI-900 Rigidized Silica Insulation (RSI) and the baseline LMSC strain arrestor and foambond system. The SK 62034B environmental test model is a stringer-stiffened-sheet panel structure, with edge fittings provided for attachment of tension loading fixtures. (The mating loading fixtures are available and have been proof-loaded and fit-checked.) The panel structure, as shown in Fig. 4.1.1-1, provides a 6.25 in. by 24 in. test surface for attachment of the RSI TPS. To this test surface was installed the baseline RSI system, comprised of three LI-900 tiles having dimensions of approximately 6.25 in. by 6.00 in. by 3.00 in. The tiles were attached to the panel structure using the foambond system. The inboard surface of each tile was fitted with a high-modulus composite strain arrestor plate.

The center test tile was instrumented with two surface thermocouples and six in-depth thermocouples. One end tile was instrumented with six in-depth thermocouples; the remaining tile was uninstrumented. In addition, three thermocouples were attached to the inboard surface of the panel structure. The two tile joints were filled with FI-600 strips from the center of tile thickness to the tile backface edge.

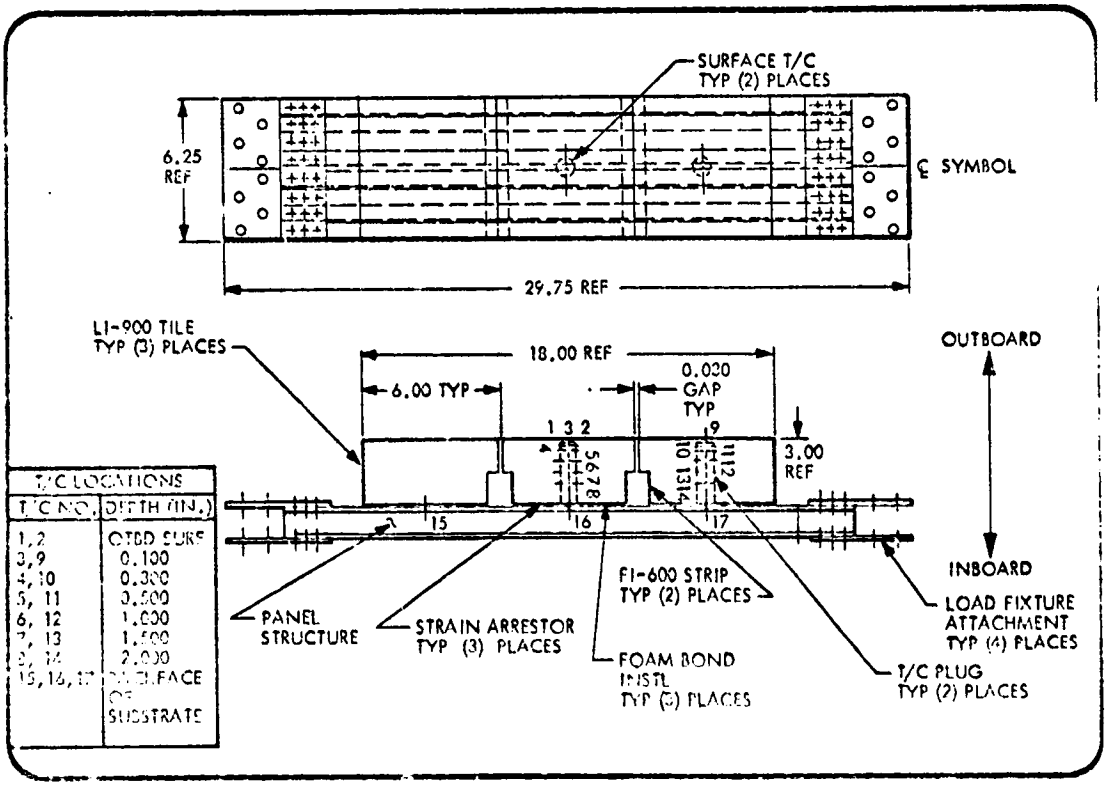

Fig. 4.1.1-1 Environmental Test Model SK 62034B

Specific tests performed under this task are discussed in this subsection.

Area 2P Entry Heating By Radiant Simulation. The test item was installed in the RADVAC facility, as shown in Fig. 4.1.1-2, and all thermocouples were connected to suitable temperature recorders. A heat rate calorimeter was installed in RADVAC to measure the incident heat flux at the specimen surface. The Area 2P temperature history, Fig. 4.1.1-3, was utilized to program the test heat pulse. The center tile surface thermocouples were utilized for test control programming. Five applications of the Area 2P heat pulse were applied to the test item. Each test was initiated with the test item at laboratory ambient temperature. The surrounding environment of the test item during test was air at ambient pressure. Test data were monitored and recorded continuously during each test cycle.

The test item was inspected for test effects and/or damage prior to and after each test pulse was applied. Color photographs of the test item were obtained at the start and end of the test series to document any visible test effects or anomalies. Test and inspection results were entered in the log book.

Cold Soak Test to Minimum Orbital Temperature Condition. The test item was installed in the cold environment facility shown in Fig. 4.1.1-4. The three thermocouples installed on the panel structure were connected to suitable recorders. The test item was cooled to -250°F, at which time cooling was terminated and the test item allowed to warm to room temperature. The test item was observed continuously during this test to determine the time/temperature of occurrence of any cracking or deforming of the test item, or of any noise emanating from the test item. The test item was inspected for test effects and/or damage prior to and after test. Photographs of the test item were obtained at the start and end of the test to document any test effects or anomalies present. Test and inspection results were entered in the log book.

Combined Cold Soak and Static Load Conditions. The test item was instrumented with strain gages, as shown in Fig. 4.1.1-4, then installed in a suitable loading device using the SK 62031 loading fixture to adapt the panel structure to the loading system. The three thermocouples installed on the panel structure were connected to suitable recorders. The test item was enclosed in a suitable cooling chamber, installed as shown in Fig. 4.1.1-5. The test item was cooled to -250°F, as measured at the substrate, and a tension line load of 500 lb/in., or 3125 lb was applied in a time duration of approximately 60 seconds. The applied load was held at the maximum level for 60 seconds, then reduced to 0-lb load in a time duration of approximately 60 seconds. The test item was then allowed to warm to -130°F, as measured at the substrate, at which time a tension line load of 2750 lb/in. or 17,187.5 lb was applied in a time duration of approximately 60 seconds. The applied load was held at the maximum level for 60 seconds, then reduced to 0-lb load in a time duration of approximately 60 seconds. The test item was then allowed to warm to -35°F, as measured at the substrate, at which time a tension line load of 4,000 lb/in., or 25,000 lb, was applied in a time duration of approximately 60 seconds. The applied load was held at the maximum level for 60 seconds, then reduced to 0-lb load in a time duration of approximately 60 seconds. The test item was then allowed to warm to room temperature and removed from the test facility. The test item was observed continuously

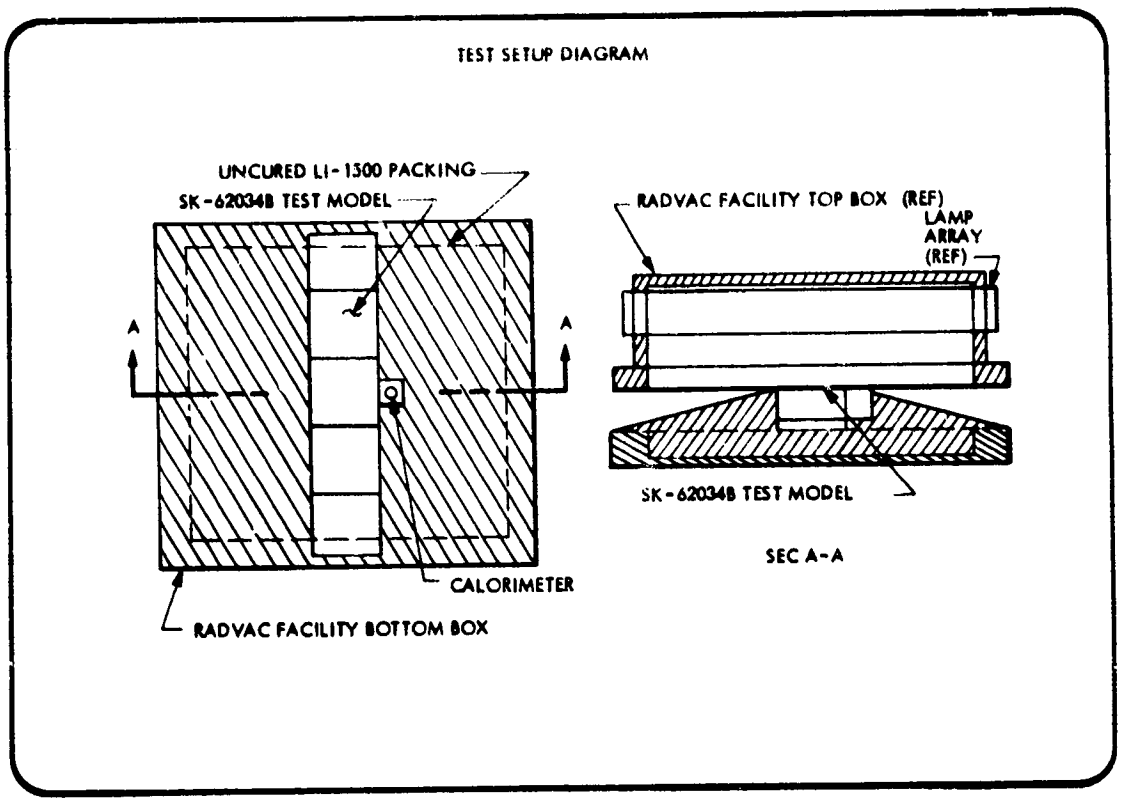

Fig. 4.1.1-2 LI-900 Thermal Response Cycling Test (Test Setup Diagram)

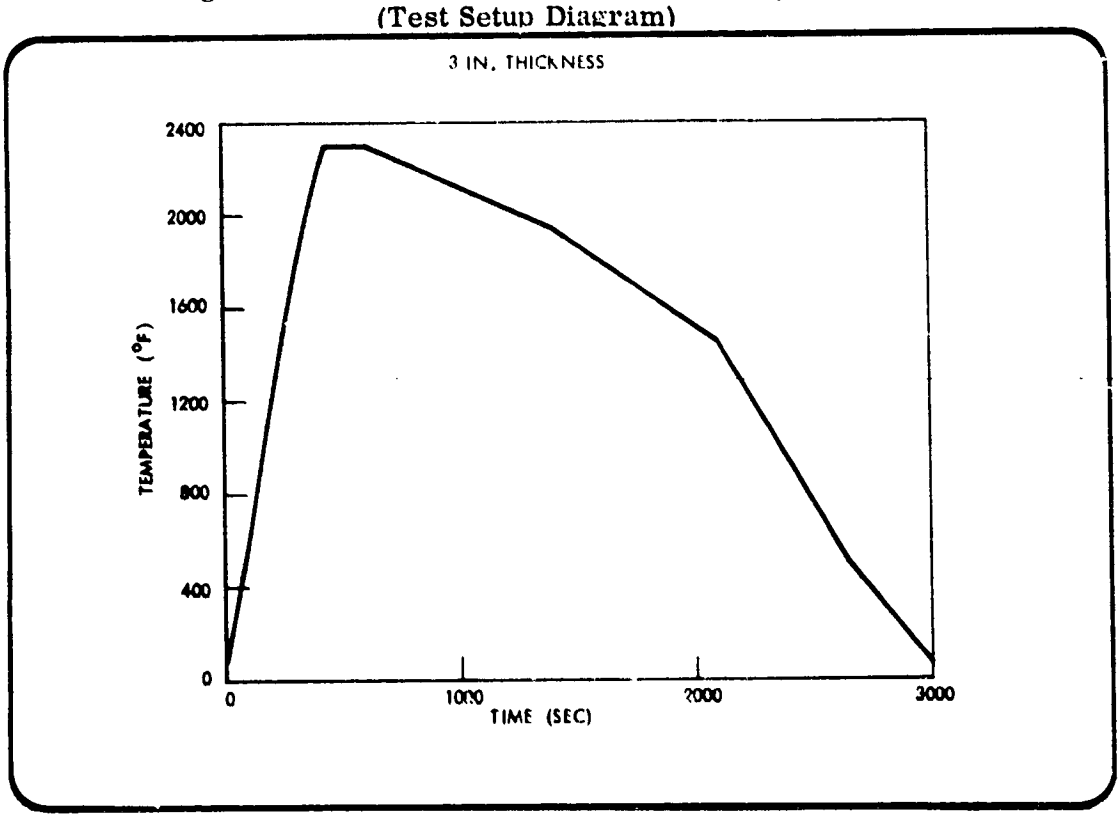

Fig. 4.1.1-3 Area 2P Heat Pulse for 3-In. Thickness LI-900 Tile

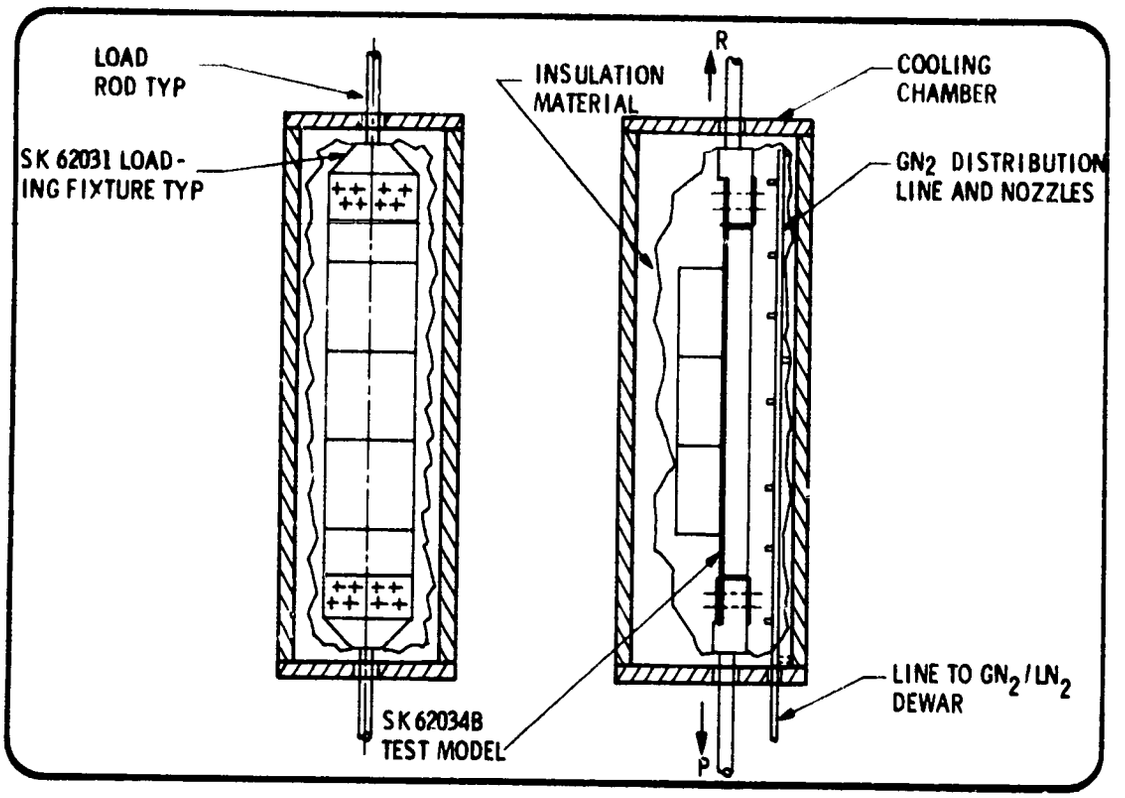

Fig. 4.1.1-4 Cold Environment/Static Load Test Setup

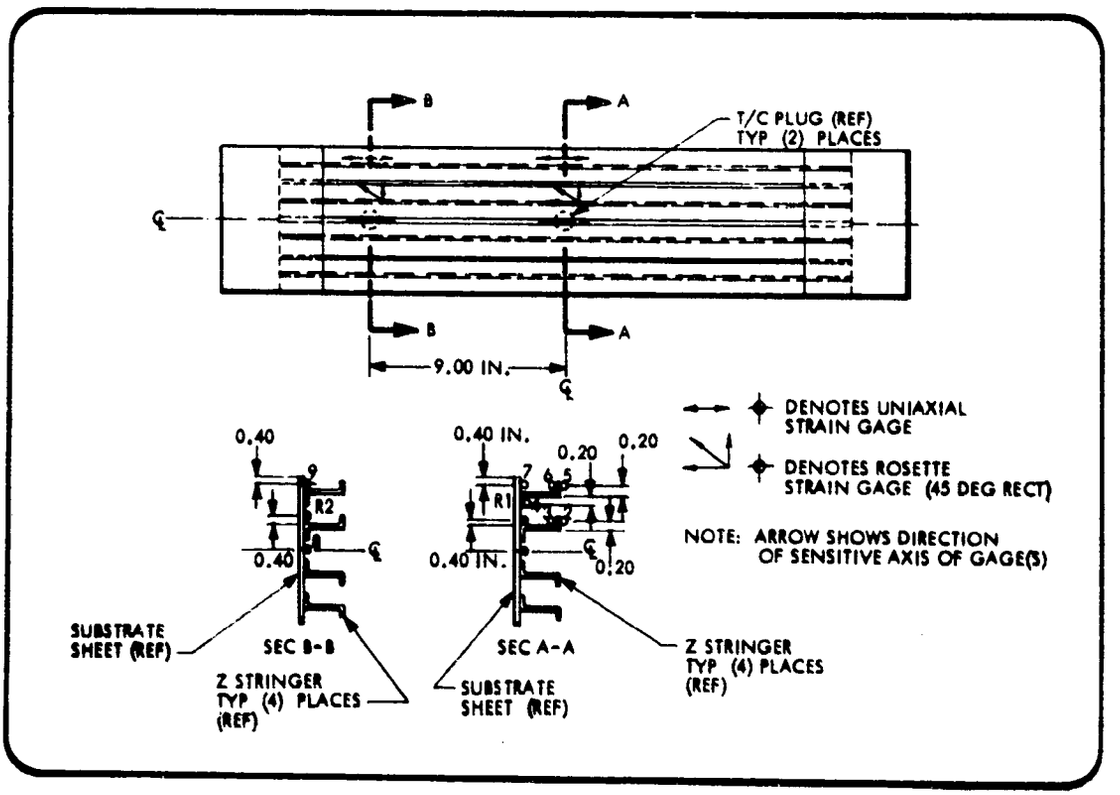

Fig. 4.1.1-5 Strain Gage Instrumentation Locations and Identification

during this test to determine the time, load, and temperature of any yielding or failure of the panel structure, or of any cracking or failure of the RSI tiles, strain arrestor, or foambond installation. The test item was inspected for test effects and/or damage prior to and after test. Documentary photographs of the test item were obtained at start and end of the test to document any test effects or anomalies present. Test and inspection results were entered in the log book. Figure 4.1.1-6 shows the test item prior to testing.

4.1.2 Test Results

Preliminary results of the five-cycle thermal test program indicate no degradation in thermal performance due to thermal cycling. Repeatability of in-depth temperature response was acceptable. In-depth temperature histories and maximum in-depth temperature data are shown for information in Figs. 4.1.2-1 and 4.1.2-2. Upon completion of test environment-based prediction, the data and prediction will be submitted as an addendun to this report.

4.1.3 Comparison and Theory

Temperature predictions based on the test environments will be to submitted as an addendum to this report.

4.2 TURBULENT DUCT TEST AT NASA/AMES

4.2.1 Test Plan and Model Geometry

The test plan and model geometry for the turbulent duct tests is included in this document as Appendix C1. Figure 4.2.1-1 shows the turbulent duct test item prior to shipment to NASA/ARC.

4.3 CONVECTIVE CYCLING TESTS AT NASA/MSC

4.3.1 Test Plan and Model Geometry

The test plan and model geometry for the convective cycling tests is included in this document as Appendix C2. Figure 4.2.1-2 shows the 100 cycle convective heating model prior to shipment to NASA/MSC.

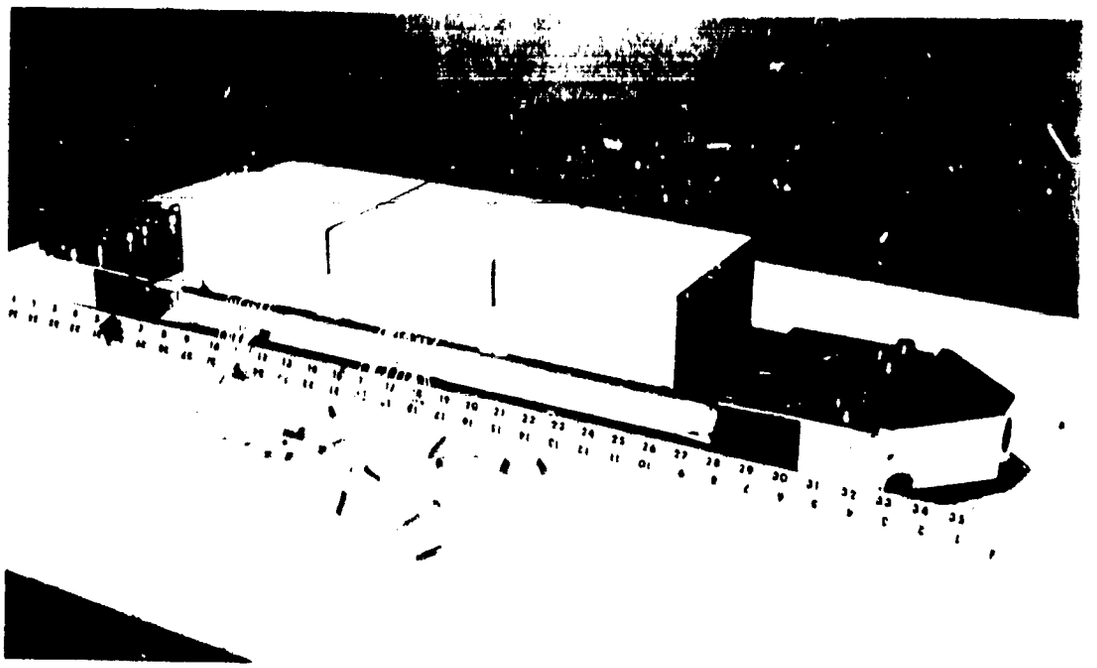

Fig. 4.1.1-6 Thermal Response Test Panel – Pre-Test

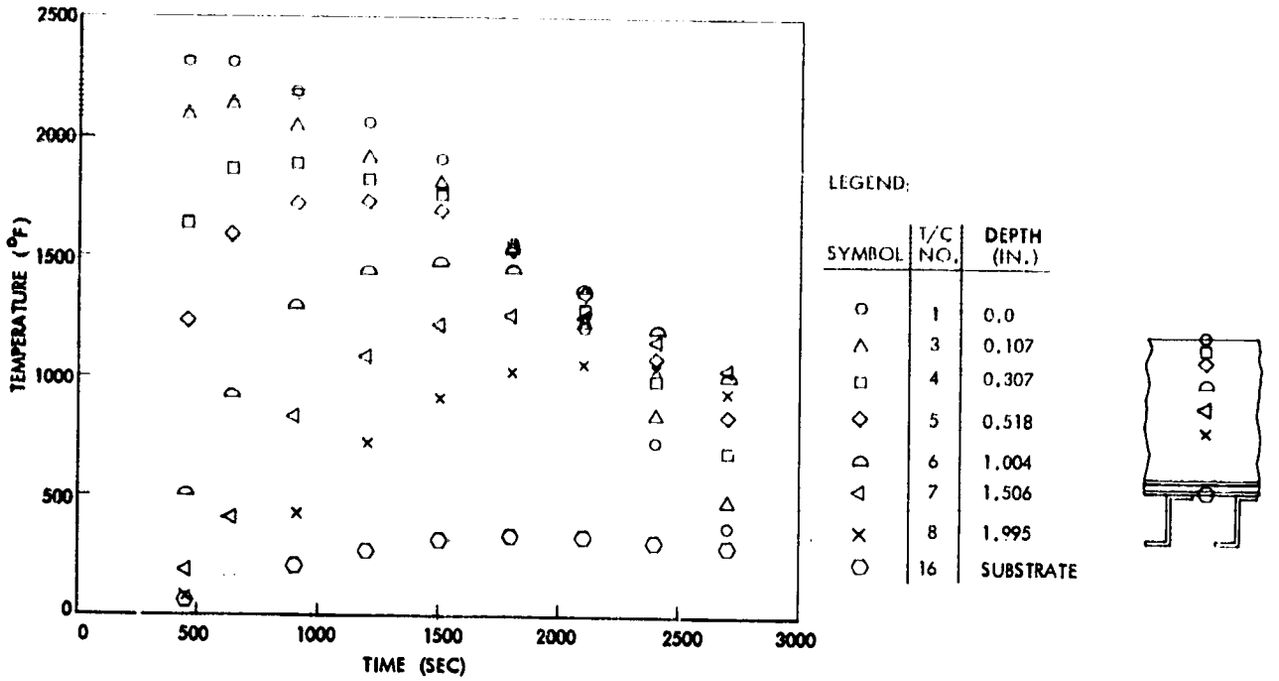

Fig. 4.1.2-1 LI-900 Thermal Response Tests – In-Depth Temperature Histories

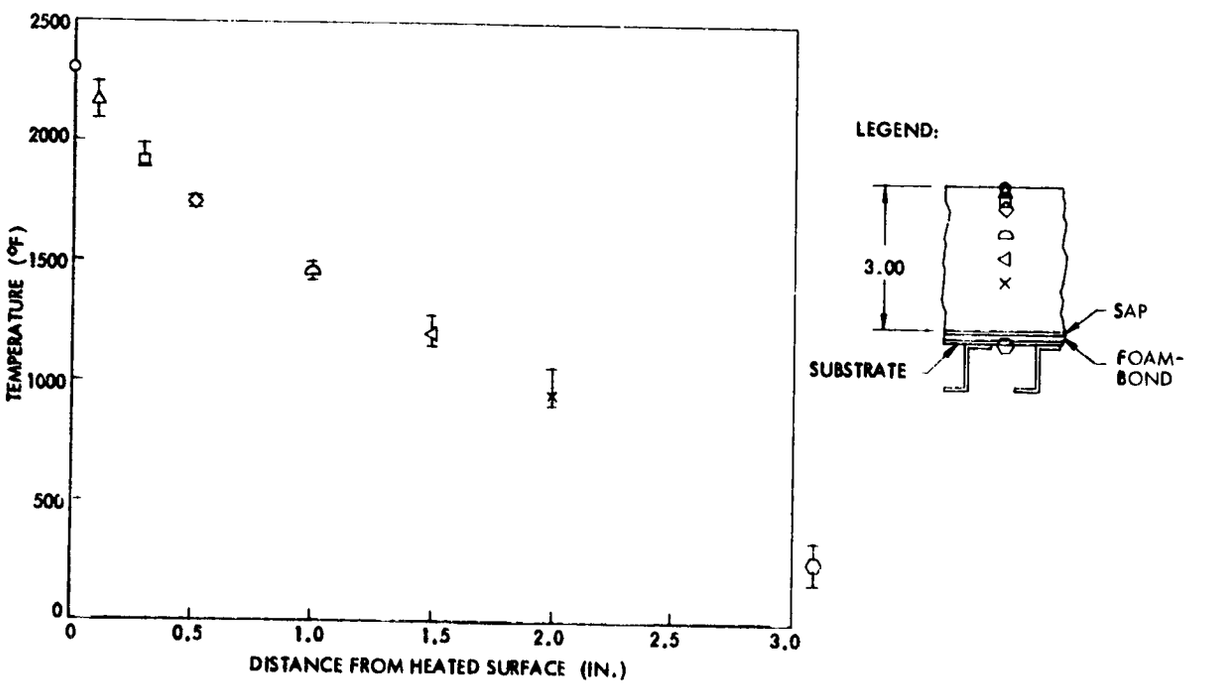

Fig. 4.1.2-2 LI-900 Thermal Response Tests – Maximum In-Depth Temperature

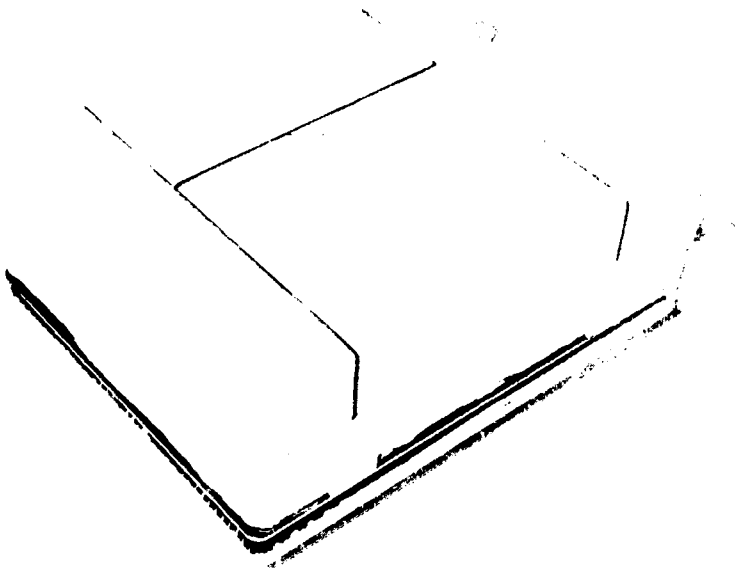

Fig. 4.2.1-1 Turbulent Duct Model (Pre-Test)

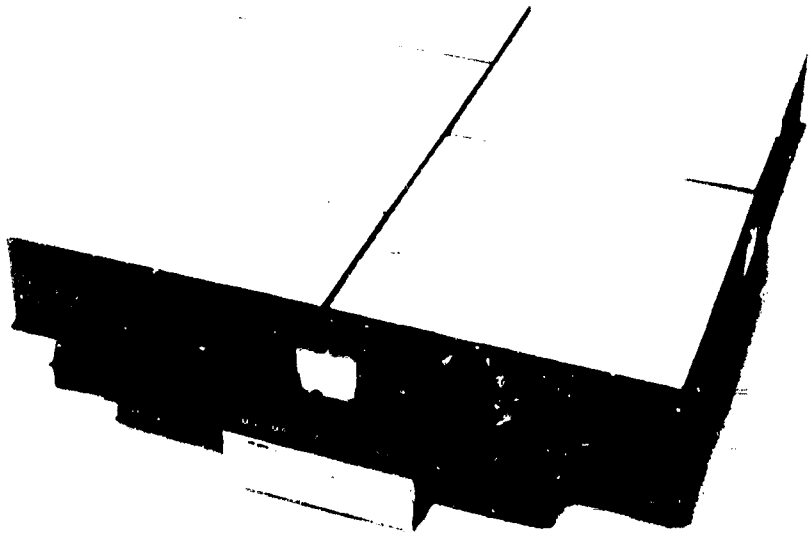

Fig. 4.2.1-2 100 Cycle Convective Heating Model

.4 CHEMICAL TOLERANCE

.4.1 Task C-4 Chemical Tolerance Tests of LI-900 RSI Material

Chemical tolerance tests were performed to establish an assessment of the effects of various materials that could possibly contaminate the LI-900 RSI material during normal shuttle operations. Approximately thirteen LMSC SK 62029 environmental test models of LI-900 RSI material, as shown in Fig. 4.4.1-1, were exposed to the following materials:

- Dilute Hydrochloric Acid (HCL)
- Dilute Sodium Hydroxide (N_4OH)
- Acetone (CH_3COCH_3)
- Methyl-Ethyl-Ketone (MEK)
- Hydraulic Fluid (MIL-L-5056)
- Gas Turbine Fuel (JP-4)
- Inhibited Red Fuming Nitric Acid (IRFNA)
- Unsymmetrical Dimethyl Hydrazine (UDMH)
- Bird Excrement
- NASA/MSC NDE Fluid (CH_3CHO)

The test models were weighed and measured, and temperature emittance characteristics were determined prior to and after test exposures.

Fluid Exposure. Exposure to fluids of interest was accomplished by partial immersion or splash methods and procedures. The duration of exposure was approximately 24 hr, after which the test models were removed from the test environment and the excess fluid wiped from the test model. After the exposure test, the models were weighed and dimensional measurements, emittance characteristic determinations, and visual examinations were performed. The test models were then subjected to the modified Area 2P heating environment, as shown in Fig. 4.4.1-2, under the laboratory ambient pressure condition. Post-test examinations were repeated after the simulated entry heating exposure was performed.

Bird Excrement Exposure. Exposure to bird excrement was accomplished by partial immersion of one test model in a slurry composed of seagull excreta and water and by coating three test models with freshly deposited seagull excreta.

Immersion Test. The test model was partially immersed in a thick slurry of seagull excreta and water for a period of 24 hours. The slurry was agitated continuously during the test period. At the end of the test period the test model was removed from the test environment and the excess slurry materials wiped from the test model. After the exposure test, the model was weighed and dimensional measurements, emittance

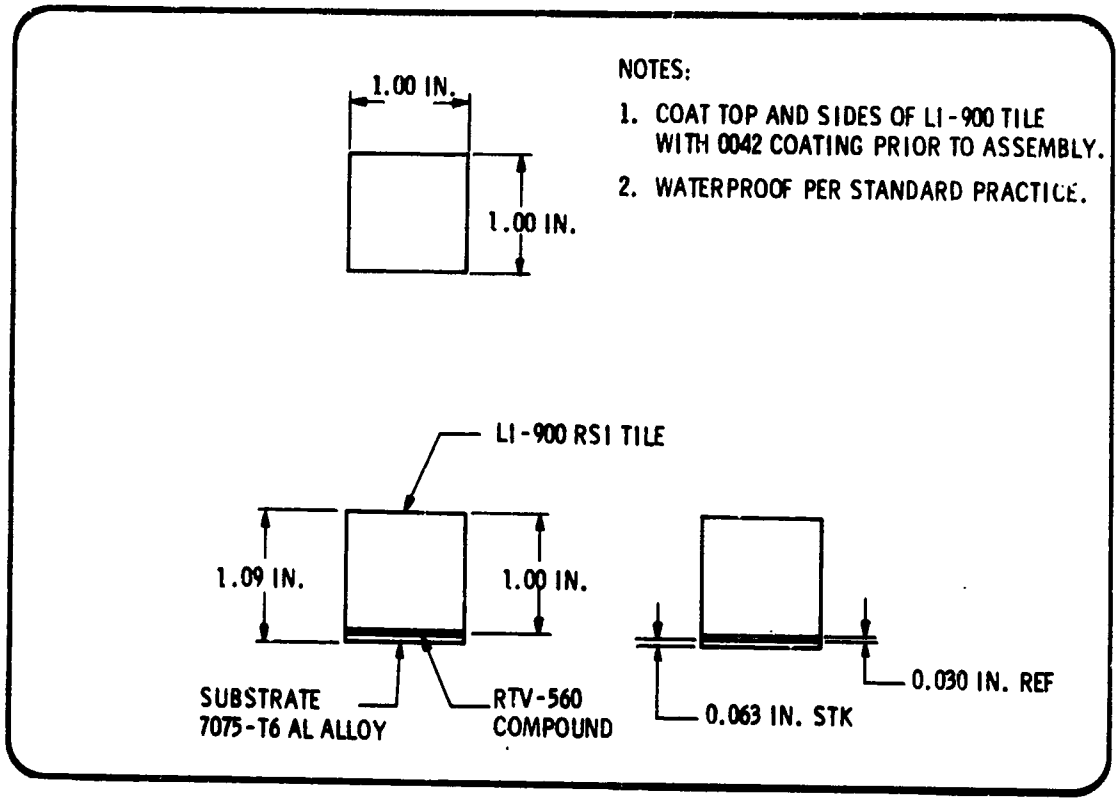

Fig. 4.4.1-1 Chemical Tolerance Test Model SK 62029

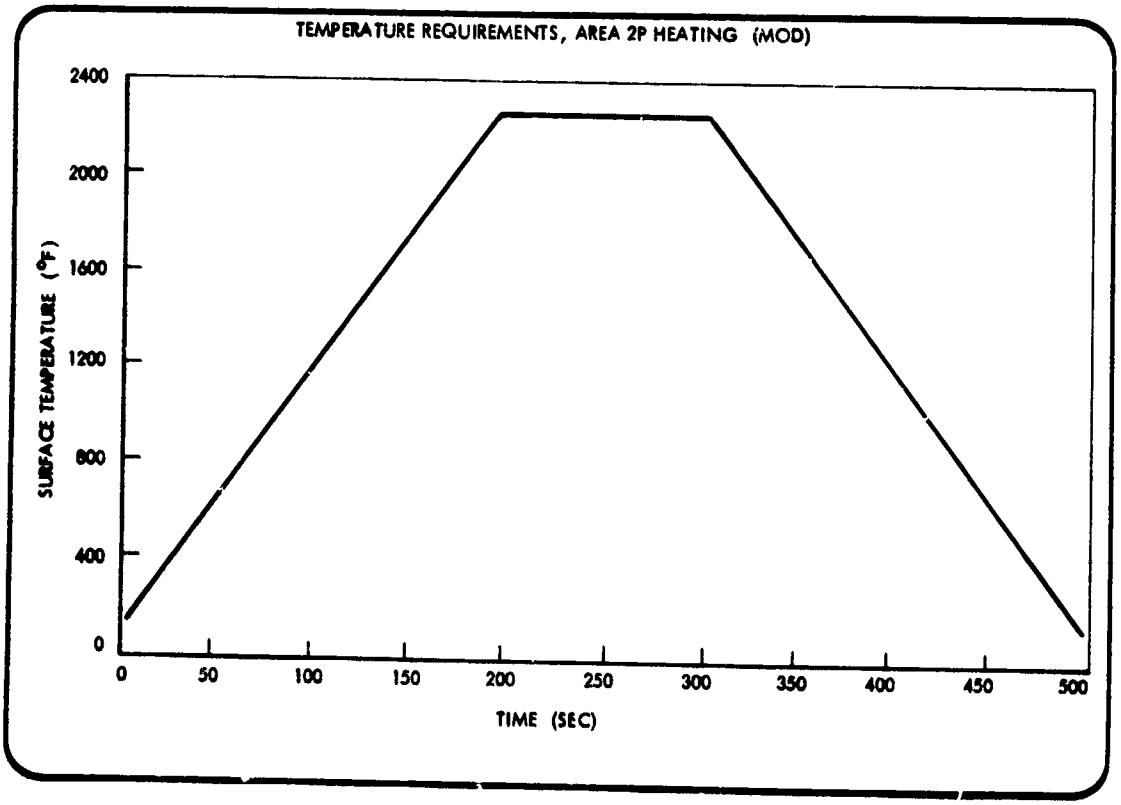

Fig. 4.4.1-2 Chemical Tolerance Tests, Temperature Requirements, Area 2P Heating (Mod)

characteristic determination, and visual examination were performed. The test model was then subjected to the modified Area 2P heating environment, as shown in Fig. 4.4.1-2, under the laboratory ambient pressure condition. Post-test examinations were repeated after the simulated entry heating exposure was performed.

Coating Tests. Three test models were coated with freshly deposited seagull excreta. An attempt was made to identify the contributing seagull by species and sex, and to establish the time interval between voiding of excreta by the subject contributing seagull and the application of same to the test model. Application of the excreta to the test model was made with a soft rubber or plastic spatula, or digitally. Only the outboard surface of the test model was coated (the coating was approximately 1/16 to 1/8 inch thick, depending on viscosity of excreta material). A total of three test models were coated; one test model was cleaned with isopropyl alcohol as soon as the excreta solidified; the second test model was cleaned with isopropyl alcohol approximately 72 hours after application of excreta; the third test model was not cleaned, but was preserved with excreta coating intact.

After the exposure test, the models were weighed and dimensional measurements, emittance characteristic determinations, and visual examinations were performed. The test models were then subjected to the modified Area 2P heating environment, as shown in Fig. 4.4.1-2, under the laboratory ambient pressure condition. Post-test examinations were repeated after the entry heating test was performed.

Test Data and Results. It is expected that the data collected as a result of the tests performed herein will provide the basis for a tentative "restricted fluids" list for LI 900 RSI material. In addition, these results will provide an evaluation of the significance of bird excrement contamination to reuse of the LI-900 RSI material.

All test data collected were tabulated for incorporation in this final report.

Color photographs were made for documentation of the appearance of the test models prior to exposure, after exposure, and after the radiant simulation Area 2P heat environment.

4.4.2 Test Results

A summary of the test results is presented in Table 4.4.2. Figures 4.4.2-1 and 4.4.2-2 show the appearance of the test models prior to and after chemical exposure. It should be noted that the only visible change in appearance due to the exposure occurred with the specimens immensed in JP-4 fuel, inhibited red fuming nitric acid (IRFNA), and unsymmetrical dimethyl hydrazine (UDMH). However, all of the models increased in weight during the exposure, as shown in the tabular data. The model immensed in JP-4 failed in the tile bond due to swelling of the RTV (Ref. Fig. 4.4.2-3). The model exposed to UDMH acquired red surface stains, as shown in Fig. 4.4.2-4.

The test model exposed to IRFNA acquired surface stains and experienced bond deterioration, as shown in Fig. 4.4.2-3. No coating cracks were evident in any of the test models after the exposure. The appearance of the three models exposed to bird excrement is shown in Fig. 4.4.2-5. It was found during these tests that the darker components of bird excrement would not adhere to the 0042 coating after drying; the white component would adhere quite tenaciously after drying. The results of the model examinations performed after the chemical exposure indicate the JP-4, UDMH, and IRFNA should not be allowed to contaminate the RSI thermal protection system. The JP-4 in particular should not be permitted to contact the RTV bond materials.

The results of the application of the modified area 2P heat pulse to the test models are also presented in Table 4.4.2. The actual surface temperature pulse applied is shown in Fig. 4.4.2-6. Heating of the models was terminated after the peak surface temperature required was achieved, because of the burning of residual volatile chemical exposure materials as they escaped from the tiles. This burning effect did some local damage to the RTV bond installation. In the case of the model exposed to JP-4, the burnoff was substantial and affected the adjacent models packed for the test, indicating that any fuels spilled and absorbed during prelaunch operation could, if absorbed, possibly burn off with resulting damage to the RTV bond. The individual effects of the heat pulse on the test models are described below:

The tabulated results of model weights indicate that all models increased in weight during the chemical exposure and decreased in weight during the modified area 2P heat pulse. Final weights are slightly less than initial weights for each test model. The tabulated results of test model emittance values show little if any change in emittance due to the chemical exposures. The only significant change was due to the bird excrement coating.

In general, the results of the heat pulse indicate that sodium hydroxide, JP-4 fuel, UDMH, and the dried white component of bird excrement are destructive to the RSI thermal protective system. A tentative list of restricted fluids for the LI-900 RSI system should include the following:

1. Sodium Hydroxide (NaOH)
2. JP-4 Turbine Fuel
3. Inhibited Red Fuming Nitric Acid
4. Unsymmetrical Dimethyl Hydrazine (UDMH)
5. Dried White Component of Bird Excrement

4.4.3 Shuttle Comparison

(Comparison of the test results to the predicted Shuttle service environments will be submitted after test completion and incorporated into an addendum.)

Table 4.4.2

SUMMARY OF CHEMICAL TOLERANCE TEST RESULTS

Specimen Ident	Exposure Material	Pre-Exposure Weight (g)	Pre-Exposure Emittance	Exposure Time (Hr)	Post-Exposure Weight (g)	Post-Exposure Emittance	Post-Heat Pulse Weight (g)	Post-Heat Pulse Emittance	Comments
TT128-3	Bird Excreta	7.9549	–	24	7.962	.84	7.690	.84	
TT128-4	Bird Excreta	7.763	.85	3	7.801	.85	7.223	.84	
TT128-5	MEK	8.3891	–	24	17.7005	.85	8.321	.84	
TT128-6	CH_3CHO	8.4182	–	24	11.3146	.85	8.380	.85	
TT128-7	HYD OIL	8.2351	–	24	8.2640	.88	8.230	.85	
TT128-9	JP-4	8.3895	–	24	17.4415	.85	8.512	.85	1.
TT128-10	Acetone	8.0540	–	24	13.8884	.85	7.907	.85	
TT128-12	Bird Excreta	7.749	.84	72	7.763	.86	7.023	.85	
TT128-14	IRFNA	8.0701	–	24	9.8744	.87	7.343	.86	2.
TT128-15	Bird Excreta	8.069	.84	–	8.172	.91	7.700	.83	
TT128-16	HCl	7.8994	–	24	7.9031	.83	7.616	.84	
TT128-17	NaOH	7.9875	–	24	8.8564	.86	7.678	.84	
TT128-18	UDMH	7.9440	–	24	10.5301	.85	7.716	.84	

1. Tile cracked above bond due to expansion of RTV.
2. RTV bond deteriorated.

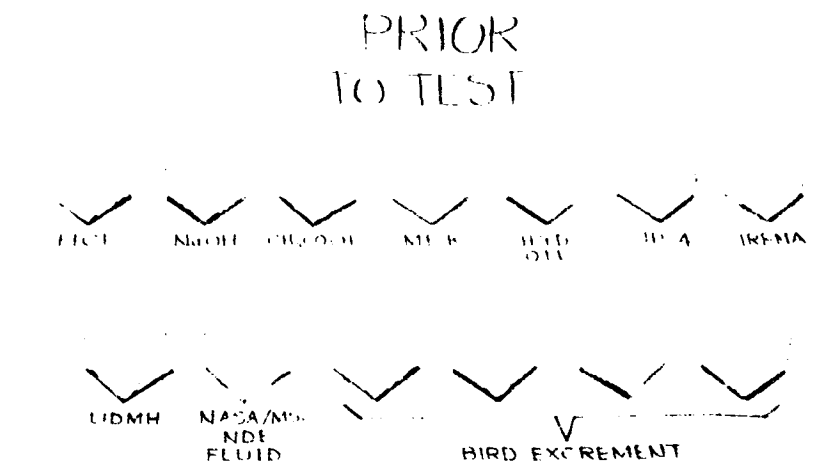

Fig. 4.4.2-1 Task C-4, Chemical Tolerance Test Models – Contract NAS9-12856

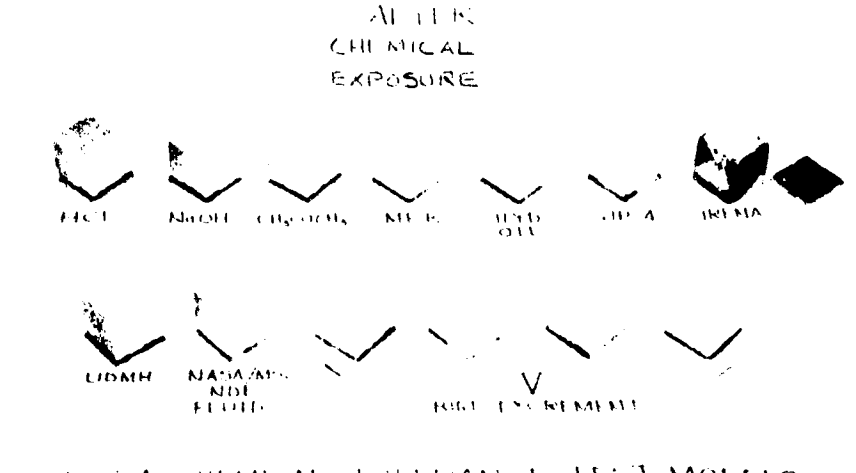

Fig. 4.4.2-2 Task C-4, Chemical Tolerance Test Models – Contract NAS9-12856

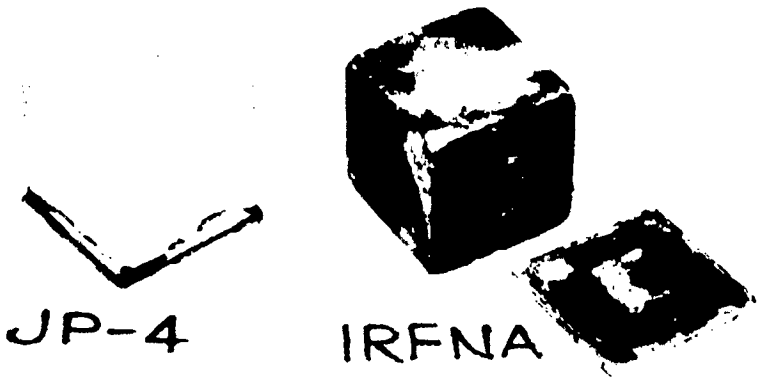

Fig. 4.4.2-3 JP-4 and IRFNA Specimen After Exposure

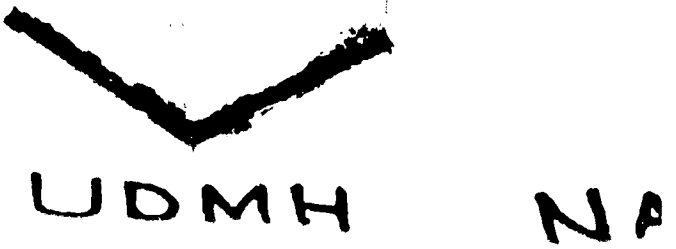

Fig. 4.4.2-4 UDMH Specimen After Exposure

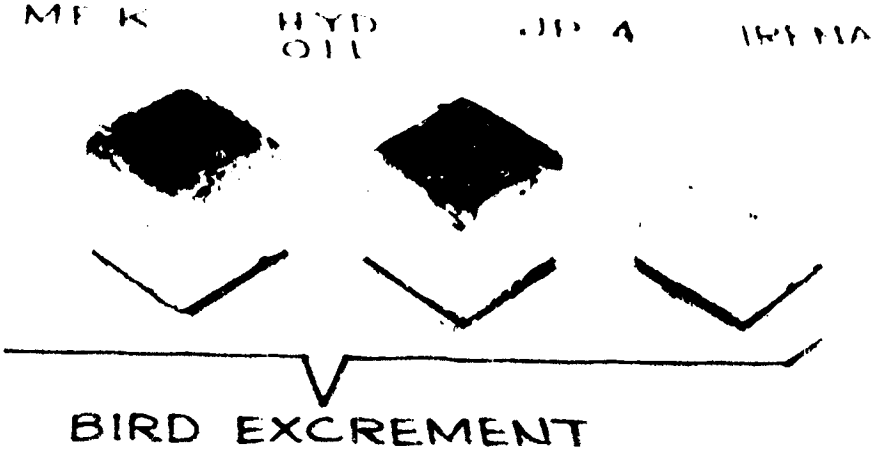

Fig. 4.4.2-5 Bird Excrement Specimen After Exposure

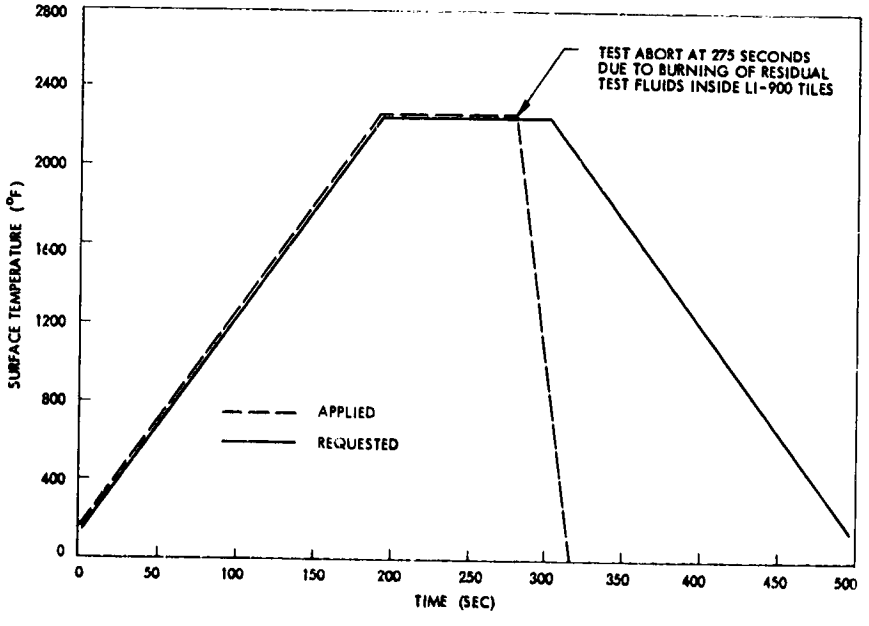

Fig. 4.4.2-6 Chemical Tolerance Tests – Temperature Requirements, Area 2P Heating (Mod)

Section 5
MATERIAL PRODUCTION SUMMARY - TASK D

The LI-900 material required to support Task C and Task E, as well as the material for MSC evaluation, were produced under Task D. In addition, LI-1500 material required under Supplemental Agreement No. 1S to the contract for MSC evaluation was also produced under this task.

Tasks C and E Material. Materials produced for other tasks at LMSC are described and detailed on pages 5-2 and 5-6.

Task D LI-900 Material for MSC Evaluation. This material was delivered in accordance with "call" requirements from NASA/MSC which stipulated configuration and quantity. These requirements are detailed on pages 5-7, 5-11, 5-17, 5-19, and 5-21.

Task D Supplemental Agreement No. 1S:LI-1500 Material for MSC Evaluation. LI-1500 material was also delivered in accordance with all requirements from NASA/MSC stipulating configuration and quantity. This requirement is detailed on pages 5-9, 5-13, and 5-15.

Photographs have been taken of all delivered material. Typical materials as supplied are shown in Figs. 5-1, 5-3, and 5-3.

The manufacture of the all-silica RSI (LI-1500 and LI-900) is closely controlled to ensure quality and reliable material. Quality control logs are maintained for each critical process step and maintenance of the logs is certified by Quality Engineering. Each specimen and test model produced has been identified as to process lot number. Copies of all radiographic NDE evaluations performed on the test specimens and/or test models have been supplied to NASA.

For Contract NAS 9-12856 and Supplemental Agreement No. 1S, a total of 11 cubic feet of RSI material was originally contracted to be produced to fulfill the evaluation requirements. For requirements added during the program performance to obtain other material test/evaluation needs, a total of 19 cubic feet of LI-1500/LI-900 RSI material was actually produced.

TILE DATA SHEET

Lot Identification	C-1 Thermal Response Test		
Basic Material	LI-900		
Surface Coating (LI-0042)	Yes		
Hydrophobic Treatment (LI-007)	Yes		
Tile Properties	TT 141-X Series		
Ident No.	-2	-4	-6
Dim (in.):			
Length (dia)	6.26	6.27	6.33
Width	6.01	6.02	5.99
Thickness	3.04	3.04	3.09
Density (pcf)	8.4	9.0	9.0
Ctg Wt (lb)	.053	.068	.066
Tile Wt (lb)	.638	.640	.627
Proc Lot No.	5790	5790	5790
Misc Data	None		
Ship Date(s)	NA		
Deliver To	NA		

TILE DATA SHEET

Lot Identification	C-2 Turbulent Duct Test			
Basic Material	LI-900			
Surface Coating (LI-0042)	Yes			
Hydrophobic Treatment (LI-007)	Yes			
Tile Properties	TT 140-X Series			
Ident No.	-1	-2	-3	-5
Dim (in.):				
Length (dia)	7.85	7.79	5.91	5.92
Width	1.95	2.42	2.93	4.93
Thickness	2.99	2.96	2.98	3.00
Density (pcf)	8.8	8.5	9.1	9.4
Ctg Wt (lb)	.033	.032	.043	.049
Tile Wt (lb)	.270	.219	.281	.474
Proc Lot No.	5790	5790	5790	4790
Misc Data	None			
Ship Date(s)	NA			
Deliver To	NA			

TILE DATA SHEET

Lot Identification	C-3 Convective Cycling Test					
Basic Material	LI-900					
Surface Coating (LI-0042)	Yes					
Hydrophobic Treatment (LI-007)	Yes					
Tile Properties	TT 142-X Series					
Ident No.	-3	-4	-5	-7	-8	
Dim (in.):						
Length (dia)	6.0	6.0	6.0	6.0	6.0	
Width	6.0	6.0	6.0	3.0	3.0	
Thickness	2.0	2.0	2.0	2.0	2.0	
Density (pcf)	8.6	9.0	8.5	8.3	9.2	
Ctg Wt (lb)	TBD					
Tile Wt (lb)	TBD					
Proc Lot No.	5790	5790	5790	5790	5790	
Misc Data	None					
Ship Date(s)	NA					
Deliver To	NA					

TILE DATA SHEET

Lot Identification	C-4 Chemical Tolerance Tests
Basic Material	LI-900
Surface Coating (LI-0042)	Yes
Hydrophobic Treatment (LI-007)	Yes
Tile Properties	TT-128 Series
Ident No.	-3 Through -18
Dim (in.):	
Length (dia)	1.0
Width	1.0
Thickness	1.0
Density (pcf)	7.7 - 9.8
Ctg Wt (lb)	Not Significant
Tile Wt (lb)	Not Significant
Proc Lot No.	5790
Misc Data	None
Ship Date(s)	NA
Deliver To	NA

TILE DATA SHEET

Lot Identification	E-Prototype Panel			
Basic Material	LI-900			
Surface Coating (LI-0042)	Yes			
Hydrophobic Treatment (LI-007)	Yes			
Tile Properties	TT 146-X Series			
Ident No.	-1	-2	-3	-4
Dim (in.):				
Length (dia)	12.0	12.0	12.0	12.0
Width	12.0	12.0	12.0	12.0
Thickness	3.0	3.0	3.0	3.0
Density (pcf)	8.4	9.4	9.3	8.7
Ctg Wt (lb)	TBD			
Tile Wt (lb)	TBD			
Proc Lot No.	5790	5790	5790	5790
Misc Data	None			
Ship Date(s)	NA			
Deliver To	NA			

TILE DATA SHEET

Lot Identification	Call Requirement No. 1
Basic Material	LI-900
Surface Coating (LI-0042)	Yes
Hydrophobic Treatment (LI-007)	Yes
Tile Properties	
Ident No.	TT 111
Dim (in.):	
Length (dia)	12.01
Width	12.01
Thickness	2.02
Density (pcf)	8.7
Ctg Wt (lb)	TBD
Tile Wt (lb)	1.56
Proc Lot No.	2086
Misc Data	None
Ship Date(s)	8-28-72
Deliver To	NASA/ARC

TILE DATA SHEET

Lot Identification	Call Requirement No. 1		
Basic Material	LI-1500		
Surface Coating (LI-0042)	Yes		
Hydrophobic Treatment (LI-007)	Yes		
Tile Properties	TT 139-X Series		
Ident No.	-1	-2	-3
Dim (in.):			
Length (dia)	12.01	12.01	12.02
Width	11.97	12.02	12.02
Thickness	2.01	2.02	2.01
Density (pcf)	14.7	14.2	14.1
Ctg Wt (lb)	.1	.1	.1
Tile Wt (lb)	2.61	2.51	2.54
Proc Lot No.	2157	2157	2157
Misc Data	None		
Ship Date(s)	11-8-72		
Deliver To	NASA/ARC		

FOLDOUT FRAME

FOLDOUT FRA

TA SHEET

E No. 1

-3	-4	-5	-6	-7	-8	-9	-11
12.02	12.01	11.99	12.02	12.02	12.01	11.93	12.05
12.02	12.01	11.98	12.01	12.01	12.01	12.00	12.06
2.01	1.98	2.02	2.01	2.01	2.00	2.02	2.01
14.1	13.5	14.4	15.3	14.5	13.8	14.4	15.8
.1	.1	.1	.1	.1	.1	.1	.1
2.54	2.36	2.53	2.72	2.59	2.42	2.50	2.77
2157	2157	2157	2157	2157	2157	2157	2157

DOUT FRAM

2

TITLE DATA SHEET

Lot Identification	Call Requirement No. 2						
Basic Material	LI-0900						
Surface Coating (LI-0042)	Yes						
Hydrophobic Treatment (LI-007)	Yes						
Tile Properties	TT 113-X Series						
Ident No.	-9	-10	-11	-12	-13	-14
Length (dia)	3.81	3.80	3.80	3.80	3.78	3.80
Width						
Thickness	2.01	2.01	2.01	2.01	2.01	2.01
Density (pcf)	10.5	10.8	11.3	10.3	8.8	9.6
Ctg Wt (lb)	.02	.02	.02	.02	.02	.02
Tile Wt (lb)	.15	.16	.16	.16	.13	.14
Proc Lot No.	5789	5789	5789	5789	5789	5789
Misc Data	Mounted on .062 in. Alu. Plate with .080 RL-1973 Sponge/RTV-560 Bond 12 Thermocouples Each Model						
Ship Date(s)	10-2-72						
Deliver To	NASA/MSC						

TILE DATA SHEET

Lot Identification	Call Requirement No. 2		
Basic Material	LI-1500		
Surface Coating (LI-0042)	Yes		
Hydrophobic Treatment (LI-007)	Yes		
Tile Properties	TT 143-X Series		
Ident No.	-5	-7	-8
Dim (in.):			
Length (dia)	6.01	6.01	6.02
Width	6.01	6.02	6.01
Thickness	2.99	2.99	3.00
Density (pcf)	14.8	14.5	14.6
Ctg Wt (lb)	.08	.08	.09
Tile Wt (lb)	1.03	1.02	1.02
Proc Lot No.	2157	2157	2157
Misc Data	6 Thermocouples on -8 only		
Ship Date(s)	11-16-72 to 11-19-72		
Deliver To	NASA/MSC		

FOLDOUT FRAME

FOLDOUT FRAME

=A SHEET

No. 2

-8	-9	-14	-15	-16	-17
6.02	6.00	6.03	6.03	6.02	6.03
6.01	6.01	6.03	6.03	6.02	6.02
3.00	2.98	2.99	2.99	2.99	2.99
14.6	14.2	14.4	15.0	14.6	15.0
.09	.08	.06	.05	.06	.05
1.02	1.00	1.00	1.02	1.00	1.02
2157	2157	2157	2157	2157	2157

on -8 only.

=-72

PRECEDING PAGE BLANK NOT FILMED

OUT FRAM

2

TILE DATA SHEET

Lot Identification	Call Requirement No. 2		
Basic Material	LI-1500		
Surface Coating (LI-0042)	Yes		
Hydrophobic Treatment (LI-007)	Yes		
Tile Properties	TT 144-X Series		
Ident. No.	-2	-3	-4
Dim (in.):			
Length (dia)	5.99	6.01	6.03
Width	5.99	6.01	6.03
Thickness	1.51	1.51	3.00
Density (pcf)	14.7	14.9	14.2
Ctg Wt (lb)	.06	.06	.06
Tile Wt (lb)	.53	.53	1.00
Proc Lot No.	2157	2157	2157
Misc Data	TT 145-X Series Mounted on 6 Thermocouples on TT 144-		
Ship Date(s)	12-4-72 to 12-10-72		
Deliver To	NASA/MSC		

OLDOUT FRA

SHEET

.. 2

TT 145-X Series

-4	-5	-1	-2	-3	-5	-6
3.03	6.00	3.84	3.84	3.85	3.85	3.87
3.03	6.01					
3.00	3.00	3.00	3.00	3.08	3.00	3.00
2.2	14.6	15.9	15.3	15.1	15.4	15.0
.06	.06	.03	.03	.03	.03	.03
..00	.98	.36	.36	.35	.35	.35
2157	2157	2157	2157	2157	2157	2157

..nted on .062 Alu. Plate with .080 RL-1973 Sponge/RTV-560 Bond
TT 144-3 &-5, TT 145-1 &-2

PRECEDING PAGE BLANK NOT FILMED

TILE DATA SHEET

Lot Identification	Call Requirement No. 3	
Basic Material	LI-900	
Surfac Coating (LI-0042)	Yes	
Hydrophobic Treatment (LI-007)	Yes	
Tile Properties	TT 114-X Series	
Ident No.	-3	-4
Dim (in.):		
Length (dia)	11.94	11.99
Width	11.95	11.99
Thickness	2.00	2.01
Density (pcf)	8.6	9.8
Ctg Wt (lb)	.12	.10
Tile Wt (lb)	1.60	1.77
Proc Lot No.	5789	5789
Misc Data	None	
Ship Date(s)	10-4-72	
Deliver To	Battelle	

FOLDOUT FRAME

1

TILE DATA SHE

Lot Identification	Call Requirement No. 4		
Basic Material	LI-0900		
Surface Coating (LI-0042)	Yes		
Hydrophobic Treatment (LI-007)	Yes		
Tile Properties	TT 129-X Series		
Ident. No.	-1	-2	-3
Dim (in.):			
Length (dia)	3.83	3.85	3.85
Width			
Thickness	3.00	3.01	3.00
Density (pcf)	8.4	8.5	8.6
Ctg Wt (lb)	.03	.04	.03
Tile Wt (lb)	.21	.21	.21
Proc Lot No.	5789	5789	5789
Misc Data	Mounted on .062 Alu. Pla 6 Thermocouples on TT 1		
Ship Date(s)	11-5-72		
Deliver To	NASA/MSC		

OLDOUT FRAME

2

TILE DATA SHEET

uirement No. 4

X Series				TT 130-X Series				
-2	-3	-12	-13	-2	-3	-5	-10	-12
3.85	3.85	3.85	3.85	3.86	3.86	3.85	3.86	3.85
3.01	3.00	3.01	3.00	1.51	1.51	1.55	1.51	1.50
8.5	8.6	8.6	9.0	10.0	9.9	8.3	9.7	9.9
.04	.03	.03	.02	.03	.02	.02	.02	.03
.21	.21	.21	.20	.12	.12	.11	.11	.12
5789	5789	5789	5789	2086	2086	5789	2086	5790

on .062 Alu. Plate with .080 RL-1973 Sponge/RTV-560 Bond
ocouples on TT 129-2 & -13, TT 130-10 & -12

SC

PRECEDING PAGE BLANK NOT FILMED

DOUT FRAME

1

TILE DATA SHEET

Lot Identification		Call Requirement No. 4		
Basic Material		LI-0900		
Surface Coating (LI-0042)		Yes		
Hydrophobic Treatment (LI-007)		Yes		
Tile Properties		TT 131-X Series		
	Ident No.	-2	-3	-4
	Dim (in.):			
	Length (dia)	6.01	6.00	6.01
	Width	6.00	6.00	6.00
	Thickness	3.00	3.00	3.00
	Density (pcf)	9.3	9.3	9.2
	Ctg Wt (lb)	.08	.08	.08
	Tile Wt (lb)	.69	.69	.68
	Proc Lot No.	5790	5790	5790
Misc Data		6 Thermocouples on TT 131-10		
Ship Date(s)		11-5-72		
Deliver To		NASA/MSC		

C-3

UT FRAME
2.

DATA SHEET

ent No. 4

TT 132-X Series

	-4	-5	-10	-11	-1	-2	-3	-4	-11	-13
	6.01	6.01	6.01	6.01	6.01	6.00	6.01	6.01	6.01	6.01
	6.00	6.01	6.01	6.01	6.01	6.00	6.01	6.00	6.01	6.01
	3.00	3.01	3.00	2.99	1.50	1.50	1.50	1.50	1.51	1.50
	9.2	8.9	9.1	8.3	8.6	8.4	8.9	8.8	9.5	10.2
	.08	.08	.09	.08	.06	.06	.05	.05	.06	.05
	.68	.68	.67	.62	.34	.34	.34	.34	.36	.38
	5790	5790	5790	5789	5790	5790	5790	5790	5789	5789

ler [illegible] TT 132-11 &-13

PRECEDING PAGE BLANK NOT FILMED

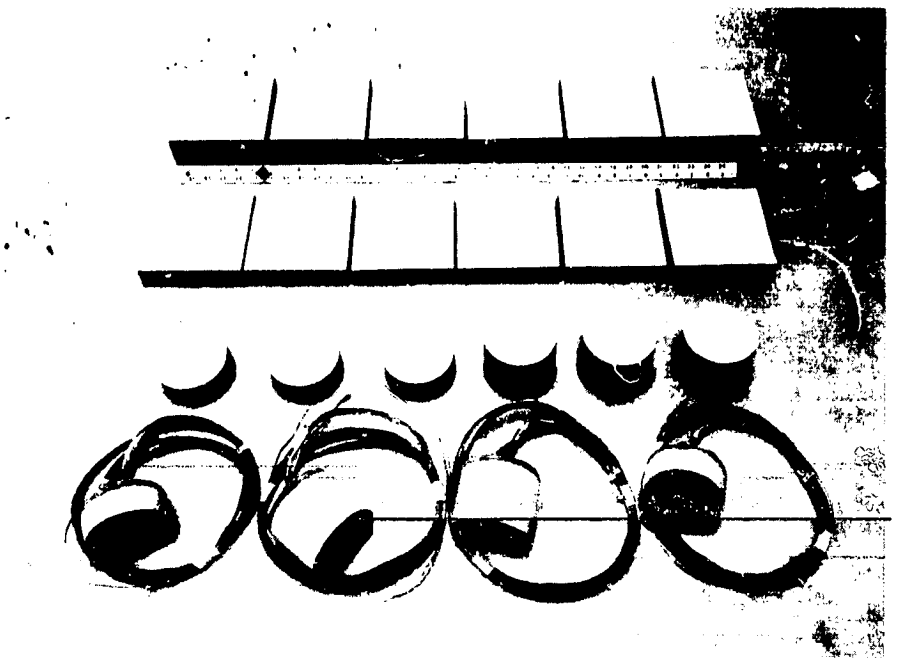

Fig. 5-1 Task D, Call Requirement No. 4 - NASA/MSC Evaluation
TT 129, TT 130, TT 131, TT 132

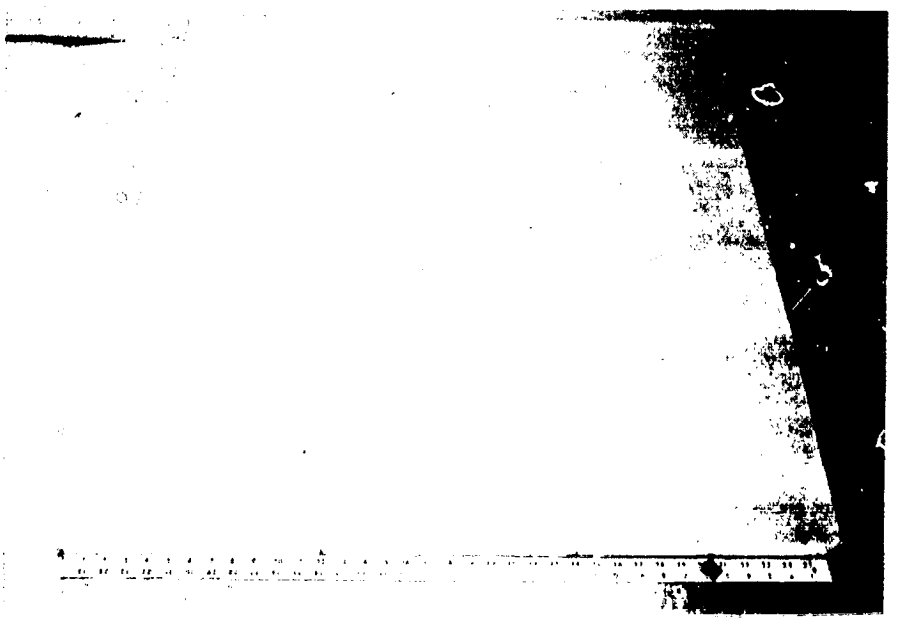

Fig. 5-2 Task D, Supplementary Agreement No. 15 – LI-1500 Material
for NASA/MSC Est. Call Requirement No. 1, TT 139

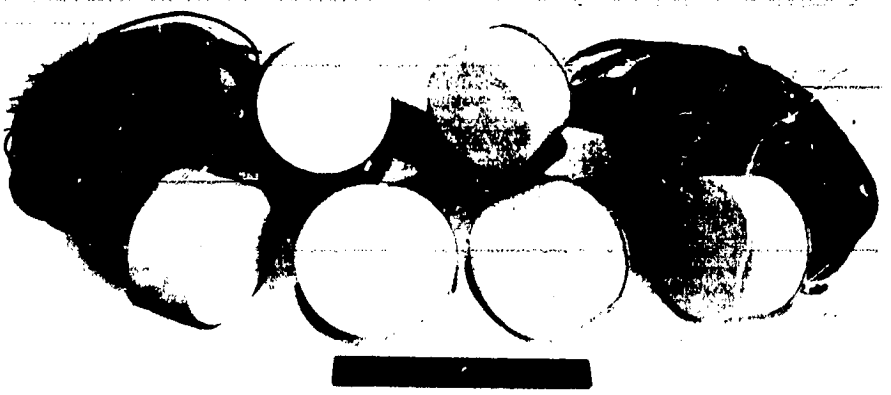

Fig 5-3 Call Requirement No. 2 - NASA/MSC Arc Jet Models TT 113

Section 6
DESIGN OPTIONS FOR MSC EVALUATION – TASK E

6.1 ENVIRONMENTAL TEST PLAN

An Environmental Test Plan for Phase III RSI Prototype Test Panel is included in this report as Appendix E1.

6.2 TPS TEST PANEL DRAWINGS – TASK E

Figures 6.2-1, 6.2-2, and 6.2-3 show the structural details of the TPS Test Panel (with instrumentation shown on Fig. 6.2-3). Figure 6.2-4 shows the geometry of the strain arrestor plate. Design description of these articles is contained in Section 2, Design – Task A of this report.

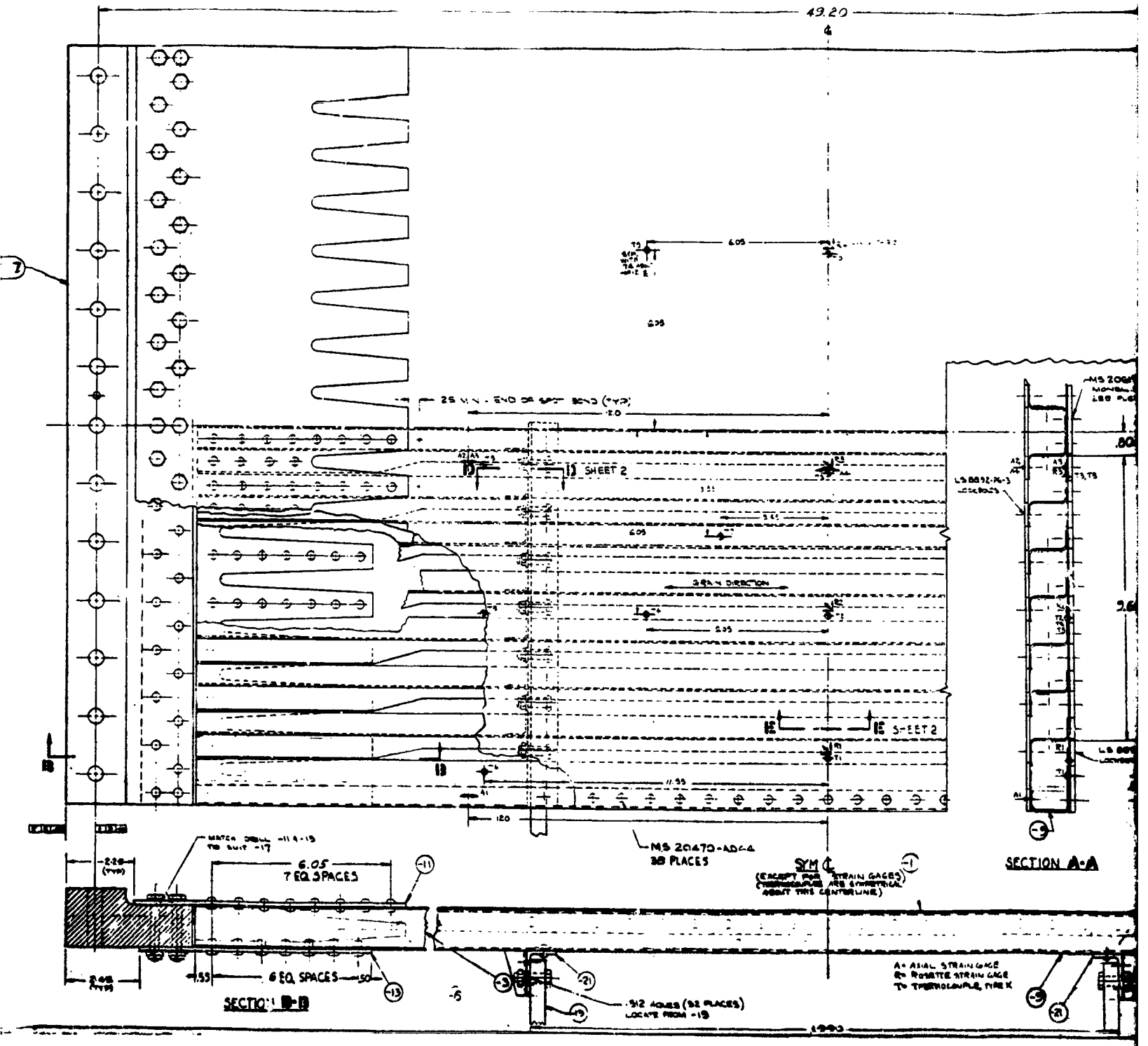

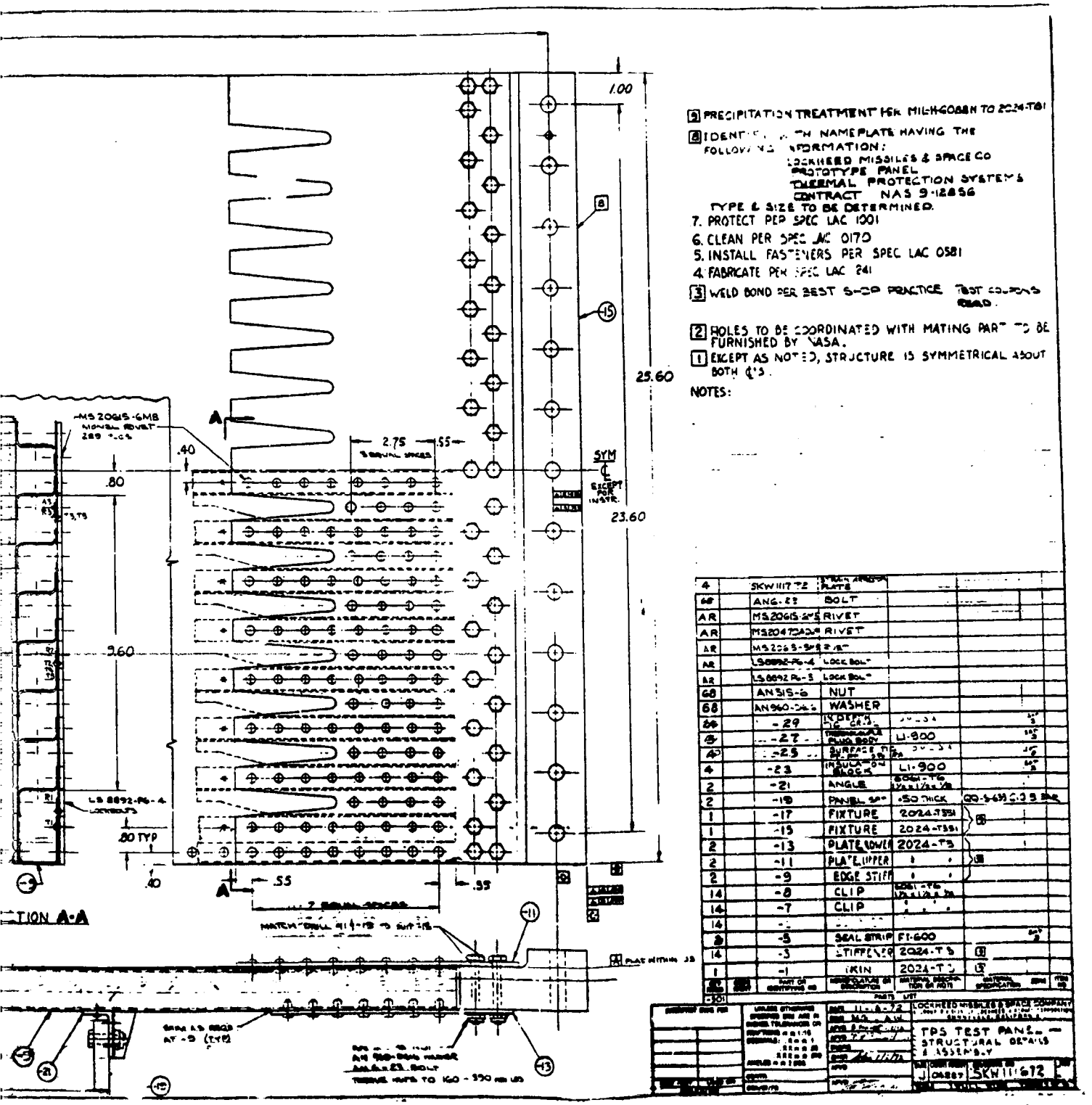

Fig. 6.2-1 TPS Test Panel Structural Details and Assembly

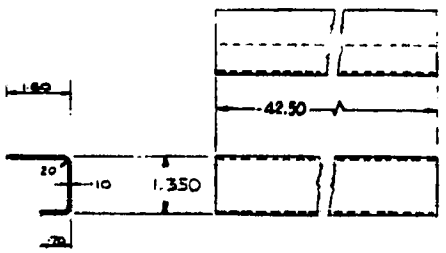

-9 EDGE STIFFENER

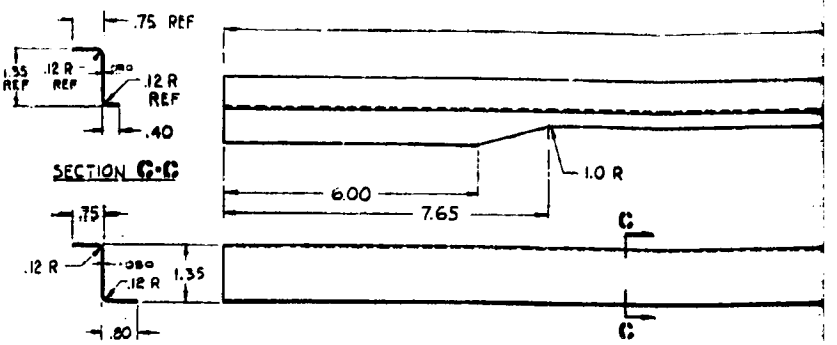

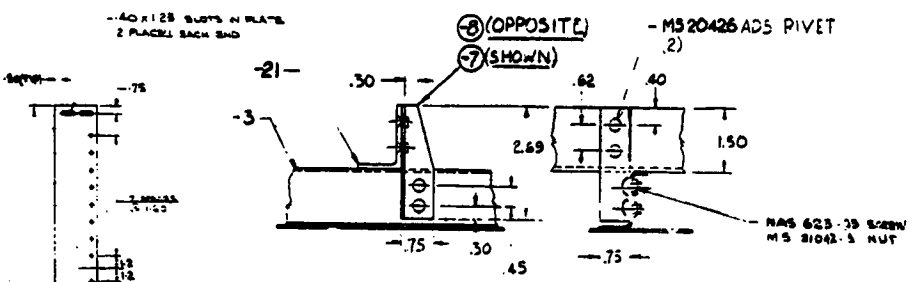

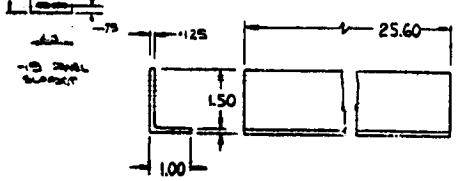

-21 ANGLE

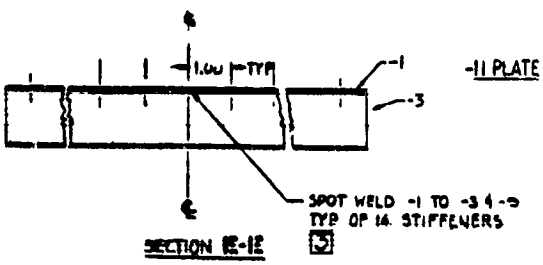

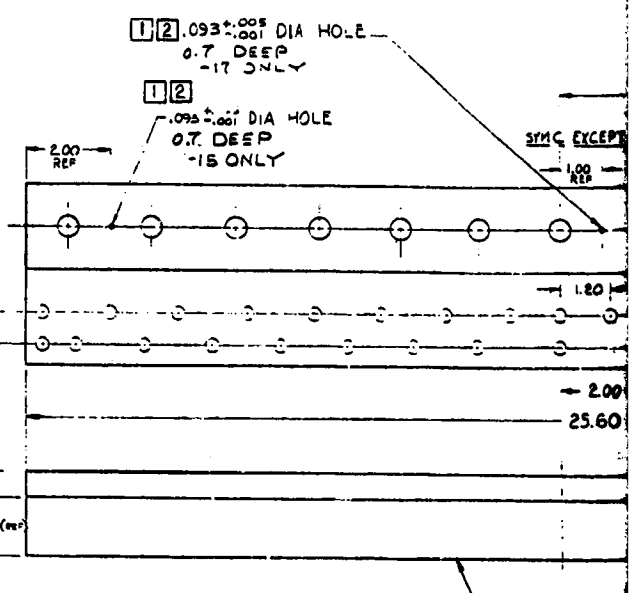

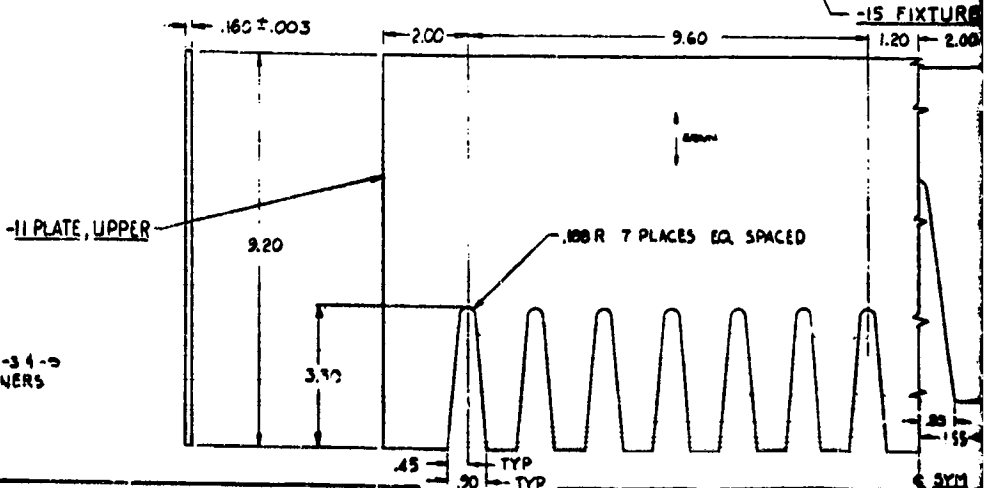

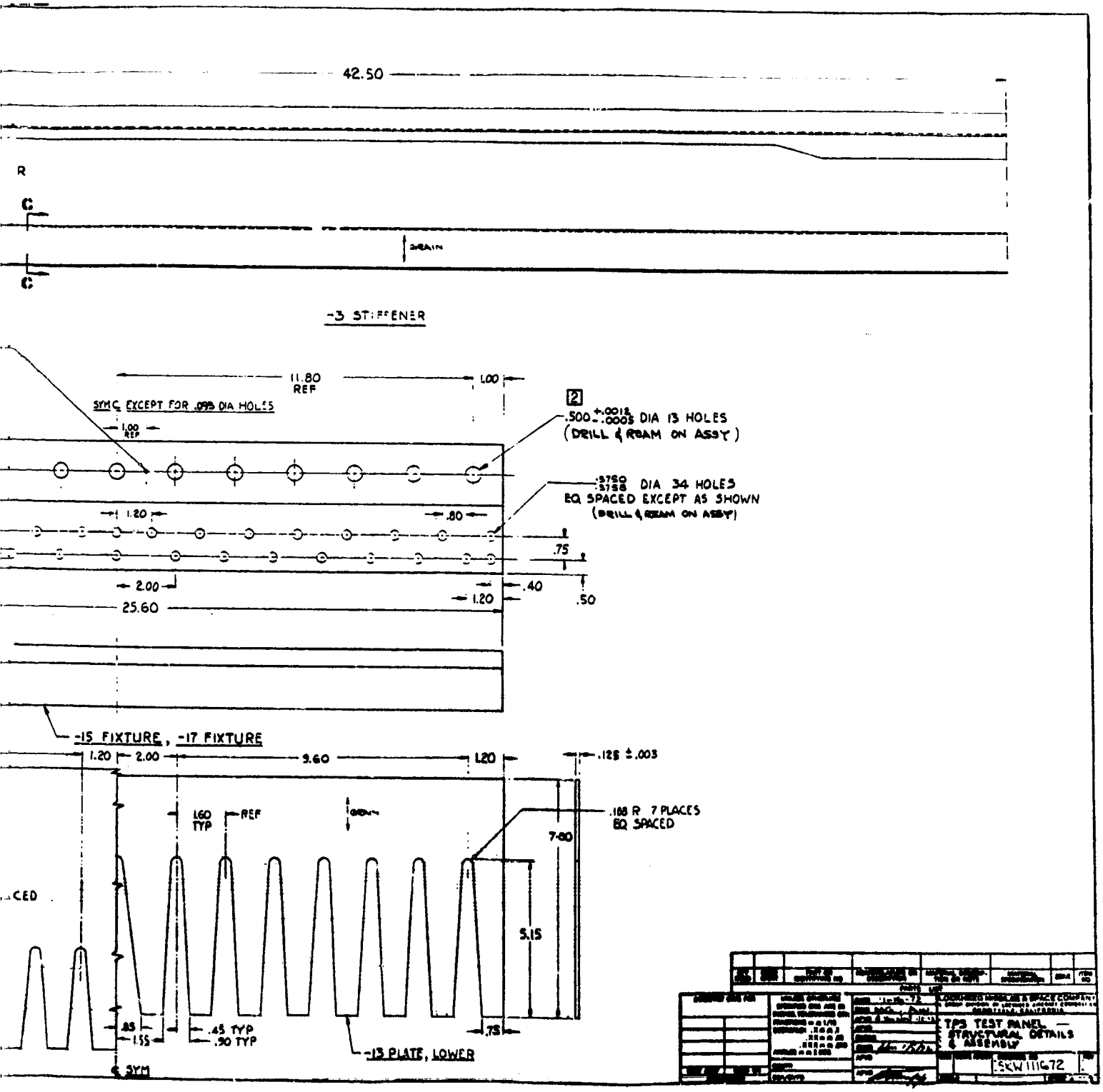

Fig. 6.2-2 TPS Test Panel Structural Details and Assembly

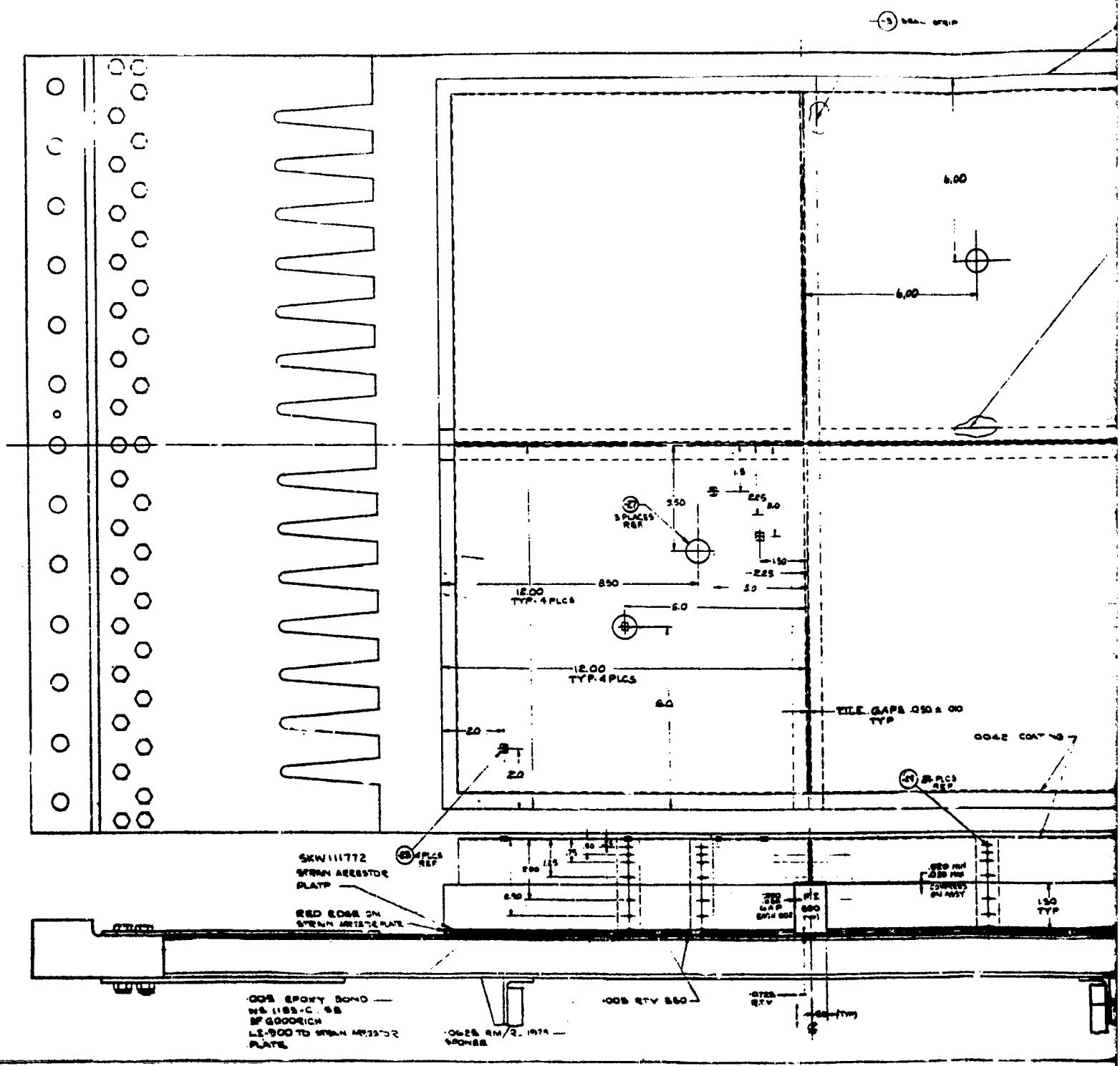

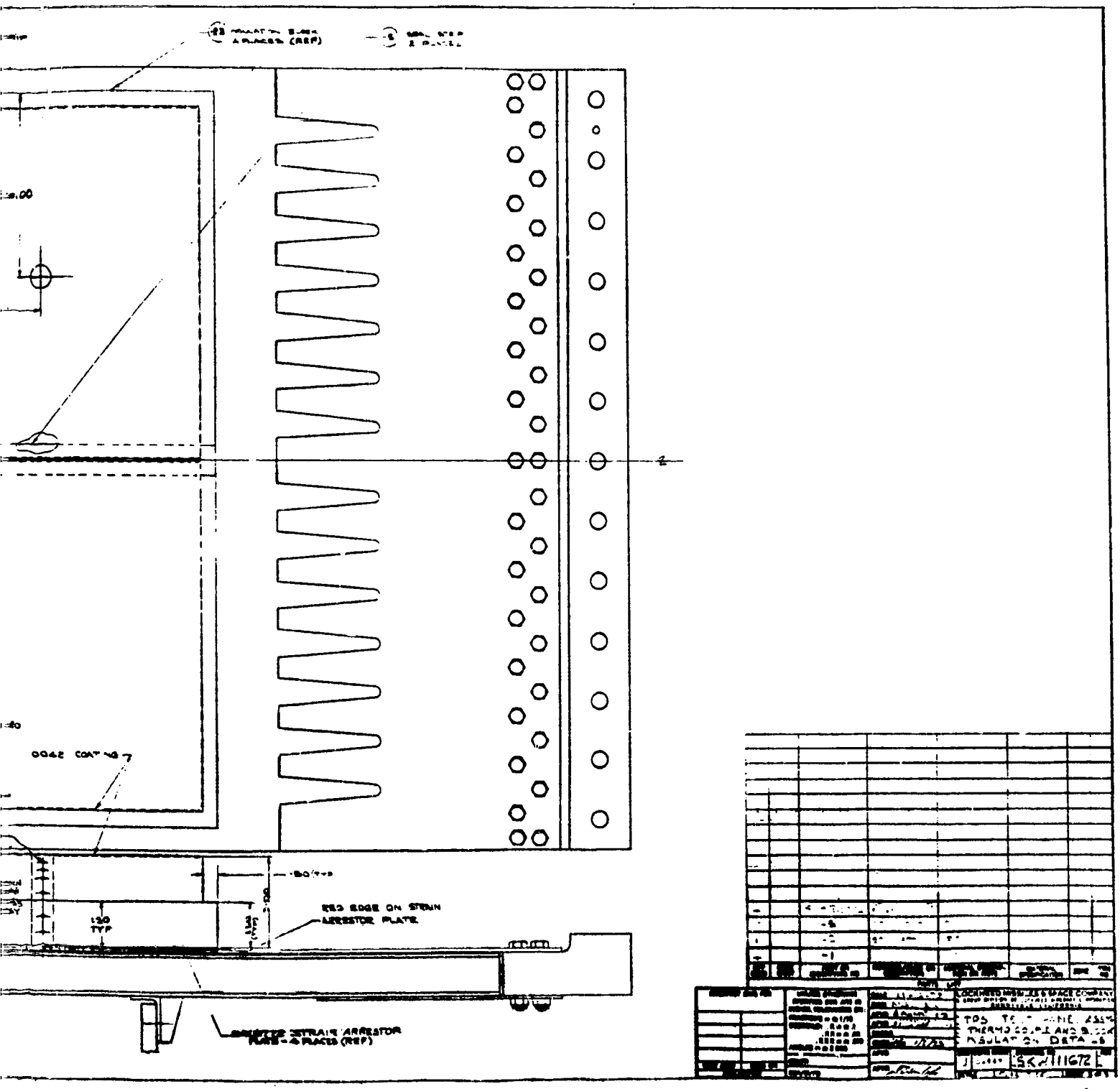

Fig. 6.2-3 TPS Test Panel

FOLDOUT FRAME 2

LAYOUT FRAME

8 7 6 5

D C B A

COLOR THIS EDGE RED

.028

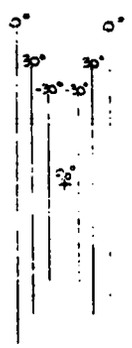

PLY ORIENTATION DIAGRAM

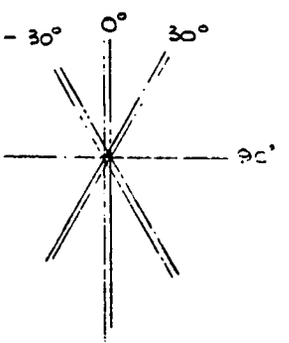

PLY ORIENTATION DIAGRAM

11.50

11.50

FOLDOUT FRAME 2

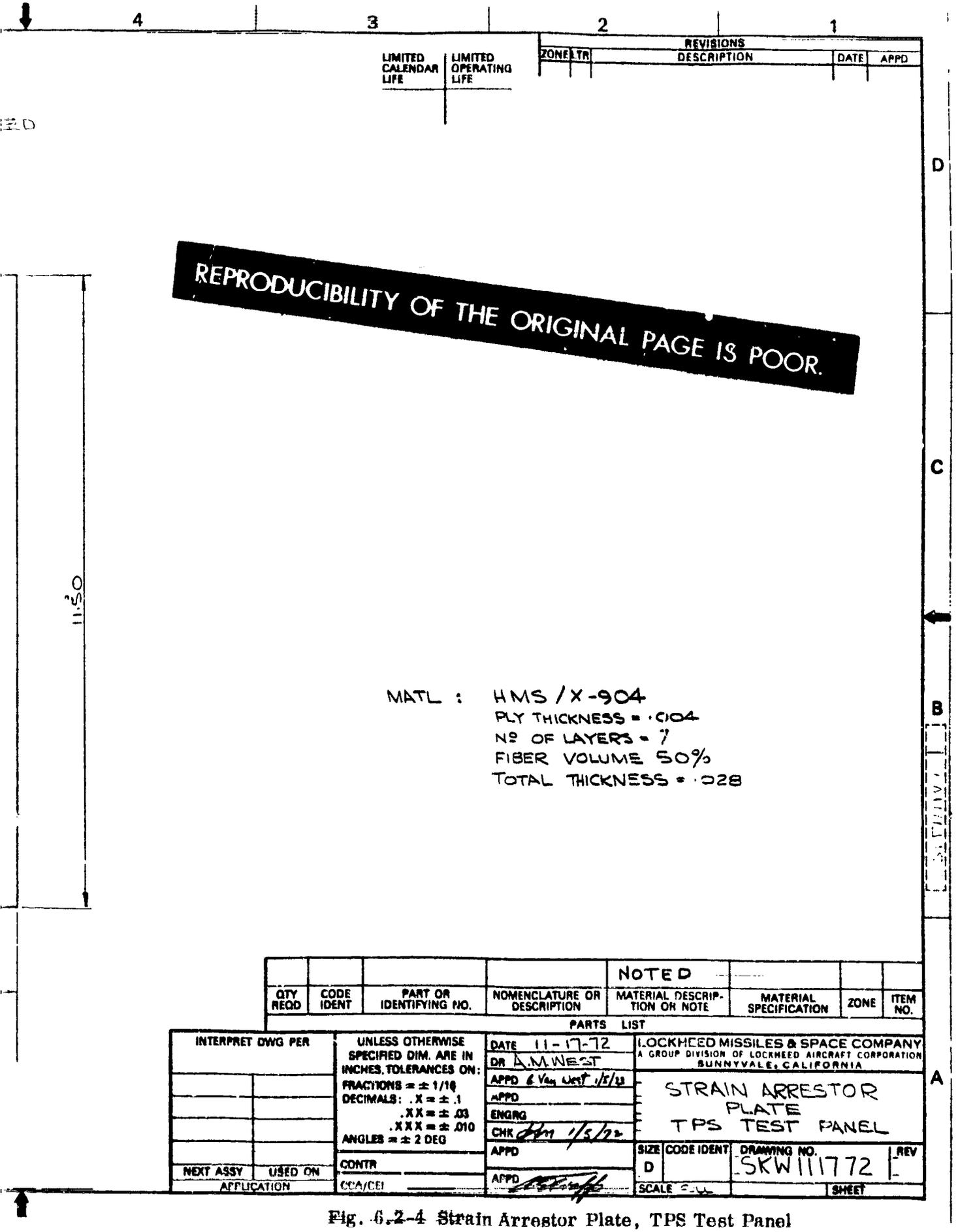

Fig. 6.2-4 Strain Arrestor Plate, TPS Test Panel

ADDENDUM TO

LMSC-D282673; MSC-07040, DRL-3

FINAL REPORT FOR

DEVELOPMENT AND DESIGN

APPLICATION OF RIGIDIZED SURFACE

INSULATION THERMAL PROTECTION SYSTEMS

31 January 1973

Contract NAS 9-12856

Prepared under direction of

A. E. Trapp
Project Leader

Approved

K. J. Forsberg, Assistant Director
Materials and Structures

J. F. Milton, Director
Manned Space Support Systems

FOREWORD

This addendum presents additional information on material property determination and environmental tests that was not available when the Final Report, LMSC-D282673; MSC-07040, DRL-3, was published. The information is presented by paragraph and page reference to the final report for ease of correlation. Sections are presented as integral parts and numbered consistent with the final report. Pages are "T" slotted to allow insertion in the final report document if so desired. An errata of corrections is also included.

CONTENTS

3.3.1.2 LI-900 Thermal Conductivity (Cont.)

Thermal conductivity measurements have been completed on specimens 2 and 3 of the radiantly cycled LI-900 material, with the results shown in Table 3.3.1. Comparison with data obtained from as-fabricated material, presented in the final report, LMSC-D282673 dated 30 December 1972, indicates that radiant cycling does not alter LI-900 conductivity properites. This conclusion is best illustrated by referring to Fig. 3.3.1.5a.

Table 3.3.1

RADIANTLY CYCLED LI-900 THERMAL CONDUCTIVITY FOR TRANSVERSE DIRECTION

Specimen No.	Mean Temperature (^{o}F)	Thermal Conductivity (Btu-in./hr-ft^2 ^{o}F)	Pressure (Torr)
RC-2	604	0.170	10^{-4}
	545	0.538	760
	1620	0.645	10^{-4}
RC-3	625	0.225	10^{-4}
	595	0.555	760
	1620	0.616	10^{-4}
	1760	0.720	10^{-2}

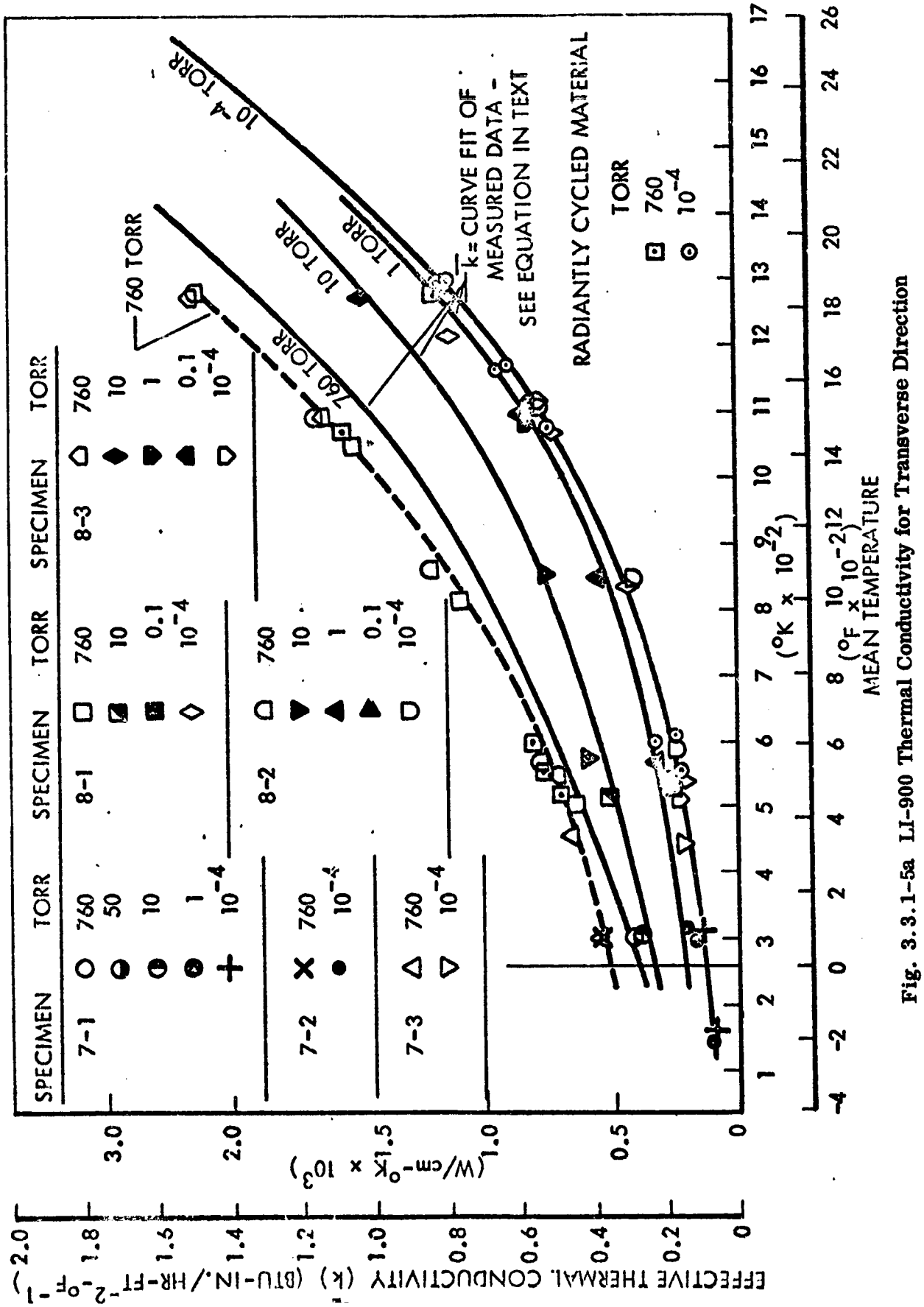

Fig. 3.3.1-5a LI-900 Thermal Conductivity for Transverse Direction

4.1.2 Test Results (Cont.)

Results of Cold Soak Test to Minimum Orbital Temperature Condition. Post-test inspection of the test model disclosed no evidence of cracking or deformation of the substrate, RSI installation, or test fixtures. The tile coating did not develop additional cracks to those present from handling and instrumentation damage. A small amount of scorching to the exposed edge of the model bond was present, caused by gap heating during the Area 2P entry heating simulation.

Results of Combined Cold Soak and Static Load Conditions. Post-test inspection was performed after application of 3,125 pounds axial tension load at -250°F. This inspection disclosed no evidence of cracking, deformation or failure of the test model. Post-test inspection was performed after application of 2,750 pounds of axial tension load at -130°F, then application of 17,200 pounds axial tension load at -35°F. This inspection disclosed no evidence of damage or degradation of the test model due to effects of the test. Strain data for the tests performed are presented in Tables 4.1.2-1 and 4.1.2-2. Figure 4.1.2-1 shows the test model installed for test. Figures 4.1.2-2 and 4.1.2-3 show the model after test.

Table 4.1.2-1

STRAINS COMPUTED ON PRE-TEST ZERO LOAD TO MAX LOAD

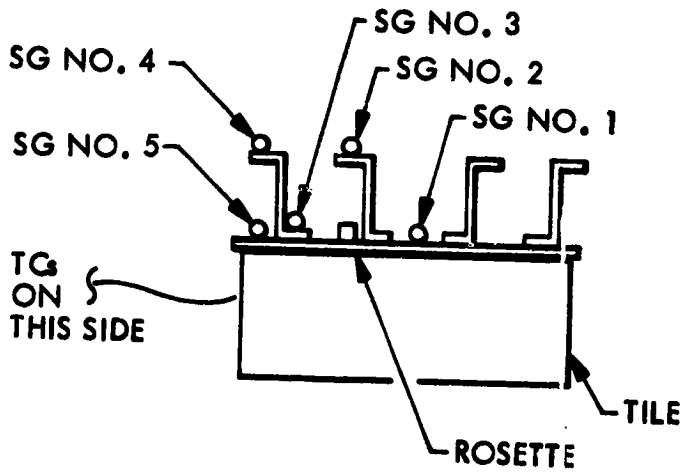

Strain Gage Number		Load - Pounds	
	3,125	17,200	25,000
	Strain	Strain	Strain
	μin./in.	μin./in.	μin./in.
1	266	2,193	3,364
2	491	2,608	Open
3	254	2,190	3,271
4	506	2,696	3,840
5	258	2,166	3,254
A	246	2,158	3,221
B	-60	-840	-1,352
C	103	645	892

Table 4.1.2-2

STRAINS COMPUTED ON MAX. LOAD TO POST-TEST ZERO

Strain Gage Number	Load - Pounds		
	3,125	17,200	25,000
	Strain	Strain	Strain
	μin./in.	μin./in.	μin./in.
1	290	2114	3325
2	426	2511	Open
3	215	1983	3261
4	504	2590	3840
5	224	2104	3254
A	218	2095	3221
B	-36	-865	-1352
C	89	622	892

The results noted in the tabulations have been corrected for temperature effects. The minus sign denotes compressive strain.

4.1.3 Comparison and Theory

To verify the adequacy of the interim design values of thermal conductivity of LI-900, temperature predictions were performed for the thermal response panel using a one-dimensional thermal model, LMSC's THERM computer code, and the thermal conductivity and specific heat values determined for LI-1500, Ref. 2, Vol II, Page 6.2-5.

Figure 4.1.3-1 shows a comparison of LI-900 thermal conductivity data for 10^{-4} and 760 ton with LI-1500 design curves. Excluding the three LI-900 data point at low pressure between 1725 and 1890°F, the low pressure design curve is slightly higher than the data and the 1-atm pressure design curve is slightly under the LI-900 data. However, the data scatter is within the experimental uncertainty of the measurements, and the same design curves are currently being used for both LI-900 and LI-1500 thermal conductivity. Additional effort will be required to define more adequately the variation of LI-900 thermal conductivity with pressure. Additional correlations of measured temperature data are required to justify modifications of the interim design values for LI-900 thermal conductivity.

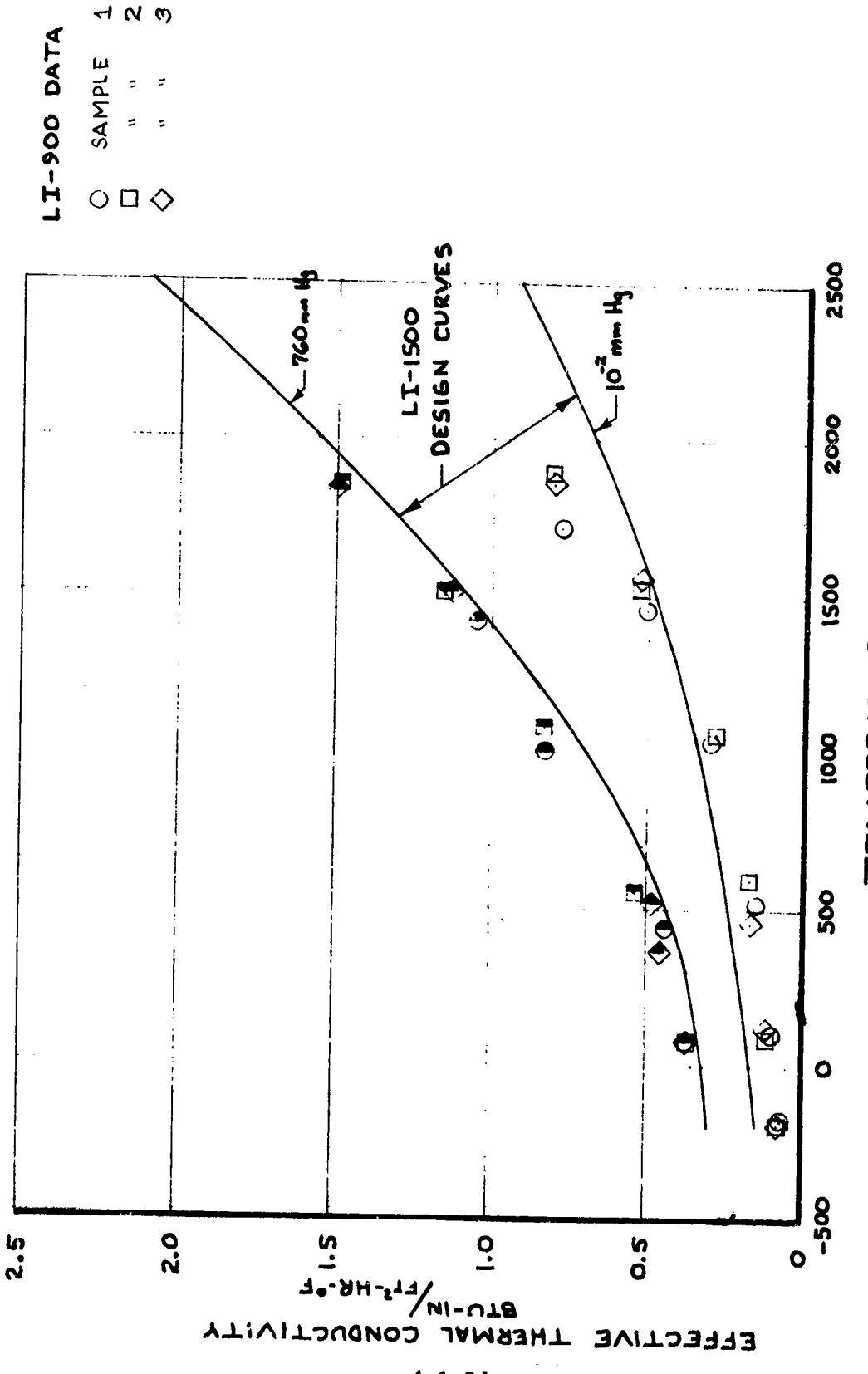

Fig. 4.1.3.1 Comparison of LI-900 Thermal Conductivity Data With LI-1500 Design Curves

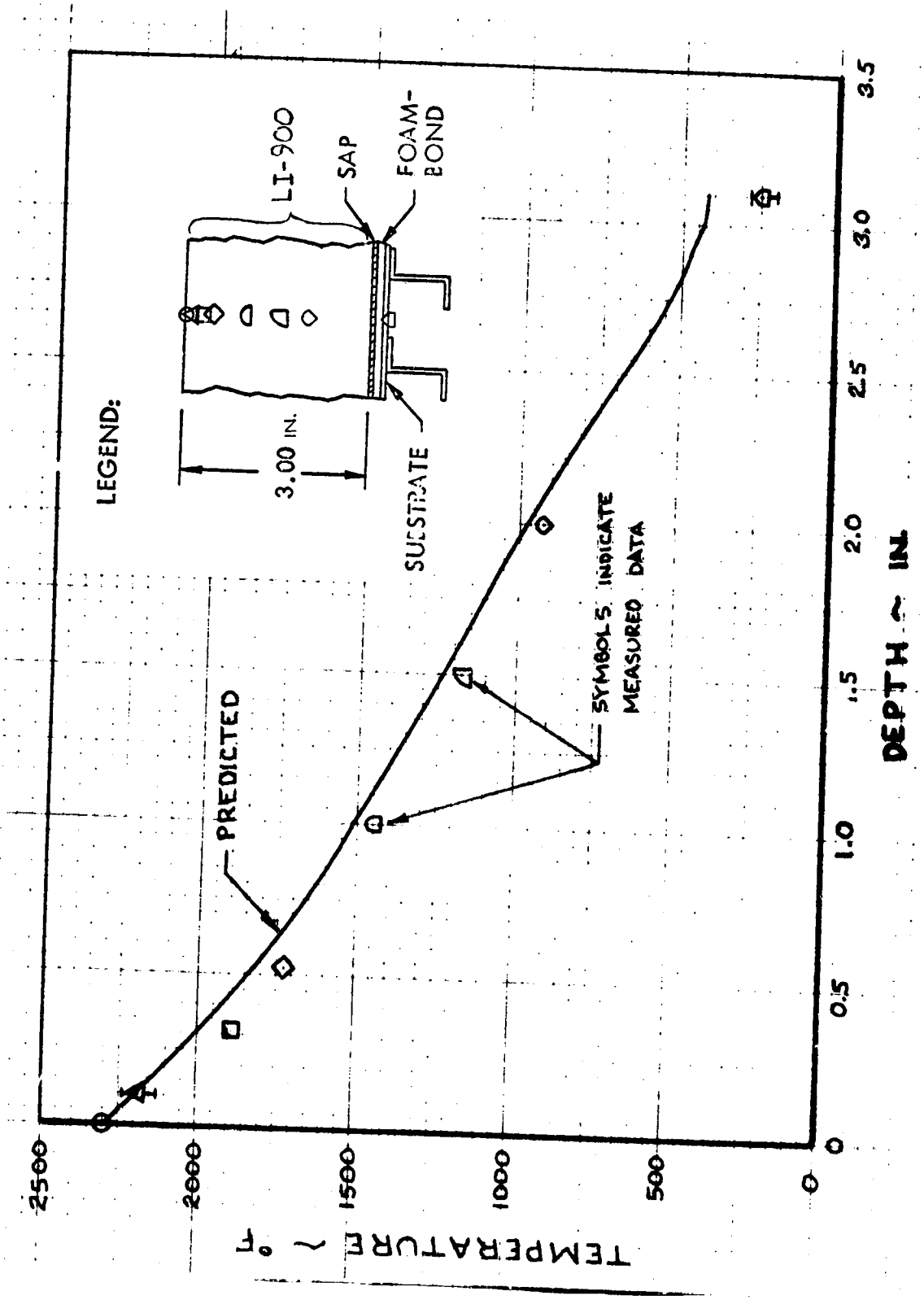

Fig. 4.1.3-2 Peak Temperature Distribution for Thermal Response Panel

Figure 4.1.3-2 depicts the maximum measured temperature distribution through LI-900 for the thermal response tests. The symbols and data bands shown represent the spread in peak measured temperature for the five tests. The predicted maximum temperature distribution indicates that the 1-atm interim design values for LI-900 thermal conductivity are conservative. Hence, use of the LI-1500 design curve of Fig. 4.1.3-1, while slightly lower than the LI-900 measured thermal conductivity, tends to overpredict the test results for the thermal response panel.

Figure 4.1.3-3 shows a comparison of the predicted and measured temperature histories for test No. 2. The thermocouple locations are also shown in Fig. 4.1.3-3. Although the data shown are for the middle LI-900 tile (Fig. 4.1.1-1), the measured temperatures for the other instrumented tile (i.e., T/C Nos. 9, 10, 11, 12, 13, and 14) were essentially the same as those shown in Fig. 4.1.3-3. Hence, the data repeatability was consistent for both tiles during the five tests. The measured surface temperature was used as the surface boundary condition and an adiabatic condition was assumed at the panel. The predicted temperatures are conservative but generally tend to reach their maximum values at the same time as the measured data. The spread in the measured panel temperatures (thermocouples 15, 16, and 17) during test No. 2 is shown by the data band associated with the symbol in Fig. 4.1.3-3.

Although the predicted panel temperature was generally within the range of the measured panel temperatures until 2000 sec and there overpredicts the panel peak temperature, it is possible that the overprediction is due to a non-adiabatic backface condition during the latter part of the test.

Comparisons of predicted and measured temperature data for a low pressure environment (1-20 mm Hg) were shown in Figs. 3.2.3.6-2 and 3.2.3.6-3 of the Final Report for Task B radiantly cycled LI-900. These predictions also used the LI-1500 design conductivity curves for LI-900 and results indicate good agreement with the measures data. Hence, these initial data correlations at both high (760 mm Hg) and low pressure (10-20 mm Hg) have shown that the LI-900 thermal conductivity values are adequate for TPS design studies.

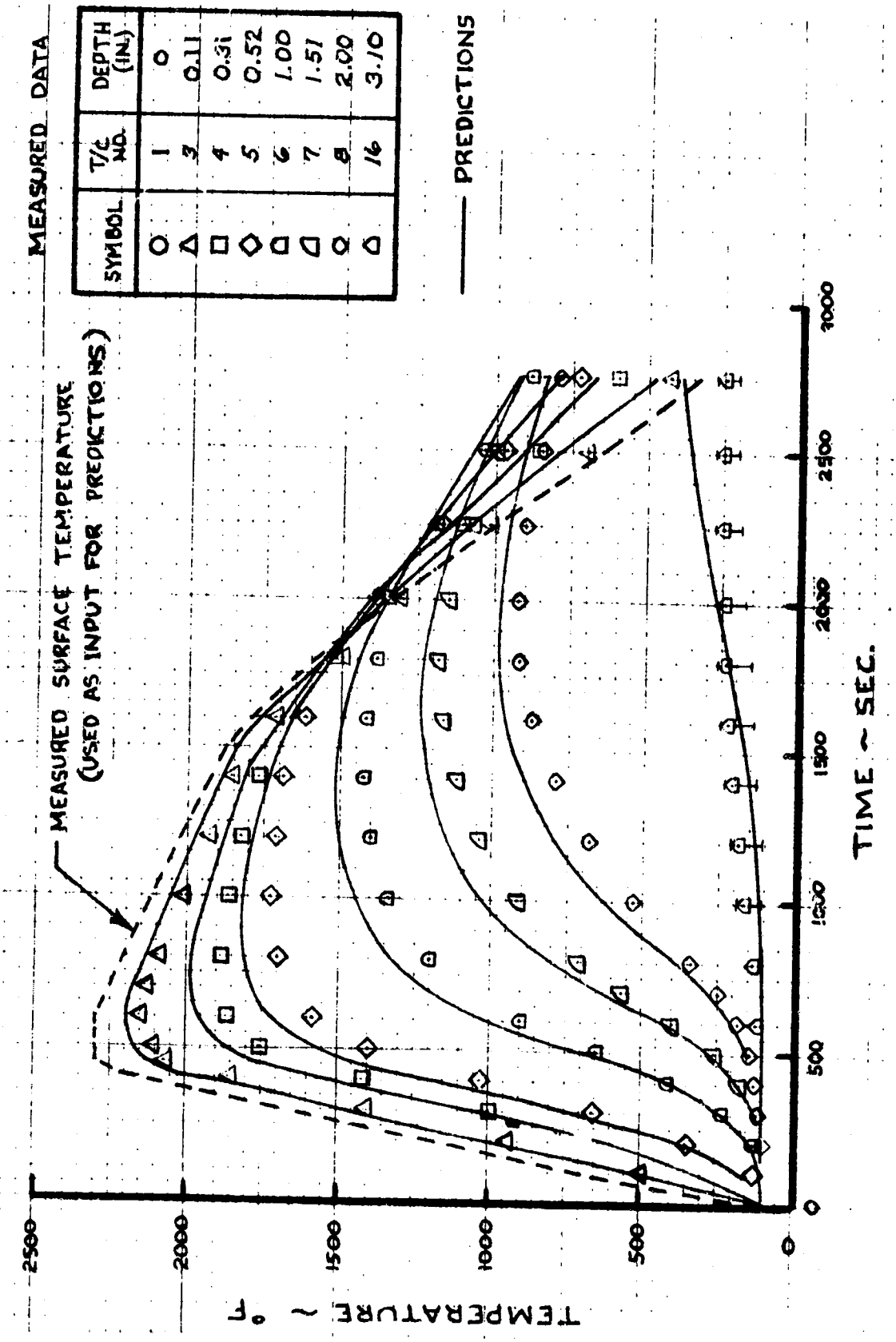

Fig. 4.1.3-3 Comparison of Predicted and Measured Temperature Histories for Thermal Response Panel

ANALYSIS OF STRAIN RESULTS

Test results show that during -250°F cold soak with axial load applied in tension the thermal response test panel undergoes bending in the aluminum substrate in the following mode.

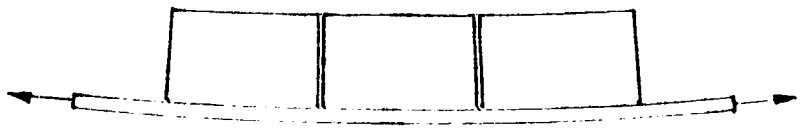

This is indicated by the higher tensile strain values on strain gages Nos. 2 and 4, on the stiffener lower flanges, than on the upper strain gages.

Table 4.1.2-3

COMPARISON OF MEASURED AND COMPUTED STRAINS

Strain Gage No.	Substrate Mechanical Strain (μ in./in.) Test Results	Computed** (Stress-Free at -250°F)	Computed* (No Stress Relaxation)
1	266	335	534
2	491	362	204
3	254	335	534
4	506	362	204
5	258	335	534
A	246	335	534
B	-60	-110	-150
C	103	—	—

*Computed strains, with no relaxation of foambond during cooldown, includes strains due to thermal distortion and mechanical load.
**Computed strains, with foambond stress relaxation, assumes no stress or strain at -250°F. Strains due to mechanical load only.

Computed strain results are shown assuming a stress-free state at room temperature so that the strains include those due to thermal distortion as well as mechanical load. Due to the high coefficient of expansion of aluminum compared with LI-900 the composite tends to bend in the opposite mode when cooled down, as indicated by the strain results.

This effect overcomes the opposite bending effect due to mechanical load.

Computed strain results, where stress relaxation in the bond is considered, give values that are closer to those of the test. This assumes that creep or stress relaxation takes place in the foam and bond during panel cooldown so that at -250^{o}F a stress-free state exists with no panel deformation. When the mechanical load is applied the strain results indicate bending in the same mode as in the test.

Strain results indicate that relaxation occurs in the bond system. This evidence is substantiated by tests on bond systems done by H. Owens at General Dynamics.

Further study on creep and relaxation phenomena in bond systems is presently being carried out at LMSC. Computer codes that include creep in the analysis are being refined and a test program is being conducted to measure the required quantities.

4.4.3 Shuttle Comparison

The tests as performed are obviously not comparable to real life orbiter environments because of the manner of exposure to the chemical contaminants. A 24-hour immersion to half the thickness of the specimen provides a means only of screening the chemicals to determine which should be subject to further investigation. A more representative test program, to simulate the accidental application and the time of exposure, should be carefully defined and closely controlled.

Broadly speaking, the results indicate that petroleum derivatives are destructive to the RTV bond used.

As expected, sodium hydroxide degrades the tile surface and the tiles are discolored by IRFNA and UDMH, although there is no apparent degradation of the coating. In addition, the results of exposure to the white portion of bird excrement were inconclusive and should be examined extensively. These reagents should be investigated further to define precautionary measures for use during orbiter servicing and operation.

ERRATA

Page	Comments
2.1-6	Fig. 2.1-3. Disregard separate scale at left. Scale shown on figure (0-4.0) is Δ P (psi)
2.1-9	Table 2.1-1. Compression Weak Direction Values for LI-900: stress – 34.2 psi, Modulus – 3400 psi
2.2-7	Fig. 2.2-8. Add "cloth" after Epoxy in title.
2.3-17	Fig. 2.3-20. Label for upper line should be R-compression
2.3-18	Fig. 2.3-21. Information is for "weak" direction
2.3-21	Table 2.3-5. Second column from right, t = 1000 sec instead of 10,000 sec
2.4-15	Table 2.4-8. For compression allowables please reference pages B2-36 and B2-37
2.5-13	Fig. 2.5-11. Replace PRD-49 with HMS/ X-904